The Application of Cellulose Nanowhiskers to Engineer Skeletal Muscle Tissue

A thesis submitted to the University of Manchester for the degree of Doctor of Philosophy in the Faculty of Science and Engineering

2019

Annchalee Eade

School of Natural Sciences

Department of Materials

Contents

Word Count: 35,690

List of figures

List of tables

List of abbreviations

General Abbreviations

2D	2 dimensional
3D	3 dimensional
AFM	Atomic force microscopy
BM-MSC	Human bone marrow derived mesenchymal stem cells
C2C12	Immortalised mouse myoblast cell line
CNW	Cellulose nanowhiskers
dH2O	Distilled water
ECM	Extracellular matrix
FTIR	Fourier transmission infrared radiography
GAG	Glycosaminoglycan
hSkMC	Human skeletal muscle
LbL	Layer-by-layer
MFR	Myogenic regulatory factors
PAH	Poly(allylamine hydrochloride
PAHCI	Polyallylamine hydrochloride
PCL	Poly(3-caprolactone)
PDMS	Poly(dimethylsiloxan)
PEI	Polyethylenimine
PG	Proteoglycans
PLLA	Polylactic acid
PSS	Polystyrene sulphonate
PTFE	Polytetrafluoroethylene
SLRP	Small leucine-rich proteoglycans
XPS	X-ray photoelectron spectroscopy

Substrate Descriptions

Glass	Glass only
Chitosan	Glass with 1 layer of spin coated chitosan
ChitCNW	Glass with 1 layer of spin coated chitosan and 1 of spin coated CNW (a bilayer)
6CNW	Glass with 6 bilayers, top layer is spin coated CNW
12Chit	Glass with 11 bilayers and a top layer of spin coated chitosan
12CNW	Glass with 12 bilayers, top layer is spin coated CNW

Abstract

Skeletal muscle has a high capacity for self-regeneration, however, this is limited when there is a significant loss of tissue. The development of cell based constructs using biomaterials that can stimulate cell proliferation and differentiation, could support the body's natural systems during regeneration. Cellulose nanowhiskers (CNWs) are rod like nanomaterials, typically 5 to 20 nm in diameter, and can range from 100's of nanometres to several microns in length. The high aspect ratio of the CNWs could provide contact guidance suitable for directing cells of highly structural tissues, like skeletal muscle. This work explores the potential of multilayer substrates composed of alternating polyelectrolyte CNW and chitosan, with an oriented CNW top layer to promote the alignment and differentiation of myoblasts in to myotubes.

Multilayer substrates were assembled through the dip coating of CNW and chitosan solutions on to glass coverslips. CNWs are produced through the partial acid hydrolysis of cellulose. The use of sulphuric acid results in a residual negative charge caused by the addition of sulphate ester groups on the whiskers. As a polyanion, CNWs can be layered with an oppositely charged polycation, chitosan, to form stable multilayer films. CNWs can then be spin coated on to the multilayer substrates forming a radial oriented nanotopography.

Once formed, the capabilities of the substrates to promote cell growth and differentiation were investigated using C2C12s, an immortalised mouse myoblast cell line. The cells showed distinct signs of differentiation through the immunofluorescence staining of key myogenic components. Broad alignment of myotubes was observed on the oriented CNW multilayers whereas only local alignment formed on the substrates without the CNWs. Other cell types also showed a morphological cell response to these substrates, as human skeletal muscle cells (hSkMCs) and bone marrow derived mesenchymal stem cells (BM-MSCs) both showed alignment and elongation on the oriented CNWs. To further encourage the proliferation and differentiation of cells, key extracellular matrix (ECM) proteins, such as fibronectin and laminin, were adsorbed onto the substrates. Both proteins showed increased cell spreading and proliferation compared to untreated controls for C2C12 and BM-MSCs. These results are extremely promising for development of nanotopographical substrates, and pave the way for more complex 3D tissue scaffolds to be developed.

Declaration

I declare that that no portion of the work referred to in the thesis has been submitted in support of an application for another degree or qualification of this or any other university or other institute of learning.

Acknowledgements

I would like to thank my supervisors, Prof. Julie Gough and Prof. John Aplin for their academic guidance. I would specifically like to thank Julie for her overall support during the PhD process, especially in the last few years. I am extremely grateful to Dr. Naa-Dei Nikoi who's direction and help have been invaluable.

Elements of this work would not have been possible without the help and training of the following: Dr. Ben Spencer and his mastery of XPS and AFM, Dr. Louise Carney for her training in cell work and general experimental disasters, Dr. Rachel Saunders for her training on the KRUSS Drop Shape Analyzer and all of the fun I had helping at Outreach events, Dr Francesco Galli of the Cossu Group who gave his time and his satellite cells and Andrew Wood and Wojciech Hahnel from PromoCell and their help with the hSkMCs. I also need to thank my masters students, Aima Noel and Moneik Schmitzfor their contributions to substrate preparation and repeats of the C2C12 viability experiments.

This thesis would not have reached this point without proof reading and editing from my mum, Benjawan Eade, and my housemate, George Severns who, along with Mike Lacey and Mia Coleman, have been my dependable pub goers from the start. A special thank you to Will Ambler for the copious amounts of coffee, biscuits and support during the writing period.

Lastly a thank you to the whole Biomaterials Group at the University of Manchester for making the last few years so enjoyable and my family for their tolerance of my perpetual studentship.

This work was funded by the (EPSRC) Doctoral Training Award and supported by the Henry Royce Institute for Advanced Materials, funded through EPSRC grants EP/R00661X/1, EP/P025021/1 and EP/P025498/1.

Preface of the Author

My undergraduate degree was done at the University of Manchester where I received a First Class MEng in Biomedical Materials Science WIE. I liked Manchester so much I stayed, joining the Gough Group within the Biomaterials Department. My interest in Biomedical Materials stems from my curiosity in mixing materials engineering and human biology.

I have been fortunate enough to have present posters at a number of international conferences, TERMIS 2017 and ESB 2018, and some closer to home, TCES 2018 and School of Material PGR Conferences 2016 to 2018. I was lucky enough to give an oral presentation at the Bioinspired Nanomaterials Meeting at the University of Strathclyde in 2019.

My Outreach work has included Dragonfly Days, ScienceX, the Community Festival, HeadStart EDT and the Blue Dot Festival. I have also been partly responsible for the Biomaterials Christmas Party for the last 2 years.

Chapter 1: Introduction

1.1 Thesis Summary

The response of cells to a surface is one of the key factors guiding tissue engineering research. The initial reaction and laying down of key extracellular matrix (ECM) proteins is the foundation of a successful tissue scaffold. Although the development of 3D scaffolds is the end goal of tissue scaffolding, it is first necessary to understand how cells interact with the topography of 2D substrates. Topographical features in the microscale such as patterned grooves are well documented, however promising new research is showing that nanoscale features can lead to even an even greater cell response. Cellulose nanowhiskers (CNWs) are biocompatible, have a low toxicity and are susceptible to chemical modifications. The high aspect ratio of their morphology (typically one hundred times longer than they are wide) could be beneficial in the guidance of highly structural tissues, such as skeletal muscle. The main functions of skeletal muscle tissue are support and mobility, however, accidents which result in tissue loss or diseases, such as muscle dystrophy, can reduce the ability of the tissue to fulfil its purpose. Substrates or scaffolds formed from biomaterials can support the culture and formation of biological structures, and could aid in the regeneration of damaged sites.

This thesis builds on the idea of using oriented CNW's and polyelectrolyte multilayer substrates, and seeks to improve the ability of such substrates to aid with engineering skeletal muscle tissue. Polyelectrolyte multilayers of alternating CNWs and chitosan layers with an oriented CNW top layer were produced following protocols developed in previous work from the Gough Group at the University of Manchester. In 2011, James Dugan investigated the response of C2C12s, a mouse myoblast cell line, on spin coated CNWs; a method which was then optimised by Naa-Dei Nikoi and applied on top of polyelectrolyte multilayers of CNW, chitosan and polystyrene sulphonate (PSS). Both studies showed the potential of the CNWs to direct myoblast alignment and encourage myotube formation. However, the PSS in the multilayers proved cytotoxic to the cells. The substrates produced in this project have been designed using the same principle of combining the polyelectrolyte layers with the spin coated CNWs, however, PSS had been omitted.

The response of different cell types linked to skeletal muscle have been explored in this thesis including bone marrow derived mesenchymal stem cells (BM-MSCs). BM-MSCs when exposed to specific stimuli have the potential to differentiate into a wide range of cell types. As possibly some of the smallest topographical features to influence cells, it is of interest to see if the nanotopography of the CNWs could direct the cells towards a muscle lineage.

Lastly, the effect of adsorbed ECM proteins, combined with the CNWs, on the response of cells is explored. Fibronectin and laminin are key ECM proteins found in the basement membrane of skeletal muscle tissue. Both proteins are crucial to cell adhesion and differentiation, to many other cell types, not just muscle. The combination of topography and adsorbed fibronectin and laminin could have a positive response from the myoblasts.

Overall, this thesis contributes to the understanding of multiple concepts, such as contact guidance and the influence of proteins, and how we combine them in the attempt to achieve the optimum cell environment.

1.2 Project Aims

This thesis hypothesises that multilayer substrates of alternating chitosan and CNW layers with an oriented CNW top layer, can be used in the application of skeletal muscle tissue engineering through the alignment of differentiated myoblasts and influence of key ECM proteins. Oriented CNWs on similarly composed substrates have already shown promise in the formation of aligned myotubes, however in the preliminary work a level of toxicity resulted from the choice of material. This thesis seeks to improve both the biocompatibility and functionality of the multilayer substrates, through the addition of fibronectin and laminin, whilst also investigating the cell response of primary cells such as human skeletal muscle cells (hSkMCs) and human bone marrow derived mesenchymal stem cells (BM-MSCs).

The principle aims of the work described in this thesis are:

1. To create multilayer substrates with an oriented CNW top layer, and to characterise the cell response (guided orientation);
    a. Formation of multilayer substrates of alternating CNW and chitosan layers, with a spin coated top layer of radially oriented CNWs,
    b. Proliferation and spreading of C2C12s to ensure there is no toxic response to the multilayer substrates,
    c. Positive differentiation of C2C12s and subsequent induction of broadly aligned myotubes across large areas of the substrate.

2. Application and response of primary cells, such as hSkMCs and BM-MSCs, on the oriented multilayer substrates;
    a. Proliferation, alignment and differentiation of hSkMCs in response to the oriented topography of the CNWs,
    b. Proliferation and alignment of BM-MSCs with the potential to differentiate towards myogenic lineage.

3. Investigate the effect on cell response of adsorbed ECM proteins on the oriented CNW topography;
    a. Confirm the adsorption of fibronectin and laminin on the multilayer substrates,

b. Observe any improvement in C2C12 proliferation and differentiation in response to the adsorbed proteins,
c. Observe any improvement in BM-MSC proliferation and alignment in response to the adsorbed proteins.

Chapter 2: Literature Review

2.1 Introduction

This introductory chapter will explore the components which piece together this thesis from understanding the tissue architecture to discussing the concepts of protein adsorption. The first step in designing a biomaterial is to understand the purpose of the tissue and the properties of the material. The structure of skeletal muscle as a whole tissue down to the cellular level is discussed with examples of tissue engineering strategies already published. The properties of CNWs and their potential as a biomaterial are explored along with current use of the material. Lastly, the comprehension of scientific approaches and the basis behind them are applied to cell mechanisms discussed in the results chapters.

2.2 Muscle Tissue

There are three types of muscle in the body; skeletal, cardiac and smooth. Skeletal muscle is the voluntary muscle of the body and is responsible for the body's mobility. Its cells are elongated and have striations, which allow the muscle tissue to contract. Along with movement, skeletal muscle is responsible for the stability of the skeleton and how the body maintains its posture. This muscle makes up the bulk of the tissue and is one of the most abundant organs in the body protecting and supporting other organs. It allows the voluntary control of swallowing, breathing, urination and defecation. Cardiac muscle is only found in the heart and although cardiac muscle cells are also striated, the contraction of the heart muscle is not considered voluntary as it cannot always be consciously controlled. Smooth muscle cells (SMCs) are elongated but do not have striations. Such muscles are found in the walls of the stomach and other hollow visceral organs responsible for the movement of fluid and other substances around the body. These muscles are not voluntarily controlled (Marieb and Hoehn, 2014).

As with all tissues in the human body, damage of the skeletal muscle can result in a loss of function. Most skeletal muscle injuries are sports related where the muscle is subjected to a large force resulting in strains or contusions (Jarvinen, Jarvinen and

Kalimo, 2013). Skeletal muscle can undergo heavier damage where there is significant tissue loss, more likely caused by accidents such as traffic collisions. Muscular dystrophy, also known as the "muscle wasting condition", is a rare genetic condition that affects 70,000 people in the UK and covers a range of symptoms and prognoses (NHS, 2018). The reduction in muscle function is due to mutations in the genes required to grow muscle and maintain the structure (North and Beggs, 1996).

2.2.1 Structure

A muscle organ consists predominately of skeletal muscle, as well as, nerves, blood vessels and connective tissue. The structure of muscle is hierarchical, as shown in Figure 2-1. Skeletal muscle cells fuse to form myotubes, which then mature and group together as muscle fibres. These fibres are wrapped up in a thin connective tissue called the endomysium, as well as, the basement membrane (Marieb and Hoehn, 2014; Christ *et al.*, 2015). The endomysium is a thin sheath of fibrillar collagen I and III in conjunction with proteoglycans and glycosaminoglycans (GAGs). The muscle basement membrane consists of mainly collagen type IV, fibronectin and laminin and although considered a different component to the endomysium, the two are closely connected (Gillies, Lieber and Lieber, 2012). The subsequent tier of the muscle structure is the perimysium, which bundles groups of muscle fibres into fascicles. The final connective tissue layer is called the epimysium and envelopes the fascicles forming the muscle organ. As with the endomysium, the perimysium and epimysium are connective tissue composed of collagen I and II, proteoglycans and GAGs. However, the structures of the endomysium and perimysium are different. Collagen in the endomysium has a web like structure and assembles as a longitudinal wave along the muscle fibre. Collagen in the perimysium runs the length of the fascicles in a coiled structure (Gillies, Lieber and Lieber, 2012; Christ *et al.*, 2015). Tendons of connective tissue then connect the muscle to the bone.

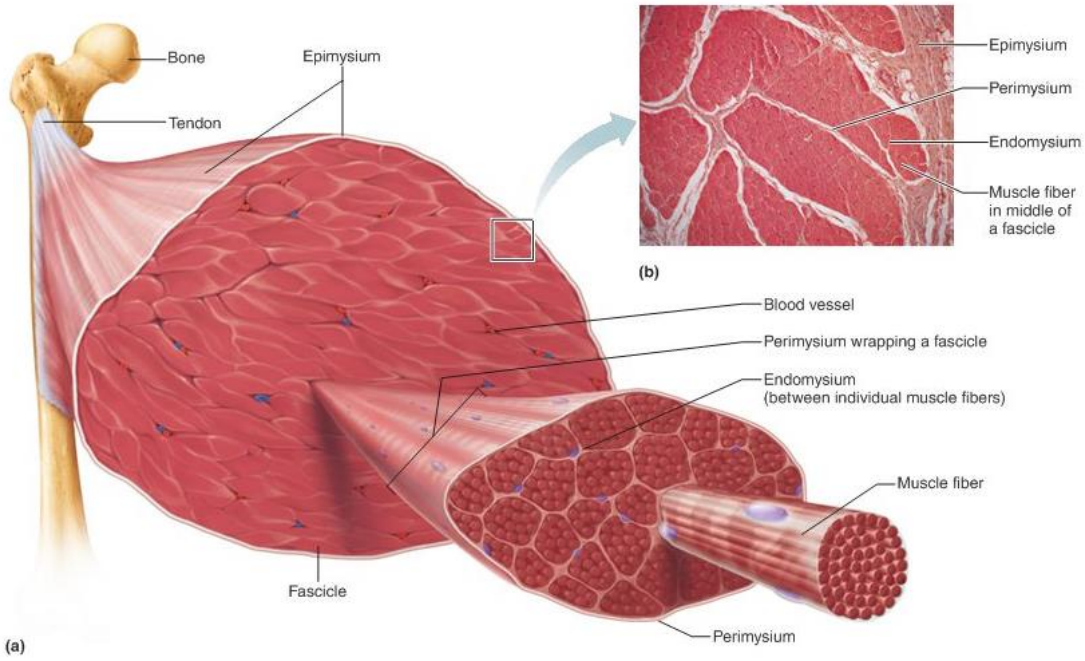

Figure 2-1: (a) Hierarchical structure of the skeletal muscle tissue and (b) layering of the connective tissue within the muscle structure (Marieb and Hoehn, 2014)**.**

Muscle fibres are formed from the fusion of muscle cells into myotubes. Myogenic differentiation is a multistep process, which includes withdrawal from the cell cycle, recruitment of transcription factors and cell morphological changes (Chiron *et al.*, 2012). Their lengths vary depending on the size of muscle, the longest being in the thigh, which can reach 30 cm however, the diameter is generally only around 100 µm thick. Due to how muscle fibres form, each fibre can contain up to several 100 nuclei. Mitochondria are also present; like the nuclei, they are found on the periphery of the fibre beneath the sarcolemma, the membrane of the muscle fibre (Marieb and Hoehn, 2014; Christ *et al.*, 2015).

Contraction is one of the main functions of muscle. The system of relaxing and contracting controls the movement of the skeleton and gives the ability of controlled mobility. Within a muscle fibre, each myofibril is composed of myofilaments, which form repeating contractile units called sarcomeres. A sarcomere is formed of thin and thick filaments, which are arranged as shown in Figure 2-2, with the Z-disc identifying the individual unit (Marieb and Hoehn, 2014). The thin filaments are predominately actin and appear as a light isotropic (I) band. The thick filaments are myosin and

appear as a dark anisotropic (A) band. The dark and light bands form the striated pattern seen on skeletal and cardiac muscle tissues. The H zone, in which is found with the middle (M) line, is located centrally in the sarcomere and contains only myosin filaments. Similarly, the Z disc only contains actin filaments. The observation of striated muscle fibres *in vitro* can be used to positively identify the maturation of myotubes although it is not seen developing myotubes (Christ *et al.*, 2015).

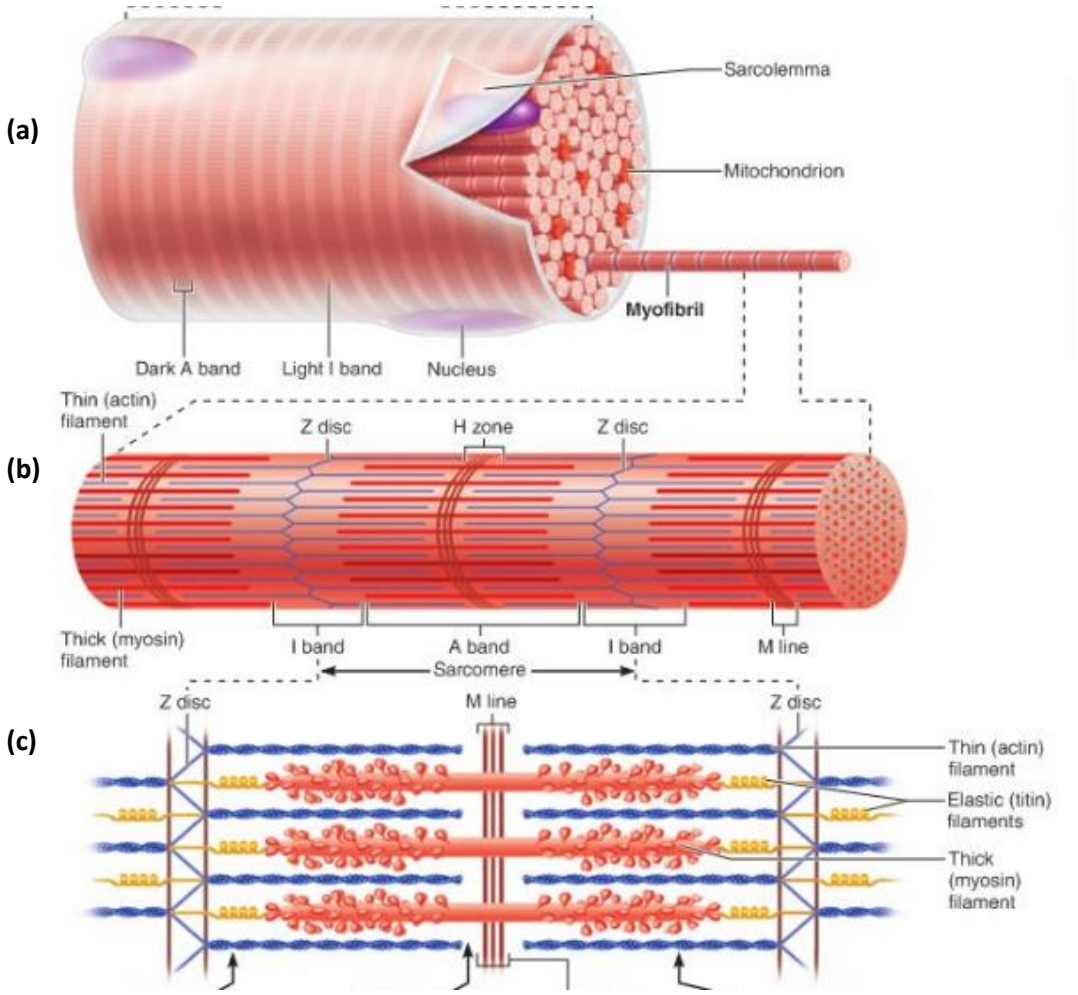

Figure 2-2: (a) The sarcolemma of a muscle fibre holds together a number of myofibrils and organelles such as mitochondria and nuclei. (b) Myofibrils contain myofilaments which form a light and dark banding pattern. (c) The sarcomere is composed of actin and myosin filaments. A muscle contracts due to the simultaneous contraction of sarcomeres. (Marieb and Hoehn, 2014)

Actin crosslinking proteins of the α-actin family, specifically ACTN-2, are often used to identify myogenic differentiation *in vitro*. ACTN-1 and -4 are non-muscle specific and found along actin microfilament bundles where they mediate membrane attachments.

ACTN-2 and -3 are also known as sarcomeric α-actinins due to their location in the sarcomere where they anchor the thin actin filaments (I band) to the Z-disc. They play a key role in the organisation of the sarcomere and defects in this protein could be linked to certain types of muscle dystrophy (Beggs *et al.*, 1992; North and Beggs, 1996; Mills, 2001; Chiu *et al.*, 2010).

Sarcomeres contract by shortening. The nervous system stimulates the muscle causing cross-bridges to form between myosin and actin filaments. A combination of these cross bridges forming and breaking moves the actin filaments towards the centre of the sarcomere, shortening it. The H zone disappears as the Z-discs move closer together. This happens across all the sarcomeres simultaneously resulting in the whole muscle contracting as a unit producing enough force for movement (Marieb and Hoehn, 2014).

Satellite cells are the precursor cells of adult skeletal muscles, known as myoblasts. They are mitotically quiescent and are found between the sarcolemma and basal lamina of muscle fibres. Activation of satellite cells can occur for example, from exercise or injury. This causes the satellite cells to proliferate extensively and express a myoblastic phenotype, which allows them to differentiate into myoblasts. They then fuse with existing myotubes and contribute new myonuclei to repair damage. Satellite cells which do not differentiate revert back to quiescence. This system allows the repair and growth of muscle throughout adulthood (Zammit, 2008; Jarvinen, Jarvinen and Kalimo, 2013; Marieb and Hoehn, 2014).

2.2.2 Myogenic Differentiation

Myogenesis is the process of forming new muscle which is initiated by the activation of quiescent satellite cells. Satellite cells migrate from the area between the basal lamina and sarcolemma and are marked with the transcription factor Pax7, which is responsible for the expression of MyoD, a myogenic regulatory factor (MRF). As the satellite cells proliferate some will self-renew and return to a quiescent state; however, the rest will express a myogenic phenotype in the form of myoblasts, a precursor cell. Myoblasts continue to proliferate until they differentiate and begin to express myogenin. At this point, either primary or secondary fusion will occur. Primary

fusion is the production of new multi-nucleated myotubes, which mature into muscle fibres while secondary fusion is when they fuse to existing damaged muscle fibres which are damaged (Juhas, Ye and Bursac, 2015). In adults, myogenenesis occurs in response to specific stimuli, such as exercise or injury (Blais *et al.*, 2005). Primary fusion is what is observed with myoblasts *in vitro* (S. Burattini, P. Ferri, M. Battistelli, R. Curci, F. Luchetti, 2004).

There are four MRFs which belong to a family of basic helix-loop-helix transcription factors, MyoD, Myf5, myogenin and MRF4. They are responsible for the determination of the myogenic phenotype expressed, the progression of myoblast differentiation and the regulation of the muscle specific genes expressed (Blais *et al.*, 2005). The pattern of their expression overlaps as the cells go through differentiation however, they do have specific roles (Pownall, Gustafsson and Emerson, 2002; Hernández-Hernández *et al.*, 2017). MyoD is activated once the satellite cells begin to proliferate. This is responsible for the balance of proliferation and differentiation of satellite cells and is required to cease proliferation and, therefore allow satellite cells to differentiate. As MyoD can activate the muscle transcription program of specific genes it can induce myogenic differentiation in other cell types and control the muscle lineage (Tapscott, 2005). Myf5 is expressed during satellite cell proliferation like MyoD; they determine the Myogenesis progression. Myogenin and MRF4, are expressed with MyoD during the onset of myoblast differentiation and fusion of the cells into myotubes. Myogenin is responsible for the amplification of present gene expression and formation of myotubes (Buckingham and Montarras, 2008). MRF4 mediates the final maturation of the myotubes into myofibres and can down-regulate myogenin (Zhang, Behringer and Olson, 1995). As well as regulating muscle specific genes, the MRFs auto-regulate each other in an on-going cycle where MyoD and myogenin induce expression of each other (Thayer *et al.*, 1989). MRFs induce the expression of key muscle specific proteins such as the actin crosslinking protein α-actinin and heavy and light myosin chains (S. Burattini, P. Ferri, M. Battistelli, R. Curci, F. Luchetti, 2004).

Pax genes are a family of transcription factors identified by the presence of a paired DNA bonding motif. Key Pax factors in myogenesis are Pax3 and Pax7, which also have a homeodomain, a sixty amino acid helix-turn-helix DNA-binding domain. Neither genes are skeletal muscle specific and can be found in other areas such as regions of

the central nervous system. However, they are important in tissue specification, which makes them significant for myogenic differentiation (Buckingham and Montarras, 2008).

The understanding of myogenic differentiation is important for the tissue engineering of skeletal muscle. The differentiation of myoblasts into myotubes can be replicated *in vitro* and the background of myogenesis will help determine the success of cell work carried out. C2C12 cells are often used *in vitro* to model myogenic differentiation and myotube formation. They are murine myoblasts derived from satellite cells, which spontaneously differentiate in response to low levels of serum. When in an undifferentiated state, they are approximately 20-80 µm in size and appear flat and adherent. When differentiating, the cells undergo an irreversible withdrawal from the cell cycle and are terminally differentiated as muscle specific genes are expressed. Nuclei, which are part of the formation of myotubes, cannot re-activate the DNA synthesis in response to mitogenic stimuli, hence the presence of the quiescent satellite cell population in the basal lamina (S. Burattini, P. Ferri, M. Battistelli, R. Curci, F. Luchetti, 2004; Ferri *et al.*, 2009).

2.2.3 Skeletal Muscle ECM

It is a well-established concept in tissue engineering to use biomaterials to replicate the native ECM of tissue types in an effort to better reproduce the ideal cell proliferation and differentiation conditions. Collagen is the major structural protein in the ECM and different types in different assemblies can be found throughout the hierarchical structure of the organ. However, it is not yet understood if the ratios of collagen types vary between muscle functions (Gillies, Lieber and Lieber, 2012).

Proteoglycans (PGs) and glycosaminoglycans (GAGs) are also abundant in the ECM. Many PGs belong to a family of small leucine-rich proteoglycans (SLRPs) such as decroin and biglycan. These PGs consist of a core protein attached to GAG chains such as chondroitin sulphate and dermatan sulphate. Negatively charged GAGs, such as heparan sulphate PGs, store growth factors required for skeletal muscle regeneration in the basement membrane and endomysium. When needed, enzymes will cleave the growth factors from the GAGs (Brandan and Inestrosa, 1987; Gillies, Lieber and Lieber,

2012). Fibronectin and laminin are also key components of the skeletal muscle ECM. Fibronectin is found in a range of tissue types and is related to cell migration and proliferation due to the presence of the RGD (Arg-Gly-Asp) motif, which interacts with integrins on cells (Sottile and Hocking, 2002).

Laminin has been shown to be a key component of myogenic differentiation due to the presence of specific integrin binding sites (Bajanca *et al.*, 2006)and has been used to prolong the myogenic potential in long term culture expansion *in vitro* (Penton *et al.*, 2016). The components of the ECM work together to support the maintenance of satellite cells and promote regeneration of myotubes if the tissue is injured; for example, collagen IV which is present in the basement membrane has been shown to bind to laminin, fibronectin and heparan sulphate PGs (Laurie *et al.*, 1986).

The biomimetic approach is often used to try and engineer skeletal muscle tissue *in vitro*. For example, using electrospun fibres which represent the structural proteins in the ECM combined with ECM protein based coatings to promote cell adhesion and differentiation (Cronin *et al.*, 2004; Zahari, Idrus and Chowdhury, 2017).

2.2.4 Response to Injury

When muscle fibres rupture due to contusions (twisting), lacerations (severing) or shearing (tensile forces) a very similar regeneration processes is followed consisting of three phases; 1) destructive, 2) repair and 3) remodelling. Figure 2-3 shows a schematic of the regeneration of an injured muscle fibre illustrating each of the phases. In the destructive phase, the ruptured fibre (a) becomes necrotized as the uninjured ends retract and seal away to leave a gap for a haematoma, and inflammation occurs as monocytes begin phagocytosis of the necrotized tissue (b). Satellite cells are activated in the repair phase and begin to proliferate and differentiate in to myoblasts with some satellite cells remaining undifferentiated for future regeneration purposes (c). Collagens and other structural ECM proteins are produced and begin forming scar tissue as myoblasts elongate and fuse, forming myotubes (d). Remodelling occurs as the myotubes mature into muscle fibres and merge with the uninjured ends of the muscle fibre (e). The muscle fibres attach to the

newly formed scar tissue through a thin layer of connective tissue (f) (Zammit, 2008; Jarvinen, Jarvinen and Kalimo, 2013).

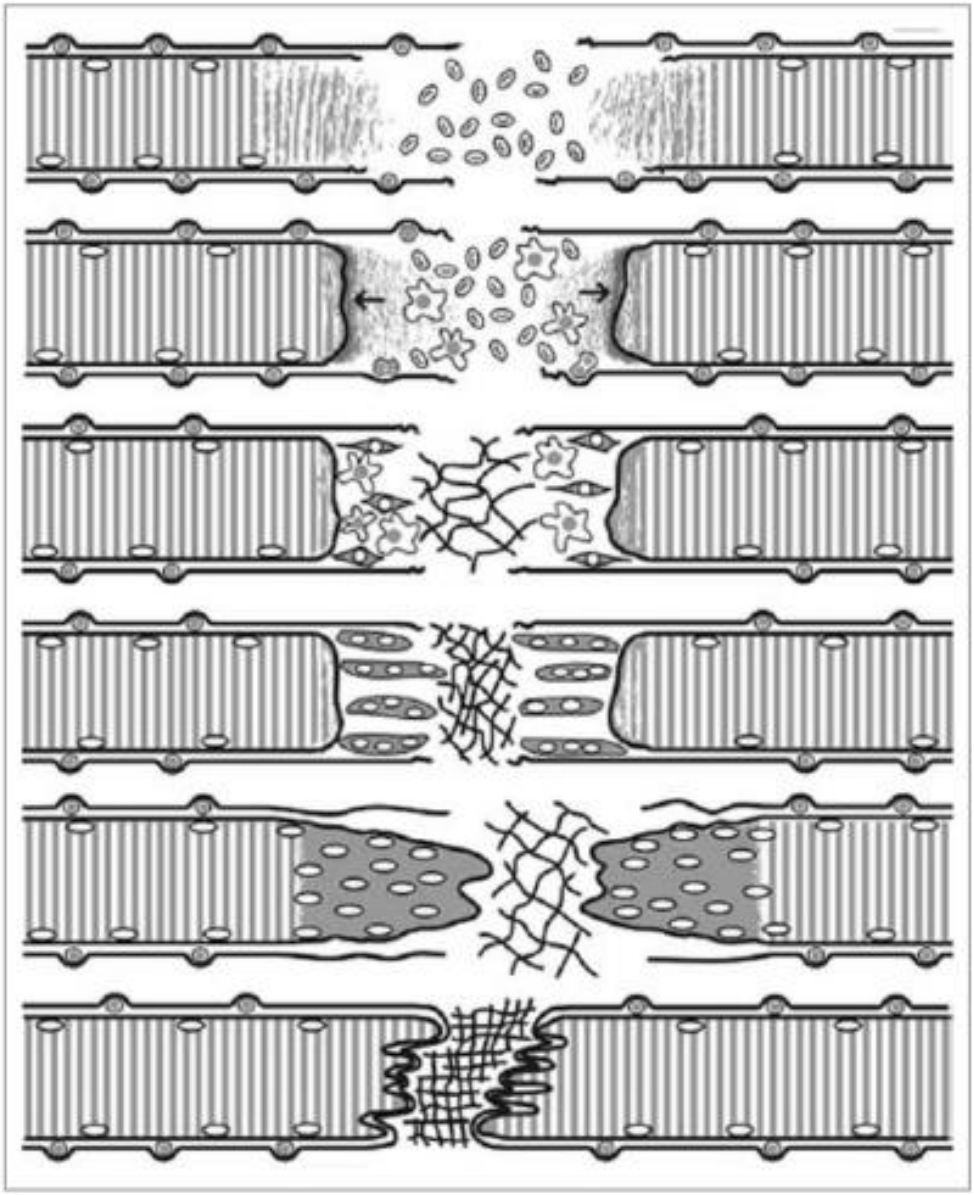

Figure 2-3: Schematic representation of regeneration of a sheared muscle fibre (Jarvinen, Jarvinen and Kalimo, 2013)**. Muscle fibres undergo regeneration through three phases, destructive, shown in (a) and (b), repair, shown in (c) and (d) and finally remodelling, shown in (e) and (f).**

Skeletal muscle has a high capacity for self-regeneration of small muscle fibre ruptures and, depending on the size of the rupture and care of the injured site, scar tissue can be negligible (Jarvinen, Jarvinen and Kalimo, 2013). However, in cases where there is a volumetric loss of tissue or if regeneration is impeded by disease, there is a limit to the extent of this regeneration.

2.2.5 Tissue Engineering of Skeletal Muscle

The application of combining cells and engineering to repair, restore or replace tissues or tissue function is classed as tissue engineering. The engineering is often the modification and use of the physiochemical and structural properties of a biomaterial with the intention to specifically influence cell response (Langer and Vacanti, 1993). Skeletal muscle has the ability to regenerate after injury or exercise due to the presence of satellite cells in the muscle fibres. However, this property can be impaired due to muscle trauma where there is large tissue loss and due to congenital myopathies. Regeneration abilities of muscle also decrease with age (Juhas, Ye and Bursac, 2015). The current treatment for muscle tissue loss is autologous grafts. However, this method is limited by tissue availability and can be impacted by further injury to the donor site (Choi *et al.*, 2008). The field of skeletal muscle tissue engineering has developed over the past 25 years, leading to a variety of research into the construction of functional 3D skeletal muscle tissue (Juhas, Ye and Bursac, 2015). The first functional human muscle tissue with the ability to contract in response to electrical stimuli was engineered by Madden et al in 2015 (Madden *et al.*, 2015). Scaffolds, tailored for the specific requirements of muscle tissue, are being developed by controlling the material properties and biochemical additives. The addition of other cells found in muscle tissue, such as fibroblasts and neural cells, could also improve the regenerative capability of a tissue engineered construct in a wound (Christ *et al.*, 2015).

Tissue engineered skeletal muscle can be used for other purposes than replacement and repair of damaged muscle tissue. The result and process of constructing tissue engineered muscle could be used to increase understanding of the physiology and biochemistry of the tissue. A tissue engineered muscle could also be used as an alternative for screening and testing pharmacological agents, adding a beneficial step in treating muscle related diseases (Christ *et al.*, 2015).

There are two main cell types used in skeletal muscle tissue engineering; satellite cells and myoblasts. Satellite cells are obtained from native muscle tissue by either explant cultures or digestion isolations (Christ *et al.*, 2015). In adults, satellite cells only make up approximately 4% of the total muscle nuclei, therefore for tissue engineering needs, the satellite cells need to be isolated, but then require continuous stimulation to

remain undifferentiated while proliferating(Juhas, Ye and Bursac, 2015). C2C12s, are the immortalised murine cell line that are often used as a model for myogenic differentiation, however, human skeletal muscles cells (hSkMCs) are also used *in vitro*. Both types within a particular environment will differentiate at confluence unless maintained in a proliferative state. Once differentiated, myoblasts will become post-mitotic and no longer useful for proliferation or differentiation studies (S. Burattini, P. Ferri, M. Battistelli, R. Curci, F. Luchetti, 2004; Juhas, Ye and Bursac, 2015).

Scaffolds are designed to mimic the native tissue in order to achieve a cellular response that will lead to confluent proliferation and stimulate differentiation. Therefore, scaffolds tend to mimic the morphology of the ECM of the tissue, in stiffness, texture and biochemically. Sometimes the manipulation of a specific factor, such as topography, can trigger the desired cell response. Muscle cells are not only responsive to 3D scaffolds, but can adhere and differentiate on 2D constructs where the topography defines their functionality (Charest, Garcia and King, 2007; Gingras *et al.*, 2009; Wang, Yu and Tsai, 2010). Lam et al (2006) reported a healthy yield of myotubes cultured on micropatterned wavy silicone surfaces. Alignment and fusion of myoblasts were observed and it was specifically noted that alignment improved with increasing cell density when seeded (Lam *et al.*, 2006).

Electrospinning of polymer matrices shows promise in mimicking the ECM of skeletal muscle tissue. Choi et al (2008) investigated the use of electrospun poly(3-caprolactone) (PCL)/collagen based nanofibres of differing orientations to guide and enhance the cellular organisation of human skeletal muscle cells. They found that there were superior alignment and myotube formation on the unidirectional fibres compared to the randomly oriented fibres (Choi *et al.*, 2008). The importance of alignment was also reported by Aviss et al (2010), who used electrospun PLGA to produce aligned fibres, which were found to induce myoblast elongation and fusion (Aviss, Gough and Downes, 2010). Although electrospun polymer scaffolds are promising, there is a difference in the stiffness of the scaffolds to that of the native muscle tissue. Extensor digitorum longus muscles of mice have an elastic modulus of around 12 KPa whereas an example electrospun scaffold has an elastic modulus of approximately 100 MPa. It has been shown that muscle precursor cells have a superior

response in differentiation to scaffolds of a similar stiffness to native skeletal muscle (Christ *et al.*, 2015).

Some studies have found that combining micro and nano-scale topographies can show successful myogenic differentiation. Jun et al (2016) placed both aligned and random polylactic acid (PLLA) nano-scale electrospun fibres on micro-scale patterned PLLA platforms and showed increased cell adhesion and differentiation to aligned myotubes (Jun *et al.*, 2016). Similarly, Yeo et al (2019) applied the same concept with electrospun alginate nanofibres and a 3D printed patterned PCL platform. Again, greater differentiation was shown on the oriented fibres with an increase in myotube formation (Yeo and Kim, 2019).

The application of ECM components to engineer skeletal muscle is also showing signs of developing myogenic differentiation. Chae et al (2019) used fibrillated collagen-coated PCL surfaces to increase the myogenic differentiation of C2C12s. The collagen nanofibres were randomly distributed however greater myotube formation was reported on the fibrillated collagen layer compared to the control (Chae, Lee and Kim, 2019). Other studies have reported using a combination of topography and ECM components to encourage myogenic differentiation of myoblasts. Cronin et al (2004) and Riboldi et al (2005) both showed an increase in myotube alignment and formation on ECM/Matrigel coated oriented polymer fibres whereas, Lee et al (2014) showed that immobilisation of fibronectin and laminin on poly(urethane acrylate) (PUA) grooved substrates also supported the differentiation of C2C12s (Cronin *et al.*, 2004; Riboldi *et al.*, 2005; Lee *et al.*, 2015).

Many directions are being explored in the tissue engineering of skeletal muscle. It appears that the combination of an oriented topography to guide myotube alignment and some biochemical cues such as ECM proteins to promote differentiation is a promising field of investigation. Some physicochemical properties can show to have a larger effect on cell response than others however it is the combination of surface charge, wettability and topography that interrelate to influence cell-material interactions. This is further explored in Section 2.4.

2.2.6 Application of MSCs

Mesenchymal stem cells (MSCs) have the potential to differentiate into a variety of cells due to their multipotent nature as shown in Figure 2-4 (Caplan, 1991). However, the pathway to a specific tissue type has to be clearly defined, requiring a combination of fundamental factors to control the expression of a specific functionalised cell lineage. One further advantage of the application of MSCs is that a patient requiring a certain tissue type could have a tissue engineered alternative constructed using their own MSCs. Stem cells harvested from the patient could be cultured on a specifically constructed scaffold for a specific tissue type and have it implanted into the damaged area. This process would not be limited by immune rejection. However, to get to this point, scaffolds need to be designed to promote the specific factors required to take MSCs to the cell phenotype (Caplan, 1991). There are different types of stem cell that are extracted from a variety of sources.

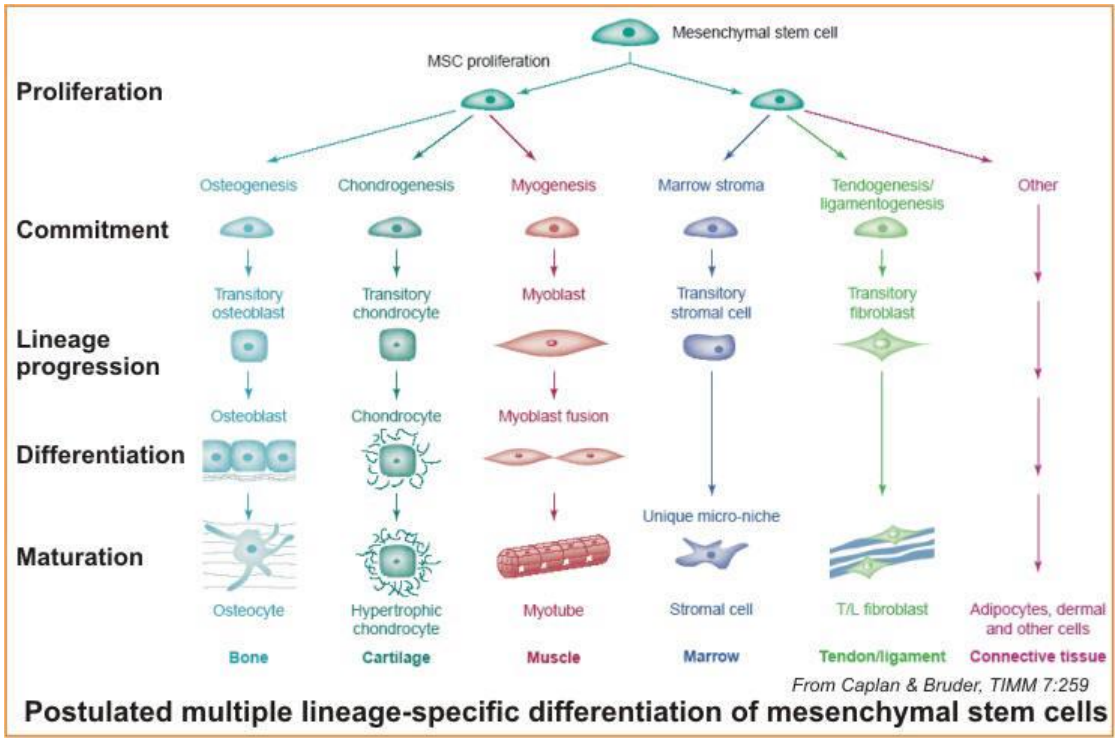

Figure 2-4: Simplified diagram of the possible different lineage-specific differentiation of MSCs (Caplan and Bruder, 2001). The myogenic lineage is shown in red, from the proliferation of the MSCs to through the commitment to the myogenic lineage and formation of a myotube.

Numerous studies have been carried out that have proven the concept that integral properties of a synthetically constructed scaffold can influence and induce differentiation of lineage-specific stem cells. Inherent properties of such scaffolds

include stiffness, nanotopography, chemical functionality and degradability (Murphy, McDevitt and Engler, 2014). A number of different methods have been published documenting the controlled myogenic differentiation of stem cells. These include the artificial up-regulation of muscle specific genes, the application of pharmacological agents and biological cues, the conditioning of media and specifically designed topography ((Constantinides, Jones and Gevers, 1977; Wakitani, Saito and Caplan, 1995; Zuk *et al.*, 2001; Santa Maria, Rojas and Minguell, 2004; Engler *et al.*, 2006; Gang *et al.*, 2008).

Gang et al (2008) reported the up regulation of the Pax3 gene promoted myogenic differentiation over other mesenchymal lineages (bone, fat or cartilage). Pax3 is required to ensure tissue specific differentiation and was reported to contribute to the early development of striated muscle (Gang *et al.*, 2008). Azacytidine, initially synthesised as a potential chemotherapeutic agents for cancer, however, has since been found to non-specifically induce activation of silenced genes by inhibiting DNA methylation. Constantinides et al. (1977) observed that azacytidine treated embryonic mouse MSCs formed striated myotubes (Constantinides, Jones and Gevers, 1977). This was built on by Wakitani et al (1995) who reported myogenic phenotypes differentiated from azacytidine treated rat bone marrow MSCs (Wakitani, Saito and Caplan, 1995). Azacytidine has also been reported to promote cardiomyocyte phenotypes in human umbilical cord-derived MSCs (Qian *et al.*, 2012). Other pharmaceutical agents used include a mixture of dexamethasone and high-dose hydrocortisone which Zuk et al (2001) showed to promote myogenic differentiation of human adipose derived MSCs (Zuk *et al.*, 2001).

A number of studies have attempted to use cells already expressing myogenic phenotypes to induce myogenic differentiation in MSCs. Shi et al (2004) found that human bone marrow derived MSCs fused with C2C12 myotubes but haematopoietic stem cells did not (Shi *et al.*, 2004). Fusion of bone marrow derived MSCs and myotubes was also reported by Gentile et al (2011) who observed that epicardial derived stem cells had a higher predisposition for fusion with myotubes. The addition of exogenous cytokines interleukin-4 or interleukin-13 was shown to increase fusion to myotubes for both cell types (Gentile *et al.*, 2011). Choi et al (2016) evidenced the potential of exosomes released from skeletal muscle cells in inducing human adipose-

derived stem cells (HASCs) to express myogenic phenotypes. Exosomes transfer specific signalling molecules for myogenesis. Exosome-treated HASCs exhibited early fusion and expression of myogenic protein *in vitro*. This type of treatment showed promise in *in vivo* studies as there was notable improved regeneration of myofibres in a muscle laceration mouse model (Choi *et al.*, 2016).

Santa Maria et al (2004) reported that medium conditioned against damaged skeletal muscle tissue from rats could induce myogenesis and cell fusion in bone marrow derived MSCs. This is possibly due to the presence of a signalling molecule or factor that is only activated in response to cell damage as media conditioned against healthy rat muscle tissue did not induce myogenesis (Santa Maria, Rojas and Minguell, 2004). This was supported by a study by Nunes et al (2007) who concluded that the conditioned media from healthy muscle did not induce myogenic differentiation, this time in stem cells derived from umbilical cord blood (Nunes *et al.*, 2007). Media conditioned with the myogenic regulatory factor MyoD has also been shown to induce efficient myogenesis in induced pluripotent stem cells (Abujarour *et al.*, 2014).

Topographical cues and mechanical properties of materials have been used in an attempt to promote myogenesis of stem cells. Engler et al (2006) investigated the effect of stiffness on MSC type expression. Using a biocompatible gel with a range of stiffness determined by the degree of crosslinking, they reported that MSCs seeded on the medium stiffness (roughly 8-17 kPa) showed potential myogenic differentiation. However, terminal myogenic differentiation was not observed. The stiffer gels (25-40 kPa) showed osteogenic differentiation and the softer gels (0.1-1 kPa) exhibited neurogenic potential (Engler *et al.*, 2006). The mechanical properties and morphology of electrospun nanofibres have shown potential for MSC differentiation into myogenic cell lineages by Dang et al (2007) who concluded that the scaffold was responsible for inducing the cells (Dang and Leong, 2007).

As described there have been a number of different approaches to inducing myogenic differentiation in adult stem cells. Most studies focus on a specific characteristic and no single characteristic has been proven to be superior at influencing a myogenic cell response from stem cells. It may be the case that there is an optimum combination of factors that would prove to be more successful.

2.3 Natural Polymers in Tissue Engineering

2.3.1 Cellulose

Research into cellulose has continuously grown since its discovery by French scientist Anselme Payen in 1838. Cellulose is mostly known as a structural component in plant cell walls and is the most abundant biopolymer in the world. It can also be found in a wide variety of living sources such as algae, bacteria and some marine animals (Eichhorn, 2011). Its properties have made it useful for a broad range of applications. Cellulose is a fibrous material and is mainly sourced from wood pulp to make cardboard and paper. As an organic polymer, it is biodegradable, biocompatible and environmentally friendly due to its renewability. It is also chemically adaptable resulting in the use of chemically modified cellulose in applications such as cellulose esters in coatings and laminates or cellulose nitrate, which is used in explosives (Klemm *et al.*, 2005; George and Sabapathi, 2015).

Structure

Cellulose is an organic polymer composed of a repeating dimer called cellobiose. Each repeating monomer is a disaccharide of two D-glucose units held together by a β(1-4) glycosidic bond. There are six carbon atoms with C6 attached to a hydroxyl group. The chain is formed by condensation resulting in each repeating unit being joined together by glycosidic oxygen bridges (Figure 2-5). In each glucose unit there are three hydroxyl groups, which are responsible for some of the characteristics of the polymer such as its hydrophilic nature and nucleophilic reactivity that allows derivatives of cellulose to form. Although hydrophilic, cellulose is insoluble in water and a very stable polymer due to the strong hydrogen bonds it can form between C2 and C6. This is also responsible for its crystalline and amorphous organisation (Habibi, Lucia and Rojas, 2010; Dugan, Gough and Eichhorn, 2013; George and Sabapathi, 2015).

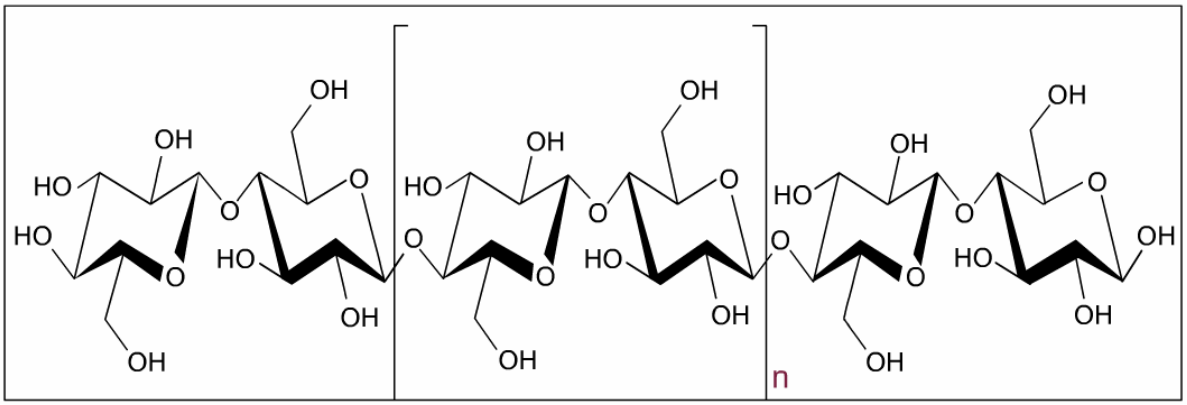

Figure 2-5: Molecular structure of cellulose (George and Sabapathi, 2015)

Sources and Crystallinity

Cellulose can be obtained from a number of sources. Plants are the main source of cellulose as they are inexpensive and abundant. Cellulose can be harvested and extracted from wood pulp and cotton on a large scale due to the industrial infrastructure available and commercial value. However, cellulose from this source requires an extensive purification process. Pure cellulose can be produced naturally by some species of bacteria. The bacterium produces microfibrils of almost pure cellulose and water, which can be hydrolysed in a dilute alkaline solution to remove impurities leaving pure cellulose pellicles, which can be processed (Klemm *et al.*, 2005; George and Sabapathi, 2015). Bacterial cellulose exhibits superior qualities than those of plant cellulose, including; a higher mechanical strength, increased capacity to hold water, a higher stability and a higher purity. This is due to the difference in arrangement of the glycosyl units within each crystallite, which gives bacterial cellulose a higher crystallinity than that of plant cellulose. Bacterial cellulose is used as a biomaterial in many applications including wound healing, nerve surgery and coatings of arterial stents (George and Sabapathi, 2015; Ul-Islam *et al.*, 2015).

Tunicates are the only animal source of cellulose. They are a marine filter feeder found attached to rocks or other coastal features or floating freely depending on their species of which there are about 300. They feed and respire by drawing in and expelling water in a one-way current system through its body, filtering out plankton. Tunicin cellulose is found in the tunic of the tunicate (Figure 2-6) and acts as a skeletal structure covering the entire epidermis of the animal. The cellulose is composed of

almost pure cellulose I crystals that are formed as microfibrils that built in multiple layers in a bundle organisation parallel to the epidermis. The cellulose microfibrils are wide and highly crystalline (Kimura and Itoh, 2007; George and Sabapathi, 2015).

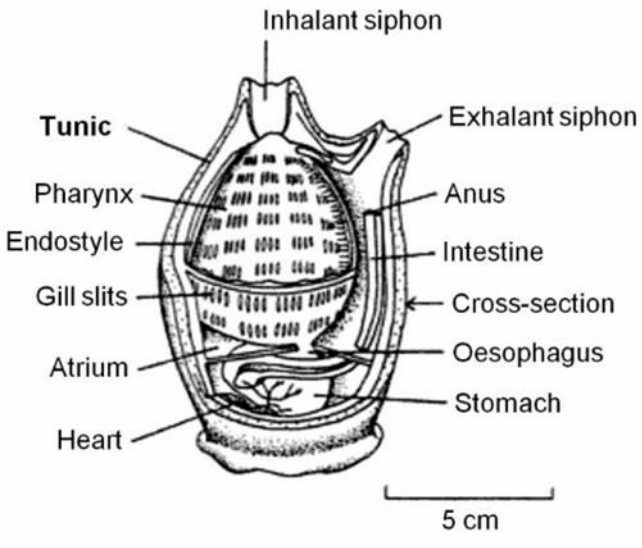

Figure 2-6: Anatomy of the tunicate such as *Ascidiella sp.,* the species used in this project (Benton, 2004)

The crystallinity of cellulose is due to the degree of polymerisation of the chains as this determines the crystalline and amorphous regions (George and Sabapathi, 2015).There are two types of cellulose I crystals; Iα and Iβ, both are found together, however, the ratio is dependent on the source. The difference between the two types is due to the types of chain and how they stack. Cellulose Iα has a triclinic one-chain unit cell where parallel cellulose chains are stacked with a parallel shear to the chain axis. Cellulose Iβ has a monoclinic two-chain unit cell where parallel chains are stacked with an alternating shear. The difference in shear is due to van der Waals interactions caused by the different structures in the unit cells. There are other polymorphs of cellulose (II, II, IV) with different crystalline structures and are formed from different chemical treatments (Nishiyama *et al.*, 2003; Wada, Heux and Sugiyama, 2004; Klemm *et al.*, 2005). The crystallinity of cellulose is determined during its biosynthesis. Individual cellulose chain-forming molecules are spun in a hierarchical order, initially assembling protofibrils, which bundle together to form microfibrils, andfurther bundle together to form cellulose fibres. The difference found in cellulose of different sources is due to

the conditions in which the biosynthesis occurs. The spinning and hierarchical bundling of the cellulose is driven by van der Waals forces and intra and intermolecular hydrogen bonds. Amorphous regions found in the crystallinity are defects linked the conditions of the biosynthesis (Saxena and Brown, 2005; Habibi, Lucia and Rojas, 2010).

Due to the structure of cellulose, the crystalline regions can be easily extracted by hydrolysis of the glycosidic bond. Although there are a number of different methods of extracting cellulose crystals, acid hydrolysis can be easily controlled. Crystalline regions within cellulose are more resistant to hydrolysis than the amorphous regions, therefore by controlling time, acid concentration and temperature; pure crystalline cellulose can be extracted. By increasing any of these parameters above the optimised treatment, crystalline regions will become susceptible to cleaving (George and Sabapathi, 2015).

The application of cellulose is dependent on its source and processing methods as these are responsible for the structure and properties of the cellulose used. Its use as a biomaterial has grown from applications such as artificial kidney membranes and coatings for drugs (Miyamoto *et al.*, 1989) to its use as a potential biomaterial in regenerative medicine. In general, cellulose has shown to be biocompatible although it's difficult to compare the studies due to the different cells used, sources of cellulose and experimental methods carried out. A few studies have shown a moderate immune response *in vivo* however numerous studies *in vitro* have shown a positive response from cells to cellulose based materials (Miyamoto *et al.*, 1989; Hart *et al.*, 2002; Svensson *et al.*, 2005; Backdahl *et al.*, 2006; Yokota, Kitaoka and Wariishi, 2008).

Applications of Cellulose in Tissue Engineering

Interest in cellulose as a biomaterial for tissue engineering has increased as the field of tissue engineering has grown and researchers look to promising new applications of materials. Due to its characteristics, specifically its biocompatibility and fibrous nature, cellulose shows a lot of potential as a biomaterial for tissue scaffolds. Its ability to be

compliant to chemical and physical modifications means that its use in tissue engineering is adaptable for many potential uses.

The use of cellulose and its derivatives have been used in a variety of different applications including as a 3D scaffold, tested *in vivo* and specifically developed for its material properties. Yang et al (2011) developed 3D nanostructured macroporous bacterial cellulose scaffolds and composite macroporous bacterial cellulose/agarose scaffolds on to which they seeded adult human bone marrow derived stromal cells. The scaffolds showed potential as a biomimetic scaffold for differentiation of the cells in to a variety of different cell types including chondrocytes for use in cartilage tissue engineering (Yang *et al.*, 2011). Zhang et al (2015) has also investigated the use of cellulose derivative based scaffold with MSCs for biological applications, specifically cellulose sulphate in both research and clinical trials (Zhang, Lin and Yao, 2015). *In vivo* studies using cellulose based vascular grafts have been carried out in pigs by Wippermann et al (2009). The scaffolds were found to be stable and able to promote rapid re-cellularisation in the pigs' arteries after 3 months (Wippermann *et al.*, 2009). Due to the potential degradation properties that bacterial cellulose can offer, it has been used in the application of wound healing as a bio-absorbable scaffold. Cellulase enzymes were incorporated into the scaffold, which was placed in a simulated wound environment. The mechanical properties were observed and showed that the scaffold exhibited similar tensile strength and extensibility to that of human skin. The degradation of the substrate was also measured and then modified in relation to the changes of the wound environment such as temperature and pH (Hu and Catchmark, 2011).

Backdahl et al (2006) proposed that bacterial cellulose had the potential for use as a material in blood vessel scaffolds as the stress-strain relationship of bacterial cellulose was similar to that of the carotid artery. The pellicles of bacterial cellulose were also shown to support smooth muscle cell adhesion and proliferation (Backdahl *et al.*, 2006). Another cellulose derived scaffold in the tissue engineering of blood vessels has been developed by Pooyan et al (2012) who were investigating the use of a cellulose acetate matrix embedded with CNWs as a possible biomaterial (Pooyan, Tannenbaum and Garmestani, 2012). Cellulose acetate and regenerated cellulose scaffolds were investigated for use in tissue engineered functional cardiac cell constructs by Svensson

et al (2005). The use of the cellulose in the scaffold showed advantageous shape conforming properties, which enabled bridging of gap junctions, as well as, supporting a perfusion structure promoting the proliferation of cardiac cells (Entcheva *et al.*, 2004). Bacterial cellulose has also been shown as a possible material for the tissue engineering of cartilage. Svensson et al showed bacterial cellulose was superior over collagen type II substrates at supporting chondrocyte proliferation and improved mechanical properties (Svensson *et al.*, 2005).

2.3.2 Cellulose to Cellulose Nanowhiskers

The discovery of cellulose nanowhiskers (CNWs) is attributed to Ranby (1949) although a number of groups were investigating the hydrolysis of cellulose between the 1940s and 1950s. Ranby (1949) initially reported the suspension of micelles of cellulose hydrolysed using sulphuric acid. CNWs of 6 nm x 60 nm were produced from wood and cotton cellulose (Ranby, 1949). Other research carried out at the time includes that done by Nickerson and Habrle (1947) who reported the hydrolysis of cellulose was limited due to the possibility that some crystalline regions of cellulose were resistant to hydrolysis. They also reported that hydrochloric acid was more effective at hydrolysing the cellulose than sulphuric acid (Nickerson and Habrle, 1947). Battista (1950) took this work further by using hydrochloric acid hydrolysis to produce microcrystalline cellulose. These crystalline particles of cellulose are used as a particulate additive in many applications, including food and pharmaceuticals (Battista, 1950). CNWs have been a useful material in tissue engineering scaffolds (Domingues, Gomes and Reis, 2014) and as a particulate supplement to nano-composites (Arjmandi *et al.*, 2016).

Methods of Extraction

There have been several methods reported for the extraction of CNWs with the majority of them using a form of partial acid hydrolysis. This is where a strong acid is used to break down cellulose through the cleaving of the glycosidic bond, destroying

the amorphous region and cutting up the crystalline region (Wertz and Bédué O, 2010). The basic mechanism of the acid hydrolysis is shown in Figure 2-7. This method results in the production of high aspect ratio nanoparticles. The rod-like nanoparticles are defined as having a high aspect ratio due to the high ratio between the diameter and the rod length. CNWs have diameters nanometres thick; however, the length of the nano-crystals can range from nanometres to micrometres. After being treated with acid the CNW solution is diluted with water and undergoes successive centrifugation before being dialysed. Further treatments include filtration and sonification. The hypothesis is that the amorphous regions have a reduced steric hindrance and due to kinetic factors are more susceptible to cleavage by acid than the crystalline regions. However, the crystalline region is not completely impervious to attack, hence, the various lengths of nanofibre produced. Amorphous regions are defects in the crystalline structure caused by mechanical deformation during or immediately following biosynthesis (Elazzouzi-Hafraoui *et al.*, 2008; Habibi, Lucia and Rojas, 2010). Due to the many variables in this method, different studies have shown value in modifying the parameters to achieve an optimum yield. These variables include the acid-to-cellulose ratio, the acid used, the time and temperature of hydrolysis and the source of the cellulose. Strict control of these parameters is required to produce uniform CNWs each time.

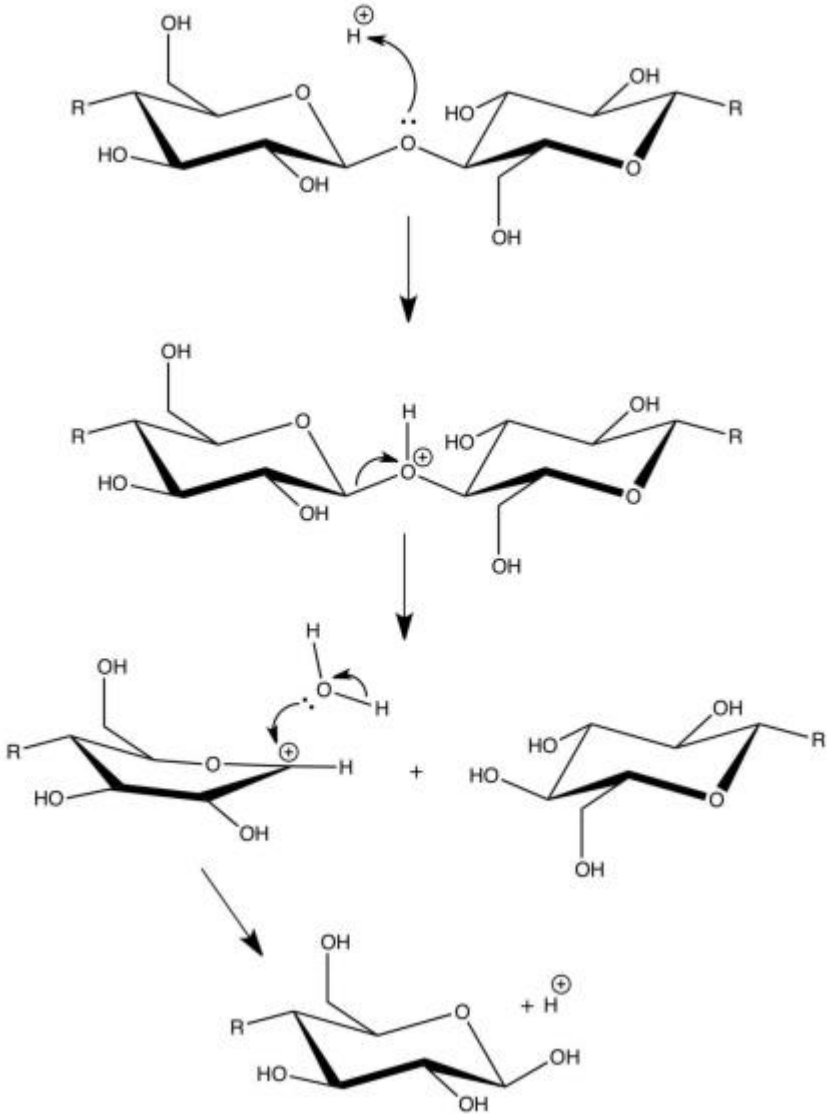

Figure 2-7: Schematic representation of the hydrolysis of cellulose. The H^+ ion protonates the bridging oxygen leaving the whole molecule susceptible to nucleophilic attack from a water molecule causing the chain to break. Diagram taken from Dugan's thesis (2011), reproduced and modified from Wertz et al (2010). (Dugan, Gough and Eichhorn, 2010; Wertz and Bédué O, 2010)

Many of the papers using partial acid hydrolysis to produce CNWs differ in the alternations applied to the method. Sulphuric and hydrochloric acid are the main acids used however the use of phosphoric and hydrobromic acids have also been reported. There is also a difference in the CNWs produced by sulphuric and hydrochloric acids. CNWs prepared with sulphuric acid gain net negative charge due to a side reaction resulting in sulphur ester groups attaching to the nanowhiskers. The use of hydrochloric acid results in unstable colloidal suspensions, which are limited in their dispersibility. Due to the surface charge of sulphuric acid CNWs, they are

electrostatically stable (Habibi, Lucia and Rojas, 2010). Temperature, time and agitation of the cellulose in acid have been shown to affect the size of the nanowhiskers. Dong et al (1998) reported that a longer hydrolysis time produced CNWs with a decreased length and higher surface charge (Dong, 1998). This was supported by the work of Beck-Candanedo et al (2005) who also stated that the CNWs were shorter and less polydispersed with increased time. Increase in acid-to-cellulose ratio during hydrolysis also reported shorter nanowhiskers (Beck-Candanedo, Roman and Gray, 2005). Shorter CNWs were also produced by increasing the temperature (Habibi, Lucia and Rojas, 2010). The source of the cellulose has an effect on the quality of the nanowhiskers produced as different sources have different ratios of crystallinity (Elazzouzi-Hafraoui *et al.*, 2008). CNWs with a higher aspect ratio were found to be produced from native cellulose with a higher crystallinity, such as tunicin. Tunicin CNWs reported by Anglès et al (2000) have diameters of 10-20 nm and can reach 1 µm in length (Anglès and Dufresne, 2000). CNWs prepared from wood, which has a lower crystallinity, produces nanowhiskers with a lower aspect ratio. Reported dimensions are around 5 nm by 150 nm (Beck-Candanedo, Roman and Gray, 2005). The CNWs used in this work are of the same origin and protocol of those used in studies by Dugan et al (2001, 2013) where the whiskers were reported to have diameter of approximately 6 nm and lengths ranging from 100s of nanometres to microns (Dugan, Gough and Eichhorn, 2010; Dugan *et al.*, 2013).

The term nanowhisker refers to nano-crystalline cellulose that has a high aspect ratio (>1:100) within the nanoscale range due to the high degree of crystallinity dependent on the source. Other terms, such as nanocrystals or nanofibrillar refer to nano-crystalline cellulose of a lower aspect ratio and to disaggregated fibres respectively (Eichhorn, 2011). The CNWs used in this work are termed nanowhisker due to the high crystallinity of the tunicin cellulose.

2.3.3 Application of CNWs in Tissue Engineering

Compared to cellulose itself, the application of specifically defined cellulose nanowhiskers is little studied. However, its potential for chemical modification and high abundance makes it a promising material for tissue engineering. Cellulose is

known to be biocompatible and bioinert as it is used as a filter in haemodialysis and micro-cellulose is used as a pill binder in the pharmaceutical industry (Clark *et al.*, 1991; Habibi, Lucia and Rojas, 2010). On the other hand, tissue engineering utilising nano-cellulose in the form of nanocrystals or nanofibres is growing.

Clift et al (2011) investigated the potential biological detrimental effects of nanofibres using a 3D *in vitro* triple cell co-culture model of the human epithelial airway barrier. CNWs derived from cotton were found to trigger a lower cytotoxicity and inflammatory response when compared with multiwalled carbon nanotubes and asbestos fibres (Clift *et al.*, 2011). Jia et al (2013) reported an increase in cell viability of vascular smooth muscle cells with increasing concentrations of cellulose content. The composite of microcrystal cellulose and CNW could mimic the native ECM and increase proliferation and adhesion (Jia *et al.*, 2013). The key factor in the biological response to CNWs appears to be the surface charge of the nanowhiskers although the size may have an effect. The surface charge determines the acceptability of CNWs to cells in their initial response and then adhesion to the nanowhiskers. Mahmoud et al (2010) investigated the surface charge of CNWs in relation to toxicity and found that they showed not cytotoxic effect (Mahmoud *et al.*, 2010).

Nanocellulose based scaffolds have been applied to the engineering of a range of different tissue types including skin, vascular, neural and cardiac (Luo *et al.*, 2019). Its application in skeletal muscle tissue engineering has been through the development of nanocrystals in electrospun fibres or hydrogels. He et al (2014) has combined aligned electrospun cellulose fibres and oriented cellulose nanocrystals to promote the formation of aligned myotubes whereas Barua et al (2015) has developed a CuO-nanofibrillated cellulose/glycerol based hyperbranched epoxy nanocomposite with a high tensile strength and anti-bacterial properties that was shown to be biocompatible both *in vitro* and *in vivo* (He *et al.*, 2014; Barua *et al.*, 2015). Different hydrogels have also shown skeletal muscle engineering potential such as cellulose nanofibril reinforcing thermo sensitive hydrogels developed by Liu et al (2016) and injectable hydrogels with tunable mechanical properties by De France et al (2017) (Liu *et al.*, 2016; De France *et al.*, 2017).

Overall the application of all forms cellulose nanocrystals is still growing in the field of tissue engineering. Despite possible reservations of their nanoscale size, they appear to have a minimal cytotoxic effect on cells when compared to similar sized nanoparticles (Clift *et al.*, 2011). When in combination with other materials, they can influence the orientation of cells and modulate cell adhesion.

2.4 Cell and Material Interactions

2.4.1 Orientation of CNWs

A biomaterial's topography can be used to control cell behaviour. The first observation of this was by Weiss (1934) who began developing the concept of contact guidance after observing the alignment of neurites extending from neurons along an oriented fibrin clot. He theorised that contact with an oriented biomolecule will cause the cells to align parallel to it (Weiss, 1934). This concept was further developed by Curtis and Varde (1964) who built upon Weiss' findings by suggesting that it is the topography that can induce cell alignment without the need for oriented biomolecules (Clark *et al.*, 1991; Curtis and Wilkinson, 1997). Many papers have been published in support of this principle also identifying other factors which contribute to a cell's response to topography, including cell type, cell origin and surface chemistry (den Braber *et al.*, 1998; Loesberg *et al.*, 2007; Anselme and Bigerelle, 2011).

With advances in manufacturing technologies, the ability to design and produce biomaterials with surfaces that are more complex and with smaller scale features has led to an increase in research directed at finding the smallest topological feature that has an effect on cell behaviour. Loesberg et al (2007) explored fibroblast response on a range of nanogrooved substrates (groove depth: 5-350 nm, width: 20-1000 nm) and found 35 nm to be the smallest feature to affect morphological behaviour of the cells. Contact guidance on features below this value was not seen, and the cells spread out in a random fashion, much like the behaviour seen on the smooth substrates (Loesberg *et al.*, 2007). Although narrower and deeper grooves were found to increase cell orientation (Biela *et al.*, 2009) it was suggested by Crouch et al (2009) that a groove aspect ratio (the ratio of width/depth) could be used as a parameter to define grooves and ridges in topographical studies (Crouch *et al.*, 2009). Crouch et al (2009) found that fibroblasts showed increased cell alignment and elongation at an aspect ratio of around 0.05. The model was applied to other published data and although there were differences in cell type and material, a similar relationship between groove width and depth was shown however the topographies were of a lateral dimension and on a microscale (Crouch *et al.*, 2009).

Focal adhesions are the mechanism by which contact guidance occurs by cells in response to an orientated topography. Focal adhesions consist of transmembrane integrin receptors, which are linked to the cytoskeleton by their associated intracellular proteins. During formation, these receptors sense and orient themselves in response to the surface therefore aligning the focal adhesions, and subsequently the cells, to the topography (Ohara and Buck, 1979; den Braber *et al.*, 1998). The influence of topography is dependent on how the integrin receptors cluster around a topographical feature. As cells adhere to a substrate, the critical dimensions at which nanotopography influences the cell morphology is dependent on the limit of size the focal adhesions can adhere to (Biggs, Richards and Dalby, 2010).

Cell response to topography is also dependent on the cell type in question. Different cell types sense the topography of a substrate through different mechanisms and therefore, will be more sensitive to different topographies than others. Topographical cues in a substrate can be physical and chemical, as some cell types are sensitive to feature size either in micro or nanometres and others may be more sensitive to the specific material of the substrate, be ECM based, organic or synthetic. If a cell shape is composed of a number of protrusions and filopodia, it might be more sensitive to the topographical cues as the cell could form strong focal adhesions in response. Cell response can also be linked to the purpose of the cell. Cells which function in alignment could potentially be more inclined to align to a patterned topography. Although studies have been carried out to investigate the different cell types and their responses to topographical cues it is difficult to form comparisons due to the range of variables in each experiment. Cell types which permanently adhere, such as fibroblasts and osteoblasts, are more sensitive to surface topography than cells which are not, such as macrophages and other blood derived cells. Due to the range of studies into cell type and topography it is hard to specifically characterise which cell type will consistently perform on a given topography as the influence of the material and size of the features are too broad. It is considered by some that nanoscale features can have more of an effect on cell response than micro scale (Huang *et al.*, 2006; Biela *et al.*, 2009; Anselme and Bigerelle, 2011). Features defined as nanoscale have or comprise of dimensions within the range of 1-100 nm (Hornyak, 2008).

Spin coating is a technique often used to deposit a thin film of a material on a surface. It is one of the techniques used in the production of layer-by-layer (LbL) films where solutions or suspensions of polyelectrolytes are built on top of each other in alternating charges. Other techniques include spray coating, dewetting and dip coating, the latter is discussed more in Section 3.4.2.

The deposition of CNWs or similar cellulose derivatives through spin coating has been explored by a number of studies. Kontturi et al (2007) investigated the spread of spin coated CNWs on surfaces of different chemical compositions and Winter et al (2010) spin coated bacterial cellulose nanocrystals to form a uniform topography (Kontturi *et al.*, 2007; Winter *et al.*, 2010).The spin coating method used in this work was adapted by Dugan et al (2010) from the work carried out by Cranston and Gray (2006, 2008) and further optimised by Nikoi (Nikoi, 2016). The CNWs were spin coated on top of cationic polyelectrolytes in both Dugan's and Cranston and Gray's work (polyallylamine hydrochloride (PAHCl) and poly(allylamine hydrochloride) (PAH) respectively) to oppose the slight negative charge of the CNWs, therefore, making the CNWs the anionic polyelectrolyte. Both reported the formation of uniform oriented CNWs in a radial pattern from the centre due to the spinning set up. The degree of alignment of CNWs to each other and the density were determined through the spinning speed and concentration of the CNW solution. Dugan et al went on to show that the topography of the CNWs can be used to direct cell alignment and encourage myogenic differentiation of aligned myotubes. The diameters of the CNWs were approximately 6 nm with lengths ranging from nanometres to microns and could be considered some of the smallest topographies to influence cell response (Cranston and Gray, 2006, 2008; Dugan, Gough and Eichhorn, 2010; Dugan *et al.*, 2013).

2.4.2 Polyelectrolyte Layers

Tissues are composed of cells and ECM and are viscoelastic meaning they exhibit both elastic and viscose properties. Adherent cells in the tissue matrix attach to other cells and the surrounding ECM through focal adhesions. A force occurs between the transmembrane integrin receptors and the cell's cytoskeleton; the strength of the force depends on the resistance sensed from the surface and is relayed through the

cytoskeleton to the cell. The same mechanism occurs when cells come into contact with a biomaterial. A stiffer substrate will give more resistance than a soft matrix resulting in a more organized cytoskeleton and more stable focal adhesions. Therefore the stiffness can be a strongly influencing characteristic in the design and choosing of materials for a substrate (Wells, 2008).

The nature of the transmembrane adhesion receptor can influence a cell's preference for a particular stiffness (Yeung *et al.*, 2005). Different cell types require a smaller range of stiffness to proliferate and differentiate on however there are some cells which are more adaptable. Neutrophils can proliferate readily on both soft and stiff matrices and myoblasts have been recorded differentiating into myotubes on a range of substrate stiffnesses (Wells, 2008).

This push-pull relationship between the cell and what it's adhered to aids the building of the 3D structure of tissues. There is a notable difference in how cells phenotypically change as they become confluent in culture. This occurs as the cells sense the change in stiffness from the initial influence of the stiff substrate to the softer matrix formed by the increasing number and density of cells (Wells, 2008). As neutrophils appear indifferent to stiffness this change is not noticeable however in cultures of fibroblasts and endothelial cells it is. The influence of the stiff substrate decreases as the cell confluence increases. This suggests that in some cell types the influence of the cell to cell adhesion is stronger than that of the cell to substrate (Yeung *et al.*, 2005).

LbL polyelectrolyte films could change the stiffness enough to influence cell adhesion and differentiation. Decher et al (1992) introduced the concept of LbL films using dip coating to achieve a multilayer film of alternating slightly charged polymer layers. Polyelectrolytes are polymers with units that can be or are ionised and can be natural, such as proteins, or synthetic, such as polyethylenimine (PEI) (Decher, Hong and Schmitt, 1992; Jenkins *et al.*, 1996). LbL of polyelectrolyte films have been used with the intention of engineering skeletal muscle tissue. Both Aggarwal et al (2013) and Nikoi (2016) showed the potential of cellulose based dip coated polyelectrolyte films in culturing C2C12s. Aggarwal assembled composite films using layers of chitosan paired with either heparin or cellulose sulphate however Nikoi, using chitosan, CNWs and poly(4-styrenesulfonic acid) (PSS), went further and used spin coating to produce an

oriented CNW top layer. Nikoi reported high myotube alignment on polyelectrolyte films of 12 layers however found PSS became cytotoxic as the layers increased (Aggarwal *et al.*, 2013; Nikoi, 2016).

Chitin is the second most abundant polymer in the world after cellulose and is the main structural component in the shells of crustaceans and insects. It consists of β-(1-4)-linked D-acetylglucosamine units and becomes chitosan deacetylated forming a polysaccharide of β-(1-4)-linked D-glucosamine units (Figure 2-8). Chitosan is used for many biomedical applications due to its anti-bacterial properties and low cytotoxicity and is often used in tissue engineering to promote cell adhesion. It is also its cationic property that makes it highly suitable for LbL assembly (Bumgardner *et al.*, 2012; Aggarwal *et al.*, 2013; Jangid, Hada and Rathore, 2019).

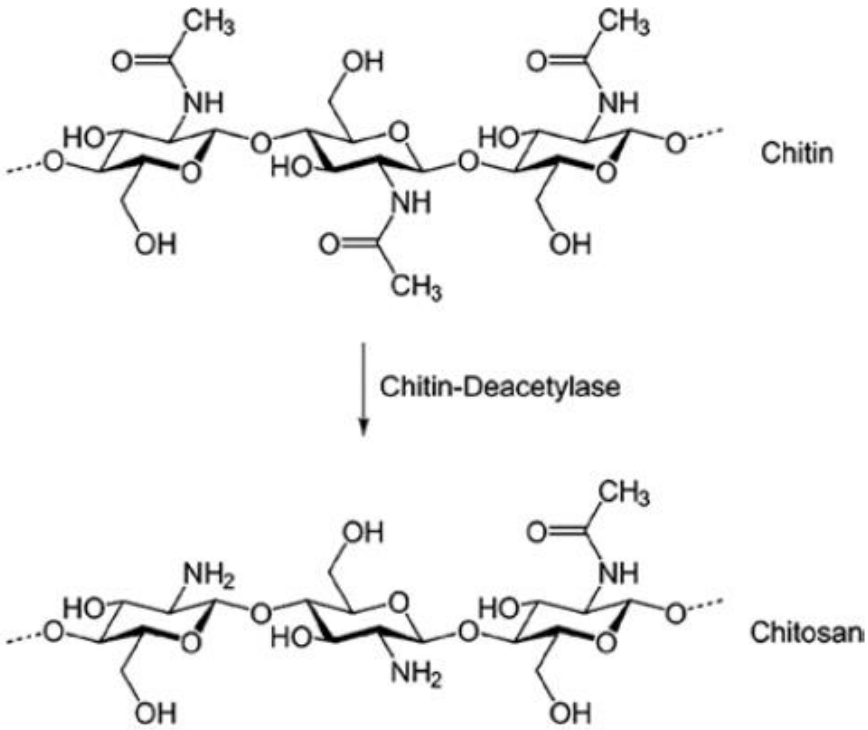

Figure 2-8: Chemical structure of chitin and chitosan. Chitosan is the de-acetylated derivative of chitin. (Jangid, Hada and Rathore, 2019)

This work builds on the concepts optimised by Dugan and Nikoi to produce CNW and chitosan multilayers to promote myoblast proliferation and differentiation.

2.4.3 Protein and Cell Interactions

The native ECM of a tissue, its composition and structure, is in the simplest terms, the environment the cells build so that the tissue can fulfil its function. It is of no surprise then that the incorporation of ECM components in tissue engineering scaffolds is a widely used technique to encourage cell adhesion and differentiation.

ECM proteins, such as collagen, fibronectin and laminin guide cell behaviour through chemical and physical mechanisms. The chemical structure and folding of proteins determine the integrins that mediate cell-ECM adhesion and communication. These integrins bind to specific motifs presented on cells. It is theorised that different cell types have different affinities for integrin binding sites and therefore some cells will strongly adhere to certain materials and others will not. Fibronectin can promote cell adhesion due to the presence of the RGD (Arg-Gly-Asp) motif, which needs to be 'visible' to the cells. When biological solutions, such as blood or serum in media, come in to contact with a material the proteins spontaneously adsorb on to the surface. This spontaneous adsorption is caused by van der Waals forces and the weak intermolecular forces caused by random polarisation multipoles in molecules. Other factors can affect initial protein adsorption such as surface charge, wettability and roughness. Ideal protein adsorption should be flexible to allow the cells to interact and recognise binding sites, however, not too strong as to deform the protein structure. Extremely hydrophobic surfaces lead to rigid adsorption of denatured proteins which no longer present recognisable binding sites. On the other hand, extreme hydrophilic surfaces can lead to saturation of the surface and again, denaturing of the protein. Nanoroughness is considered to be, theoretically, a desirable quality of a material, to better resemble the nano-architecture of the native ECM as ECM proteins will adsorb in the correct conformation to present binding sites. The validity of this concept is still in discussion. Other physical mechanisms can influence cell behaviour such as the elasticity of ECM protein. In tissue types were the ECM plays a crucial structural and mechanical role, such as ligament or tendon, the mechanical properties of the ECM protein can have an effect on the cell response (Guilak *et al.*, 2009; Hynes, 2009; Bacakova *et al.*, 2011; Trappmann *et al.*, 2012) .

Fibronectin and laminin are key ECM proteins found in the basement membrane of skeletal muscle tissue. Neither proteins are specific to skeletal muscle however, both play vital roles in the cell adhesion and differentiation of myogenic cells. Fibronectin mediates cell adhesion and collective migration that can encourage cells to align to each other. Laminin, on the other hand, has more of the specific role in myogenic differentiation as it facilitates myoblast motility and promotes myoblast to myoblast adhesion crucial for cell fusion. Both have been used in combination with other myogenic stimuli with some success. Increases in myoblast adhesion and differentiation in response to fibronectin and laminin adsorption have been reported by Cronin et al (2004) and Lee et al (2014) (Cronin *et al.*, 2004; Riboldi *et al.*, 2005; Sengupta *et al.*, 2012; Lee *et al.*, 2015). The combination of key ECM proteins and the oriented CNW topography could potentially lead to an increase in myogenic differentiation and myotube formation.

2.5 Summary

Starting with the structure and function of skeletal muscle followed by the origin and potential biomaterial properties of the CNWs; this literature review should have given an informative and concise background of the components of this thesis. This includes an exploration of current approaches to tissue engineering and the different techniques applied to encourage a positive cell response. Concepts such as nanotopography, contact guidance and the influence of ECM proteins have been discussed. The understanding of all of these elements will support the work carried out in this thesis.

Chapter 3: Methods and Materials

3.1 Reagents

Gutted tunicates from *Ascideilla spp.* were obtained from Glycomar, Oban, Scotland in March 2012 by Dr. Allison Harvey on behalf of the Gough research group. Smaller batches were divided up and stored at -20 °C.

Sulphuric acid (H_2SO_4, >95%, 'Extra Pure', S/9160/PB17), acetic acid (CH_3COOH, glacial, 'Extra Pure', A/0360/PB17), 18mm x 18 mm coverslips (no.1 thickness, Menzel 'Best', MNJ-400-010X) and AFM specimen discs (12mm diameter stainless steel, AGF7001) were obtained from Fisher Scientific, Loughborough, UK.

hSkMCs (cryopreserved, C-12530), Skeletal Muscle Cell Growth Medium (C-23160), Skeletal Muscle Differentiation Medium (C-39366), Freezing Medium Cryo-SFM (C-29912) and Mesenchymal Stem Cell Growth Medium 2 (C-28009) were purchased from PromoCell, Heidelberg, Germany.

ProLong™ Diamond Antifade Mountant (P36965), UltraPure™ DNase/RNase-Free Distilled Water (10977035), Quant-iT™ PicoGreen™ dsDNA Assay Kit (P11496) and NanoOrange™ Protein Quantitation Kit (N6666) were all purchased from Invitrogen, Paisley, UK. Secondary antibodies Alexa Fluor™ 488 goat anti-rabbit (A31627), Alexa Fluor™ 568 goat anti-mouse (A11004) and Hoechst 33342 (62249)were purchased from Thermo Fisher.

Primary antibodies against myogenin (monoclonal rabbit anti-human, ab1835), α-sarcomeric actinin (monoclonal mouse anti-rabbit, ab9465) and Cytopainter ™ 647-conjugated phalloidin (ab176759) were all purchased from Abcam, Cambridge, UK. Tween-20 (663684B) was purchased from VWR, UK.

Hydrogen Peroxide (H 2 O 2 , 30%, Perdrogen™, 31642), sodium hydroxide (NaOH, pellets, reagent grade, S5881), sodium hypochlorite (NaClO, 4% active Cl, 23,930-5), dialysis tubing (27mm diameter, MWCO 12-14 kDa, D9527), Chitosan (Chi, medium molecular weight, M w ≈ 190 -310 kDa, 75-85% deacetylated, 448877) and Polyethyleneimine (PEI, branched, M w ≈ 25 kDa, 408727) were bought from Sigma-Aldrich, U.K.

Fetal bovine serum (FBS, heat-inactivated, sterile-filtered, non-USA origin, F9665), adult horse serum (HS, heat-inactivated, sterile filtered, H1138), antibiotic (AB, 10000 units penicillin, 10 mg streptomycin and 25 μg amphotericin per ml, A5955), low glucose Dulbecco's Modified Eagle's Medium (LG-DMEM, with L-glutamine and sodium pyruvate,), high glucose Dulbecco's Modified Eagle's Medium (HG-DMEM, with L-glutamine and without sodium pyruvate, D5796), Dulbecco's phosphate buffered saline without calcium and magnesium (PBS, sterile-filtered, D8537), trypsin/EDTA solution (0.05% trypsin, 0.02% EDTA in Hanks' balanced salt solution, 59417C), trypan blue solution (0.4%, sterile-filtered, T8154), resazurin sodium salt for the Alamar Blue cell viability test ('BioReagent', R7017), dimethyl sulfoxide (DMSO, ≥99.5% (GC), plant cell culture tested, D4540), Triton™ X-100 (for molecular biology, T8787), bovine serum albumin (BSA, ≥96%, 'BioReagent', A9418), cold water fish skin gelatin (2% in water, 'BioReagent', G1393), adult goat serum (GS, USA origin, sterile-filtered, G6767), Laminin from Engelbreth-Holm-Swarm murine sarcoma basement membrane (L2020), Fibronectin bovine plasma (F1141-1MG) and formalin solution (neutral buffered, 10%, HT501128) were all purchased from SigmaAldrich, U.K.

Minimum essential medium (MEM) non-essential amino acids (NEAA, 1140-035)was purchased from Gibco Life Technologies, UK, through ThermoFisher Scientific.

3.2 Production of CNWs and Layer-by-Layer Films

3.2.1 Cellulose Purification

Tunicates, *Ascidiella aspersa*, were received from GlycoMar, already gutted and stored frozen at -20^{o}C. When required for purification, the tunicates were defrosted and washed in running tap water. Care was taken to remove any sea debris, such as seaweed, shells and sand. Once washed, excess water was squeezed out and the tunicates were weighed.

Scissors were used to chop the tunicates into 1-2 cm pieces which were placed in a beaker of deionised water (300 ml per 50 g of tunicate) with a magnetic stirrer. A hotplate was used to heat the solution to 80^{o}C. To deproteinize the tunicates, sodium hydroxide pellets were slowly added to form a 5% w/v solution and the whole solution was left stirring overnight. After removal from heat, the solution was left to cool to room temperature before being rinsed in running tap water for at least 5 min followed by a few rinses with deionised water. If any debris could still be seen upon inspection of the tunicates, this deproteinization step was repeated.

The tunicates were bleached by suspending the material in deionised water (300 ml per 50 g of tunicate) and heated on a hotplate to 60^{o}C. 1 ml of sodium hypochlorite was added and the solution was left stirring for 5 h. Once cooled to room temperature, the material was washed with deionised water through a sieve. If the tunicate still looked too discoloured, the bleaching process was repeated.

The tunicate cellulose was squeezed of excess water and frozen at -80^{o}C overnight before undergoing freeze drying. Tunicin cellulose was left in the freeze dryer (Edwards Modulyo) until all liquid had been removed. The tunicate material is now termed cellulose and stored in centrifuge tubes in a desiccator until use.

3.2.2 CNW Extraction

Tunicin cellulose was used to produce cellulose nanowhiskers through partial acid hydrolysis. Partial acid hydrolysis works by breaking down the amorphous regions within the crystalline cellulose structure leaving behind rod shaped pieces of cellulose. The parameters to control achieve high aspect ratio CNWs were adapted from

Cranston and Gray by Dugan et al (Cranston and Gray, 2006; Dugan, Gough and Eichhorn, 2010). The key parameters are acid concentration and type, time and temperature.

Sulphuric acid (64% w/w) was prepared from concentrate (95%) and the density resulting solution adjusted to 1.542 g/ml at 20 °C using a specific gravity hydrometer (range 1.480 to 1.550 g/ml, VWR U.K., catalogue number 34627-479). A reaction vessel was suspended in a water bath set at 45^{o}C with 87.5 ml of 64% w/w sulphuric acid per 1 g of cellulose. A PTFE stirrer on a glass rod was mounted above the reaction vessel and set to stir at a slow rate. 1 g of grinded cellulose was added slowly to the reaction vessel and the whole set up was left for 30 min. Once complete, the solution was immediately neutralised by rapidly pouring the solution in to 9x volume ice cold deionised water. Dregs were washed out of the reaction vessel.

The diluted acid-CNW solution was centrifuged in 50 ml centrifuge tubes at 8000 rpm for 5 min and the most of supernatant removed leaving behind the CNWs in solution. Deionised water was then added and the solution centrifuged again to wash the CNWs. This was done 2-3 times and then collated into about 100 ml in total. The CNW dispersion was then poured into a number of pre-soaked dialysis tubing (cellulose, 27mm diameter, MWCO 12-14 kDa) to less than half full. These were then suspended in a large beaker of deionised water and left to stir for 7-10 d. The water was changed daily until the beaker water pH matched that of the dH_2O.

The CNW dispersion was removed from the dialysis tubing and sonicated. A (Model 250, Branson) sonicator was used with a flat tip for 10 min, amplitude 30% and maximum temperature was 40^{o}C. A droplet of the CNW dispersion from before sonicifcation and afterwards was observed under the microscope. Beforehand, whiskers could be seen in the CNW dispersion, this was not observed in the post-sonicated sample. The CNW solution was then stored in a Winchester bottle at 2-8^{o}C.

The concentration of CNW solution was determined as a weight percentage by measuring the difference in water weight. 1 ml of CNW solution was weighed and frozen at -80^{o}C for at least 12 h before freeze drying. Once freeze dried, the sample was then weighed again and the percentage weight calculated. The partial acid

hydrolysis of 1g of cellulose would make a solution with a concentration of approximately 0.45% CNWs.

3.2.3 Substrate Preparation

Substrate cleaning

Glass coverslips used in the majority of the substrate characterisation and all of the cellular work was cut from 18x18 mm borosilicate glass. The glass cover slips were cut using a custom made cutting guide into rectangles of 9x18 mm. Cleaved glass cover slips were washed in detergent solution (Neural-Con, Decon labs, 2% in dH2O) in an ultrasonic bath for 15 min. After rinsing well with dH2O, the glass was then washed in ethanol (50% in dH2O) in an ultrasonic bath for 15 min. Further rinses were carried out with 100% ethanol before being stored in 100% ethanol until required. When the rectangular glass coverslip were needed for spin coating, dip coating or cell work, the glass was dried with nitrogen gas held in custom made slide holders and plasma treated.

RF generated glow discharge air plasma (20 watt power) was used to plasma treat the glass and the glass was used within 24 h. All treatments were done at a pressure of 1.2 x10 mBar for 2 min. Plasma treatment is often used to prepare glass surfaces for LbL to increase the wettability and adhesion properties and has been used as a preparation step for spin coating (Wade 2000, Valtakari 2015, Terpilowski 2016).

Single bilayers and alignment of CNWs

Single layers and individual bilayers of chitosan and chitosan/CNW respectively were produced using a Laurell Technologies Spin coater (model WS-650SZ-6NPP-LITE) supplied with nitrogen gas (oxygen-free nitrogen, BOC gases UK). The chitosan solution was made by dissolving chitosan at 10 mg ml^{-1} in 1 M acetic acid overnight, filter and dilute with dH_2O to produce a solution at 1 mg ml^{-1}. Glass coverslips were placed plasma-treated surface up on a 5 mm diameter vacuum chuck. The spin coating parameters for each substrate type are summarised in Table 3-1 and a schematic of the spin coating is shown in Figure 3-1. For a single layer of chitosan, 200 µl of chitosan

solution was applied at 3000 rpm, followed by 3x 500 µl of dH_2O and finished with a drying step at 4000 rpm. For the bilayer of chitosan and CNW, 200 µl of chitosan solution was applied at 3000 rpm, followed by 2x 500 µl of dH_2O. After the speed reached 8000 rpm, 200 µl of CNW solution was applied and followed by a rinsing step of 3x dH_2O at 4000 rpm. The spin coating parameters to achieve optimal radial alignment of the CNWs was augmented by Nikoi (Nikoi, 2016).

Spin coated Chitosan Layer

Step	RPM	Acceleration	Time (s)	Description
1	3000	6000	30	200 µl chitosan, x3 500 µl deionized water
2	4000	10000	40	

Spin coated Chit/CNW layer

Step	RPM	Acceleration	Time (s)	Description
1	3000	6000	30	200 µl chitosan, x2 500 µl deionized water
2	8000	2000	30	200 µl 0.04% CNW
3	4000	10000	40	x3 500 µl deionized water

Table 3-1: Summary of the parameters used to spin coat the Chitosan and Chit/CNW layers

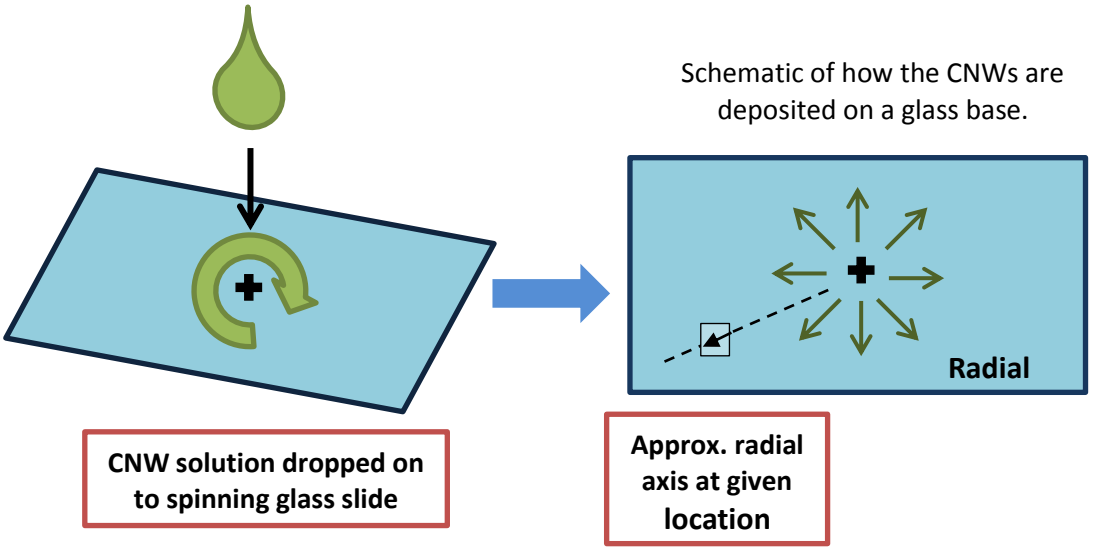

Figure 3-1: Simplified diagram showing the spin coating and radial pattern produced.

Once spin coated, substrates were stored at room temperature in 12 well plates. Pieces of plastic pipette tips were glued to the bottom of each well as spacers to improve handling of the substrates.

Multiple Bilayers

The CNW solution has a slight negative charge due to the presence of sulphuric acid ions, a consequence of the acid chosen for the partial acid hydrolysis of the cellulose. This slight charge gives the polysaccharide polyelectrolyte properties, specifically polyanionic (Dugan, Gough and Eichhorn, 2010). The layer-by-layer (LbL) deposition method comprises of alternate adsorption of polyelectrolytes on a material's surface, resulting in the formation of polyelectrolyte multilayer films (Decher, Hong and Schmitt, 1992). Chitosan has a slight positive charge (Bumgardner *et al.*, 2012) and therefore can be used as the alternate polyelectrolyte solution to the CNWs. Dip coating was used to achieve multi-layered substrates of alternating CNW and chitosan layers (Figure 3-2). This method was used as opposed to spin coating each layer to save time and energy. Custom made slide holders allow multiple glass slides to be dip coated simultaneously.

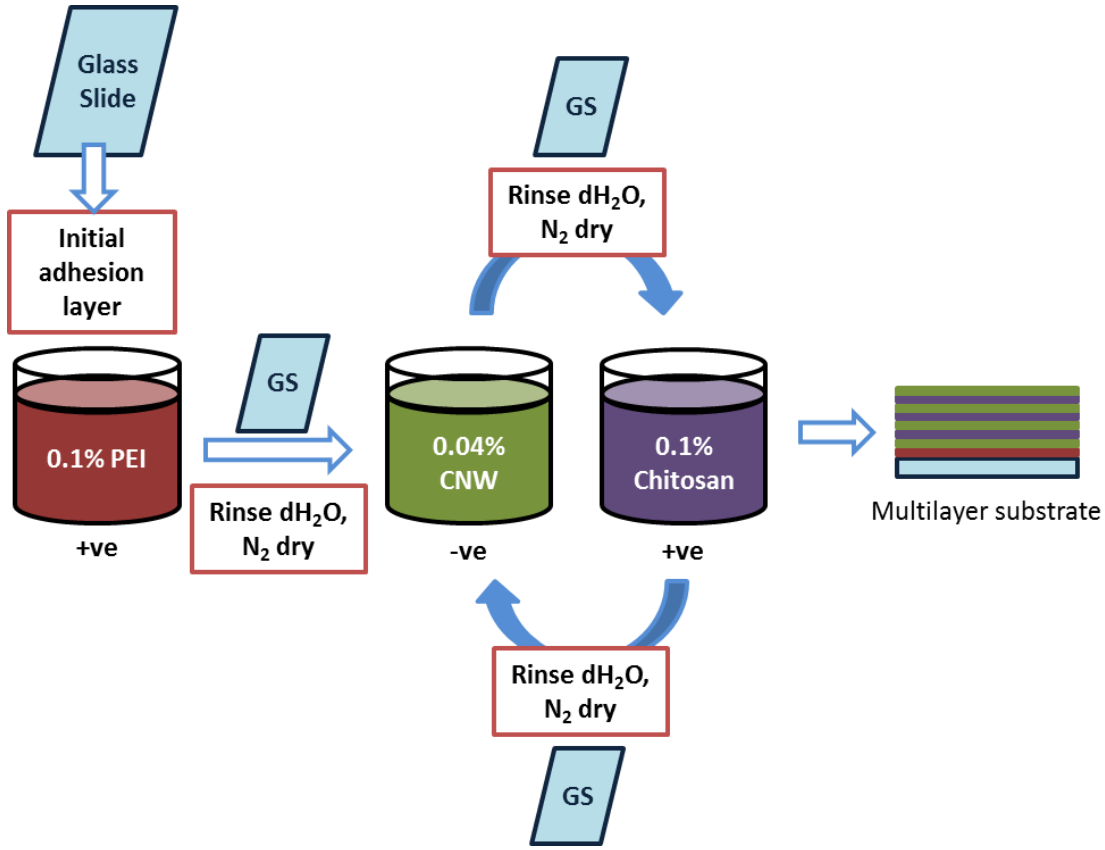

Figure 3-2: Schematic of the dip coating process to produce multilayer substrates

Once plasma treated, glass slides were placed on custom made slide holders, ensuring the direction of the plasma treated surface was noted. The holders were then placed fully submerged in the polyethylenimine (PEI) solution for 1 min before being rinsed with dH_2O three times. PEI was used as the base layer as it is a strong polycation with the intention it will provide stability for the polyelectrolyte multilayers and stop them peeling off the glass. Nitrogen gas was used to dry the glass before placing the holder in the CNW solution (polyanion) for 1 min. Three rinses in distilled water followed and the glass was dried with nitrogen gas. The holder was then fully submerged in chitosan solution (polycation) for 1 min, three rinses in distilled water followed and the glass was dried with nitrogen gas. The process was repeated with CNW solution followed by alternate dips in chitosan solution and CNW solution. This cycle was repeated to build multilayer substrates of different numbers of layers. The multilayer substrates produced for this work are shown in Figure 3-3. Substrates were stored at room temperature in 12 well plates on top of spacers until they could be spin coated.

Substrate	#Layers in total	Top Layer
Glass	None	None
Chitosan	Chit	sChit
ChitCNW	Chit/CNW	sChit/sCNW
6CNW	PEI/CNW/(Chit/CNW)^5	sChit/sCNW
12Chit	PEI/CNW/(Chit/CNW)^{10}/Chit	sChit
12CNW	PEI/CNW/(Chit/CNW)^{11}	sChit/sCNW

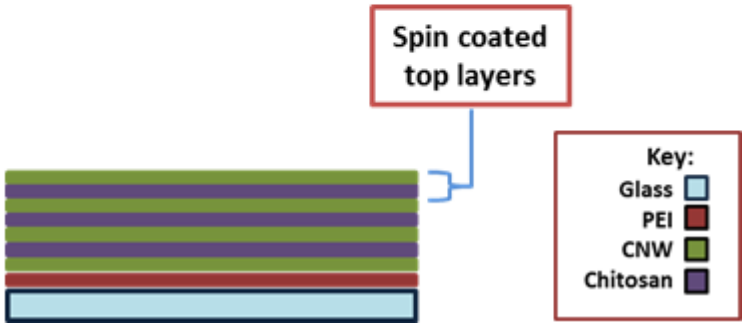

Figure 3-3: Substrates were named based on the number of layers and what the top layer was. The description of the #Layers in total refers to the number of bilayers of chitosan and CNW and what the top layers were. The 's' denotes that the top layers were spin coated.

3.2.4 Material Characterisation

Cellulose Nanowhisker Purity

Fourier Transmission Infrared Radiography (FTIR) was carried out on all samples of cellulose and CNWs to confirm purity and ensure consistency. It was carried out on the (Thermo Fisher Nicolet 5700 FT-IR). Background was taken every 15 min during readings and subtracted from the sample measurements. Peaks were identified and compared against both old samples from previous work and literature.

CNW Morphology and Orientation

Atomic force microscopy (AFM) was used to characterise the morphology and orientation of spin coated CNWs. A Bruker Multimode AFM running Nanoscope V and software Research Nanoscope 9.2 (Build R3Sr6 100600, Bruker) was used to scan areas of deposited CNWs using tapping mode in air. TESP-V2 tips were used (Bruker, nominal resonant frequency 230-410 kHz, nominal tip radius 8 nm) and areas of 5 um^2 were scanned with a resolution of 512x512 points in three different areas, scanning at 0.5 Hz. Put simply, AFM works by moving an oscillating tip across a surface, measuring the difference in frequency as the driving force is returned from the surface allowing a 3D map of the surface to be complied. To measure the morphology of the CNWs, the CNWs were spin coated at 0.01% to spread the CNWs at a lower density and reduce the number of whiskers overlapping each other. Unaligned CNWs were produced through the dip coating method for comparison to the oriented whiskers. Images were processed through the Gwyddion SPM software (Czech Metrology Institute, Czech Republic) and thresholded and binarized using ImageJ (National Institutes of Health, USA). What was measured for the length and height of the CNWs are shown in Figure 3-4. For the height, the diameter was used due to the rod shape nature of the whiskers proven by Dugan et al (Dugan, 2011). To measure orientation, the whiskers were treated like grains with the angle of the longest dimension to the bottom of the image used to show whisker orientation. Angles measures were normalised to zero so that data could be complied.

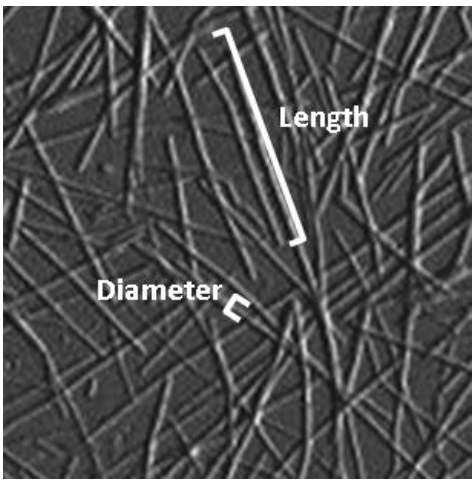

Figure 3-4: To measure the length and height of the CNWs, the features above were measured using ImageJ. The measurement for the diameter was used for the height due to the rod like morphology of the whiskers.

Presence of Sulphates

X-ray photoelectron spectroscopy (XPS) was carried out by Dr Ben Spencer on the Kratos Axis Ultra Hybrid system to identify specific elements through the analysis of the kinetic energy of the emitted photoelectrons. Due to the training required to use the XPS system, substrates were prepared on glass cover slips and the passed along for analysis. Analysis of the data collected was carried out by Annchalee Eade using the CasaXPS V2.3.22 software. Three spots were measured per substrate type and the full range was carried out twice.

The XPS and AFM facilities are both supported by the Henry Royce Institute for Advanced Materials, funded through EPSRC grants EP/R00661X/1, EP/S019367/1, EP/P025021/1 and EP/P025498/1.

Roughness

The roughness of each substrate type was measured using the Bruker White Light Contour GT system and the data collected using the Vision64 software. Variations in the surface of the substrate were measured using white light and complied to give an

area roughness value. Three random areas were measured across ten samples of each substrate type at different times throughout the project. The roughness was measured with the value Sa, which is a measurement of area surface roughness, specifically the deviation from the normal vector of its ideal form on a surface. This value, Sa, is different to the more commonly used value Ra, which is a measurement of roughness along a profile. Although not the same, the values are similar in magnitude and can be used as an approximate comparison.

Wettability

The contact angle of each substrate type was measured using the KRUSS Drop Shape Analyzer (DSA100) and the related software. dH_2O was used to understand the hydrophilic nature of the surfaces. Each drop was modelled as a sessile drop and the angle measured using Tangent Method-1. The basic equation for calculating the wettability of a surface is the Young's Equation, shown in Figure 3-5. γ denotes the surface free energy or the interfacial tensions between the different states (solid, liquid, vapour). The Young's Equation is rearranged to give the contact angle shown as Equation 3-1. Three random areas were measured across ten samples of each substrate type at different times throughout the project.

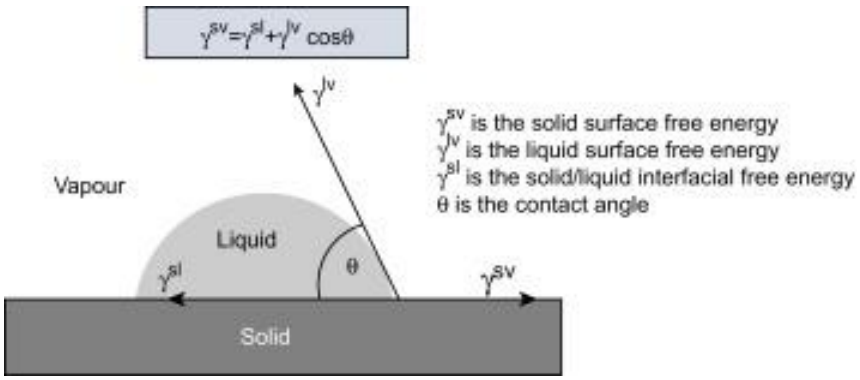

Figure 3-5: Schematic of the Youngs Equation (Soleimani-Gorgani, 2016)

$$cos\theta = \frac{\gamma^{sv} + \gamma^{sl}}{\gamma^{lv}}$$

Equation 3-1: Young's Equation to calculate contact angle

Where:

θ = contact angle

γ^{sv} = solid surface free energy

γ^{sl} = solid/liquid interfacial free energy

γ^{lv} = liquid surface free energy

The wettability of plasma treated glass vs clean glass was also measured to confirm the effect of the plasma (Figure 3-6). The increase in hydrophilicity of the plasma treated glass agrees with the literature (Valtakari 2015, Terpilowski 2016).

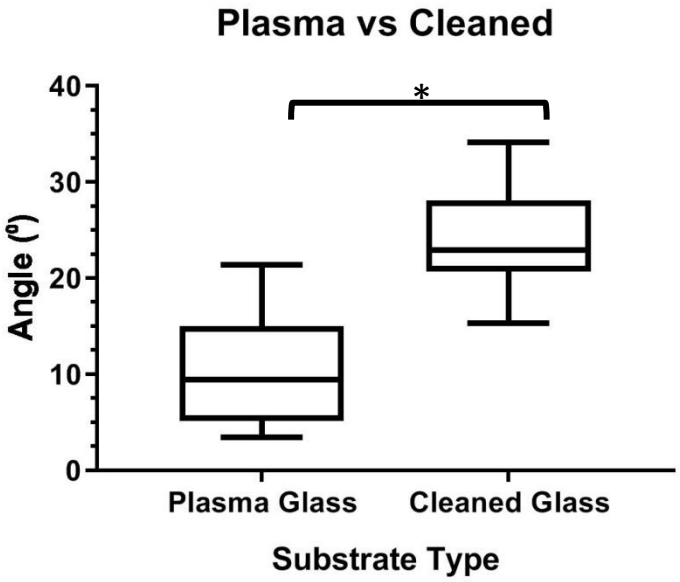

Figure 3-6: Box whisker plots (whiskers are minimum to maximum value) of the contact angle (°) of the plasma treated glass and ethanol cleaned glass taken from random batches of substrate preparation. Due to the high hydrophilic nature of the glass, only one drop was measured on each, N = 30. Data analysis carried out using T-test with Welch's correction. * = $p < 0.05$

Protein Adsorption

Adsorption of fibronectin and laminin on the substrates was measured using the NanoOrange™ Protein Quantitation Kit (Molecular Probes, Invitrogen™, ThermoFisher, Cat #: N6666). It is a fluorescence assay that can detect between 10 ng mL^{-1} and 10 µg ml^{-1} of protein in solution. The full range of substrates, including TCP, was processed as if being prepared for cell culture. Two sets were prepared to look at fibronectin and laminin adsorption separately. The assay was carried out as per the manufacturer's instructions. Each protein solution was prepared at 4 µg ml^{-1}in the NanoOrange reagent working solution and 250 µl was placed on each sample for 2 h at 37°C. After the 2 h, the solution was transferred in to eppendorfs before being heated for 10 min at 90°C. Once the solution had cooled back down to room temperature (at least 20 min), it was transferred to a black 96 well plate (Nunc, Thermo Scientific) and measured on a fluorescence reader (excitation 485 nm, emission 590 nm)(BMG Labtech, model FLUOstar Optima). Standards were taken for each protein using the same protein stock used in the assay (Figure 3-7). This was used to calculate the amount of protein adsorbed on to each sample.

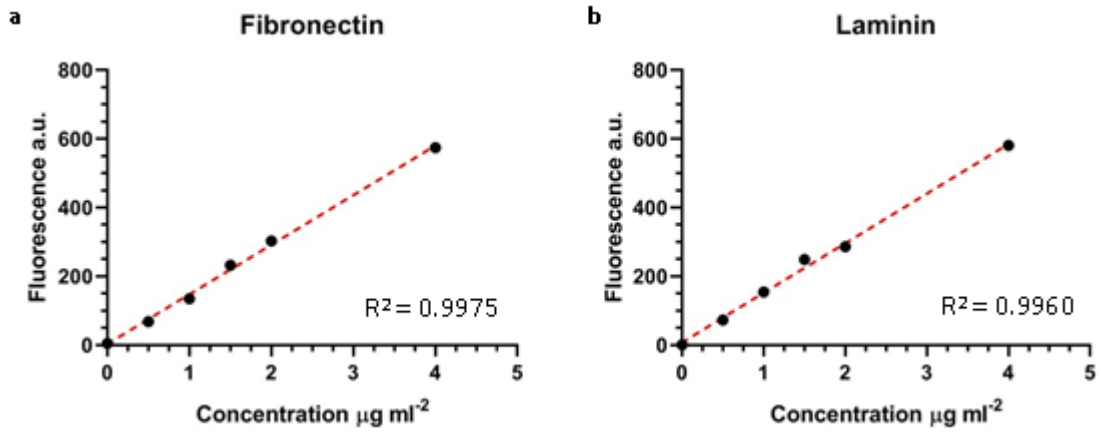

Figure 3-7: Standard curves of each protein (a) fibronectin and (b) laminin for the NanoOrange assay with R^2 values of 0.9975 for fibronectin and 0.9960 for laminin.

3.3 Cell Culture on the Cellulose Nanowhisker Substrates

3.3.1 Maintenance and Subculture of Cells

All cell work was carried out in Class 2 Biological Safety Cabinets which were thoroughly cleaned with 70% ethanol before every use.

C2C12s used in this project were taken from stock originally obtained from ATCC towards the end of 2016. The cells were expanded as per the recommended protocol and frozen down in aliquots of 1 $x10^6$ cells per vial in 90% FBS/10%DMSO freezing solution. The cells were stored in liquid nitrogen. C2C12s for experimental use were revived with C2C12-GM (growth media, DMEM High Glucose with L-glutamine, 10% FBS, 1% AB) approximately 5 d before seeding depending on the size of the experiment. Cells were placed in flasks at 10,000 cells cm^{-2}. The Trypan Blue dye was used to count viable cells using a haemacytometer. Cells were fed with C2C12-GM every 2 days and split 1:5 once the cells reached 70% confluency. Cells were maintained in an incubator at 5% CO_2 at 37^{o}C.

For differentiation purposes the C2C12s required cell-cell contact and low serum differentiation media. Cells were subcultured for seeding to approximately 90% confluency. Warmed sterile PBS was used to wash the cells twice before detaching with Trypsin/EDTA. After detachment, the Trypsin/EDTA was inhibited with an equivalent volume of C2C12-GM. The cell suspension was collected in a centrifuge tube and centrifuged at 300G for 5 min to form a cell pellet. The cell pellet was suspended in fresh C2C12-GM of known volume and counted.

hSkMCs were obtained from PromoCell (C-12530) and expanded following their recommended protocol. Cells were frozen down in aliquots of 375 $x10^3$ to 500 $x10^3$ cells per vial in Freezing Medium Cryo-SFM. The cells were stored in liquid nitrogen. Cells were frozen between these concentrations to facilitate the unfreezing straight into T75s; PromoCell recommends a seeding density between 5,000-7,500 cells cm^{-2}. The Trypan Blue dye was used to count viable cells using a haemacytometer. Cells were fed with hSkMC-GM every 3 d and subcultured once the cells reached 70% confluency. Cells were maintained in an incubator at 5% CO_2 at 37^{o}C.

hSkMCs for experimental use were revived with hSkMC-GM (Skeletal Muscle Cell Growth Medium, PromoCell) approximately 1 week before seeding depending on the size of the experiment. Warmed sterile PBS was used to wash the cells twice before detaching with Trypsin/EDTA. After detachment, the Trypsin/EDTA was inhibited with an equivalent volume of hSkMC-GM. The cell suspension was collected in a centrifuge tube and centrifuged at 300G for 5 min to form a cell pellet. The cell pellet was suspended in fresh hSkMC-GM of known volume and counted.

Two donors of BM-MSCs were used in this work. Both were contributed from stock population of other members of the Biomaterials Group at the University of Manchester. Donor 1 BM-MSCs were isolated from the femur of a 27-year old female after hip replacement surgery at Wrightington Hospital, Lancashire by the Richardson Laboratory. Donor 2 BM-MSCs were obtained from Lonza as part of a bone marrow aspirate and their isolation and characterisation was done by Dr. Deepak Kumar. Cells were fed with MSC2-GM every 5-7 d and split once the cells reached 80% confluency. Cells were maintained in an incubator at 5% CO_2 at 37^{o}C.

BM-MSCs for experimental use were revived with MSC2-GM (Mesenchymal Stem Cell Growth Medium 2, PromoCell) approximately 1-2 weeks before seeding. Warmed sterile PBS was used to wash the cells twice before detaching with Trypsin/EDTA. After detachment, the Trypsin/EDTA was inhibited with an equivalent volume of MSC2-GM. The cell suspension was collected in a centrifuge tube and centrifuged at 300G for 5 min to form a cell pellet. The cell pellet was suspended in fresh MSC2-GM of known volume and counted. Both set of BM-MSCs were observed for cell viability before use in this work, and personal aliquots were frozen down from different passages.

3.3.2 Substrate Sterilization and Cell Differentiation

All substrates were prepared for cell seeding using the following protocol. Substrates were placed in in a 24 well plate and washed twice with PBS before undergoing UV sterilisation in the biological safety cabinets for 30 min. The substrates were then preconditioned by submersion in 0.5 ml of appropriate growth media overnight in an incubator. This media was removed before cell seeding.

C2C12s were seeded at 10,000 cells cm^{-2} in C2C12-GM. After 24 h, C2C12-DM (differentiation media, DMEM High Glucose with L-glutamine, 2% HS, 1% AB) was added through partial media changes every 24 h for the duration of the experiment. hSkMCs were seeded at 5,000 cells cm^{-2} as per PromoCell's instructions. Differentiation media was swapped for hSkMC-DM (Skeletal Muscle Differentiation Medium , PromoCell) when the cells had reached 60-80 % confluency. After 2-8 d cell fusion should be observed. For a stable differentiation of hSkMC the hSkMC-DM was switched back to hSkMC-GM after 5 d incubation as per PromoCell's protocol. BM-MSCs were seeded at 5,000 cell cm^{-2} in MSC2-GM. When the cells had reached 80-90% confluency, MSC-DM (differentiation media, low-glucose DMEM, 5% HS, 1%AB, 1% NEAA) was added through partial media changes every 2 days. This media composition was chosen as a one of the simplest differentiation media reported as successful in promoting myogenic differentiation of human MSCs (Gang *et al.*, 2004).

At specific time points cells were either fixed or used in with the Alamar Blue or PicoGreen assays. To fix the cells, media was removed and the cells washed twice with warm sterile PBS. 100 µl of formalin solution (neutral buffered, 10%) was placed in each well and left for 10 min at room temperature. The formalin solution was then removed and the cells washed twice with PBS again. 0.5 ml of PBS was left in each well and the plate stored at 4^{o}C until staining.

The satellite cells extracted from biopsies of human muscle by Dr. Francesco Galli, Division of Cell Matrix Biology and Regenerative Medicine, University of Manchester. Due to ethic restrictions, the work was carried out by him in his laboratory. Satellite cells were seeded on the full range of substrates after the preconditioning step described above. After 2 days, cell adhesion was observed and differentiation media was added. The cells were fixed after 10 d in differentiation media and stored at 4^{o}C in PBS until staining.

3.3.3 Adsorption of Proteins

The effect of the preconditioning the substrates is investigated in Section 6.2.1. The substrate preparation for cell seeding described above was carried out however instead of submersion in 0.5 ml of C2C12-GM; the substrates were preconditioned

with the following, C2C12-GM, C2C12-GM without FBS, PBS and UltraPure™ dH_2O. The substrates were left in an incubator overnight and the solutions were removed before cell seeding.

For protein adsorption, the substrates were sterilised as described above. After the UV sterilisation step, 250 µl of fibronectin or laminin solution was placed on top of each substrate. The proteins were delivered in UltraPure™ dH_2O at a concentration 4 µg ml^{-1}. This concentration was chosen based off preliminary data from the NanoOrange assay. The plates were then left in an incubator for 2 h. The protein solution was removed before cell seeding.

3.3.4 Characterisation of Cells

Alamar Blue

Cell metabolic activity was measured using the Alamar Blue™ assay at different time points across multiple experiments. A 10x intermediate stock solution (5 mM) was prepared by dissolving 5 mg of resazurin salt in 40 ml PBS and filtering through a 0.22 µm syringe filter. The stock solution was diluted in the relevant cell culture media at a 1:10 ratio to produce a working solution. Media was removed from each well and replaced with 1 ml of working solution. This was left for 2 h at 37^{o}C and kept dark. After 2 h, 100 ul in triplicate was removed from each well and transferred to a black 96 well plate (Nunc, Thermo Scientific). The fluorescence was measured on a fluorescence plate reader (excitation 560 nm, emission 590 nm) (BMG Labtech, model FLUOstar Optima) and the data was collected by the Optima software package (BMG Labtech, Version 2.20R2, Firmware Version 1.26). Samples were then washed twice with PBS before being prepared for either PicoGreen or new media. Blank values were taken away from fluorescence readings before data analysis.

An estimate of the population doubling time was made using the following equation:

$$T_d = (t_2 - t_1)\frac{ln2}{ln\left(\frac{f_2}{f_1}\right)}$$

Equation 3-2: Population Doubling Time

Where:

t1 = Time (h) at measurement 1

t2 = Time (h) at measurement 2

f1 = Fluorescence (background subtracted) at time 1

f2 = Fluorescence (background subtracted) at time 2

PicoGreen

Cell number was measured using the Quant-iT™ PicoGreen™ dsDNA Assay Kit (Invitrogen™, ThermoFisher, Cat #: P7589). Media was removed from each well and washed twice with PBS. 1 ml of lysis buffer (what is it) was placed in each well and depending on the experiment, the solution was either frozen in the well or transferred to an eppendorf and then frozen at -80^{o}C. If the sample was transferred to an eppendorf, cell scrapers were used to ensure all of the cellular content was collected. The cells in solution were further broken down through at least 2 sets of freeze thaw cycles. To measure the PicoGreen fluorescence, 100 ul per well in triplicate was mixed with 100 ul of PicoGreen working solution in a black 96 well plate (Nunc, Thermo Scientific). The fluorescence was measured on a fluorescence plate reader (excitation 560 nm, emission 590 nm) (BMG Labtech, model FLUOstar Optima) and the data was collected by the Optima software package (BMG Labtech, Version 2.20R2, Firmware Version 1.26). Standards were taken for each cell type and used to calculate the cell number (Figure 3-8) and blank values were taken away from fluorescence readings before data analysis.

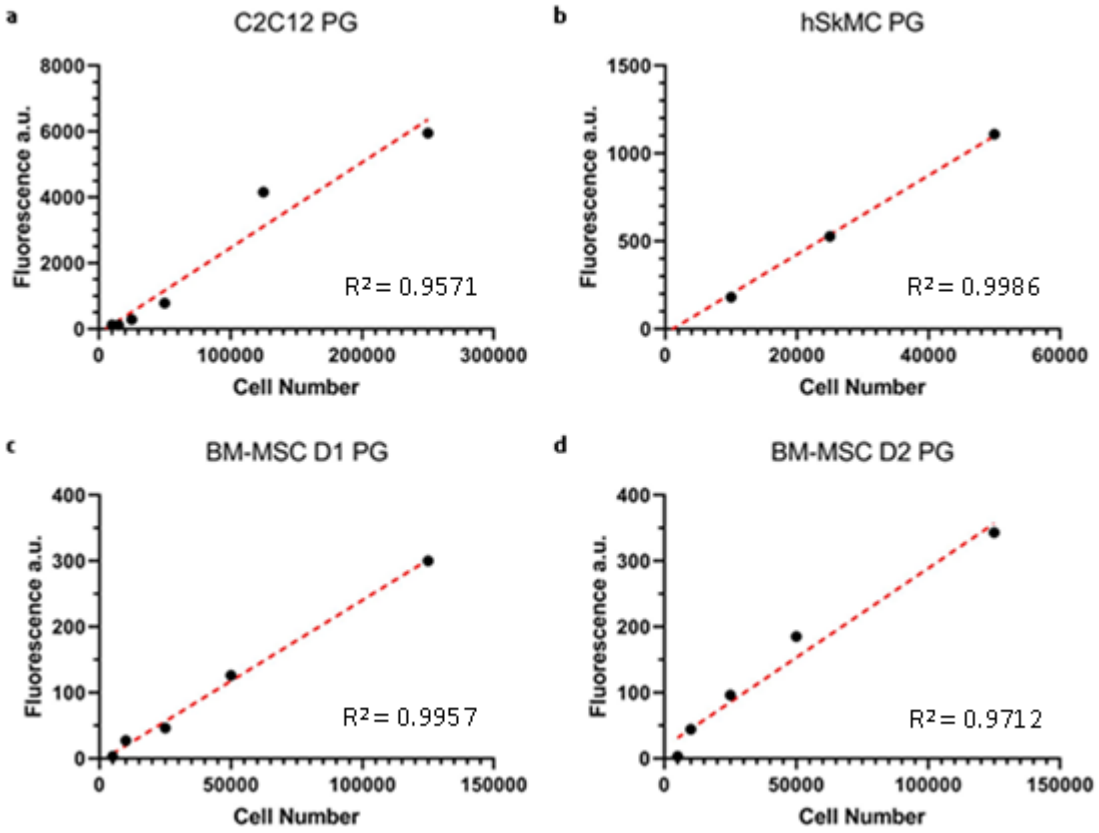

Figure 3-8: Standard curves for the PicoGreen assay of each cell type: (a) C2C12 (R^2 = 0.9571), (b) hSkMC (R^2 = 0.9986), (c) BM-MSC Donor 1 (R^2 = 0.9957) and (d) BM-MSC Donor 2 (R^2 = 0.9712).

Immunofluorescence Staining

Immunofluorescence staining is often used to label proteins and areas of interest in cell work. The primary antibody binds to the protein of interest and the secondary antibody with its tagged fluorphore labels the primary. Multiple antibodies can bind at each site therefore amplifying the signal. It is a useful method for labelling multiple proteins on the same sample.

All staining was done at room temperature. The PBS on the fixed cells was removed and 100 µl permeabilisation buffer (0.5% Triton X and 0.05% Tween in PBS) to each well for 5 min. This was then replaced with 100 µl ICC buffer (2% GS, 1% BSA and 0.1% gelatin in PBS) for 30 min to block the samples. For large amounts of staining, the substrates were removed from the wells and placed on parafilmed glass slides. This

allowed for lower volumes of primary and secondary antibody solutions to be used. 45 µl of primary antibody (rabbit myogenin, mouse sarcomeric-α-actinin in ICC buffer) was carefully deposited on top of each substrate and left covered for 1 h. Warm wet paper towels were rolled up and left with the substrates to maintain the humidity and prevent evaporation of the antibody. The substrates were then washed twice with PBS (+ 0.05% Tween) and 45 µl of secondary antibody (anti-rabbit 488, anti-mouse 568, phalloidin 647 in PBS with Tween 0.05%) was added and left covered for 1 h. The substrates were then washed twice with PBS (+ 0.05% Tween) and 45 µl of Hoechst was placed on top for 5 min. The substrates were then washed twice with dH2O and mounted on to glass slides with ProLong™ Diamond Antifade Mountant. Slides were left to cure overnight and stored at 4^{o}C when not being imaged.

Controls were also stained to observe the back ground staining that sometimes appeared on the multilayer substrates. Immunofluorescence staining was carried on glass and 12CNW substrates to show what background staining was visible (Figure 3-9). No background was seen on the glass however, the stain appeared 'cloud' like on the 12CNW. This is sometimes seen when cell density is low. The same was done on 3T3s, immortalised mouse fibroblast cell line, which were seeded on to glass and 12CNW. The nuclei were shown clearly on both substrates as expected. The myogenin stain, green, was only present as background on the 12CNW which means there was no non-specific staining of the cells.

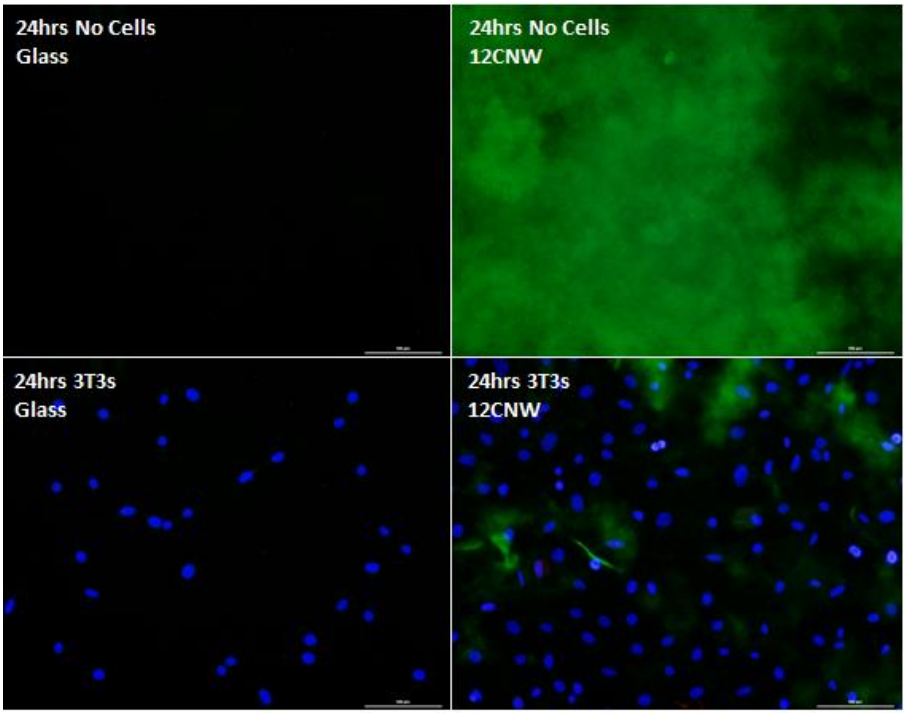

Figure 3-9: Confocal fluorescence micrographs of the controls taken at 20x mag. It shows background is often seen when there is a low cell density with the multilayer substrates. Blue = nuclei, green = myogenin

Imaging

Nearly all imaging was carried out on the CQ1 CQ1 Yokogawa Benchtop System curtsey of the Henry Royce Institute. The CQ1 is a bench top confocal microscope that can facilitate imaging of live and fixed cells on a large scale. Images were taken through different channels and saved as split and merged images. The function to image large areas with the stitching function was used to observe the broad alignment of cells. Images were stitched together using Microsoft ICE (Image Composite Editor) and analysed using ImageJ.

3.4 Data Analysis

Data analysis was carried out using GraphPad Prism 8. Ordinary one-way anova with Turkey's multiple comparison tests with a single pooled variance was used when there was one variable, such as substrate type. Two- way anova with the Geisser-

Greenhouse correction and Turkey's multiple comparison tests with individual variances was used when there were two variables, such as substrate type and time point. Data was considered to be significantly different if the P value < 0.05. Greek labels have been used to indicate groups within which no significant difference was observed (Figure 3-10).

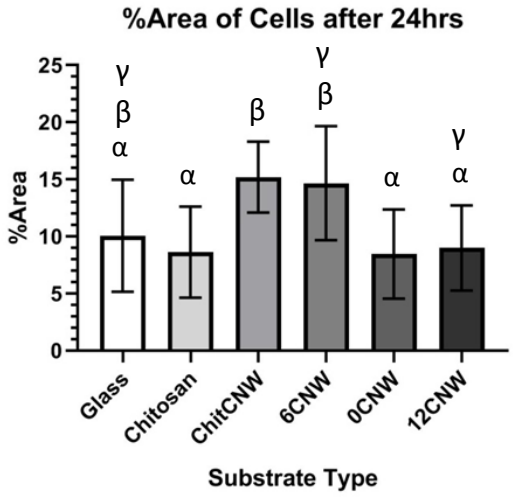

Figure 3-10: Example graph to explain the Greek letter labelling of significant difference. All substrates with the same Greek letter are not significantly different to each other. Glass is not significantly different to any other substrates. Chitosan is significantly different to ChitCNW and 6CNW but not the others. 12CNW is significantly different to ChitCNW but not to 6CNW.

Data analysis was focused between specific substrate types to give information on how specific variables changed the data recorded. Chitosan and ChitCNW are the bilayer samples and 12Chit and 12CNW are the multilayer samples. These 2 sets were compared to see if there was a statistical difference between a substrate with an oriented CNW topography (ChitCNW and 12CNW) and one without (Chitosan and 12Chit).

Box whisker plots have been used at times to show the spread of data as well as the mean (Figure 3-11). Some data has been shown in this form to show the range of the data (whiskers of the upper and lower extremes) and where most of the data lies (the box formed from the upper and lower quartile). Sometimes data had a large range overall but the majority of the data was within a small range. For example, box whisker plots were used to compare the orientation of cells and CNWs as a smaller box clearly shows a greater orientation in one direction whereas a larger box shows the data is

more spread out and therefore, the cells/CNWs are not all aligned in the same direction.

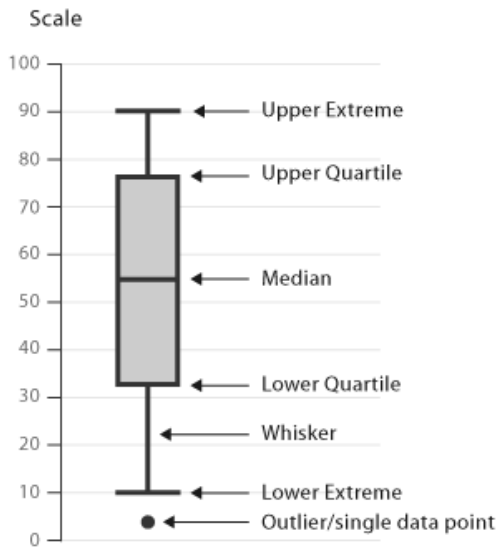

Figure 3-11: Diagram explaining the box whisker plots (Image from https://datavizcatalogue.com/methods/box_plot.html, 25/09/19)

Chapter 4: Characterisation of the Cellulose Nanowhisker Substrates

4.1 Analysis of the CNWs

4.1.1 Quality of the Cellulose

FTIR was used to confirm and compare the purity of the bleached tunicin cellulose (Cellulose (A)) used in this project and the nanowhiskers (CNWs (A)) derived from the partial acid hydrolysis of Cellulose (A) to the cellulose used in previous work (Cellulose (B)) (Figure 4-1).

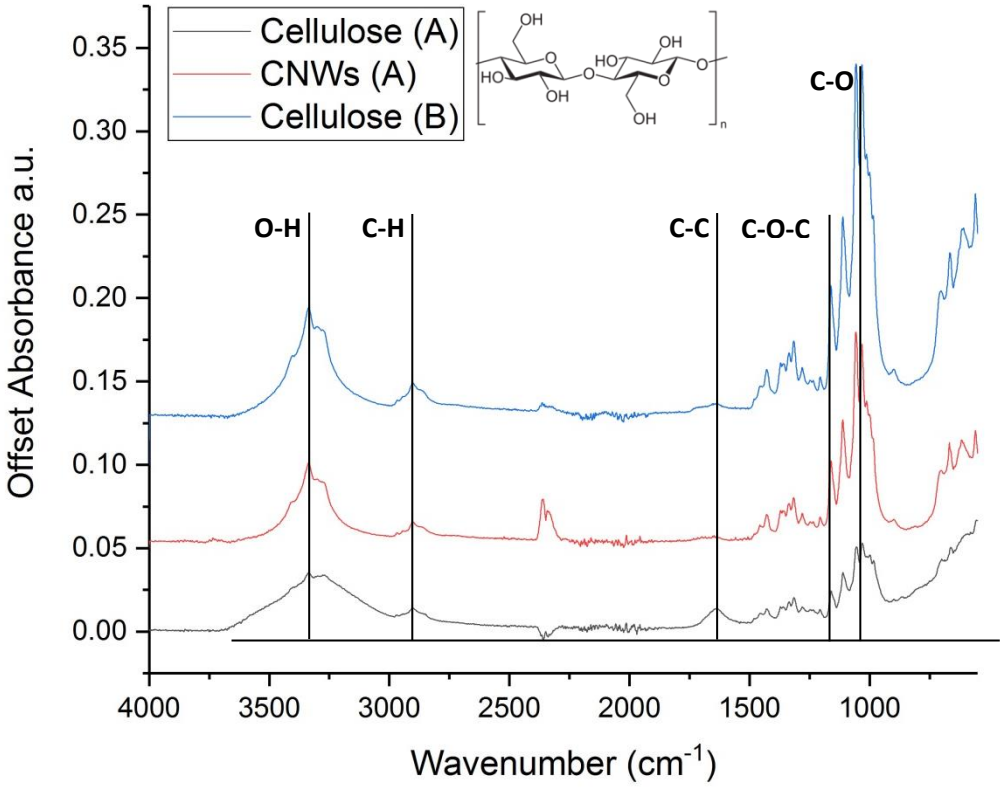

Figure 4-1: FTIR spectra of tunicin cellulose: Cellulose (A) and CNWs (A) were used in this project and Cellulose (B) was used in previous work. Important peaks are labelled and the chemical structure of cellulose is also shown.

Overall the spectra are comparable, including to Mitchell's FT-IR studies on tunicin and Valonia cellulose (Michell, 1993). It noted that tunicin cellulose was mainly comprised of highly crystalline Iβ cellulose shown by the presence of peaks at 3270 and 710 cm^{-1}. These are present, confirming the crystallinity of the cellulose samples. There is a peak shift of about 10 cm^{-1} compared to the literature, which could be related to the source of the cellulose and its processing.

The broad peaks between 3550-3200 cm^{-1} are consistent with the stretching of the O-H bonds and the small peak at around 2900 cm^{-1}, with C-H bonds. The highest peaks at around 1085-1050 are consistent with the stretching of the C-O bonds in polysaccharides. The difference in peak size is related to the number of bonds and can be affected by the processing.

The data confirms the bleached cellulose and derived CNWs produced are equivalent to the cellulose previously used in this work and to literature.

4.1.2 Heights and Length of CNWs

AFM is used to measure the average heights and lengths of the CNWs (Figure 4-2). Due to the highly crystalline Iβ cellulose structure, nanowhiskers of a high aspect ratio were produced as expected when compared to previous work and other studies. The height (mean = 5.097 nm ±0.486 nm) was similar to CNWs produced from the same species of tunicate (Dugan *et al.*, 2013), however, this was smaller than those measured of unspecified tunicate species in other literature (Elazzouzi-Hafraoui *et al.*, 2008). The lengths (mean = 0.505 µm ±0.667 µm) were within the range measured by other studies (Eichhorn, 2011).

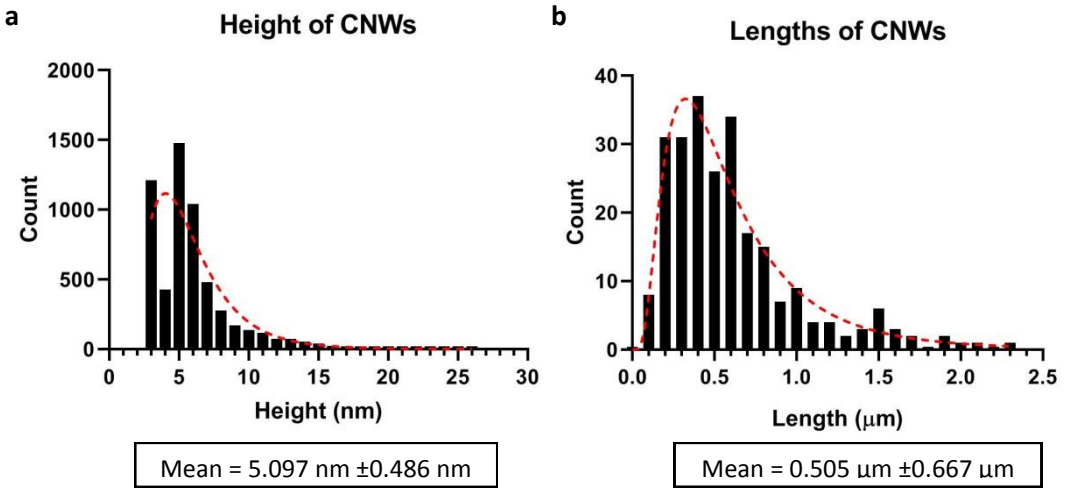

Figure 4-2: Histograms showing the heights (a) and lengths (b) of the CNWs produced.

4.1.3 Presence of Sulphates

It has been shown that the partial acid hydrolysis of cellulose with sulphuric acid leaves the CNWs produced with a slight negative charge due to sulphate ester groups (Revol *et al.*, 1992; Dugan *et al.*, 2013). XPS was used to confirm the presence of sulphur from the sulphate ester groups. Multilayer substrates were measured and the atomic percentage (%At) calculated from the peaks of each spectra. Specific elements were focused on to narrow the analysis.

The atomic percentage measured on each substrate is shown in Table 4-1. Carbon and oxygen are the main elements. There is no clear pattern with oxygen, which is most likely due to its presence in air. Carbon is shown to increase as the number of layers increase. Nitrogen is also present in air however it is also found in the amine group in chitosan. This may be why there is a slight increase in the Chitosan and 12Chit samples as the top layer is chitosan. Sulphur was only found in samples that contained CNWs, which supports the evidence from literature and previous work. Lastly, silicone shows a large decrease as there are more layers. Silicone is one of the components of glass on which all of the substrates are built on.

Sample	O1s	C1s	N1s	S2p	Si2p
Glass	56.67	17.21	1.20	-	24.92
Chitosan	48.87	28.19	2.32	-	20.62
6CNW	37.58	59.62	0.93	0.22	1.65
12Chit	41.69	51.74	2.88	0.41	3.28
12CNW	36.95	60.16	0.76	0.26	1.86

Table 4-1: %At of oxygen, carbon, nitrogen, sulphur and silicon calculated from XPS spectra of multilayer substrates

XPS spectra of the Glass and 6CNW substrates are shown in Figure 4-3 and 4-4 respectively. The area where the sulphur peak should be is highlighted.

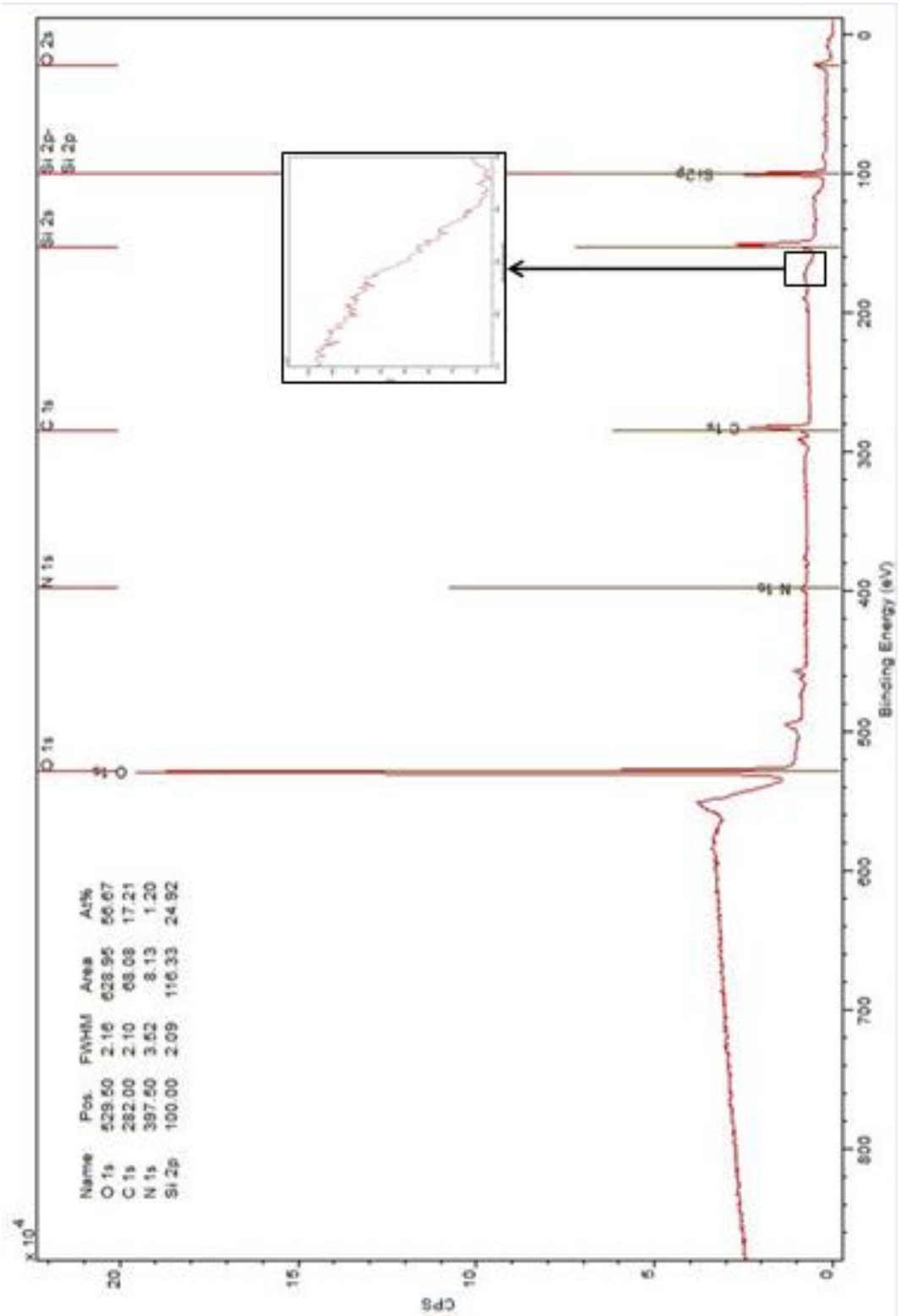

Figure 4-3: XPS spectrum of glass. No peak is seen at the binding energy of S2p.

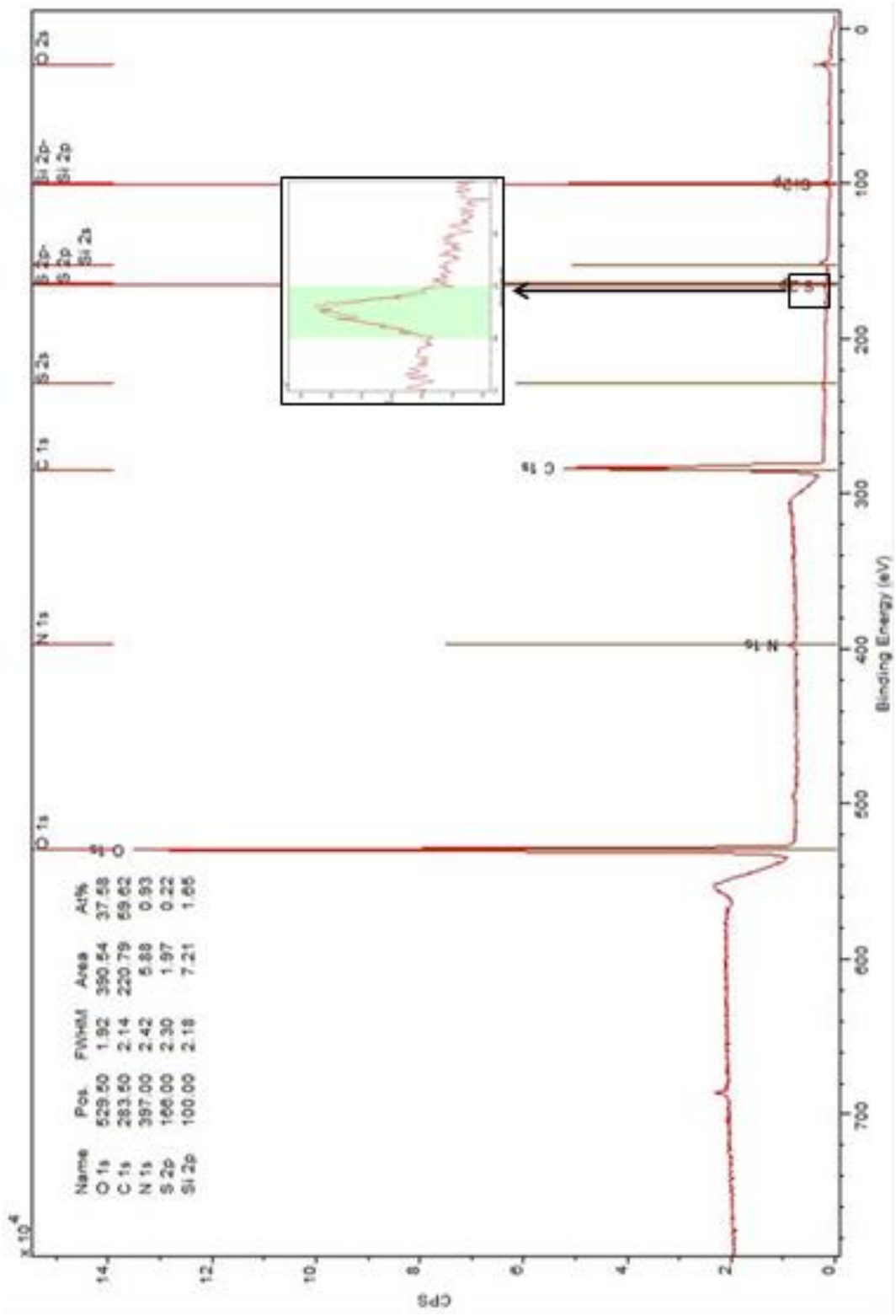

Figure 4-4: XPS spectrum of 6CNW. A peak can be seen at the binding energy of S2p.

4.2 Analysis of the Multilayer Substrates

The range of substrates used in this work is described in Figure 4-5. The naming of the substrates is dependent on the number of layers and the terminal layer. Glass, Chitosan and ChitCNW are the thinner substrates and 6CNW, 12Chit and 12CNW are the multilayers. The difference between 12Chit and 12CNW is the top layer which is chitosan and CNWs, respectively.

Substrate	#Layers in total	Top Layer
Glass	None	None
Chitosan	Chit	sChit
ChitCNW	Chit/CNW	sChit/sCNW
6CNW	PEI/CNW/(Chit/CNW)^{5}	sChit/sCNW
12Chit	PEI/CNW/(Chit/CNW)^{10}/Chit	sChit
12CNW	PEI/CNW/(Chit/CNW)^{11}	sChit/sCNW

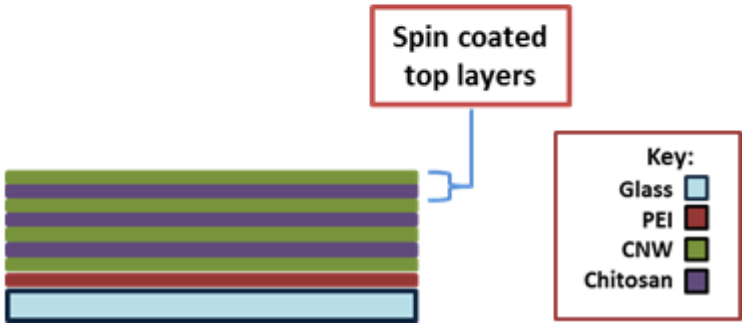

Figure 4-5: Substrates were named based on the number of layers and what the top layer was. For example, 12CNW refers to 12 bilayers of Chit/CNW deposited on glass; the final layer was spin coated CNW. The 's' denotes that the top layers were spin coated.

4.2.1 Alignment of the CNWs

The CNWs were spin coated to produce the aligned topography. The spin coating technique with these CNWs was initialised by Dugan and optimised by Nikoi. Alignment has been quantified for both the spin coated and non-spin coated topography (Figure 4-6). The oriented CNWs have a smaller distribution from 0° with 27.52% of the whiskers within ± 10°. The unaligned surface only has 8.90% of its whiskers within ± 10° of 0° and the alignment is also seen by the larger distribution of angles. Although both topographies have whiskers at a wide range of angles (Figure 4-6 (e)), the distribution of the unaligned whiskers is broader.

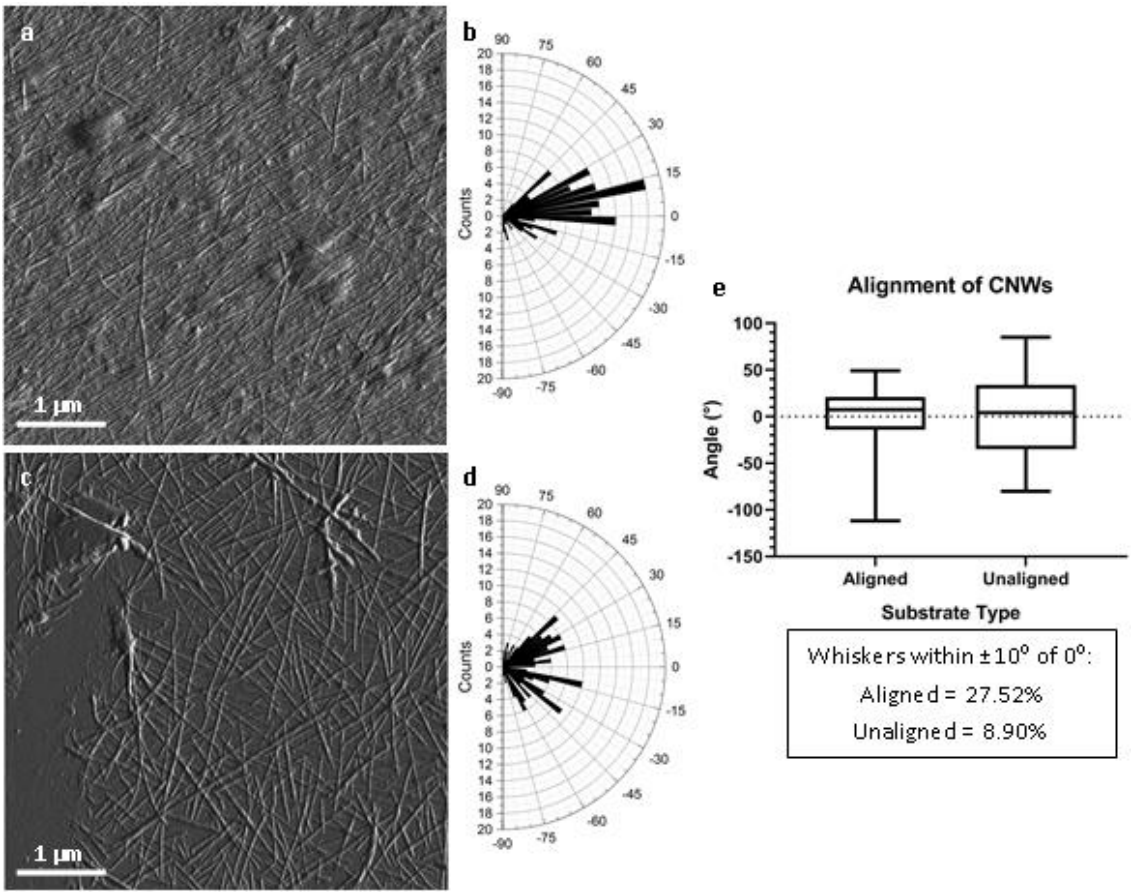

Figure 4-6: Data showing the difference in alignment of spin coated and non-spin coated CNWs. (a) and (b) show the AFM map and radial graph, respectively, of the aligned CNWs produced through spin coating. (c) and (d) show the AFM map and radial graph, respectively, of the unaligned CNWs, these were not spin coated. (e) Box and whisker plot of the range of alignment measured. N=3, the data has been normalised to zero. The smaller box on the aligned data shows that most of the data (angles) are in a narrower range than the unaligned data.

4.2.2 Roughness

Sa is a measurement of area surface roughness, specifically the deviation from the normal vector of its ideal form on a surface. Smaller Sa values are less rough than larger. Overall, the roughness of the substrates was similar to that of polymer films, but a lot smoother when compared to 3D scaffolds (Ricotti *et al.*, 2010; Yang, Lee and Kim, 2019). The difference between single layer substrates and multilayers was significant (Figure 4-7) likely due to the LBL technique used to build the multilayers.

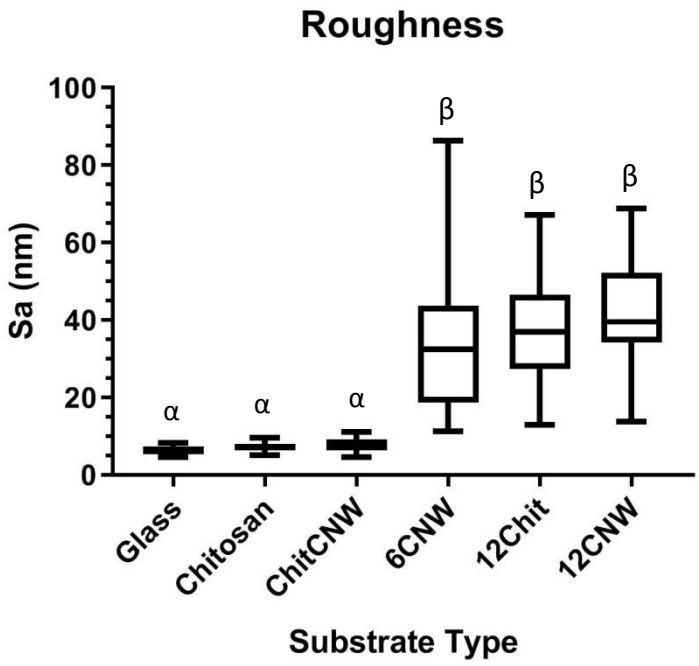

Figure 4-7: Box whisker plots of the roughness (Sa (nm)) of the range of substrate types taken from random batches of substrate preparation. Three random areas were measured across N=10 of each substrate type. Data analysis carried out using ordinary one-way anova with Turkey's multiple comparison tests with a single pooled variance. Greek labels indicate groups within which no significant difference was observed. For those that are significantly different = $p < 0.05$.

4.2.3 Wettability

Contact angle is used to quantify the wettability of a surface. A surface's wettability can have a large effect on cell attachment and proliferation (Bacakova *et al.*, 2011). It is dependent not only on the topography of the surface, but its chemical interactions. Glass was found to have a very low contact angle due to its smooth surface and plasma treatment and is therefore hydrophilic. Figure 4-8 shows the wettability of the Glass was significantly different to the other substrates. The differences between the other substrates are likely related to the compositions and top layer of each substrate.

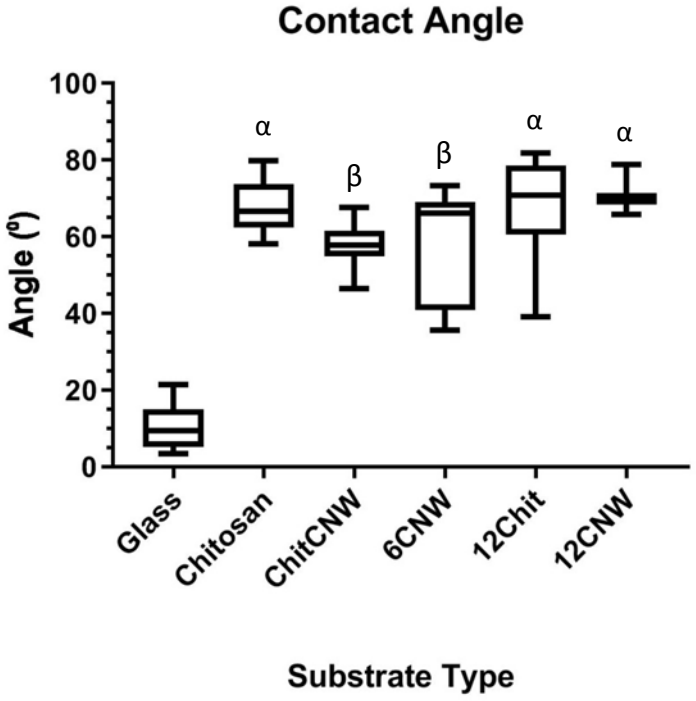

Figure 4-8: Box whisker plots of the contact angle (°) of the range of substrate types taken from random batches of substrate preparation. Three random areas were measured across N=10 of each substrate type. Data analysis carried out using ordinary one-way anova with Turkey's multiple comparison tests with a single pooled variance. Greek labels indicate groups within which no significant difference was observed. For those that are significantly different = $p < 0.05$.

4.2.4 Protein Adsorption

The NanoOrange assay was used to measure the protein absorbance of the substrates, specifically fibronectin and laminin (Figure 4-9). Both proteins are abundant in the ECM of skeletal muscle tissue. TCP was also measured as a standard due to its use *in vitro* for cell adhesion and subculture. Overall, >64% of both the proteins were adsorbed on to the substrates. Not all of the substrates could match the TCP, however, the multi-layered substrates were found not to be significantly different. Protein adsorption is important for the adhesion of cells on to biomaterials (Bacakova *et al.*, 2011).

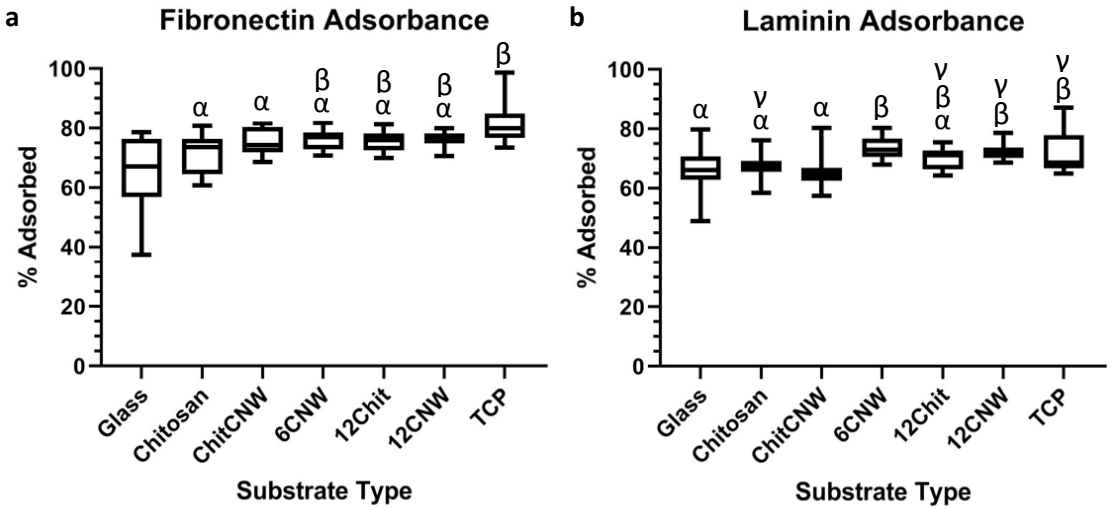

Figure 4-9: Box whisker plots of the percentage of (a) fibronectin and (b) laminin adsorbed on to the range of multilayer substrates. The data was calculated from fluorescence readings using the NanoOrange assay. The NanoOrange assay was carried out twice (N=2) and in triplicate each time (n=3). Data analysis carried out using ordinary one-way anova with Turkey's multiple comparison tests with a single pooled variance. Greek labels indicate groups within which no significant difference was observed. For those that are significantly different = $p < 0.05$.

4.3 Discussion of the Characterisation of the CNW Substrates

4.3.1 Material Characterisation

Confirmation of the quality of cellulose and the nanowhiskers produced was by FTIR. Comparisons made to samples used in previous work and that of Mitchell et al, 1993 (Michell, 1993), showed that the cellulose used in this work was Type Iβ cellulose. This is in agreement with results found by Favier et al, 1992, and Belton et al, 1988, who both confirm Type Iβ cellulose is found in tunicates, which is the higher crystalline form of cellulose I (Belton *et al.*, 1989; Favier, Chanzy and Cavaillé, 1995). The CNWs were produced through partial acid hydrolysis using sulphuric acid to cleave the amorphous regions of the cellulose, leaving behind crystal aggregates of high aspect ratio. The use of sulphuric acid resulted in the presence of sulphate esters on the whiskers, which are responsible for giving the CNWs the slight negative charge suggested by Revol et al and proven by Dugan et al (Revol *et al.*, 1992; Dugan *et al.*, 2013). XPS was used to confirm the presence of sulphur on the CNWs produced in this work and they were only present on substrates that contained CNWs. The Glass and Chitosan substrates did not show any presence of sulphur and therefore it can be confirmed that the sulphur presence is due to the whiskers.

The length and height of the CNWs were determined using AFM and compared to other studies which derived CNWs through partial acid hydrolysis. The dimensions of the whiskers depend on the source of the cellulose and its type (Eichhorn, 2011). Height and width are considered to be comparable due to the rod like shape of the whiskers. Dugan found that the width measured through TEM and the heights measured through AFM were not significantly different (Dugan *et al.*, 2013). Elazzouzi-Hafraoui, Angles and Favier all produced CNWs from tunicin sources with a width of 10-20 nm and typical lengths ranging from 100s nm to 1-2 µm (Favier, Chanzy and Cavaillé, 1995; Anglès and Dufresne, 2000; Elazzouzi-Hafraoui *et al.*, 2008). These widths are bigger than the ones measured in this project and those of Dugan and Nikoi. Dugan measured mean widths of 6.6 nm ± 1.2 nm (standard deviation) and mean heights of 5.5 nm (Dugan *et al.*, 2013) whilst Nikoi measured mean heights of 4.8 nm with mean lengths of 0.64 µm (Nikoi, 2016). It is suggested that the dimensions of the CNWs may also be dependent on tunicin species. The mean heights of the CNWs in this work were measured as 5.10 nm ±0.49 nm and the mean lengths as 0.50 µm ±0.67

µm, which are similar to those of Dugan's and Nikoi's. The species of tunicate used in this work and Nikoi's is *Ascidiella aspersa* and in Dugan's it was a mixture of *Halocynthia roretzi* and *Ascidiella aspersa*. The tunicate species has not been stated in the other literature studied here. This difference could be the reason for the slight differences in CNW dimensions.

The data compiled in this section prove that the nanowhiskers produced in this work were comparable to those used in previous work. The FTIR shows that the cellulose used is highly crystalline and produces a slightly negatively charged solution of CNWs of a high aspect ratio.

4.3.2 Substrate Characterisation

Multilayer substrates of CNWs and chitosan were built on glass cover slips. The layers were assembled using the layer-by-layer (LbL) technique using the polyelectrolyte properties of the CNW and chitosan solutions. This concept was adopted from Decher et al by Nikoi who applied it using the dip coating method (Decher, Hong and Schmitt, 1992). Nikoi (2016) produced polyelectrolyte multilayers composed of CNWs, chitosan and PSS. However, it was discovered that the increased layers of PSS had a cytotoxic effect on the cells (Nikoi, 2016). This work focuses on the multilayers of CNW and chitosan with the terminating layer that of oriented CNWs.

The spin coating used by Dugan et al (Dugan, Gough and Eichhorn, 2010) was improved by Nikoi and it is those parameters that are used in this work. Alignment of the CNWs was checked through AFM as the whiskers are too small to be observed through a light microscope. Of the oriented CNWs, 27.52% of the whiskers were within ± 10^{o} of 0^{o} whereas the unaligned surface only had 8.90% of its whiskers within the same range. Both surfaces had whiskers oriented at a large range from 0^{o} however the distribution of the angles for the oriented whiskers is narrower than the unaligned. It is noticeable that not all of the oriented whiskers are aligned at the exact same angle; instead the alignment is produced from the collective mass of whiskers roughly angled in the same direction. From previous work, it has been suggested that the cell response to the alignment is to the bulk effect of the orientation, not individual whiskers (Dugan, Gough and Eichhorn, 2010). Odd whiskers at completely different angles may not have an effect on the bulk alignment of the cells.

The roughness, wettability and protein adsorption potential of the multilayers were investigated. Roughness when quantified measures the difference in heights of peaks/features across a surface. The area surface roughness (Sa) was measured on the full range of substrates. The thinner substrates had very low roughness (Sa < 10 nm) compared to the multilayers where the averages were more than triple and had a greater range. In the literature, the roughness is often measured as the profile of surface roughness (Ra). This value is not directly comparable to Sa however their magnitudes are very similar and an approximate comparison can be made. Other studies have found that polymer films have Ra values <100 nm (Ricotti *et al.*, 2010), patterned topographies with features um in size have Ra values in the 100s of nm range (Shimizu, Fujita and Nagamori, 2009) and 3D scaffolds, such as fibres, can have Ra values in the 100s of um range (Yang, Lee and Kim, 2019). The examples chosen are all materials being developed towards the engineering of skeletal muscle tissue, showing that a wide range of topographies can be used to direct myoblast differentiation. In this case, the roughness of the ChitCNW substrate is due to the CNWs (Sa = 7.72 nm ± 1.85 nm), which is a little rougher than just Chitosan (Sa = 7.10 nm ± 1.11 nm) and Glass (Sa = 6.28 nm ± 0.88 nm), though not significantly different. On the other hand, the increased roughnesses of the multilayer substrates are due to the undulating surface caused by the LbL deposition and not just by the composition of the top layer (6CNW = 33.92 nm ± 16.99 nm, 12Chit = 37.64 nm ± 14.45 nm and 12CNW = 42.09 nm ± 12.81 nm).

Contact angle is used to determine the wettability of a surface. Hydrophilic surfaces have low contact angles whereas hydrophobic surfaces have contact angles >100^{o} (Bacakova *et al.*, 2011). Glass is plasma treated, clean, very smooth and hydrophilic, proven by a low contact angle (10.49^{o} ± 5.90^{o}). The possible reason for the significant difference between ChitCNW, 6CNW and the others substrates could be the chitosan content. Chitosan films have been reported to have a contact angle of around 70^{o} (Bumgardner *et al.*, 2012). This agrees with the contact angles averaged in this work for the chitosan topped substrates (Chitosan = 67.60^{o} ± 6.41^{o}, 12Chit = 67.66^{o} ± 13.34^{o}). There is less research on the contact angle of CNWs, however, the slight negative charge of the sulphate ester groups could be responsible for the lower contact angles measured for the ChitCNW (57.85^{o} ± 5.71^{o}) and 6CNW (56.67^{o} ± 14.09^{o})

substrates. The lower contact angles suggest the CNW surface is slightly more hydrophilic than the chitosan. Although the 12CNW multilayer's terminal layer is the CNWs, the increased chitosan content could balance out the hydrophilic effect seen on the other CNW topped substrates as the contact angle for the 12CNW multilayer ($70.85^{o} \pm 3.39^{o}$) was similar to that of the 12Chit.

The adsorption of proteins on to a surface is important in all biomedical material applications. Exposure to cell media, blood or cell deposited proteins, leads to the spontaneous adsorption of ECM proteins on to biomaterial surfaces in order to mediate cell adhesion (Bacakova *et al.*, 2011).The NanoOrange assay was used to quantify the protein adsorption on the substrates after incubation with laminin and fibronectin; two proteins chosen due to their role in the ECM of the skeletal muscle tissue (Marieb and Hoehn, 2014). TCP was used as the control as it has been designed to support the attachment of adhesive cells for study *in vitro*. TCP showed the most protein adsorption and glass had the largest range. The multilayer substrates showed no significant difference to the TCP, adsorbing >75% of fibronectin and >70% of the laminin in solution. Overall the protein adsorption on the substrates was greater than 64% for fibronectin and >65% for laminin. There was only a slight difference in the adsorption of fibronectin and laminin and it was not significant. Glass had the lowest adsorption percentage for both types of proteins. Protein adsorption was measured to see if there was a difference in levels of proteins adsorbed due to substrate type and although small, an increase was seen between the thinner layered substrates and the multilayers. It is also of interest to see if the addition of ECM proteins to the substrates would improve cell response; this is investigated in Section 6.2.2.

Roughness and wettability could have an influence on protein adsorption. Adsorption on to different types of surface occurs in response to a combination of factors, roughness and wettability only being two (Bacakova *et al.*, 2011). The multilayer substrates used in this work have a low roughness with Sa values in the nano-meter range, which appear to have little influence on the protein adsorption. However nano-roughness is suggested to be preferential for protein adsorption as the nano-features are more representative of the ECM proteins native to tissue structure (Webster *et al.*, 2000; Price *et al.*, 2004). Therefore, the range of roughness of the substrates may be too small to see a difference in protein adsorption through this technique and a

difference may be more obvious through cell response. The wettability of the multilayer substrates might have more of an influence on protein adsorption due to the slight charges on the polyelectrolyte layers. Extremely hydrophilic (contact angles <5^{o}) and extremely hydrophobic (contact angle >100^{o}) surfaces have a negative effect on protein adsorption and it is suggested that moderate hydrophilic surfaces are the most optimal (Bacakova *et al.*, 2011). Highly hydrophilic surfaces can adsorb too many proteins resulting in the proteins obstructing each other's binding sites and reducing cell adhesion. However, if the protein adsorption is too low, the protein-cell interactions may not be significant enough to promote cell adhesion. Highly hydrophobic surfaces can adsorb proteins however they are rigid and denature, making them useless for cell adhesion. The balance is moderate hydrophilic surfaces where proteins are more flexible and their binding sites are open and more easily recognisable for cell interactions (Bačáková *et al.*, 2004; Lim *et al.*, 2007).The contact angles measured for these substrates are between hydrophilic and hydrophobic, slightly leaning towards hydrophobic. This could be an optimum range of wettability for good protein adsorption.

Cell response to roughness and wettability in the literature ranges depending on the cell type and the wide variety of biomaterials being applied. Some have found the ideal wettability for cell adhesion and culture to be around 80-90^{o} depending on the cell type (Clem *et al.*, 2008; Kopecek *et al.*, 2008), however, other factors could positively influence increased cell adhesion. This is promising for the multilayer substrates used here. However, the general consensus is that it is the adsorption of proteins before cell adhesion that is the main influence. This is also suggested about the relationship between roughness and cell adhesion; it is the adsorption of proteins from the media on the surface topography that influences a cell's adhesion *in vitro* (Bacakova *et al.*, 2011). The cell itself is attaching to integrin binding sites on the ECM proteins such as fibronectin or laminin (Lee *et al.*, 2015).

Cell response was investigated on the full range of substrates examined in this section through the application of different cell lines. The adsorption of proteins to the multilayer substrates and the cell response to the combination of nanotopography and ECM protein are also explored.

Chapter 5: Cell Response to the Cellulose Nanowhiskers Substrates

5.1 Chapter Summary

The responses of three cell types are explored in this chapter. There were different degrees of success in reaching fully differentiated myotubes. C2C12s are an immortalised mouse myoblast cell line often used in the testing of skeletal muscle engineering and can differentiate readily in response to differentiation media on a range of surfaces. The oriented topography of the CNWs was used to improve the broad alignment of the formation of myotubes to better emulate basic skeletal muscle structure. Primary cells are harder to grow in 2D environments as they are extracted from human tissue which is of a 3D environment. The use of primary cells (hSkMCs and BM-MSCs) was to examine the initial response and observe if the cells responded to the oriented CNWs. The application of the multilayers was to reduce the effect of the glass and provide a softer layer to support cell proliferation.

5.2 Application of C2C12s

Many studies have used C2C12s in the development of materials for skeletal muscle tissue engineering (Sengupta *et al.*, 2012). They have been proven by Dugan et al to respond to the CNWs and to some PEMs by Nikoi (Dugan, Gough and Eichhorn, 2010; Dugan *et al.*, 2013; Nikoi, 2016). It is of interest if these cells can respond similarly to substrates composed of multilayers of chitosan and CNW.

5.2.1 C2C12 Viability

C2C12s were cultured on the full range of substrates for a period of 7 days. The myoblasts were observed to start aligning on the oriented surfaces after 24 h. Alamar Blue and PicoGreen were used to monitor the viability of the cells over the full time period. Cells were seeded in growth media and switched to differentiation media through partial media changes every day after 24 h.

The Alamar Blue assay measures the metabolic activity of the cells (Figure 5-1). The metabolic activity of the C2C12s shows a large increase from Day 1 to Day 3 followed

by a decrease from Day 3 to Day 7. When myoblasts differentiate, they can no longer proliferate (Chargé and Rudnicki, 2004; Huang *et al.*, 2006). Differentiation has been observed from Day 4 therefore the decrease in metabolic activity could be from the reduced number of cells proliferating. Data analysis was carried out between certain substrates at each time point (see Section 3.4). No significant difference was found between Chitosan and ChitCNW, 12Chit and 12CNW and between the increasing number of bilayers, ChitCNW, 6CNW and 12CNW at any time point.

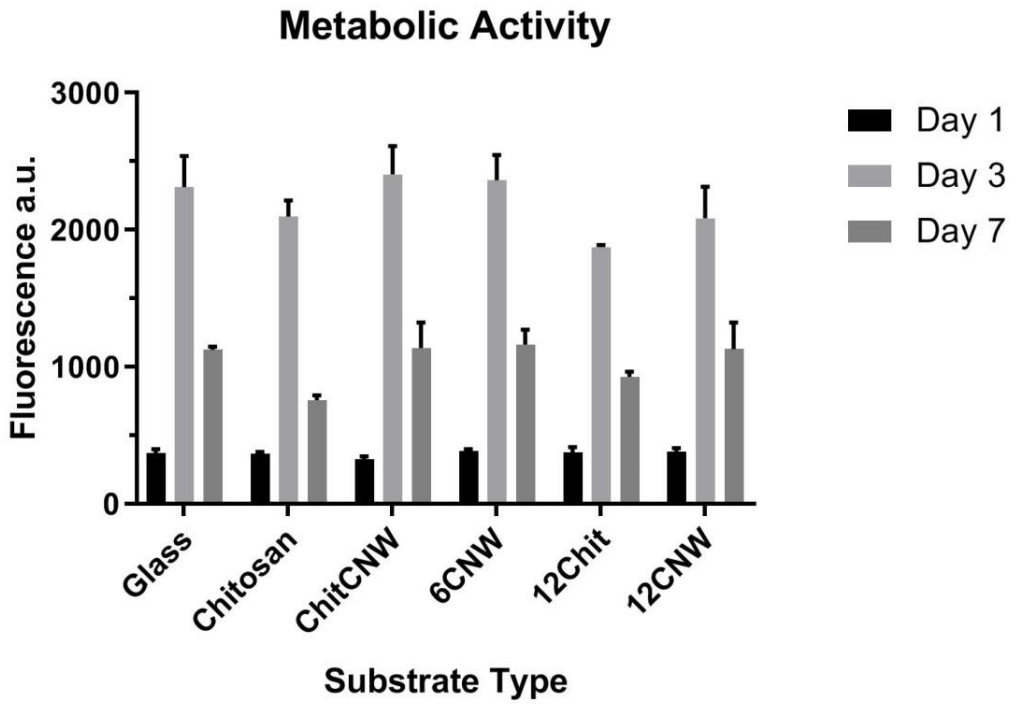

Figure 5-1: Metabolic activity of C2C12s on the full range of substrate types across 3 time points using the Alamar Blue assay. The assay was run 4 times using C2C12s of different passages and also by a Masters student. The data shown is a representative of the trend given by 3 of the 4 sets of data (all sets can be found in Figure 5-2 and Appendix A). The metabolic activity on TCP also followed a similar trend.

Alamar Blue was carried out on the C2C12s on each substrate type a total of 4 times. Although every effort was made to ensure each experiment was carried out the same, variables between sets include the passage number of the cells, general experimental and human inconsistency. All the data collected is shown in Figure 5-2. This data could not be collated due to the different magnitudes of the fluorescence readings.

Therefore the main information gathered from this data are the trends observed. Each set was compared per substrate type and the most representative set is shown in Figure 5-1.

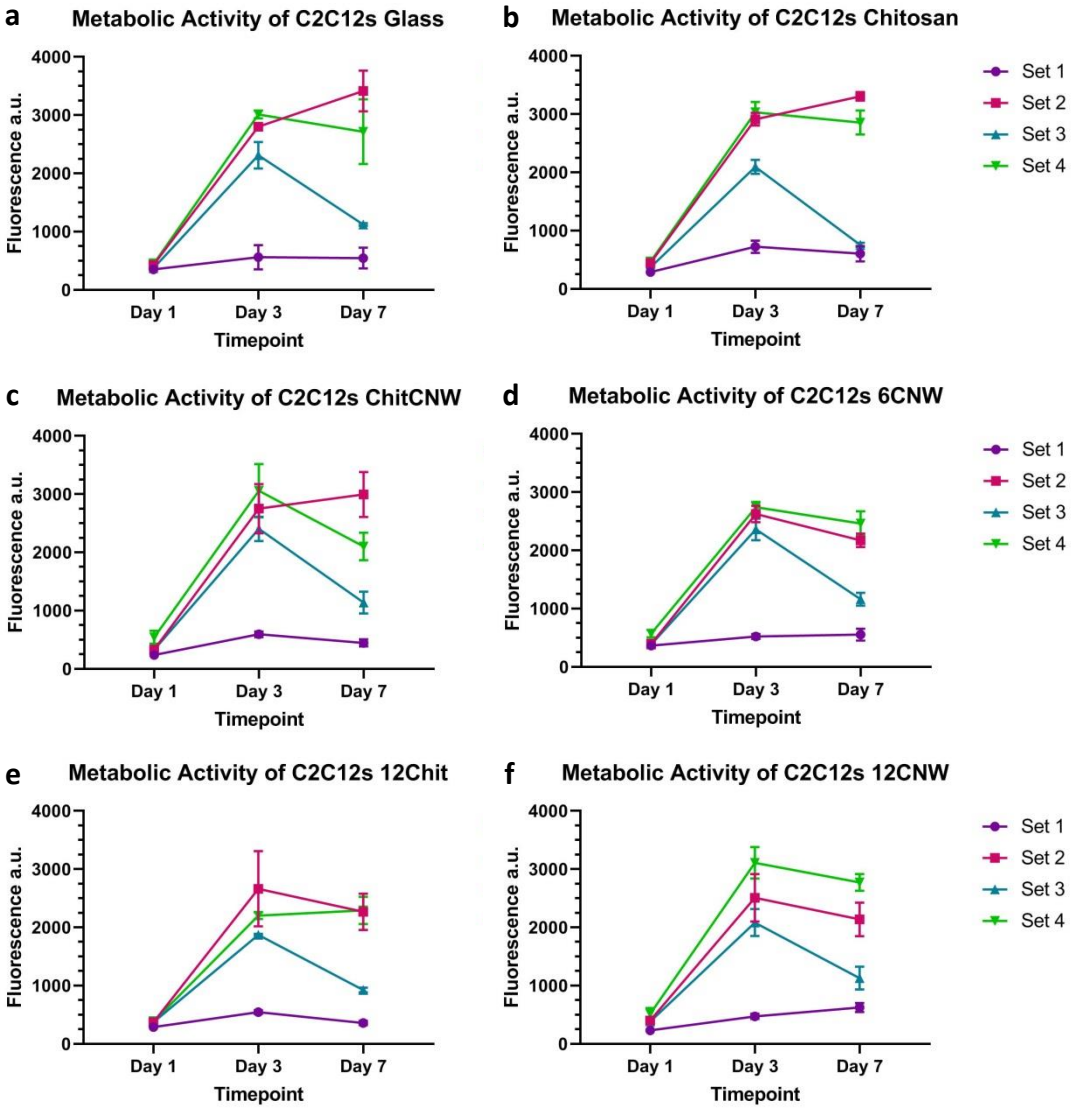

Figure 5-2: Metabolic activity of C2C12s on the full range of substrates at different time points over a 7 day period. The experiment was carried out in triplicate 4 times shown per substrate type as Sets. Error bars are the standard deviation. (a) Glass, (b) Chitosan, (c) ChitCNW, (d) 6CNW, (e) 12Chit and (f) 12CNW

The mean population doubling time was calculated from the Alamar Blue data using the equation given in Section 3.3.4 and shown in Figure 5-3. Little difference was seen between the substrates; however there was a significant difference between the

ChitCNW and 12 multilayer substrates (12Chit and 12CNW). The mean population doubling time increase by a small fraction as the number of layers increased.

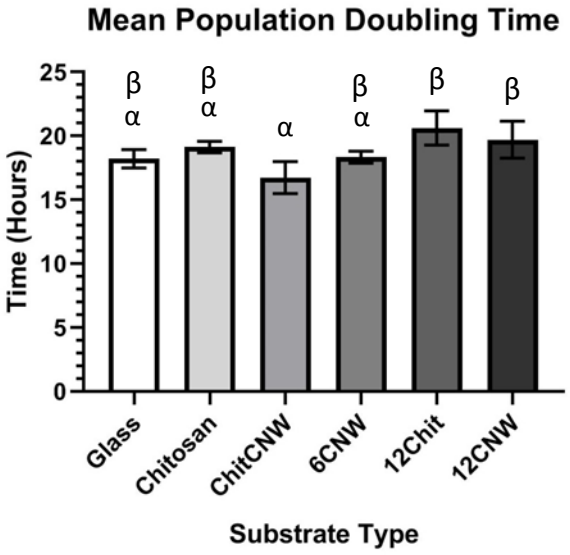

Figure 5-3: Mean Population doubling time with SD calculated with the equation found in Section 3.3.4. Data analysis carried out using ordinary one-way anova with Turkey's multiple comparison tests with a single pooled variance. Greek labels indicate groups within which no significant difference was observed. For those that are significantly different = $p < 0.05$.

The PicoGreen assay was used to measure cell number and Day 1, 3 and 7 (Figure 5-4). The cell number of the C2C12s was shown to increase over the 7 days. The rate of increase slows between Day 3 and Day 7, most likely due to the drop in proliferation rate and therefore there are fewer cells proliferating. An increase is still seen between Day 3 and 7 as although the rate of increase is lower than between Day 1 and 3, there are more cells on Day 7 compared to 3. Data analysis was carried out between certain substrates at each time point (see Section 3.4). No significant difference was found between Chitosan and ChitCNW and between the increasing number of bilayers, ChitCNW, 6CNW and 12CNW at any time point. The only significant difference was found between 12Chit and 12CNW on Day 3 where there is a much larger cell number on Day 3 for 12CNW compared to 12Chit.

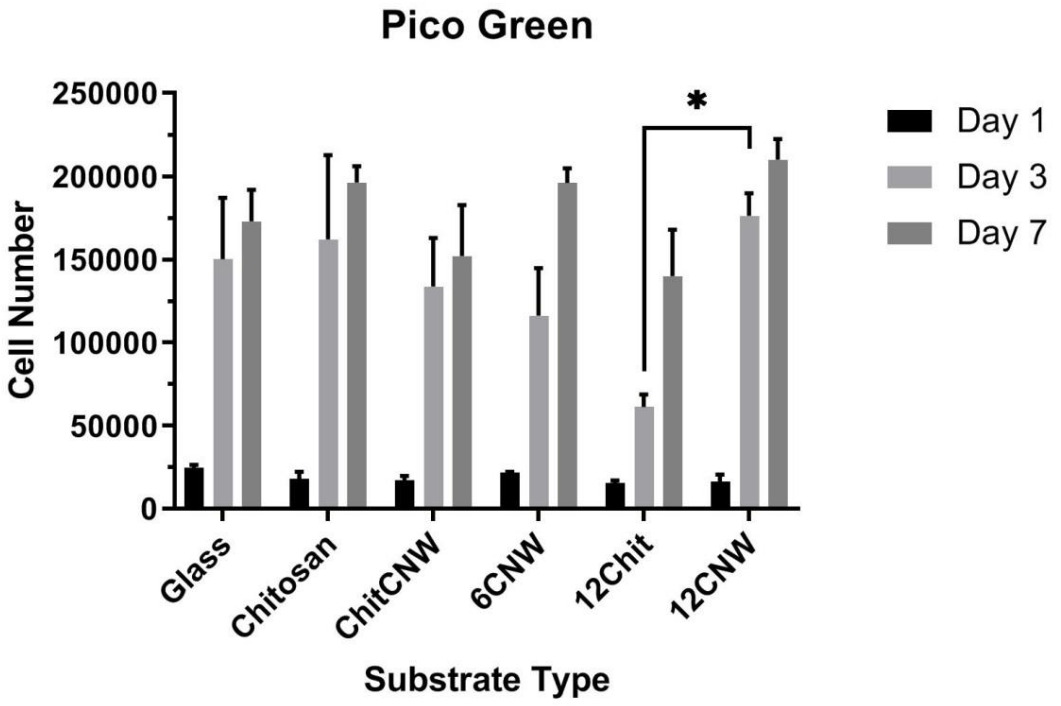

Figure 5-4: Cell number of C2C12s on the full range of substrate types across 3 time points using the PicoGreen assay. The assay was run 4 times using C2C12s of different passages and also by a Masters student. The data shown is a representative of the trend given by 3 of the 4 sets of data (all sets can be found in Appendix B). The cell number on TCP also followed a similar trend. Data analysis carried out using RM two-way anova with the Geisser-Greenhouse correction and with Turkey's multiple comparison test. For those that are significantly different (*) = $p < 0.05$.

As with the Alamar Blue data, the Pico Green assay was repeated 4 times and had the same variability in the repeats. Figure 5-5 shows all the repeated sets of the data of the cell number of the C2C12s on the full range of substrates. Each set was compared per substrate type and the most representative set is shown in Figure 5-4.

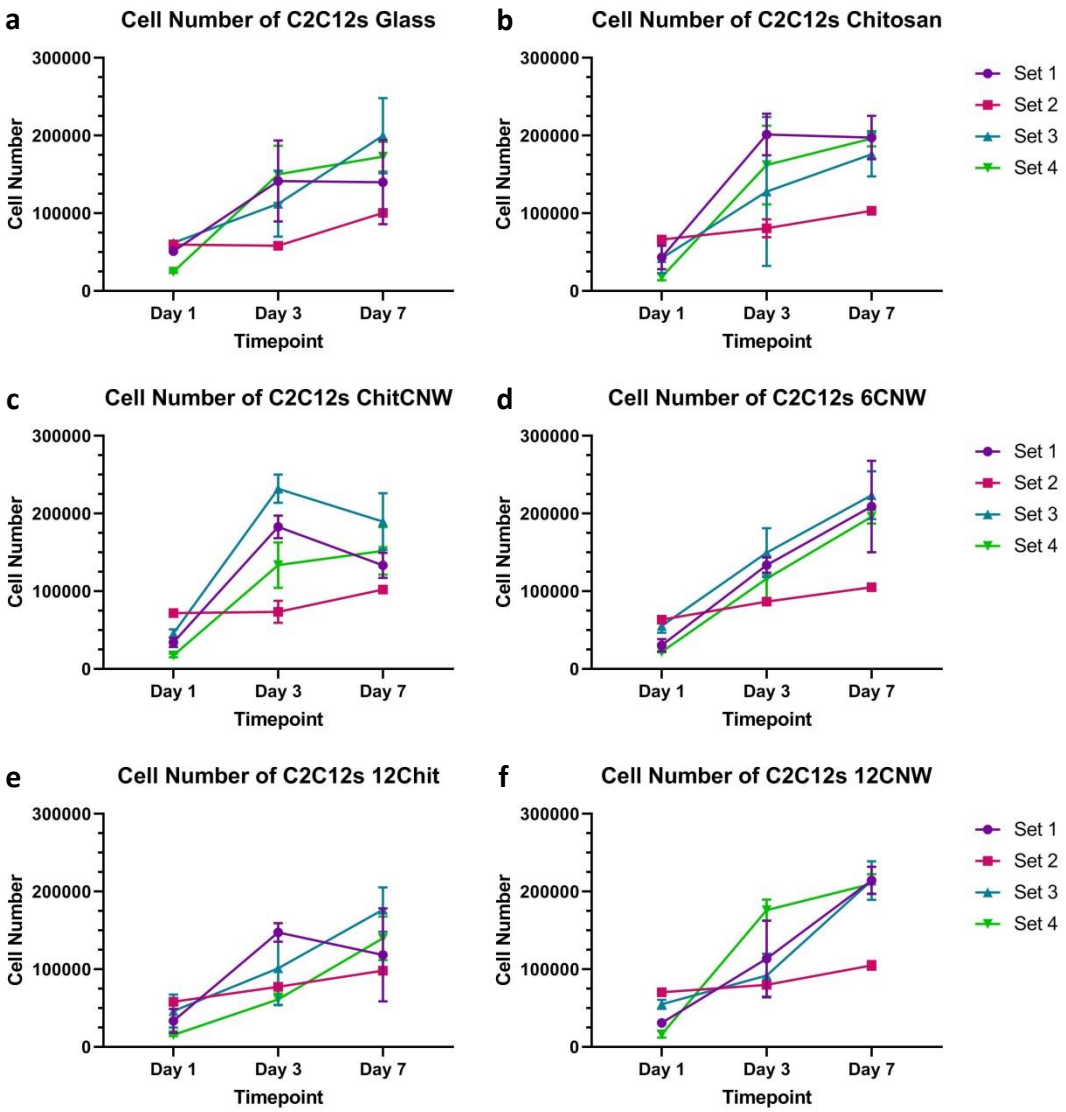

Figure 5-5: Cell number of C2C12s on the full range of substrates at different time points over a 7 day period. The experiment was carried out in triplicate 4 times shown per substrate type as Sets. Error bars are the standard deviation. (a) Glass, (b) Chitosan, (c) ChitCNW, (d) 6CNW, (e) 12Chit and (f) 12CNW

After 24 h, the C2C12s could be seen spreading across all of the substrates (Figure 5-6). Alignment of the cells can already be seen on the substrates with spin coated CNWs and they appear to have a higher cell density on the multilayer substrates. The higher cell density on the 6CNW and 12CNW multilayers is also shown by the higher number of nuclei per area and the higher surface coverage (Figure 5-6 (a) and (b) respectively), which were found to be significantly different to the other substrates.

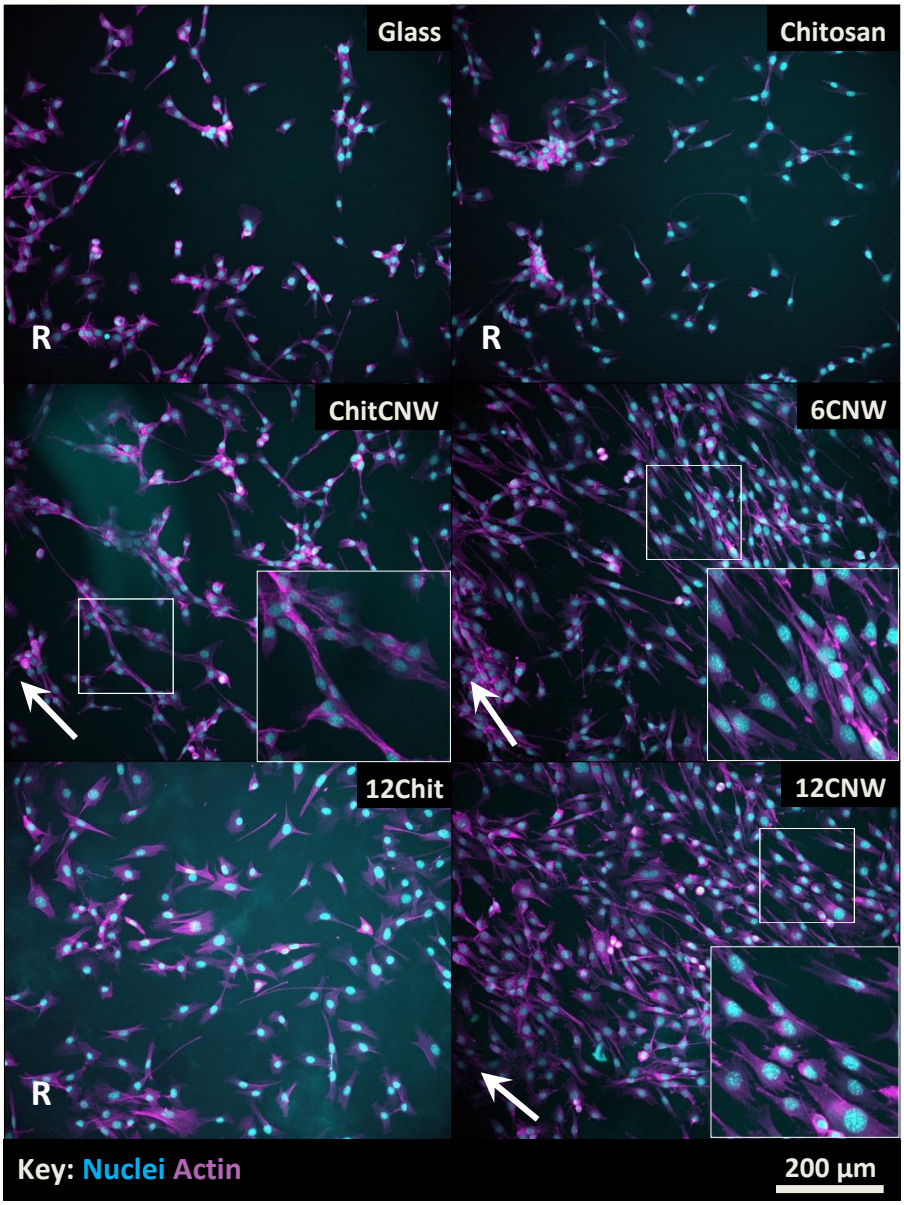

Figure 5-6: Confocal fluorescence micrographs of C2C12s on each substrate type 24 h after seeding, taken at 20x mag. The arrows indicate the general direction of the cell alignment and the R denotes where the cells are randomly oriented. Substrates named with CNW have the oriented topography. Cells can be seen elongating and aligning on the oriented substrates (ChitCNW, 6CNW and 12CNW).

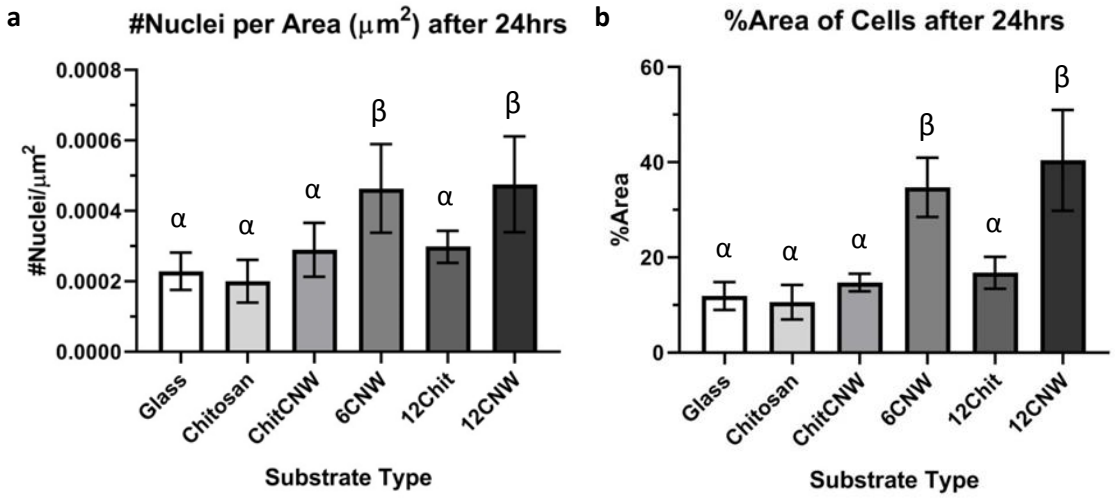

Figure 5-7: (a) The mean number of nuclei per area (μm^2) with SD on each substrate type and (b) the surface coverage of the C2C12s on each substrate type, shown as mean %Area with SD, both 24 h after seeding. Data analysis carried out using ordinary one-way anova with Turkey's multiple comparison tests with a single pooled variance. Greek labels indicate groups within which no significant difference was observed. For those that are significantly different = $p < 0.05$.

5.2.2 C2C12 Differentiation and Myotube Formation

Differentiation media was added to the C2C12s through partial media changes 24 h after seeding. Confocal fluorescence micrographs were taken at Day 7 to investigate the differentiation of the myoblasts and myotube formation (Figure 5-8). Broad alignment of the differentiated C2C12s can be seen on the oriented CNW substrates whereas only local alignment can be seen on the Glass and chitosan topped substrates.

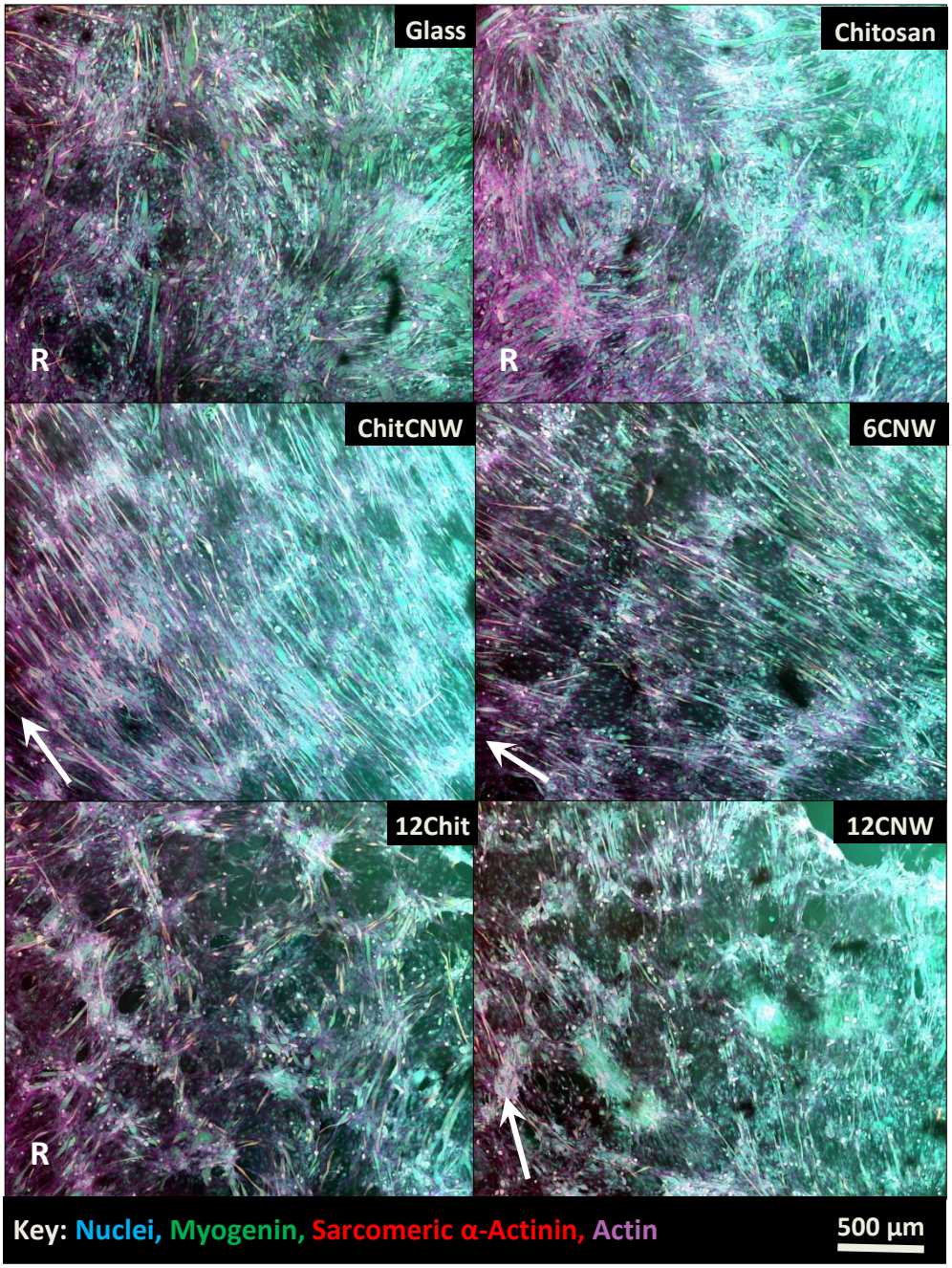

Figure 5-8: Confocal fluorescence micrographs of C2C12s on each substrate type 7 days after seeding, taken at 20x mag and stitched together in maps of 3x3. The arrows indicate the general direction of the cell alignment and the R denotes where the cells are randomly oriented. Substrates named with CNW have the oriented topography. Differentiation of C2C12s into myotubes along with local alignment can be seen on all the substrate types. Broad alignment was observed on the oriented substrate types only.

Myotube length was measured using the sarcomeric alpha actinin channel on ImageJ because this protein is present only in differentiated fused cells or cells beginning to fuse that make up the myotube. Due to this method, a large population of myotubes were measured at approximately 25 µm as individual cells were starting to fuse but

had not quite joined yet. Therefore, the number of myotubes over 100 µm was extracted as this data could not be seen in the full histograms and it is the formation of myotubes above 100 µm that is of interest. Figure 5-9 shows that the oriented substrates ChitCNW and 6CNW have the highest number of myotubes over 100 µm and that the range is over 400 µm.

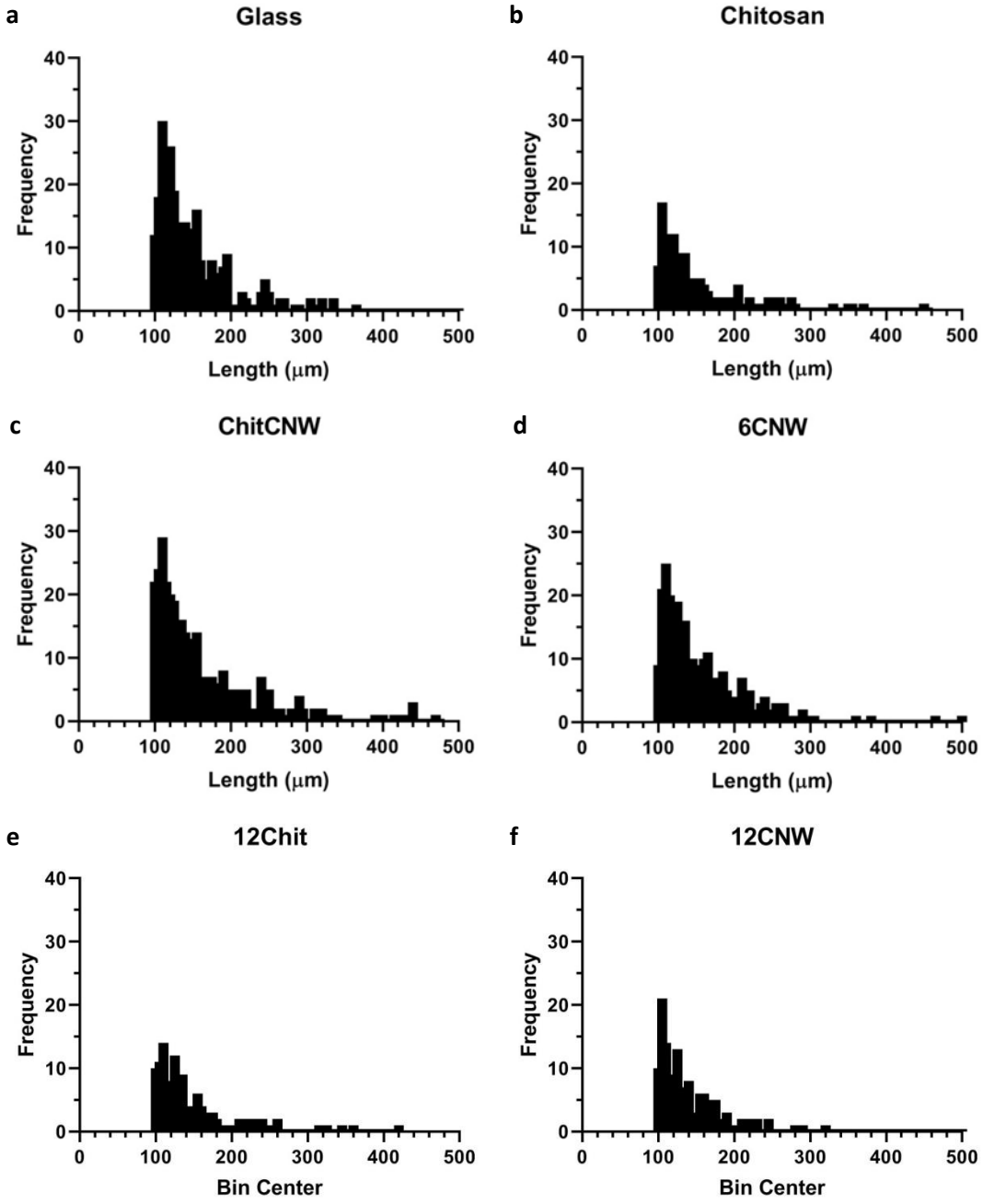

Figure 5-9: The average myotube length was measured on all substrate types. Full histograms can be found in Appendix C where the average myotube length was around 25 µm. There was a larger population of myotubes of this length which over shadowed the data of the longer tubes. Measurements of myotubes >100 µm were extracted for each substrate type (a) Glass, (b) Chitosan, (c) ChitCNW, (d) 6CNW, (e) 12Chit and (f) 12CNW.

To show the distribution of the longer myotubes, the percentage of myotubes over specific lengths were calculated and shown in Table 5-1. ChitCNW and 6CNW had a larger number of counts as there were a higher number of cells undergoing differentiation (Figure 5-10) which is also shown by the higher percentage of myotubes over 200 µm compared to the unaligned substrates. On the histograms shown in Figure 5-9, Glass also has a high number of counts above 100 µm however the total number of counts is much lower than ChitCNW and 6CNW. Therefore, it is possible that overall there is more cells differentiating on the oriented substrates and therefore more sarcomeric alpha actinin compared to the Glass surface. 12CNW, although oriented, has the lowest number of counts, possibly to the aggregation of cells explored further in the discussion.

Substrate Type	Total Count	>50µm (%)	>100µm (%)	>200µm (%)
Glass	3181	24.58	9.12	1.16
Chitosan	3000	20.57	4.83	0.87
ChitCNW	5646	20.40	6.09	1.35
6CNW	5430	17.20	4.86	0.98
12Chit	2839	16.80	4.47	0.60
12CNW	2247	27.73	6.50	0.62

Table 5-1: The percentage of myotubes above specific lengths show the distribution of the myotube lengths over 25 µm.

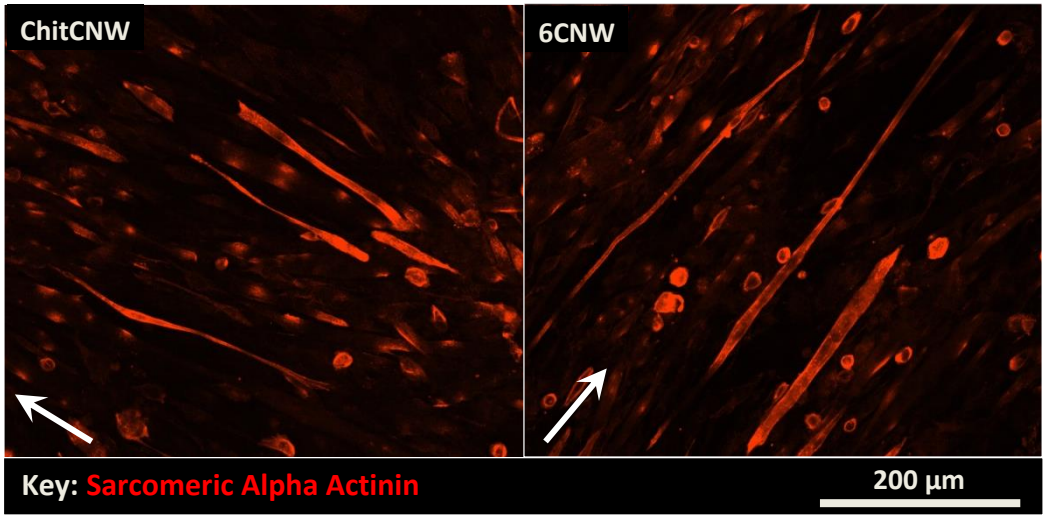

Figure 5-10: Confocal fluorescence micrographs of C2C12s on ChitCNW and 6CNW substrates 7 days after seeding, taken at 20x mag. This channel shows only the sarcomeric alpha actinin which was used to measure the lengths of the myotubes. The arrows indicate the general directions of the cell alignment.

Alignment of myotubes, as an important feature of the basic skeletal muscle tissue structure, was measured using again the data collected through ImageJ of the sarcomeric alpha actinin channel. The radial graphs show the normalised angles of the myotubes and the data for all of the substrate types are summarised in the box graph (Figure 5-11). The ChitCNW and 6CNW had the narrower boxes confirming that the myotubes are aligned on the orientated topography however the 12CNW did not show the same degree of alignment.

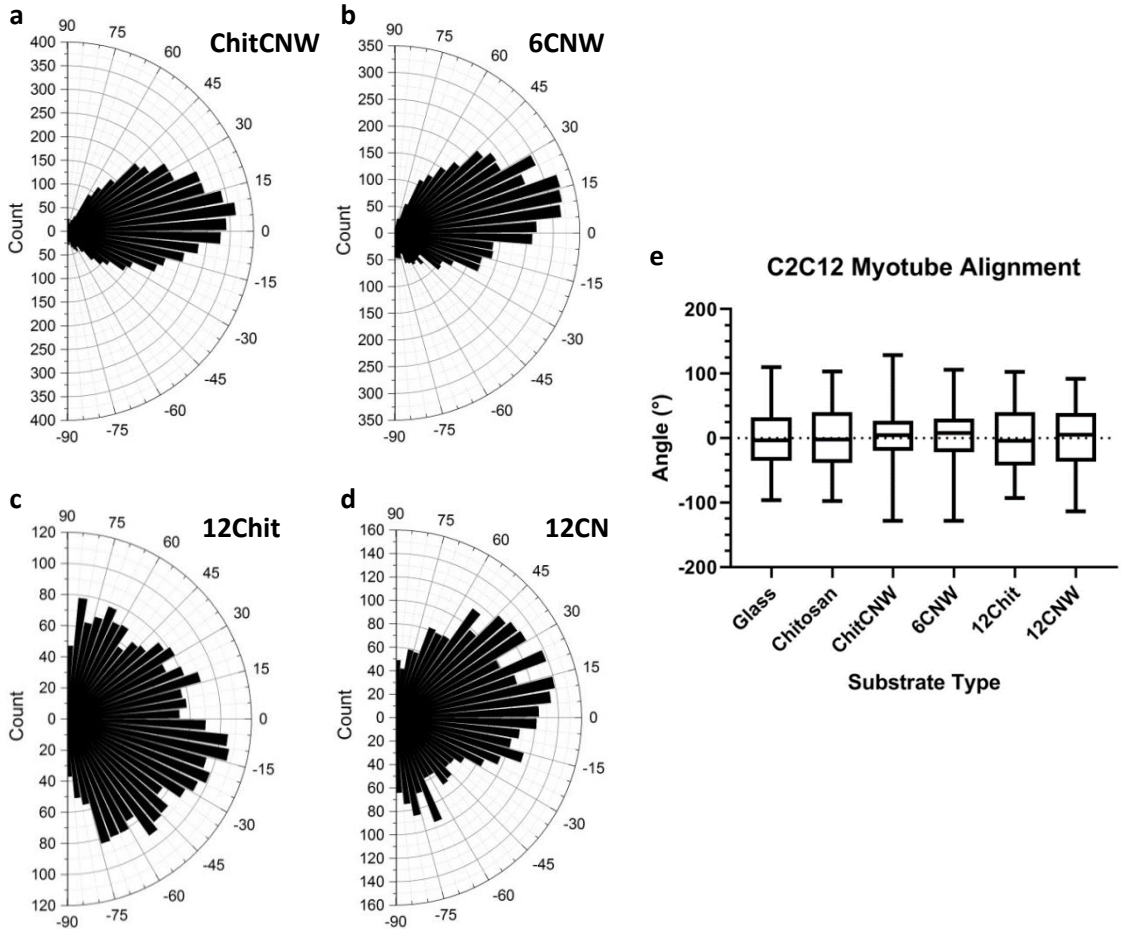

Figure 5-11: Alignment of the myotubes was measured on each substrate type. Radial graphs show normalised data on the (a) ChitCNW, (b) 6CNW, (c) 12Chit and (d) 12CNW multilayer substrates. The distribution of the angles from 0^{o} is shown by the box whisker graph (e) for the full range of substrate types. A smaller box shows that most of the data (angles) is in a narrower range and therefore the cells are more aligned. A larger box shows that most of the data (angles) is in a wider range and therefore the cells are not as aligned.

The confocal fluorescence micrographs (Figure 5-12) were further used to measure the percentage area coverage of sarcomeric alpha actinin, the percentage of myogenin positive nuclei and the mean number of nuclei per myotube (Figure 5-13 (a), (b) and (c) respectively). As mentioned before, sarcomeric alpha actinin and myogenin are positive indicators for myogenesis and have been quantified. ChitCNW and 6CNW substrates have the highest percentage of sarcomeric alpha actinin coverage which is not surprising given the myotube length data. Glass is also quite high however surprisingly, so is the 12CNW multilayer which suggests that although there is less quantified alignment, there still is a high number of cells differentiating. The only significant difference was between the 6CNW and the chitosan topped substrates. The percentages of myogenin expressing nuclei on Glass and 6CNW substrates were found significantly different to those on ChitCNW and 12CNW. This was unexpected as it does not quite follow the trend in data seen so far. The number of nuclei per myotube was shown to be high on the Glass and the oriented substrates compared to the unaligned chitosan topped substrates. Interestingly, myotubes on the Glass had high numbers of nuclei, however it was noticed that the tubes were not always one nucleus thick. An example is shown in Figure 5-13 (d) where the myotube on ChitCNW is one nucleus thick compared to the myotube on Glass.

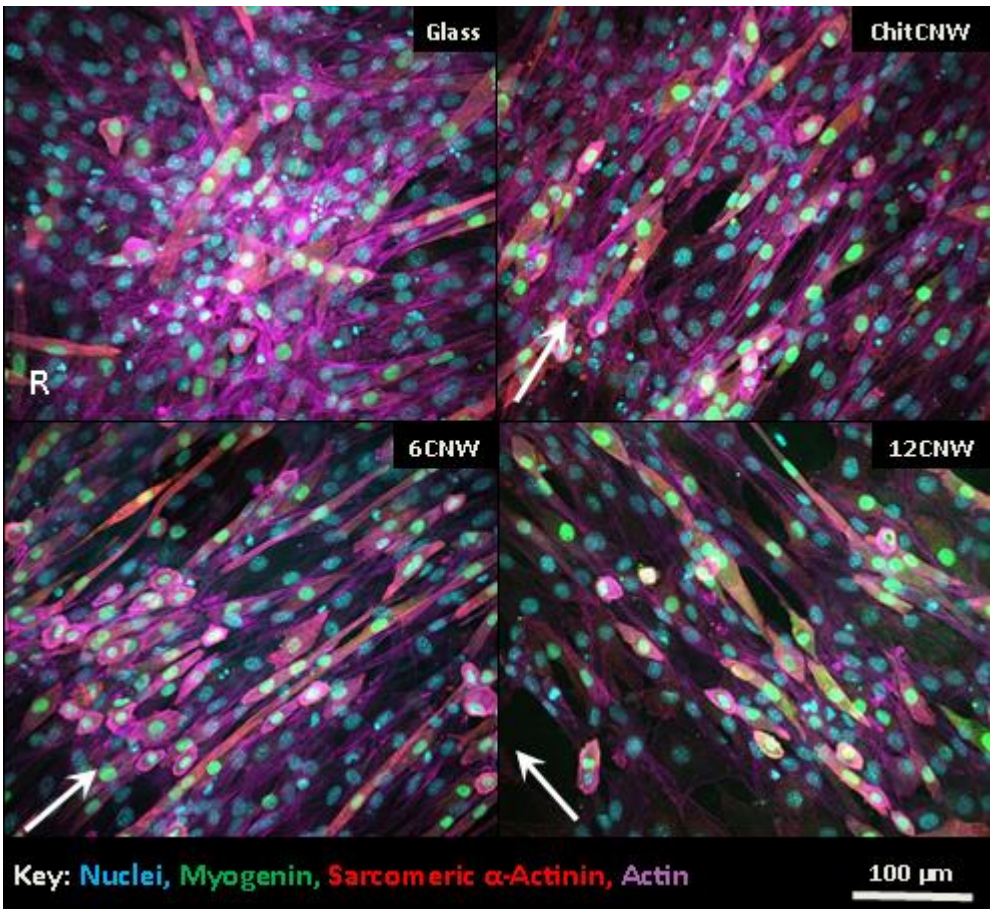

Figure 5-12: Confocal fluorescence micrographs of C2C12s on each substrate type 7 days after seeding, taken at 40x mag. Multinucleated tubes can be seen forming where there is sarcomeric alpha actinin (red) and myogenin positive nuclei (green). The arrows indicate the general direction of the cell alignment and the R denotes where the cells are randomly oriented. Substrates named with CNW have the oriented topography.

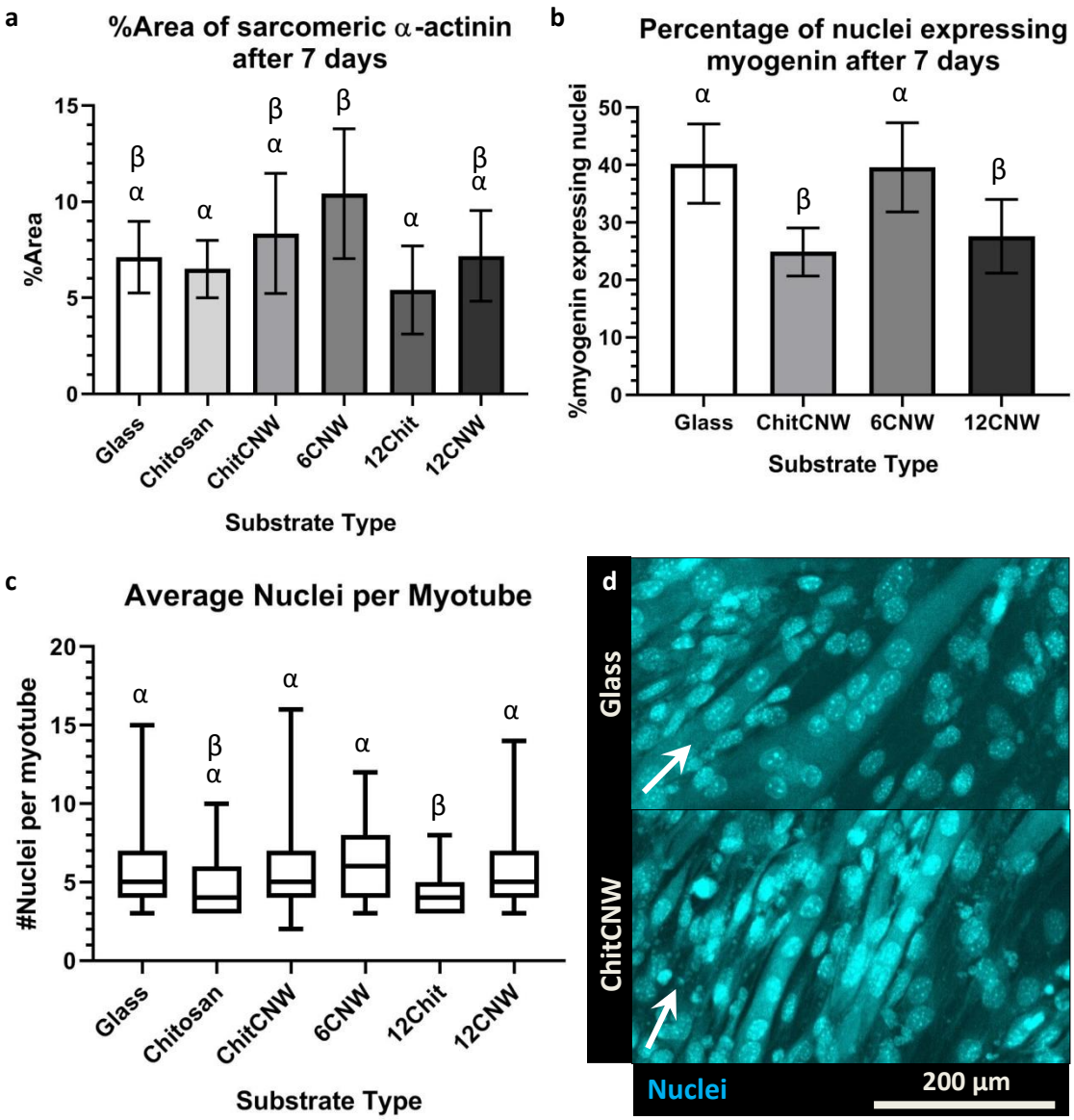

Figure 5-13: Differentiation of the C2C12s was measured on day 7 by (a) the percentage area coverage of sarcomeric alpha actinin, (b) the percentage of nuclei expressing myogenin and (c) the average number of nuclei per myotube on all substrate types. (d) Confocal fluorescence micrographs of myotubes on Glass and ChitCNW substrates showing the difference in nuclei arrangement in the myotube. Data analysis carried out using ordinary one-way anova with Turkey's multiple comparison tests with a single pooled variance. Greek labels indicate groups within which no significant difference was observed. For those that are significantly different = $p < 0.05$.

5.3 Application of hSkMCs

C2C12s have been proven to align and differentiate on the oriented CNWs. As an immortalised cell line, C2C12s are often used in the literature compared to primary hSkMCs which are not as frequently used. hSkMCs can be obtained through biopsies of skeletal muscle tissue from human donors. The cells used in this work were bought from PromoCell who sourced their hSkMCs from different muscles of adult donors. The cells are tested for sarcomeric myosin and confirmed negative for smooth muscle specific α-actin.

5.3.1 hSkMC Viability

Alamar Blue was used to observe the hSkMC viability through metabolic activity on the full range of substrates (Figure 5-14). The hSkMCs were subcultured, seeded and differentiated following PromoCell's protocol and media. Cells were seeded on each substrate type and a full media change from growth media to differentiation media occurred when the cell confluence reached 60-80%; this is noted as Day 0. Differentiation was expected between 2-8 days and differentiation media was replaced with growth media on day 5 as per PromoCell's protocol for differentiation. There is little difference in metabolic activity seen between Day 0 and 4, probably because the cells are in differentiation media. An increase in metabolic activity is seen on all substrate types from Day 4 to 8, probably because the media was changed to growth media on day 5 leading to an increase in proliferation. Data analysis was carried out between certain substrates at each time point (see Section 3.4). No significant difference was found between Chitosan and ChitCNW, 12Chit and 12CNW at any time point. A significant difference was found between ChitCNW and 6CNW on Day 8 where a higher metabolic activity was seen on the ChitCNW compared to 6CNW. These differences are specific to this set of data; repeats showed approximately a similar trend.

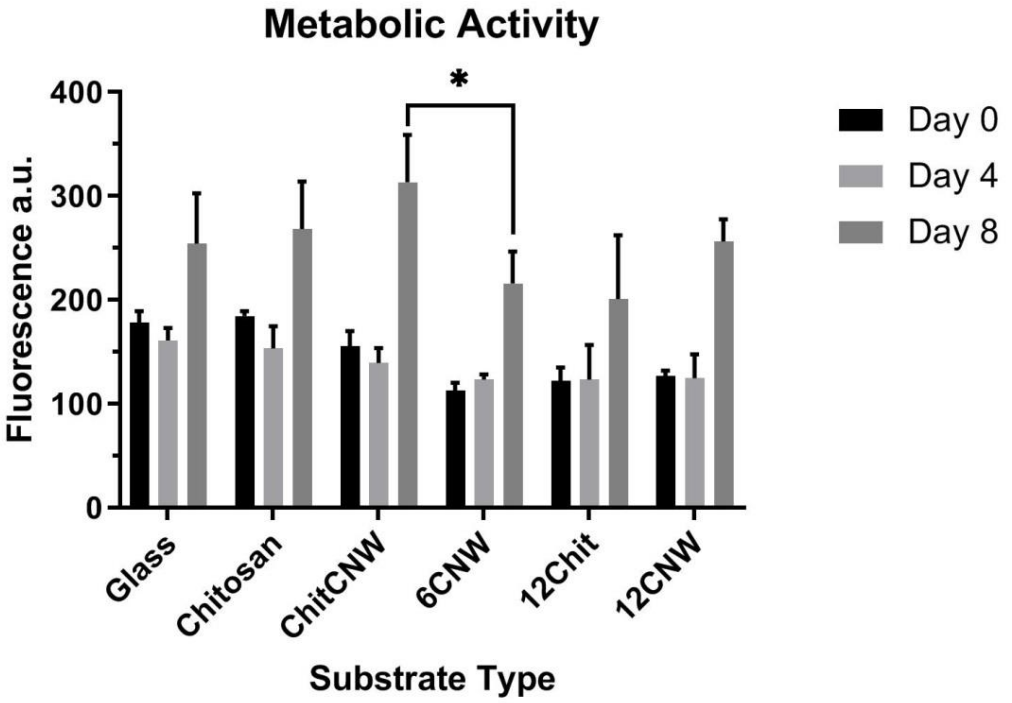

Figure 5-14: Metabolic activity of hSkMCs on the full range of substrate types across 3 time points using the Alamar Blue assay. The assay was run 3 times using hSkMCs of different passages. The data shown is a representative of the trend given by 2 of the 3 sets of data. Data analysis carried out using RM two-way anova with the Geisser-Greenhouse correction and with Turkey's multiple comparison test. For those that are significantly different (*) = $p < 0.05$.

Alamar Blue was carried out on the hSkMCs on each substrate type a total of 4 times. All the data collected is shown in Figure 5-15. Similar to the metabolic activity data collected for the C2C12s, there was a lot of variability between the different repeats of data and the data could not be collated due to the differences in magnitudes of each set. Therefore, each set was compared per substrate type and the most representative set is shown in Figure 5-14. For the data shown in Figure 5-15, Set 2 was normalised to the other sets as the magnitude was so much larger it was difficult to see the trends of each set on the same graph.

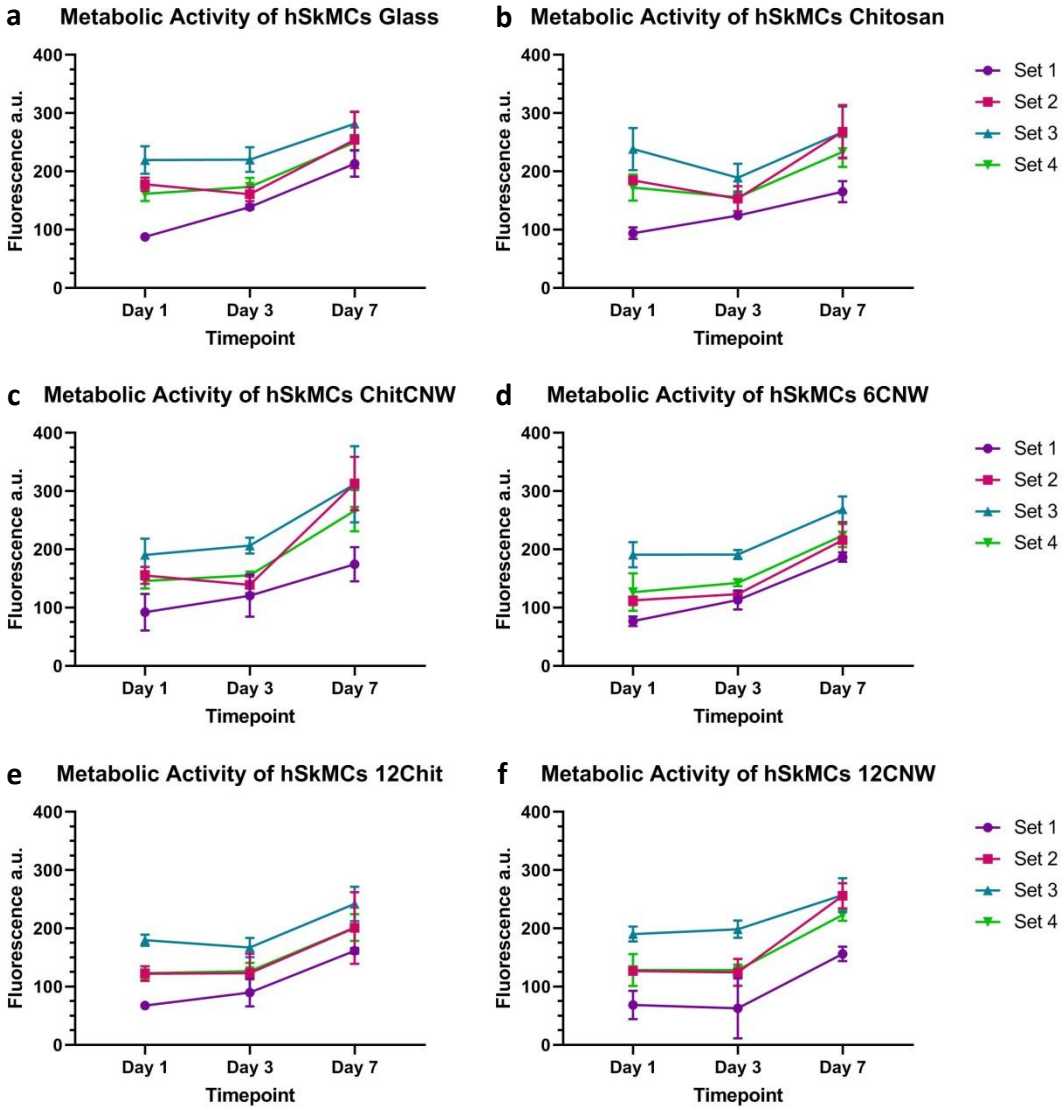

Figure 5-15: Metabolic activity of hSkMCs on the full range of substrates at different time points over a 7 day period. The experiment was carried out in triplicate 4 times shown per substrate type as Sets. Error bars are the standard deviation. (a) Glass, (b) Chitosan, (c) ChitCNW, (d) 6CNW, (e) 12Chit and (f) 12CNW

Cell number was quantified using the PicoGreen assay (Figure 5-16) on the same time points as the Alamar Blue assay. Cells were seeded within the optimum density as suggested by PromoCell and left to culture for 1-2 days until 60-80% confluent. This was not reached on each substrate at the same time therefore when at least half the substrates showed the ideal confluence, differentiation media was added. This explains the higher cell numbers seen on the first three substrate types compared to

the last set (the multilayers). The increase in cell number between Day 4 and Day 8 is likely due to the addition of growth media on day 5 which would lead to increased cell proliferation. Data analysis was carried out between certain substrates at each time point (see Section 3.4). No significant difference was found between Chitosan and ChitCNW, 12Chit and 12CNW at any time point. A significant difference was found between ChitCNW and 6CNW, 12CNW on Day 0 and between ChitCNW and 12CNW on Day 8 where a higher cell number was seen on the ChitCNW compared to 6CNW and 12CNW. These differences are specific to this set of data; repeats showed approximately a similar trend.

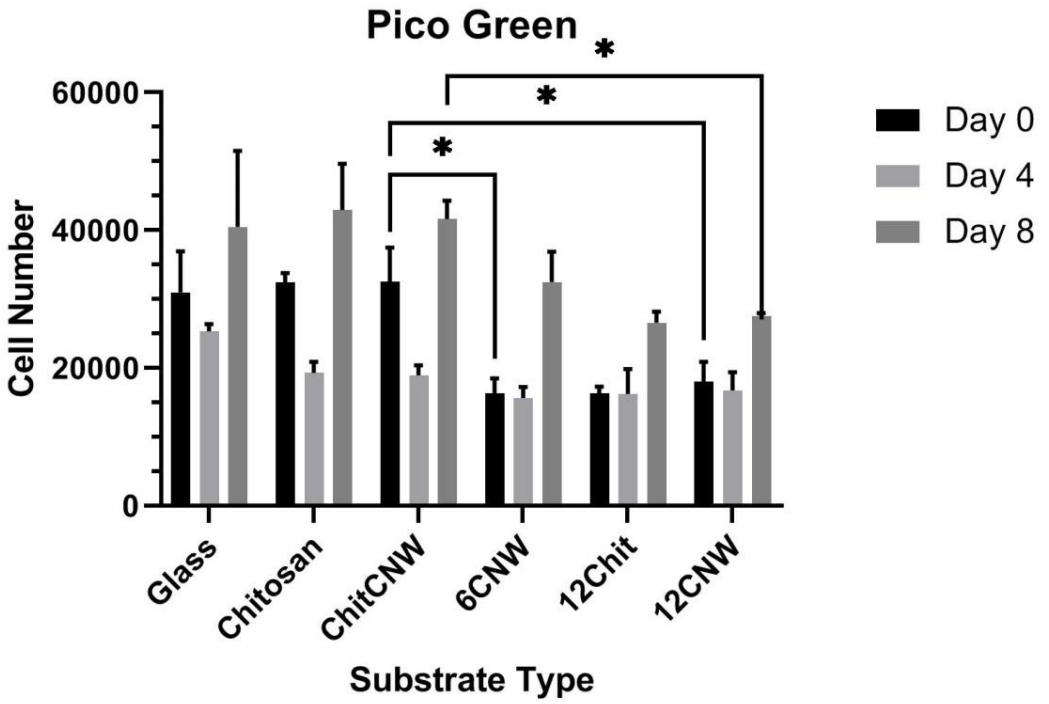

Figure 5-16: Cell number of hSkMCs on the full range of substrate types across 3 time points using the PicoGreen assay. The assay was run 3 times using hSkMCs of different passages. The data shown is a representative of the trend given by 2 of the 3 sets of data. Data analysis carried out using RM two-way anova with the Geisser-Greenhouse correction and with Turkey's multiple comparison tests. For those that are significantly different (*) = $p < 0.05$.

Again, repeats of the Pico Green assay was carried out and all the data is shown in Figure 5-17. Only 3 repeats were carried out of this assay on the hSkMCs and each set was compared per substrate type; the most representative set is shown in Figure 5-16.

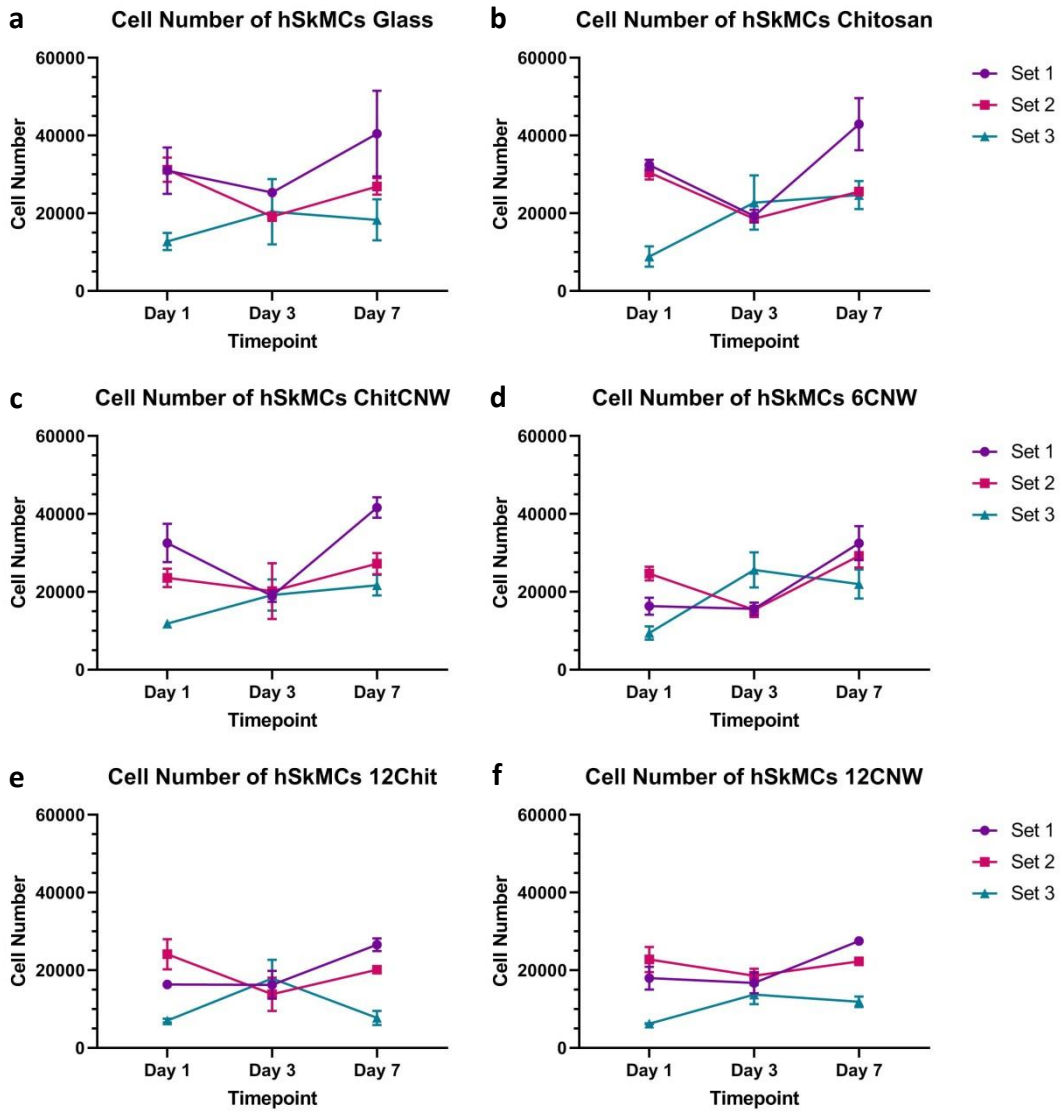

Figure 5-17: Cell number of hSkMCs on the full range of substrates at different time points over a 7 day period. The experiment was carried out in triplicate 3 times shown per substrate type as Sets. Error bars are the standard deviation. (a) Glass, (b) Chitosan, (c) ChitCNW, (d) 6CNW, (e) 12Chit and (f) 12CNW

Substrates were fixed and stained 24 h after seeding to see the initial response of the hSkMCs. Initial spreading and alignment of cells on the ChitCNW and 6CNW substrates can be seen on the confocal fluorescence micrographs shown in Figure 5-18. However, this was not observed on the 12CNW multilayer. The number of nuclei per area (Figure 5-19 (a)) was quantified and showed no significant difference between substrate types. On the other hand, the percentage area of cell coverage (Figure 5-19 (b)) was shown to be higher on the Glass and oriented substrates. The cells were least spread on the chitosan topped substrates.

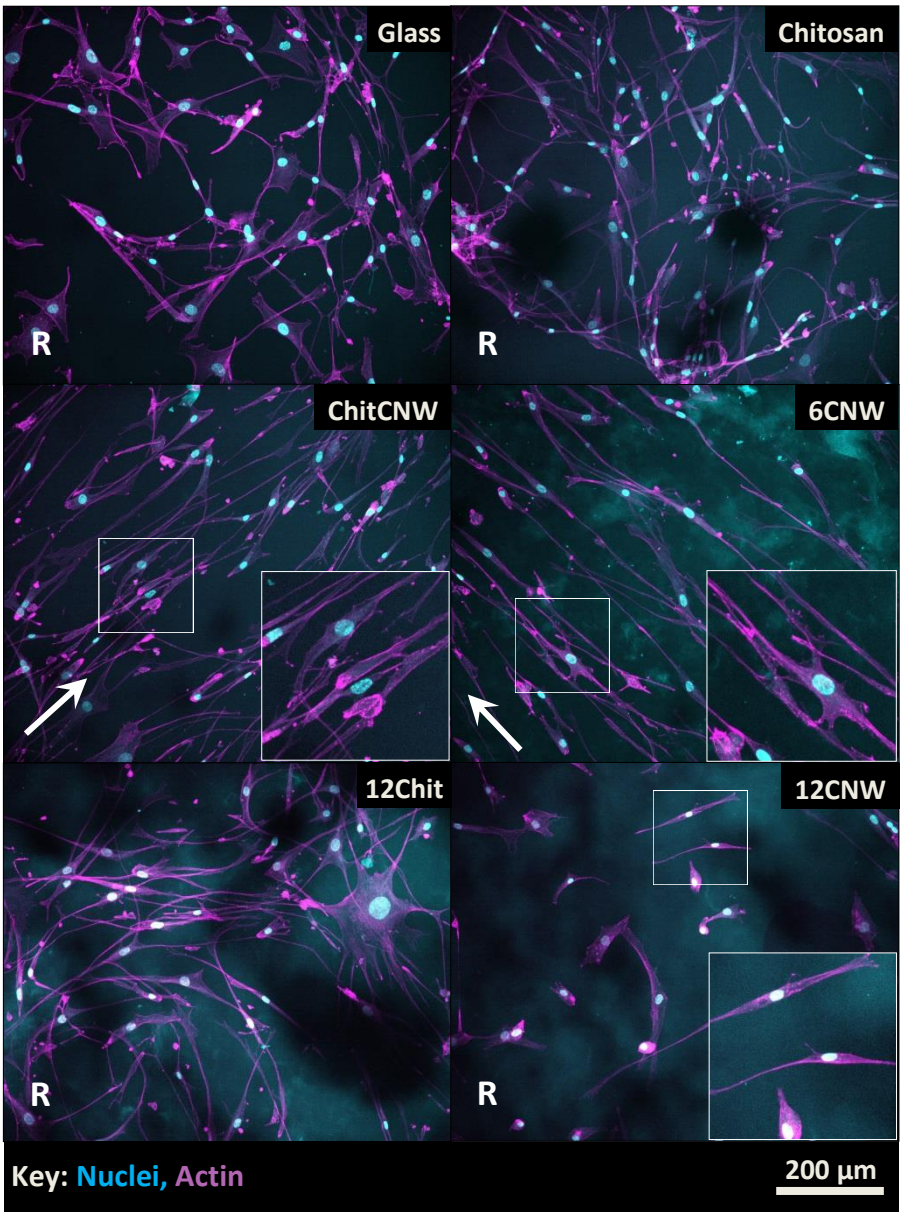

Figure 5-18: Confocal fluorescence micrographs of hSkMCs on each substrate type on 24 h after seeding, taken at 20x mag. Cells can be seen aligning on some of the oriented substrates (ChitCNW and 6CNW). The arrows indicate the general direction of the cell alignment and the R denotes where the cells are randomly oriented. Substrates named with CNW have the oriented topography.

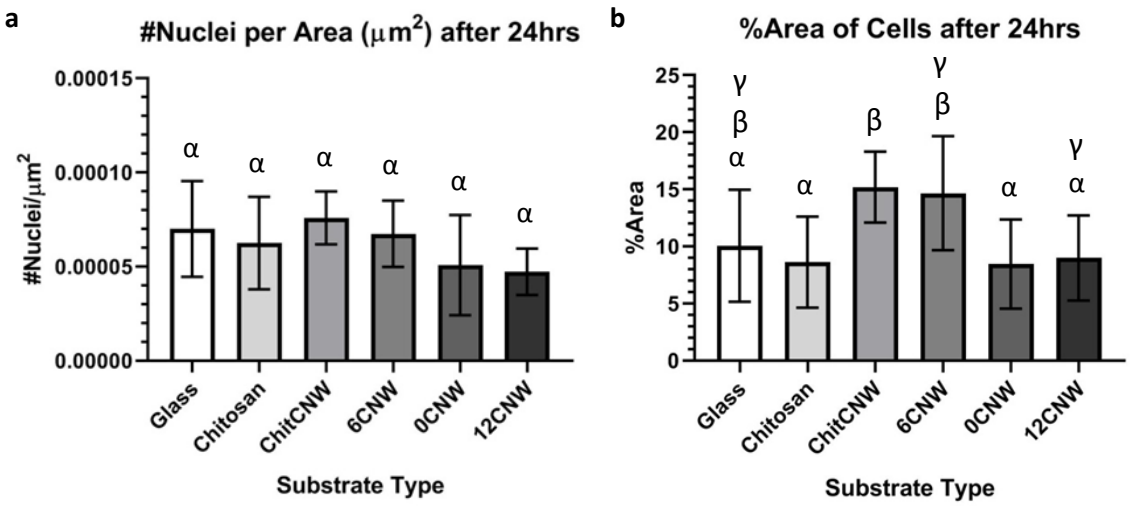

Figure 5-19: (a) The mean number of nuclei per area (μm^2) with SD on each substrate type and (b) the surface coverage of the hSkMCs on each substrate type, shown as mean %Area with SD, both 24 h after seeding. Data analysis carried out using ordinary one-way anova with Turkey's multiple comparison tests with a single pooled variance. Greek labels indicate groups within which no significant difference was observed. For those that are significantly different = $p < 0.05$.

5.3.2 hSkMC Differentiation and Elongation

The hSkMCs were shown to elongated and align on the oriented substrates, however full differentiation was not observed. Figure 5-20 shows the confocal fluorescence micrographs of areas of hSkMCs on each substrate type. Broad alignment can be seen on the ChitCNW and 6CNW substrates and partial on the 12CNW multilayer. The cells of the oriented substrates also appear thinner than those on the chitosan topped substrates.

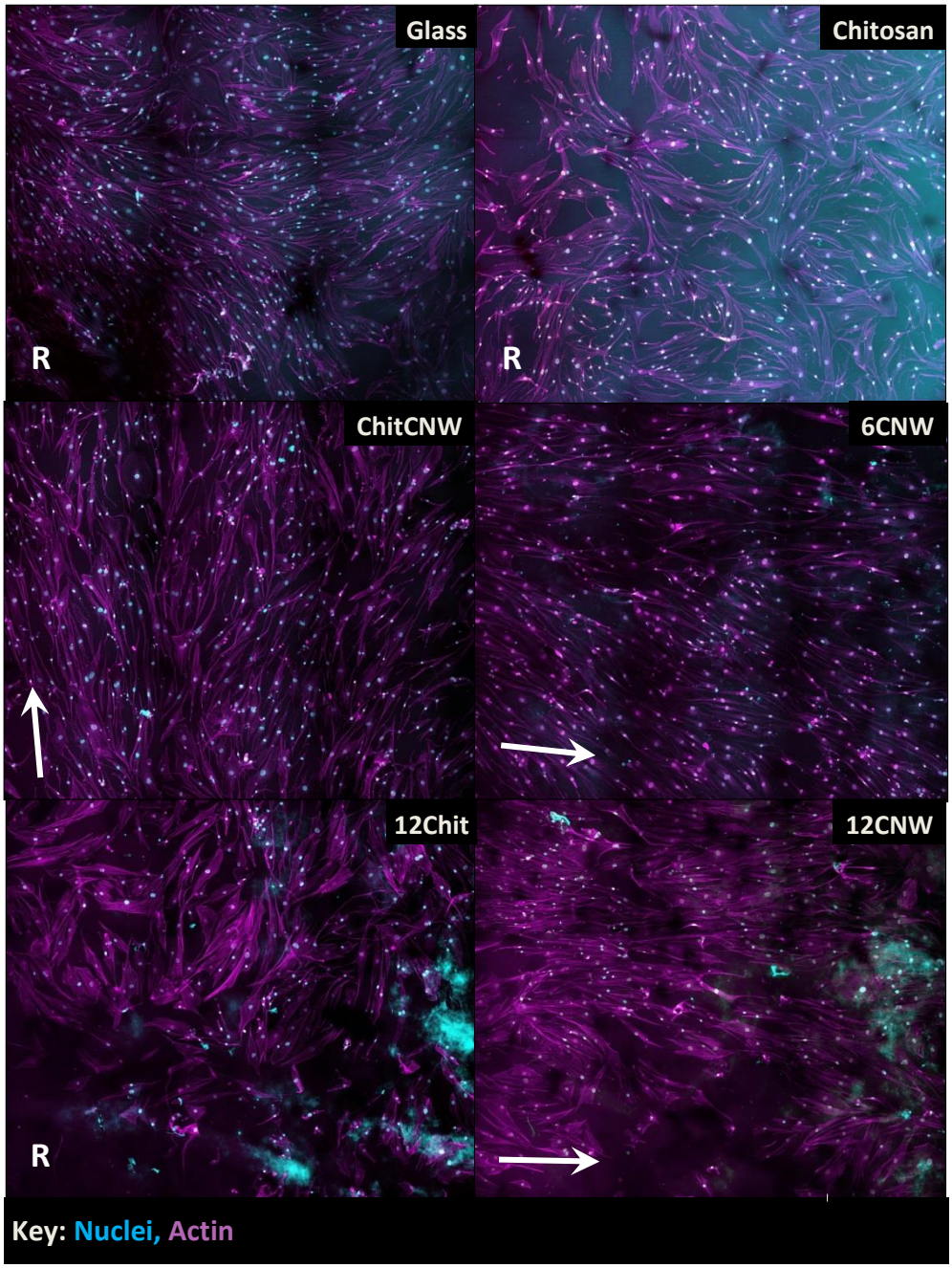

Figure 5-20: Confocal fluorescence micrographs of hSkMCs on each substrate type 8 days after differentiation media was added, taken at 20x mag and stitched together in maps of 3x3. The arrows indicate the general direction of the cell alignment and the R denotes where the cells are randomly oriented. Substrates named with CNW have the oriented topography. Broad alignment was observed on the ChitCNW and the 6CNW and to a certain degree on the 12CNW multilayer.

Alignment of the hSkMCs was carried on actin channel of the confocal fluorescence micrographs with cells' angle given by the direction of the actin fibres. The radial graphs show the normalised angles of the cells and the data for all of the substrate types are summarised in the box graph (Figure 5-21). The CNW oriented substrates, ChitCNW, 6CNW and 12CNW, showed the highest degree of alignment suggesting that the hSkMCs are influenced by the nano-topography.

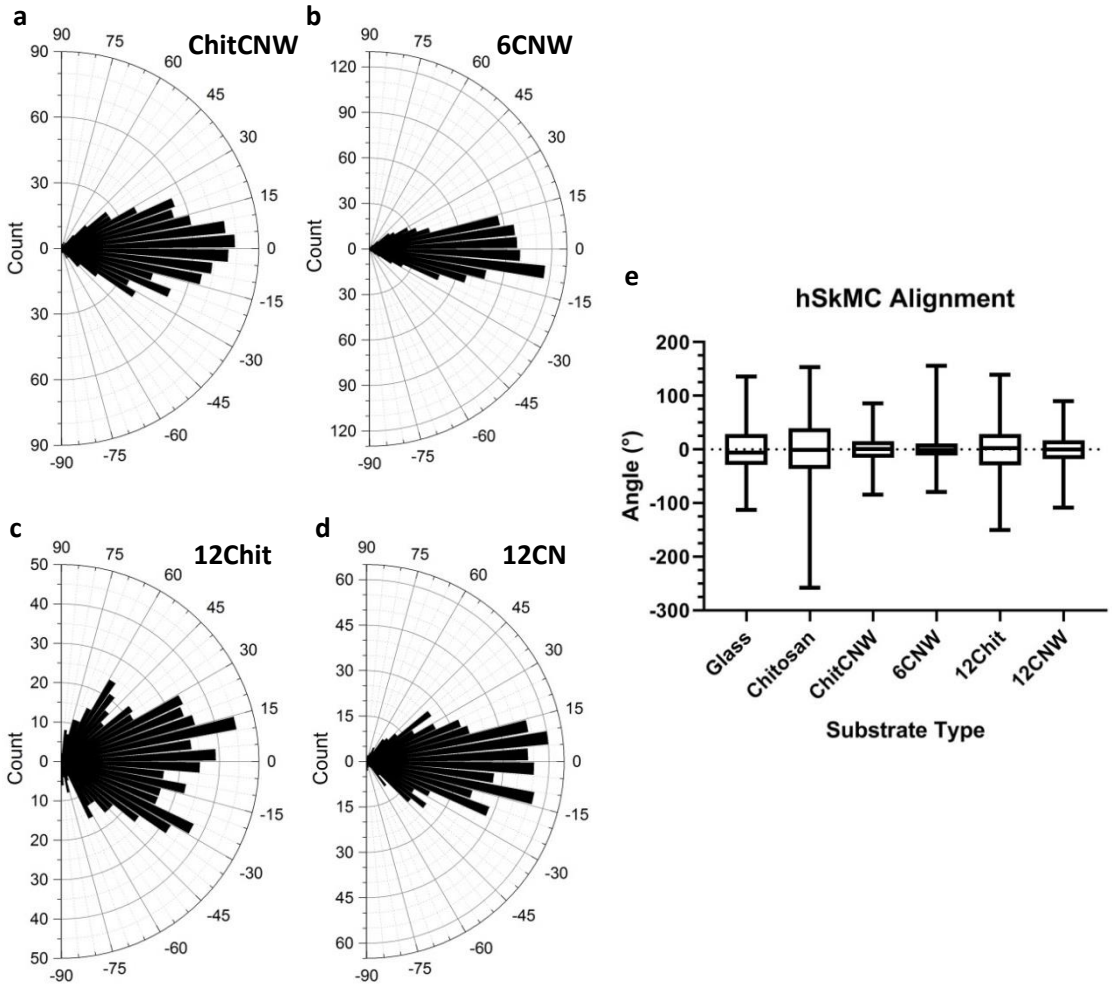

Figure 5-21: Alignment of the hSkMCs was measured on each substrate type. Radial graphs show normalised data on the (a) ChitCNW, (b) 6CNW, (c) 12Chit and (d) 12CNW multilayer substrates. The distribution of the angles from 0^{o} is shown by the box whisker graph (e) for the full range of substrate types. A smaller box shows that most of the data (angles) is in a narrower range and therefore the cells are more aligned. A larger box shows that most of the data (angles) is in a wider range and therefore the cells are not as aligned.

hSkMCs were stained for myogenin and sarcomeric alpha actinin to confirm the cells were undergoing myogenic differentiation, however these stains did not appear as clearly as on the C2C12s. Figure 5-22 shows an example of where the myogenin staining worked although this was not seen on all confocal fluorescence micrographs and could not be quantified. The presence of myogenin around the nuclei in these micrographs suggests that the cells are in the process of myogenic differentiation. On the other hand, sarcomeric alpha actinin could not be seen in the associated channel.

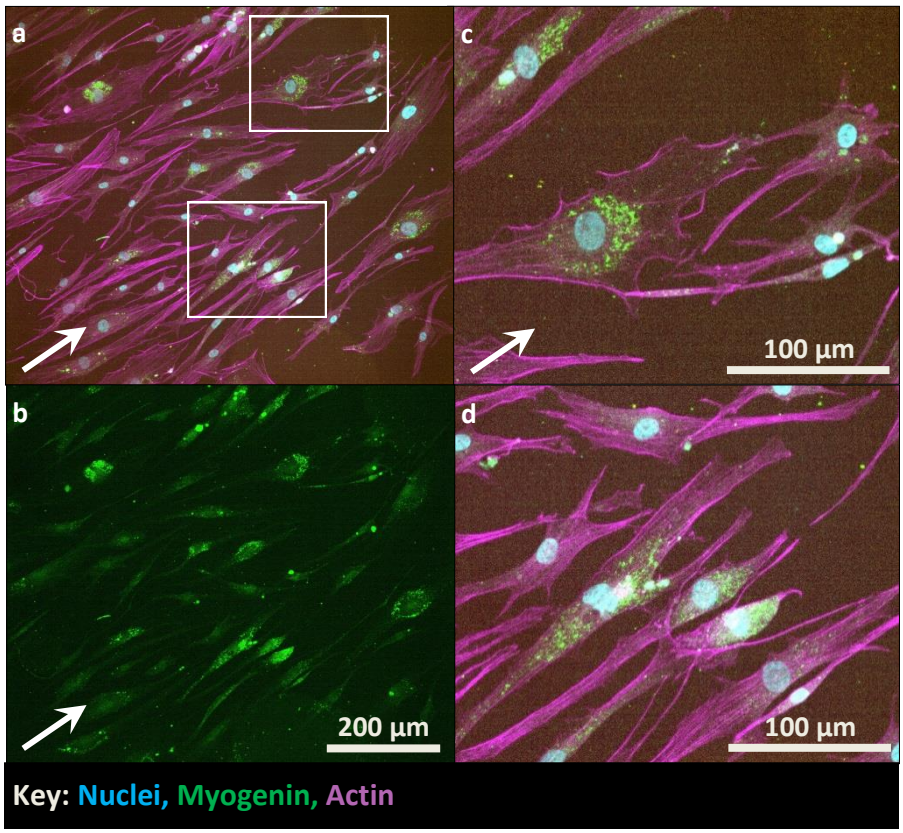

Figure 5-22: Confocal fluorescence micrographs of hSkMCs on ChitCNW taken at 20x mag 8 days after the addition of differentiation media. (a) shows the original image with all channels, (b) shows the myogenin channel and (c) and (d) are enlarged images of the sections indicated in image (a). Myogenin can be seen around the nuclei of the cells.

Although full differentiation of the hSkMCs was not achieved the cells were shown to elongate. Figure 5-23 shows confocal fluorescence micrographs taken at x40 mag illustrating the difference in hSkMC response to the substrate types. The cells appear denser and thinner on the oriented substrates compared to those on Glass and Chitosan. However, it is also noted that the cells on the 12CNW multilayer appear wider although still aligned. The approximate lengths of the cells lengths of the cells were measured (Figure 5-24) and shows the longest cells were found on the multilayers. Glass was found to be significantly lower than all the other substrate types

and 6CNW had the largest range of lengths. The elongation of the cells over time is further shown in Figure 5-24 (b) where the cells on Day 8 appear much longer and wider than those 24 h after seeding.

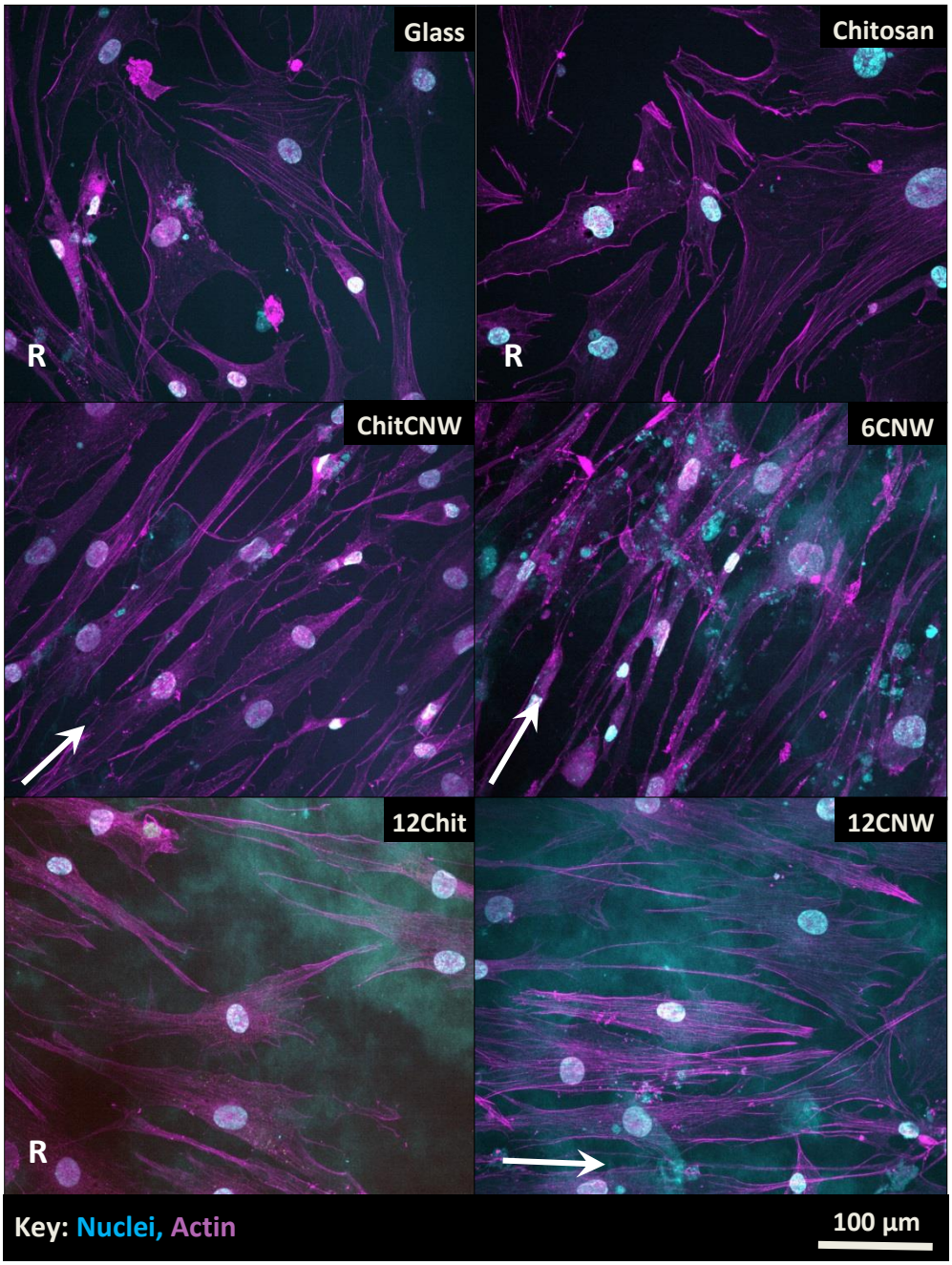

Figure 5-23: Confocal fluorescence micrographs of hSkMCs on each substrate type 8 days after differentiation media was added, taken at 40x mag. Cells are shown to be thinner and longer when aligned. On the unaligned surfaces, the cells appear flatter and are spreading out. The arrows indicate the general direction of the cell alignment and the R denotes where the cells are randomly oriented. Substrates named with CNW have the oriented topography.

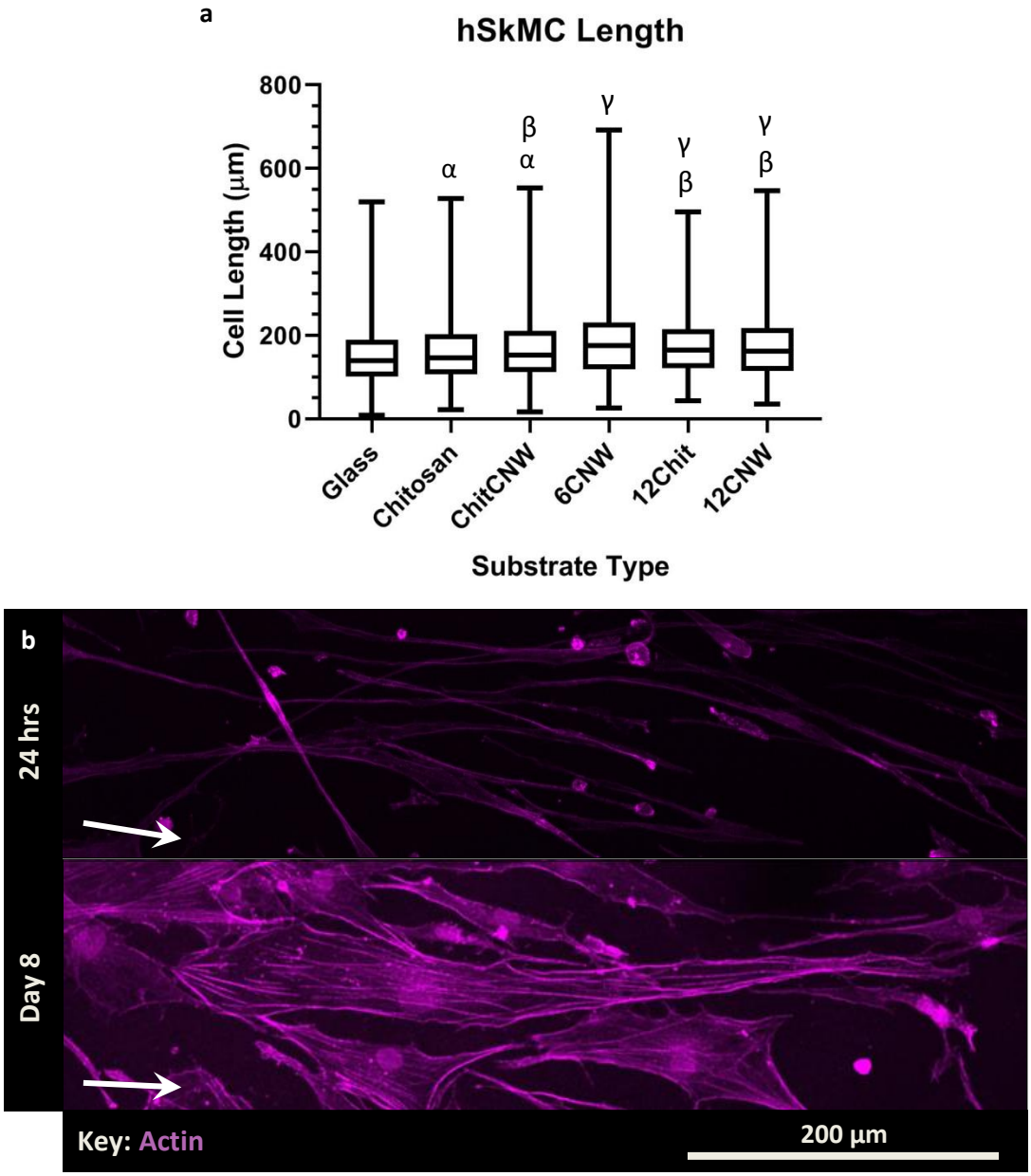

Figure 5-24: (a) the approximate mean lengths of the hSkMCs 8 days after being treated with differentiation media. Data analysis carried out using ordinary one-way anova with Turkey's multiple comparison tests with a single pooled variance. Greek labels indicate groups within which no significant difference was observed. For those that are significantly different = $p < 0.05$. (b) magnifications of confocal fluorescence micrographs, taken at 20x mag, 24 h after seeding and 8 days after treating with differentiation media. An increase in cell length and width can be seen from the first time point to the second along with cell migration and spreading in the direction of the CNWs.

5.4 Application of BM-MSCs

Bone marrow derived mesenchymal stem cells (BM-MSCs) have the potential to differentiate in to a range of different cells depending on the chemical and physical cues applied. Here, BM-MSCs from two different donors were seeded on the full range of substrates to investigate if the topography of the CNW alone could direct the BM-MSCs towards myogenic lineage. Cells were seeded on the full range of substrate types and left for 1-2 days to reach 60-80% confluency before differentiation media was added through partial media changes. The differentiation media described in Section 4.3.2 was chosen to be simple to understand the topographical cues given by the oriented CNWs. Both donors were contributed from stock population of other members of the Biomaterials Group at the University of Manchester. Donor 1 BM-MSCs were isolated from the femur of a 27-year old female after hip replacement surgery at Wrightington Hospital, Lancashire by the Richardson Laboratory. Donor 2 BM-MSCs were obtained from Lonza as part of a bone marrow aspirate and their isolation and characterisation was done by Dr. Deepak Kumar.

5.4.1 BM-MSC Viability

Metabolic activity was measured for both donors using the Alamar Blue assay (Figure 5-25). A trend can be seen for Donor 1 however not for Donor 2. The metabolic activity increases over time for Donor 1 although the only significant difference was found between the 12Chit and the 12CNW multilayer on Day 3. Donor 2 showed no trend and no relationship can be seen between different substrate types.The only significant difference found was between Glass and 12Chit on Day 3, otherwise there is no significant difference between substrate types on different days.

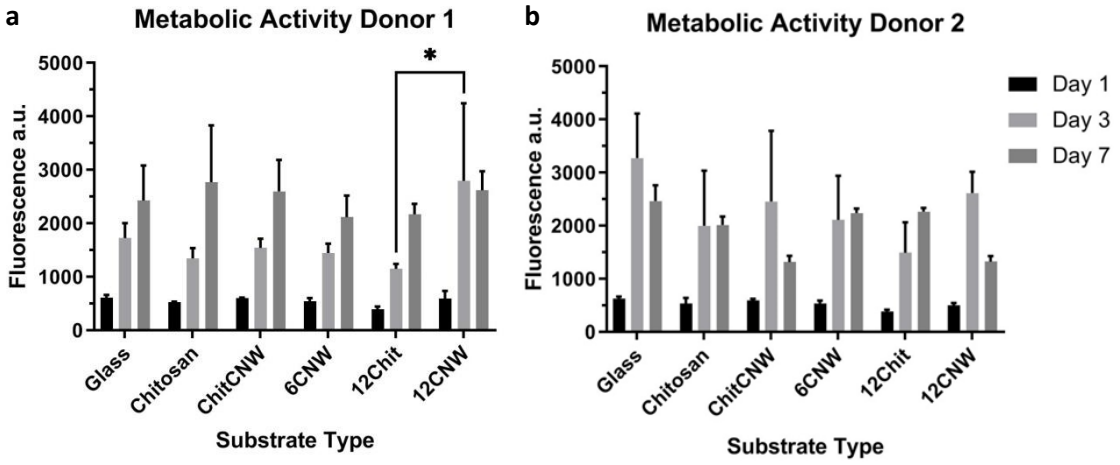

Figure 5-25: Metabolic activity of BM-MSCs on the full range of substrate types across 3 time points using the Alamar Blue assay. The assay was run on 2 different cell donors: (a) Donor 1 and (b) Donor 2. Data analysis carried out using RM two-way anova with the Geisser-Greenhouse correction and with Turkey's multiple comparison test. For those that are significantly different (*) = $p < 0.05$.

The mean population doubling time was calculated using the Alamar Blue data and the equation found in Section 3.3.4 (Figure 5-26). No significant difference was found within each donor however Donor 1 appears to have a more consistent mean doubling time across the susbrate types. On the other hand, Donor 2 has a shorter population doubling time on the Glass and 12CNW substrates and overall shorter mean doubling time compared to Donor 2.

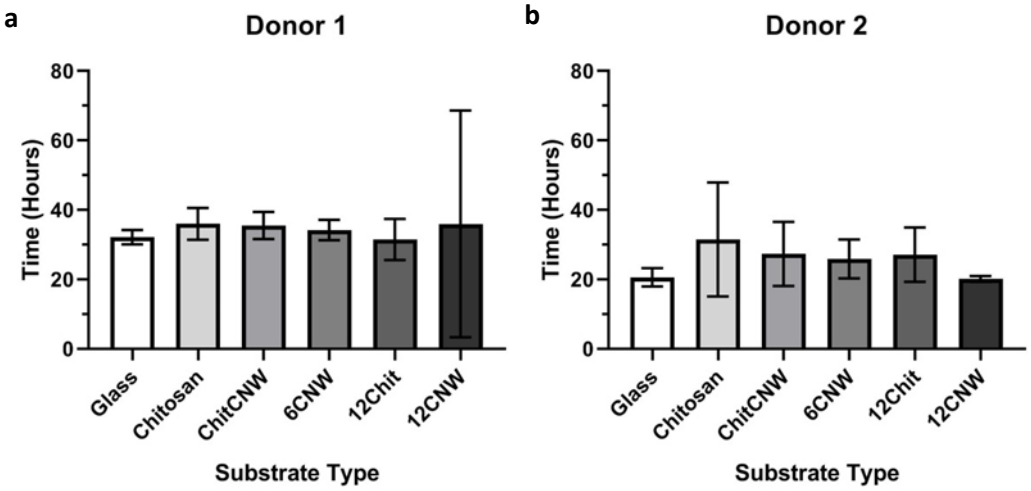

Figure 5-26: Mean population doubling time with SD calculated with the equation found in Section 3.3.4. Data analysis carried out using ordinary one-way anova with Turkey's multiple comparison tests with a single pooled variance. No significant difference was found between substrate types within each donor: (a) Donor 1 and (b) Donor 2.

The cell number was calculated for both donors using the PicoGreen assay (Figure 5-27). Donor 1 shows a greater number of cells on days 3 and 7 compared to Donor 2. Significant differences between substrate types per donor were only found on Day 3. For Donor 1, significant differences were found between Glass and the 12 multilayer substrates, Chitosan and all of the multilayer substrates. The cell number decreases from Day 3 to 7 on the thinner substrates of Donor 1 but increases between the same time points on the multilayers. For Donor 2, significant differences were found between Glass and all of the other substrates, Chitosan and ChitCNW and the 12 multilayer substrates, ChitCNW and 6CNW and lastly 6CNW and 12 multilayer substrates. Although of different magnitudes, the cell number is shown to increase over the 7 days for Donor 2. The total cell number for Donor 2 is lower than that of Donor 1 and can be seen the bright field microscope images in Figure 5-28. The PicoGreen data combined with the Alamar Blue does not give a clearer picture of the BM-MSCs initial response to the substrate types. Only the relevant significant difference are shown on the graphs, explained in Section 3.4.

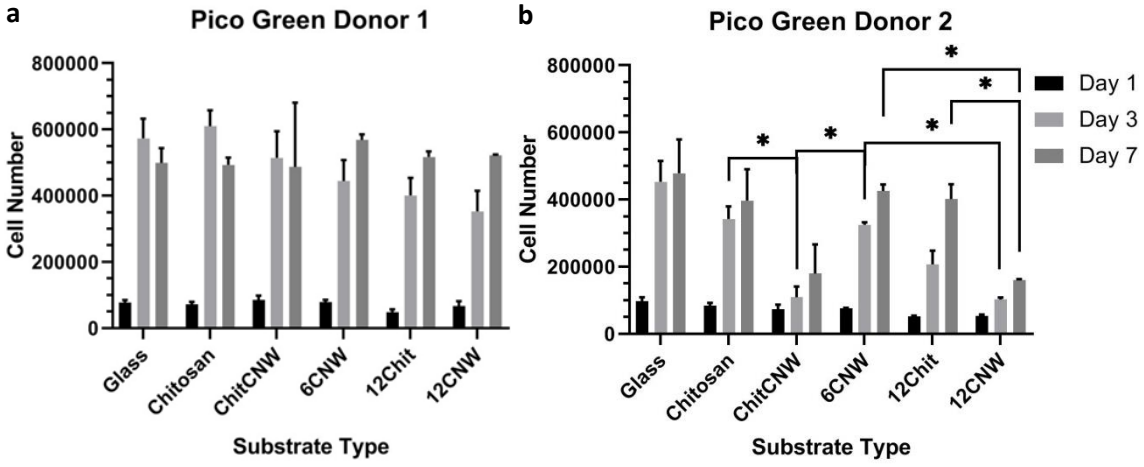

Figure 5-27: Cell number of BM-MSCs on the full range of substrate types across 3 time points using the PicoGreen Assay. The assay was run on 2 different cell donors: (a) Donor 1 and (b) Donor 2. Data analysis carried out using RM two-way anova with the Geisser-Greenhouse correction and with Turkey's multiple comparison test. For those that are significantly different (*) = $p < 0.05$.

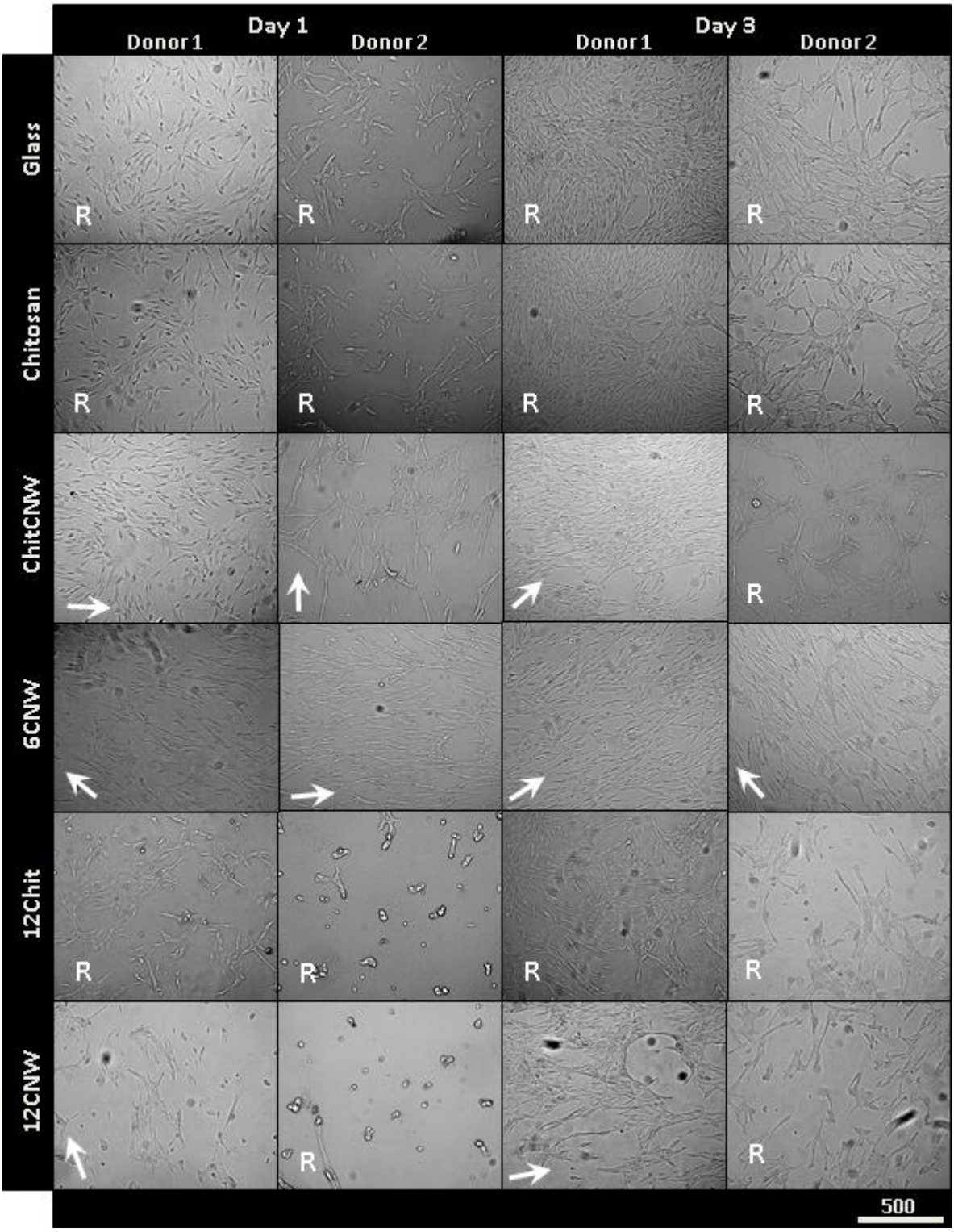

Figure 5-28: Bright field microscope images taken at 20x mag of random areas on the full range of substrate types for both Donors on Day 1 and 3. The arrows indicate the general direction of the cell alignment and the R denotes where the cells are randomly oriented. Substrates named with CNW have the oriented topography. BM-MSCs from Donor 1 appears to have a better initial response to the substrates as there is more cell spreading compared to the cells of Donor 2.

5.4.2 BM-MSC Elongation and Potential Differentiation

Sets from both donors were stained for myogenin, sarcomeric alpha actinin and actin however, when imaged, samples from Donor 2 showed no cells. This could be contributed to a mixture of cell death or peeling off the surfaces therefore no micrographs are shown for Donor 2. The micrographs in Figure 5-29 and 5-30 are of Donor 1 cells on all substrate types.

The BM-MSCs showed a strong response to the oriented CNWs on the 6CNW and 12CNW multilayers however a poor response was observed on the ChitCNW substrate (Figure 5-29). Broad alignment can be seen of the 6CNW and 12CNW multilayers and only local alignment on the Glass and chitosan topped substrates. Large patches of no cells were seen in some areas of all the substrates however this was mostly seen on the ChitCNW substrate. Figure 5-30 shows in more detail the alignment of the BM-MSCs on the 6CNW and 12CNW multilayers and even the nuclei appear to be unidirectional. At the higher magnification, the actin filaments on the oriented substrates can be seen to be oriented and stretching in the same direction as each other. The morphology of each individual cell is not clear therefore that could be some fusion in the aligned cells. Another notable difference between the oriented and randomly oriented cells is the overlapping of groups of cells. The oriented cells appear like a cell sheet across the surface while there appears to be more cells on top of each other on the substrates without CNWs.

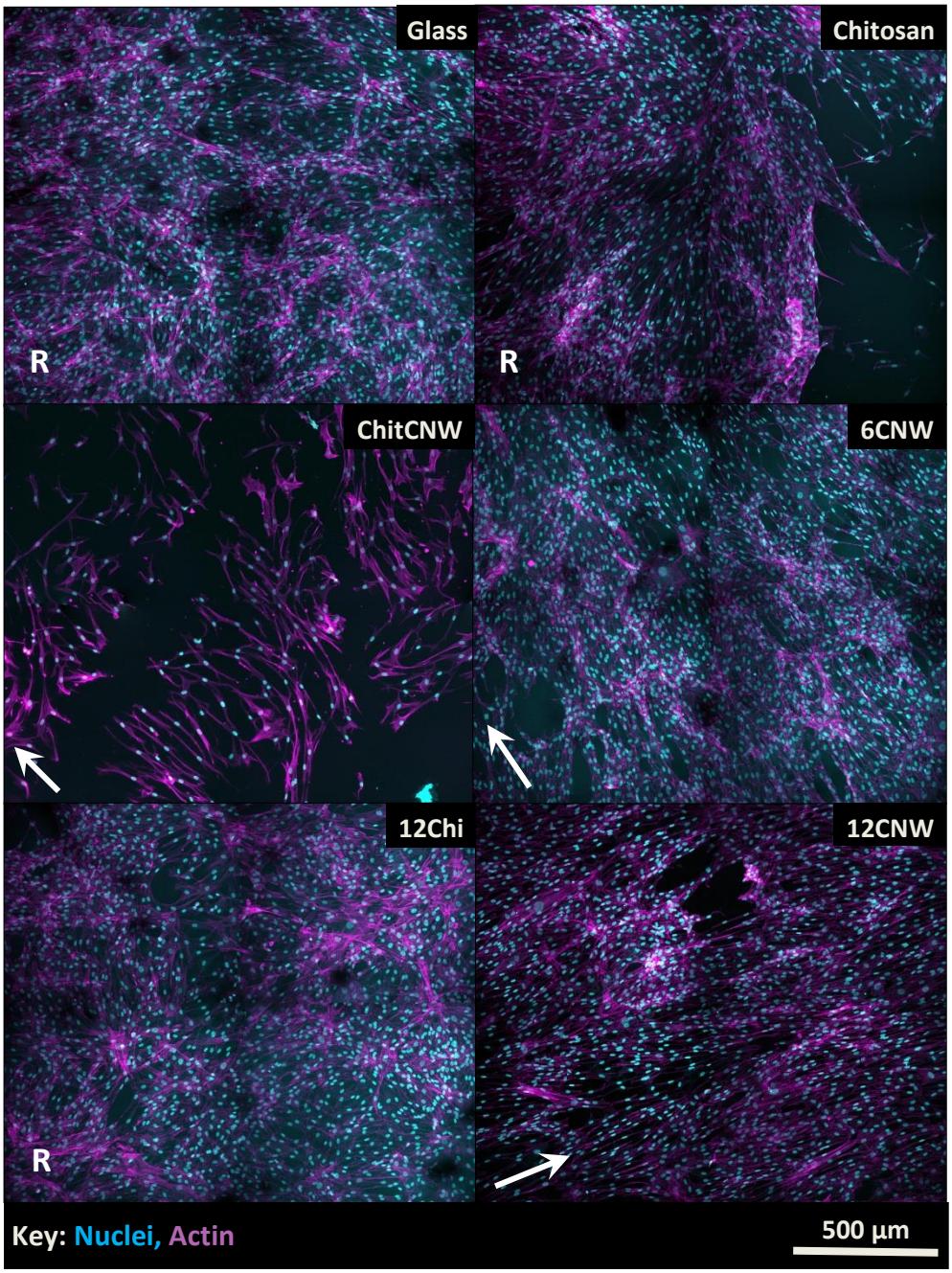

Figure 5-29: Confocal fluorescence micrographs of BM-MSCs from Donor 1 on each substrate type 7 days after differentiation media was added, taken at 20x mag and stitched together in maps of 3x3. Broad alignment was observed on the 6CNW and the 12CNW and to a certain degree on the ChitCNW substrate however there was poor cell spreading. The arrows indicate the general direction of the cell alignment and the R denotes where the cells are randomly oriented. Substrates named with CNW have the oriented topography.

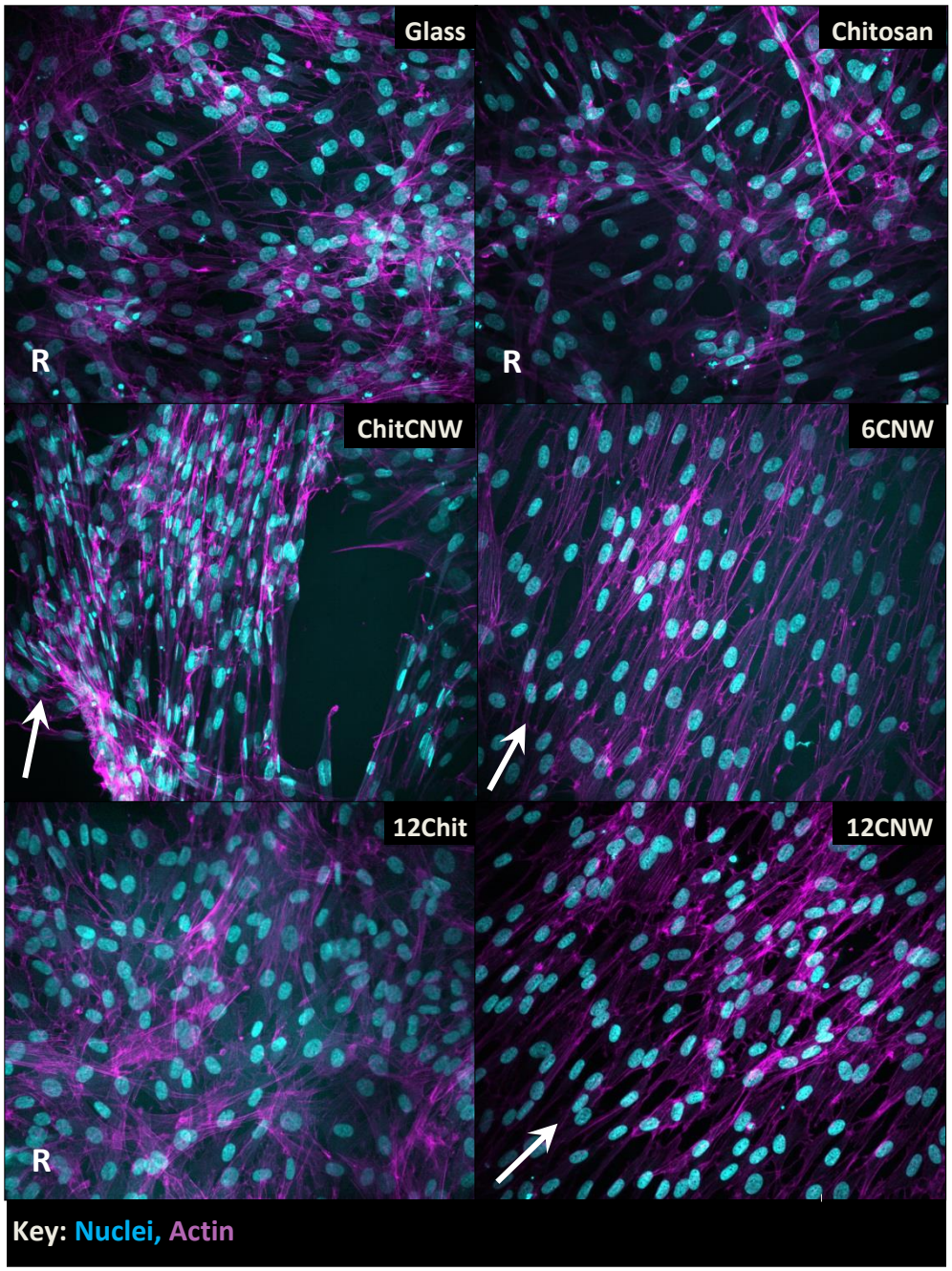

Figure 5-30: Confocal fluorescence micrographs of BM-MSCs from Donor 1 on each substrate type 7 days after differentiation media was added, taken at 40x mag. The alignment of the cells on the oriented substrates can be more clearly seen. The arrows indicate the general direction of the cell alignment and the R denotes where the cells are randomly oriented. Substrates named with CNW have the oriented topography.

5.4.3 Preliminary Response of Satellite Cells

Satellite cells are also used in the engineering of skeletal muscle tissue. They are known as the muscle stem cells as their role is to remain quiescent state until stimulated to multiple and begin differentiating in to myoblasts (Cossu *et al.*, 2000). Satellite cells, extracted from muscle biopsies by the Cossu Group at the University of Manchester, were seeded on to the full range of substrates; this was carried out by Dr. Francesco Galli. The cell attachment was seen within 24 h and once at a suitable confluence, differentiation media was added. Figure 5-31 shows the satellite cells after 10 days in differentiation media. Broad cell alignment can be seen on the substrates with the oriented CNW top layer. As with C2C12s and hSkMCs, local alignment can be seen to the Glass substrate. The alignment of the satellite cells to the CNWs shows promise for future work.

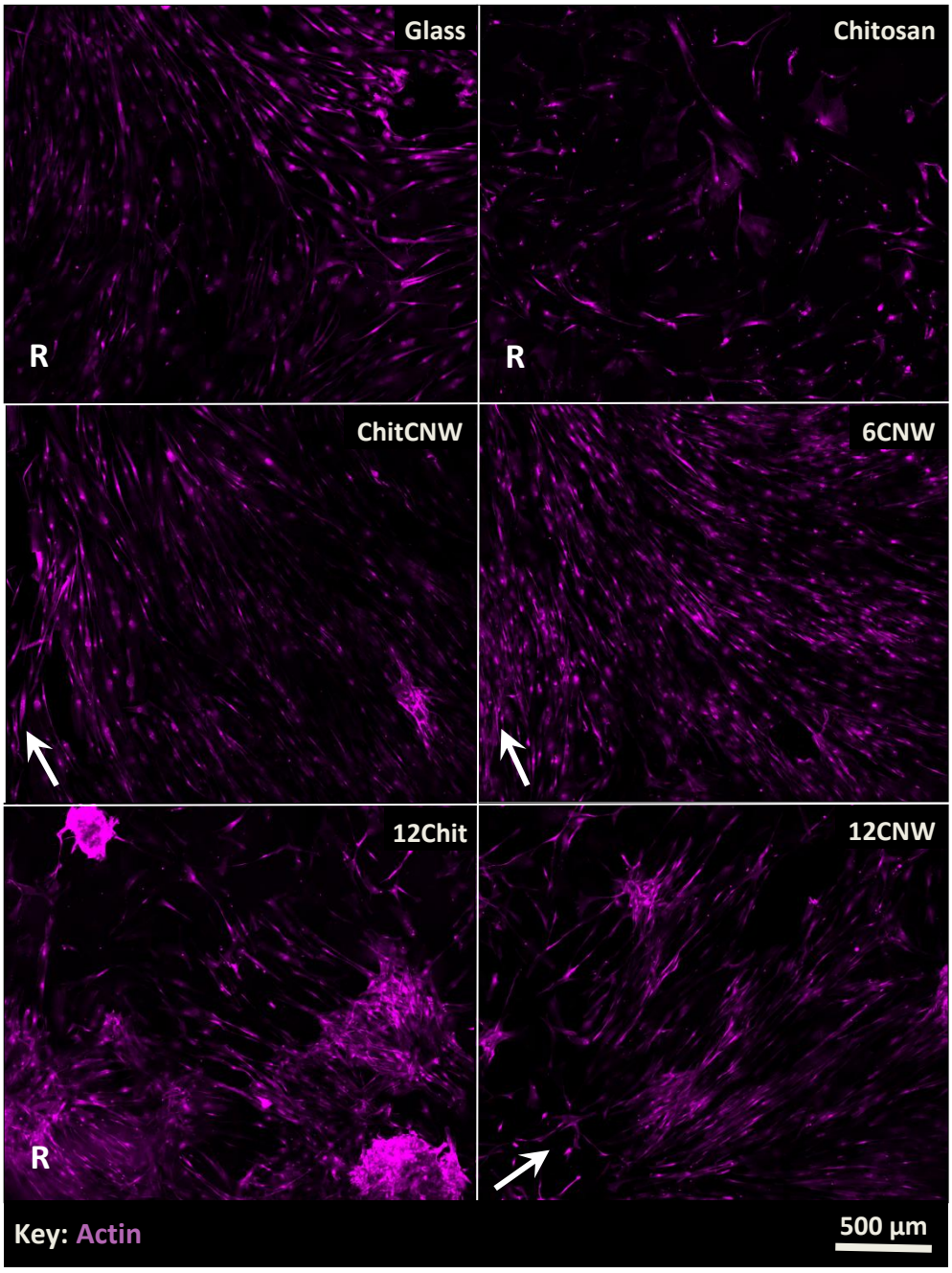

Figure 5-31: Confocal fluorescence micrographs of satellite cells taken at 10x mag on the full range of substrates 10 days after differentiation media was added. The cells were stained for actin to examine the alignment to the CNWs. The arrows indicate the general direction of the cell alignment and the R denotes where the cells are randomly oriented. Substrates named with CNW have the oriented topography.

5.5 Discussion of Cell Response to the Multilayer Substrates

5.5.1 C2C12 Response

Previous work in this group has shown that oriented CNWs can direct myotube alignment and the application of PEMs composed of CNWs, chitosan and PSS could potentially replicate the skeletal muscle tissue (Dugan *et al.*, 2013; Nikoi, 2016). The aims of this section was to confirm that these multilayers of CNWs and chitosan could align the myotubes to a similar extent and to explore the response of other cell types related to skeletal muscle.

The response of the C2C12s to the multilayers was promising and similar to that for previous work. Alignment and cell spreading over the multilayer substrates was observed. Increasing cell number and the differentiation of multi-nucleated tubes showed a positive response to the combination of CNWs and chitosan with no cytotoxic effects from either layer.

The Alamar Blue assay was used to monitor the viability of the cells by measuring the metabolic activity. The data showed a large increase between Day 1 and Day 3 before a decrease from Day 3 to 7 (Figure 5-1). The metabolic rate of cells is a representative value of how the cells are proliferating and how hard they have to work to differentiate. The increase between the first two time points is expected as cell proliferation should increase as the cell population rises. Cell number increase between Day 1 and 3 was also shown in the Pico Green data (Figure 5-4). The mean population doubling time (Figure 5-3) was calculated from the Alamar Blue data using the equation given in Section 3.3.4. There was an increase in mean doubling time of the CNW topped substrates as the number of layers increased and similarly an increase between the Chitosan and 12Chit substrates. However, the only statistical significant difference was seen between the ChitCNW and the 12 multi-layered substrates (12Chit and 12CNW). The decrease in metabolic activity between Day 3 and 7 are due to the decrease in cell proliferation and differentiation. Although, there is an increase in cell number, notably not as large an increase as between the first two time points, the drop in metabolic activity can be contributed to the increase in differentiated cells and formation of myotubes. Myoblast fusion results in the cells no longer able to proliferate as myogenesis cannot be reversed. However, a small population of

undifferentiated myoblasts remain proliferating (Chargé and Rudnicki, 2004; Huang *et al.*, 2006). Differentiation of C2C12s is triggered by the addition of differentiation media, which is lower in protein serum. It has been noticed that C2C12s grown in culture that have been starved of media with serum will begin to differentiate when a suitable cell density is reached (S. Burattini, P. Ferri, M. Battistelli, R. Curci, F. Luchetti, 2004). Differentiation media was added through partial media changes during the experimental time period so that the decrease in serum proteins was gradual. Initial differentiation and high cell density could be seen from Day 4 onwards. Overall the trend for both the Alamar Blue and PicoGreen assays was similar for all the substrates types. At Day 7, the cell number on the CNW topped substrates was shown to increase as the number of layers increased; however, there was no significant difference. The oriented substrates also had a higher cell number although there was no significant difference found between substrates types on Day 7.

Both assays are very simple in execution; however the data produced has not been entirely the same in repeats. Variations in cell metabolic activity and cell number can be due to slight differences in experimental work. Although the highest effort was done to carry out every repeat the same, some variations are expected. The data shown in the results chapters are representative of the general trends observed (see Appendix A and B for the repeats). This can be said for all the Alamar Blue and PicoGreen data in this work.

Confocal fluorescence micrographs of the C2C12s after 24 h were used to calculate the number of nuclei per area and percentage cell area (Figures 5-7). The initial response of C2C12s can be seen by the cell spreading with the most nuclei and cell spreading seen on the 6CNW and 12CNW substrates. Both values are around double those of Glass and Chitosan. The other oriented substrate, ChitCNW and the other multilayer, 12Chit, are slightly larger, however not significantly different to Glass and Chitosan. This suggests the combination of the oriented surface and multilayers are favourable to the C2C12s. Alignment of the cells can be seen on the oriented surfaces (Figure 5-8 and 5-11) and was observed on all repeats. Myoblasts are communicative cells as they try to align to each other. If the majority of the cells are aligning to an oriented topography, the message is carried along resulting in broad alignment (S. Burattini, P. Ferri, M. Battistelli, R. Curci, F. Luchetti, 2004). Cells seeded at a lower density did not

show as much alignment after 24 h possibly due to insignificant cell-cell interaction. Wragg et al also observed that cell proximity increased the myoblast differentiation and formation of more myotubes (Wragg *et al.*, 2019).

Differentiation of C2C12s is seen by the elongation and fusion of the myoblasts in to myotubes. The first observation made of the Day 7 confocal fluorescence micrographs (Figure 5-8 and 5-12) is the difference in type of myotube alignment across the substrate types. Myotube formation is seen on all of the substrate types. However, broad alignment is observed only on the ChitCNW and 6CNW substrates. As stated earlier, myoblasts prefer to align to each other, however, this does not occur over a large area without stimuli and the alignment is describe as localised. Broad alignment of C2C12s requires the influence of a stimulus such as the oriented topography used here, electrospun unidirectional fibres (Choi *et al.*, 2008) or mechanical cues such as applying a tensile force (Powell *et al.*, 2002). Alignment of the myotubes was measured and showed quantitatively that the ChitCNW and 6CNW had the most aligned myotubes (Figure 5-11). The 12CNW multilayer which is topped with oriented CNWs did not show the same degree of alignment when quantified, however, some alignment could be seen and individual myotubes appeared to be oriented the same direction. Looking at the cell spreading and myotube formation, it appears that the cells are grouping together in cell aggregates and it is these aggregates that are appearing aligned. This aggregation of cells is also observed on the 12Chit multilayer, noticeably not aligned, and some aggregation of cells can be seen on the 6CNW multilayer but not on the ChitCNW bilayer. Therefore, it is possible that the number of layers is having an influence on the cell aggregation.

Muscle fibres in the body can range in length depending of the purpose and size of the whole tissue for example there is a large difference in the size of fibres found in the extraocular muscles of the eye and the quadriceps of the legs (Porter *et al.*, 2001). These sizes are proportional to the force the muscle tissue is required to generate (Lieber and Fridén, 2000). Bundles of myotubes mature in to muscle fibres and therefore, myotube length is often reported in studies interested in engineering skeletal muscle. The most reported length of myotubes cultured *in vitro* is frequently between 100 and 500 µm where differentiation has been promoted from a range of different stimuli. This included aligned fibres, micro-patterned films and piezoelectric

materials (Ebrahimi *et al.*, 2018; Ribeiro *et al.*, 2018; Guo *et al.*, 2019; Yeo and Kim, 2019). However, longer myotube lengths have also been reported such as Huang et al, who achieved myotube lengths of around 1.8 mm with 30-40 nuclei per myotube on nano-fibrous PLLA scaffolds (Huang *et al.*, 2006). The longest myotubes measured in this work are over 400 um long after 7 days in culture, which when compared to the literature is average. Magnifications of the myotube length histograms (Figure 5-9) show that alignment may contribute to culturing more myotubes over 100 um, which was also indicated by Yeo et al who also showed an increase in myotube length from an unaligned to aligned substrate (Yeo and Kim, 2019). However, the lengths recorded for Glass are as high as those on the ChitCNW and 6CNW substrates although the longest myotubes have been measured off these aligned substrates. The number of multilayers could have an effect of the myotube length as both the 12Chit and 12CNW multilayers have less myotubes over 100 um. Fewer myotubes over 100 um were on the 12Chit compared to the 12CNW which again contributes to the theory that aligned myoblasts produce longer myotubes. This can be seen more clearly in Table 6-1 where the percentages of myotubes over specific lengths were calculated. For myotubes >100 um, the oriented substrates showed the greatest percentage compared to those with the chitosan top layer. For myotubes >200 um, it was the ChitCNW and 6CNW that had the larger percentages. The percentages of myotubes on Glass that were greater than 100 um and 200 um were also as high however it should be noted that less myotubes in total were recorded on the Glass substrate. Overall there were more myotubes in total on the ChitCNW and 6CNW substrates and a higher percentage of the myotubes measured were over 100 um.

Myogenic differentiation was also confirmed by the positive staining of myogenin and sarcomeric alpha actinin. Myogenin is a skeletal muscle transcription factor and sarcomeric alpha actinin is a structural fibrous protein found in skeletal muscle responsible for the attachment of actin filaments to the Z-discs in sarcomeres; it is often used as an indicator for sarcomere assembly (Mills, 2001; Juhas, Ye and Bursac, 2015). Myogenin is found in the nuclei after elongation and fusion has begun and is partly responsible for the production of sarcomeric alpha actinin (Buckingham and Montarras, 2008), which is only seen in forming myotubes where the nuclei are positive for myogenin (Figure 5-12). The percentage of myogenin positive nuclei was

calculated for the Glass and the aligned substrates (Figure 5-13 (b)). More than 20% of the nuclei expressed myogenin on Day 7 on the aligned substrates; however, it is highest on Glass and 6CNW substrates (40.2% ± 6.2% and 39.6% ± 7.7% respectively). Bian et al also reported myogenin positive nuclei present in myotubes with 32.7% ± 7.1% on a 2D sheet (unaligned) and an increase to 70.5% ± 4.7% on a 3D fibrin hydrogel (Bian and Bursac, 2009).

The amount of sarcomeric alpha actinin produced was measured using the confocal fluorescence micrographs of Day 7 (Figure 5-13 (a)). Although both Glass and 6CNW show around 40% of the nuclei as myogenin positive, the percentage of sarcomeric alpha actinin is higher on the 6CNW multilayer. No significant difference was found between any of the substrates; however, the substrates with the oriented CNWs had the highest percentage. The amount of sarcomeric alpha acitinin dropped between 6CNW and 12CNW suggesting the increase in layers and possibly the aggregation of cells on the 12CNW multilayer, reduced the production of microfilament protein. There was an increase in sarcomeric alpha actinin between the 12Chit and 12CNW multilayers, again supporting the theory that the alignment of the cells encourages differentiation. The presence of more sarcomeric alpha actinin on the ChitCNW and 6CNW substrates also supports the higher number of myotubes and myotube lengths measured on the same substrates.

Most literature agrees that the multinucleated feature of myotubes is important for the formation of skeletal muscle tissue, however, not all studies report it. Of those that do, the number of nuclei per myotube can range from 8 to 40 nuclei in studies cultured *in vitro* (Huang *et al.*, 2006; Jones *et al.*, 2018; Guo *et al.*, 2019). Length is often the main morphological feature measured as the number of nuclei per tube can be linked to myotube length. The length of a muscle fibre (and therefore the myotubes that form it) can vary depending on function and therefore have different numbers of nuclei depending on what is required (Christ *et al.*, 2015). The number of nuclei per myotube formed on these substrates again showed a similar trend to before (Figure 5-13 (c)). The aligned myotubes on the oriented substrates had a greater range of nuclei (3 to 16 nuclei per myotube) compared to the chitosan topped substrates (3 to 10 nuclei per myotube). Again, the Glass substrate was comparable to the aligned myotubes. What was noticeable about some of the myotubes on the Glass substrate

was the thickness and accumulation of nuclei in the myotubes (Figure 5-13 (d)). The myotubes on the oriented topography were almost always one nucleus thick, whereas some myotubes on the Glass substrate had clumps of nuclei forming the tube shape. This has been observed by Burattini et al (2004) who found the nuclei in unaligned myotubes either localised, clumped or distributed along the length the of myotube (S. Burattini, P. Ferri, M. Battistelli, R. Curci, F. Luchetti, 2004).

Overall the C2C12s have formed the longest myotubes and undergone the most differentiation on the aligned substrates. The increasing multilayers lead to the cells aggregating but still in some sort of alignment on the 12CNW multilayer. The myoblasts have responded well to Glass, however they did not broadly align without the presence of the oriented CNWs.

5.5.2 hSkMC Response

C2C12s are an immortalised cell line and proven to differentiate in to myotubes with differentiation media. Although they are a good standard to test the substrate's potential for skeletal muscle engineering, they are not completely representative of human primary cells. hSkMCs from PromoCell were used to investigate the primary cell response to the CNWs and the multilayers. These cells are biopsied from human skeletal muscle and were grown and differentiated in PromoCell hSkMC Growth Medium and PromoCell hSkMC Differentiation Medium respectively.

The time points for these cells were different to that of C2C12s. differentiation media was added when the cells reached 60-80% confluency and this was labelled as Day 0. Differentiation was expected between 2-8 days. On day 5, differentiation media was swapped back to growth media as per PromoCells protocol. Alamar Blue was used to measure cell viability through metabolic activity and PicoGreen was used to measure the cell number (Figure 5-14 and 5-16 respectively). There was no change between Day 0 and Day 4, however, there was a large increase from Day 4 to 8. Between Day 0 and Day 4 the cells were in differentiation medium and similar to the C2C12s, the proliferation slows as the cells undergo differentiation (Chargé and Rudnicki, 2004; Huang *et al.*, 2006). This is supported by the PicoGreen data as there is also no increase seen in cell number between Day 0 and 4. After Day 4, differentiation medium

was replaced with growth medium and both the metabolic actively and cell number increase. The most notable difference was seen between the thinner layers and the multilayers. Both the metabolic activity and the cell number on Day 8 are higher on the thinner substrates than on the multi-layered substrates and this likely due to the experimental set up. The cells on each substrate type reached 60-80% confluency at different rates therefore a decision was made to add the differentiation media once half the wells had reached the desired confluency. The cells on the Glass, Chitosan and ChitCNW substrates were of a higher density when the media was added than those on the 6CNW, 12Chit and 12CNW multilayers. As the cells were seeded at the same density originally, it can be concluded that the hSkMCs initial response was more positive to the thinner substrates than the multilayers. Again, variations were seen in repeats using these assays and the repeats can be found in the Appendix D and E.

The initial response of the cells to the substrates can be seen on the confocal fluorescence micrographs taken of the hSkMCs 24 h after seeding (Figure 5-18). Alignment is clear on ChitCNW and 6CNW substrates but not on the 12CNW multilayer. The number of nuclei per area and the percentage area covered by the cells were measured from the images (Figure 5-19 (a) and (b) respectively). The 12Chit and 12CNW multilayers had the lowest average for the number of nuclei per area although no significant difference was found between the substrate types. Some alignment could be seen on the 12CNW multilayer where individual cells can be seen stretching in the same direction as neighbouring cells although the cell density is low. ChitCNW and 6CNW had the highest percentage area coverage and was found to be significantly higher than the chitosan topped substrates. Chiron et al also reported seeing alignment and cell spreading after 24 h (Chiron *et al.*, 2012).

The hSkMCs were fixed on Day 8 and stained for myogenin, sarcomeric alpha actinin and actin. Figure 5-20 shows that the hSkMCs broadly align to the oriented CNWs on the ChitCNW and 6CNW substrates and partial alignment of the cells could be seen on the 12CNW multilayer. Similar to the myoblasts, local alignment was observed on the Glass and the chitosan topped substrates. The alignment was quantified shown in Figure 5-21 and measured from the direction of the actin filaments. Choi et al also reported actin filament alignment to oriented fibres and disordered filaments on randomly oriented fibres. The fibres used had diameters in the 100s of nano-meter

range and fusion of cells was seen after 7 days of differentiation (Choi *et al.*, 2008). Little or no cell fusion was observed with the hSkMCs, although some myogenin was seen on some of the elongated cells on the oriented substrates (Figure 5-23). The literature approximately agrees that differentiation is most often seen by day 7 although with that the general finding is the rate of differentiation increased from a 2D surface to a 3D scaffold (Mudera *et al.*, 2010; Chiron *et al.*, 2012). Other indication of myotube formation, apart from cell fusion, is the thickening of actin filaments and the presence of sarcomeric alpha actinin once differentiation has been initiated (Cronin *et al.*, 2004; Chiron *et al.*, 2012). It is likely that the hSkMCs did not reach differentiation by Day 8 on these substrates, however the increased elongation of the cells on the oriented substrates and initial presence of myogenin suggests the cells were in the process of or in the early stages of differentiation. Another point the literature agrees on is the effect of a high cell density when culturing hSkMCs (Cronin *et al.*, 2004; Mudera *et al.*, 2010). Like C2C12s, hSkMCs require cell- cell interaction and high cell proximity could contribute to increased differentiation (Wragg *et al.*, 2019). It could be possible that an increased cell density and longer culture time could lead to myotube formation from hSkMCs on the CNW-chitosan multilayers.

Some studies have compared the validity of using C2C12s in place of hSkMCs. As stated before, C2C12s are often used due to their dependability, reproducibility and volume of literature the results can be compared to. The cells are also very easy to maintain in the lab and can be quite forgiving to the least graceful scientist. hSkMCs on the other hand require more attention and planning as primary cells and they are more sensitive to discrepancies in cell work such as becoming over confluent or missing a feeding. Sengupta et al, found that human and mouse myoblasts were comparable for elongation and alignment, however, not for cell spreading or differentiation (Sengupta *et al.*, 2012). This was observed in this work as the hSkMCs respond well to the oriented topography and showed elongation. There was less cell spreading compared to the C2C12s and differentiation was not observed. Cronin et al examined the difference in gene regulation of the C2C12s compared to the hSkMCs when undergoing differentiation. It reported that genes related to cell adhesion, cellular metabolism, cell cycle control and cell-ECM interaction were similar in C2C12s to hSkMCs. However, genes related to myogenesis and muscle contraction were differently regulated

(Cronin *et al.*, 2004). This agrees with Sengupta et al, who also came to the conclusion that C2C12s do not faithfully recapitulate the differentiation of hSkMCs, however it can be used to replicated myoblast elongation and alignment to topographical cues.

Sengupta et al also reported that the human myoblasts responded well to smaller topographical cues (at 20 µm) than larger grooves (200 µm) and suggested it was either the size or the increased volume of cues that influenced the cell response. It was also reported that the wider grooves resulted in wider myotubes with high number of nuclei per myotube (Sengupta *et al.*, 2012). The hSkMC have been shown to align to the oriented CNWs, which are in the nano-meter range suggesting that hSkMC can respond to topographical features smaller than microns and of similar magnitudes of the native ECM.

5.5.3 BM-MSC Response

BM-MSCs of 2 donors were seeded on to the full range of substrates and the cell responses were mixed. Donor 1 showed a positive response to the substrates and showed higher cell numbers than those of Donor 2. The cells of Donor 2 appeared less dense than those of Donor 1 (Figure 5-28), which was shown in the PicoGreen data (Figure 5-27). Specifically, Donor 2 had a poor cell response to the 12 layered substrates shown in both the bright field images and PicoGreen data. Immunofluorescence staining of the BM-MSCs showed the alignment of the cells and the actin fibres stretching (Figure 5-29 and 5-30). Micrographs of Donor 2 on Day 7 are not shown as no cells were found on the substrates probably due to cell death or detachment. The poor cell response seen from the BM-MSCs of Donor 2 could be due to experimental error or problems which occurred before freezing.

Donor 1 showed broad alignment to the oriented CNW topography on the 6CNW and 12CNW substrates and the actin fibres were seen to stretch in a unidirectional pattern. This alignment is promising of structural tissues like skeletal muscle. Through the staining, only background was observed for the myogenin and sarcomeric alpha actinin channels. Noticeably, poor cell spreading was observed on the ChitCNW substrate which is different from the C2C12s and hSkMCs which responded well to the same substrate.

The differentiation of BM-MSCs is widely researched as there are many different approaches to different cell types with different degrees of successes. It is generally agreed that BM-MSCs need to have the right combination of stimuli in order to be directed towards a specific tissue lineage. Engler et al (2006) has shown that by controlling the stiffness of variably compliant polyacrylamide gels, MSCs could be guided towards different tissue lineages as the cells responded to the mechanical properties of the gel. Myogenic expression of MSCs was observed on moderately stiff matrices with a Young's modulus of 11 kPa, which is close to that of native muscle (10 kPa). Although there was an up-regulation of myogenic factors, the cells remained early myoblasts and cell fusion into myotubes was not reached (Engler *et al.*, 2006). Other studies have explored the topographical approach through the use of electrospun fibres or micropatterned grooves. Dang et al (2007) cultured MSCs on aligned electrospun nanofibres of thermally responsive hydroxybutyl chitosan and found no expression of MyoD but some myogenin on the aligned cells. Li et al (2011) developed a biodegradable polymer substrate on which channels were machined in using a laser. Cell alignment and highly organised bundles of actin were observed on the narrower channels with depths on 20 µm and widths of 30 µm and an up-regulation of the MyoD1 gene was found. However in both studies, good contact guidance was seen but cell fusion and the formation of myotubes was not (Dang and Leong, 2007; Li *et al.*, 2012). Smaller topographies have also influenced MSCs, such as the nano-printed poly(dimethylsiloxan) (PDMS) substrates developed by Yim et al (2007) with channels 350 nm wide. Alignment of the cytoskeleton and nuclei of the cells was observed to follow the pattern however the MSCs up-regulation of gene related to neural lineages (Yim, Pang and Leong, 2007).

The literature suggests that a combination of different types of stimuli is needed to direct MSCs towards specific lineages. The alignment of the BM-MSCs on the oriented CNW topography could support other stimuli such as mechanical or chemical.

Overall the oriented CNWs have shown to broadly align C2C12s, hSkMCs and BM-MSCs. Satellite cells have also been shown to follow the nanotopography (Figure 5-31). C2C12s and hSkMCs responded well to the ChitCNW and 6CNW whereas the BM-MSCs found the 6CNW and 12CNW multilayer more favourable. Although no cell fusion or myotube formation was observed of the hSkMCs or BM-MSCs, both cell types could

potentially undergo myogenic differentiation with the optimum combination of stimuli with the oriented CNWs.

Chapter 6: Influence of the Addition of Key ECM Proteins on Cell Response

6.1 Chapter Summary

One of the key concepts of biomaterials is its use in tissue engineering to simulate the native ECM of a tissue and sometimes this is aided with the use of actual ECM proteins. The idea to support biomaterials with additional proteins has been seen across the literature in the engineering of many different tissue types (Bacakova *et al.*, 2011). In skeletal muscle engineering, fibronectin and laminin are the most popular apart from collagen although collagen is often used as a base biomaterial in scaffold formation (Cronin *et al.*, 2004; Riboldi *et al.*, 2008; Lee *et al.*, 2015).

6.2 Protein Adsorption

6.2.1 Presence of Proteins

Protein adsorption of fibronectin and laminin were confirmed using the NanoOrange Assay (Section 4.2.4) and further confirmed with immunofluorescence staining. Substrates were treated as if for cell seeding before staining and stained for both proteins. The proteins appear speckled across the surface (Figure 6-1). Background staining can be seen on the multilayer substrates. This has been noticed before when cells are not present. Figure 6-2 shows the negative staining on the 12CNW multilayer. The positive images show the fibronectin and laminin on the 12CNW multilayer whereas the negatives show the opposite protein channel. The images of the negatives are cloudy which is how the background had appeared before.

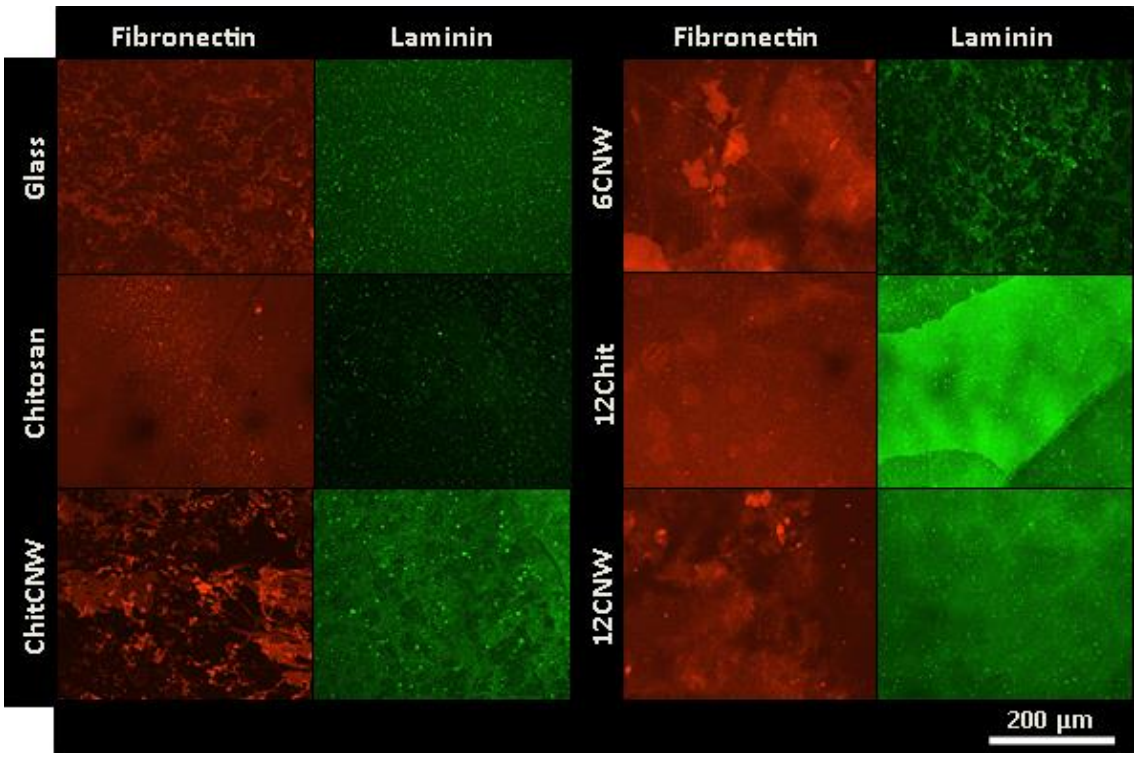

Figure 6-1: Confocal fluorescence micrographs taken at 20x mag of fibronectin and laminin adsorbed on to the surface of the full range of substrates.

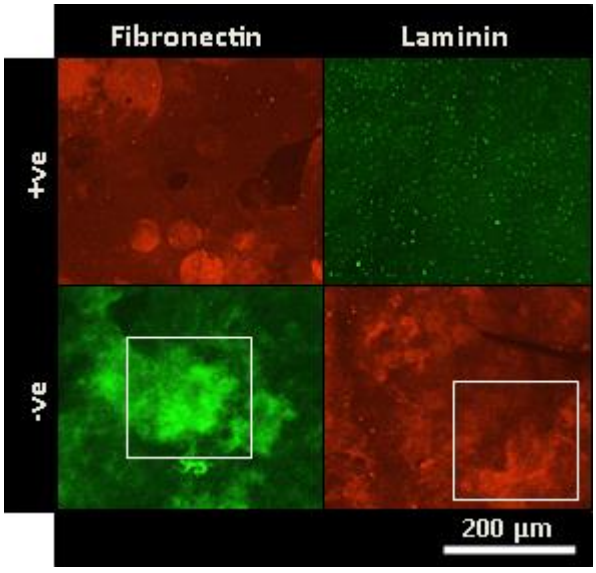

Figure 6-2: Confocal fluorescence micrographs taken at 20x mag of the 12CNW multilayer substrate showing the negative staining on the fibronectin and laminin treated surfaces. Background can be seen on the negatives as cloudy features.

6.2.2 Roughness and Protein Adsorption

After protein adsorption the roughness of the substrates was measured again. Figure 6-3 shows that there was no change in the roughness of any of the substrates after the addition of the proteins. No significant difference was found between each protein and no treatment.

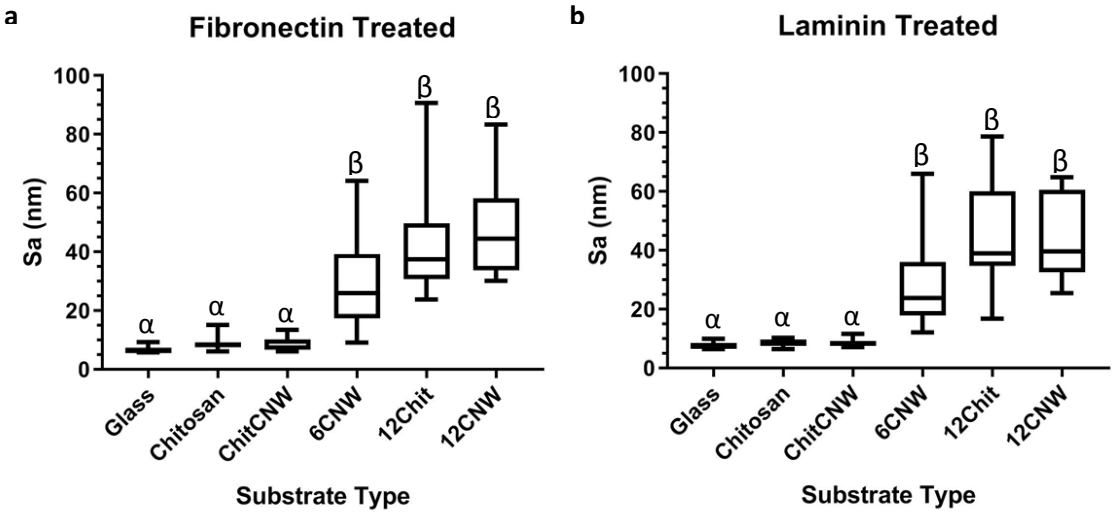

Figure 6-3: Box whisker plots of the roughness (Sa (nm)) of the range of multilayer substrates after being treated with (a) fibronectin and (b) laminin. Four random areas were measured across N=3 of each substrate type. Data analysis carried out using ordinary one-way anova with Turkey's multiple comparison tests with a single pooled variance. Greek labels indicate groups within which no significant difference was observed. For those that are significantly different = $p < 0.05$.

6.2.3 Wettability and Protein Adsorption

After protein adsorption the wettability of the substrates was measured again. Figure 6-4 shows the contact angle of all the substrates are now near 60^{o}. The Glass substrate was the only one to show any large change in contact angle, which increased from 10.49^{o} ± 5.90^{o} to 64.05^{o} ± 14.25^{o} on fibronectin and 65.64^{o} ± 8.86^{o} on laminin. No significant difference was found between each protein per substrate however the chitosan topped substrates were found to be significantly lower on the protein treated samples compared to the non-treated.

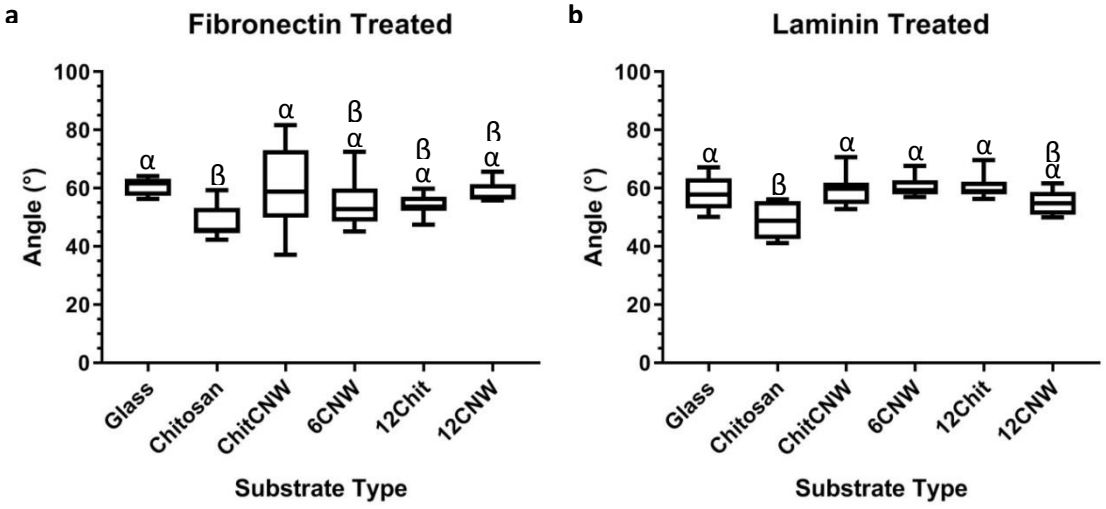

Figure 6-4: Box whisker plots of the contact angle (^{o}) of the range of multilayer substrates after being treated with (a) fibronectin and (b) laminin. Three random areas were measured across N=3 of each substrate type. Data analysis carried out using ordinary one-way anova with Turkey's multiple comparison tests with a single pooled variance. Greek labels indicate groups within which no significant difference was observed. For those that are significantly different = $p < 0.05$.

6.3 Cell Response to Protein Adsorption

6.3.1 Influence of Conditioning Substrates

As described in the materials and methods section, the substrates were pre-conditioned with growth media overnight before cell seeding. In order to investigate the effect of the pre-conditioning on cell response, an experiment was carried out to see if there was a decrease in cell proliferation if the substrates were not left in growth media overnight. The conditions were growth media with and without serum, PBS and UltraPure™ dH_2O and the cell response was examined on a smaller range of the substrate types through Alamar Blue, bright field light microscope images and Pico Green.

The Alamar Blue assay was used to measure the metabolic activity of the cells in response to the different pre-conditioning treatments (Figure 6-5). No difference was found in the first two time points for ChitCNW (Figure 6-5 (a)) however on Day 2 there is a significant difference between the PBS and UltraPure™ dH_2O to the media without serum samples. The only significant difference found on the 12CNW metabolic activity data (Figure 6-5 (b)) was on Day 1 between the media without serum and UltraPure™ dH_2O samples. The other significant differences labelled in Figure 6-5 follow the change in metabolic activity between time points per substrate. There is a statistical significant difference between 4 hrs and Day 2 for all substrates. The metabolic activity graphs for Glass and 6CNW substrates can be found in Appendix F.

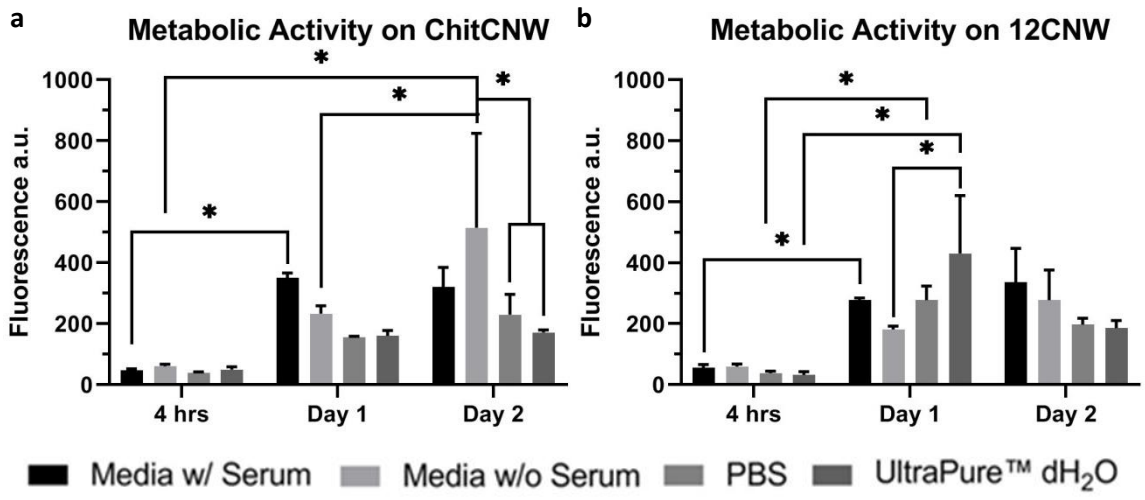

Figure 6-5: Metabolic activity of C2C12s on the preconditioned (a) ChitCNW and (b) 12CNW substrates at 4 h, 1 d and 2 d after seeding using the Alamar Blue Assay. Data analysis carried out using RM two-way anova with the Geisser-Greenhouse correction and with Turkey's multiple comparison test. For those that are significantly different (*) = $p < 0.05$.

Bright field light microscope images taken throughout showed little difference in cell spreading on all the substrate types regards of what they were pre-conditioned with. Figure 6-6 shows example images taken on Day 8 where cells are seen spreading and aligning on the oriented topography. There is also no formation of myotubes which is expected as the cells were kept in growth media for the full 8 days.

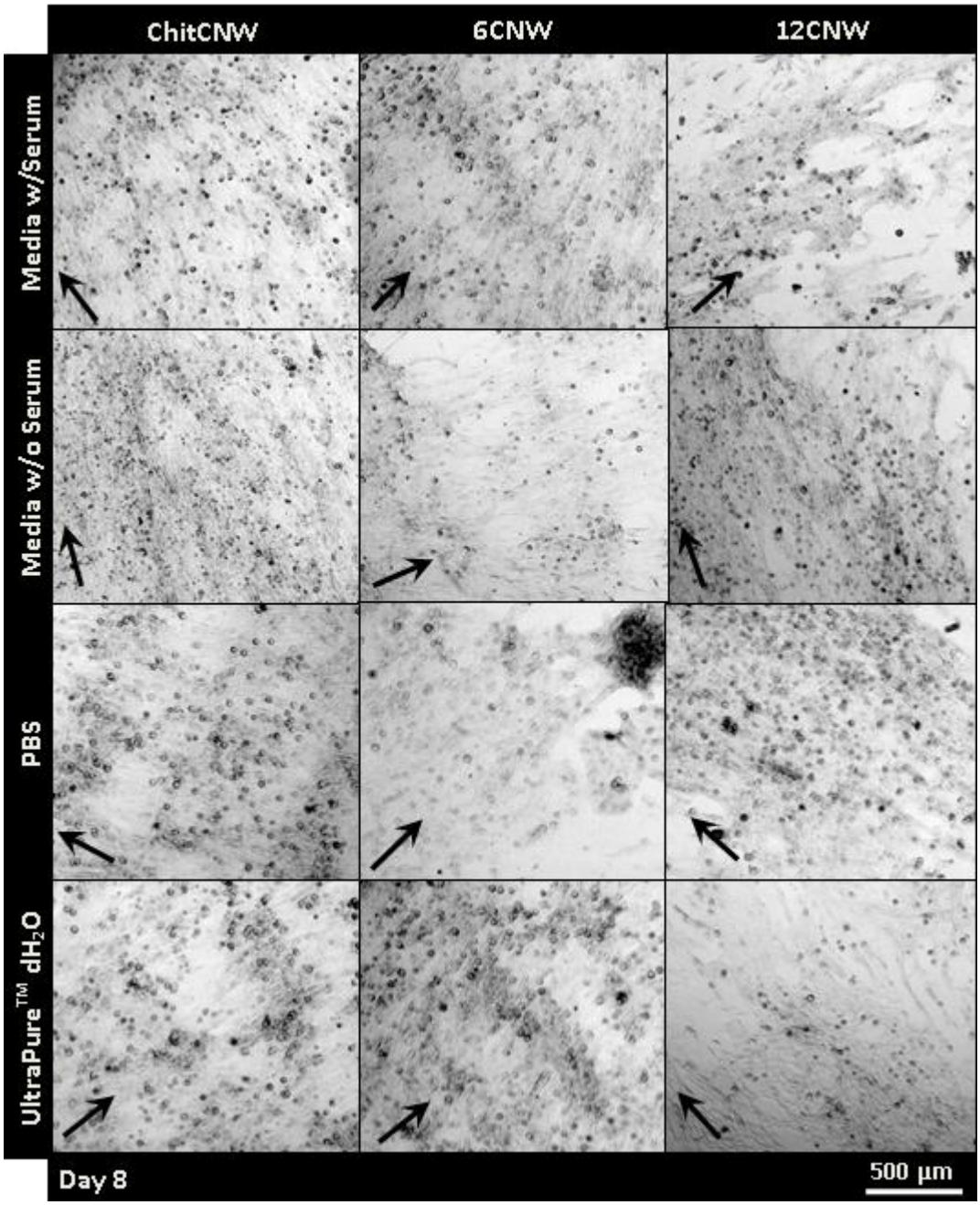

Figure 6-6: Bright field light microscope images taken at 4x mag showing the C2C12s 8 days after seeding. Cell alignment and spreading can be seen on all the oriented substrates irrelevant of pre-conditioning. The arrows indicate the general direction of the cells.

The cell number was measured using the Pico Green assay shown in Figure 6-7. Cell number was shown to increase on all substrates over the 8 days. The only significant difference was found on the ChitCNW (Figure 6-7 (a)) on Day 4 between the substrates conditioned in media and the UltraPure™ dH_2O whereas no significant difference was found on the 12CNW multilayer. The other significant differences labelled in Figure 6-7 follow the change in cell number between time points per substrate. For both ChitCNW and 12CNW, there were significant differences between Day 1 and Day 4, Day 8 for all the substrate types. The cell number graphs for Glass and 6CNW substrates can be found in Appendix G. Overall, the cells recovered from any negative effects of not conditioning the substrates with media before seeding therefore the removal of this step was not considered detrimental to examining the effect of protein adsorption on C2C12 growth and differentiation.

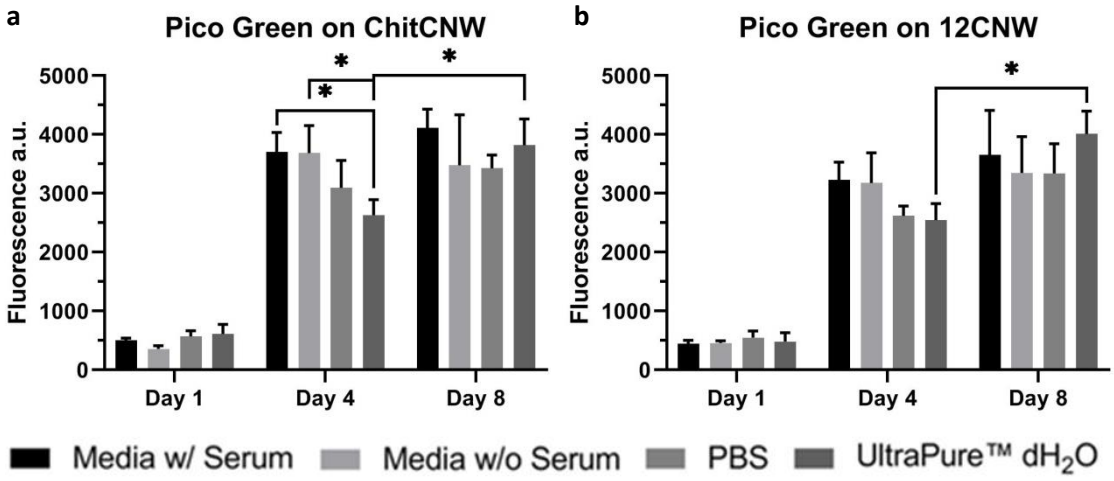

Figure 6-7: Cell number of C2C12s on the (a) ChitCNW and (b) 12CNW substrates at 1 day, 4 days and 8 days after seeding using the Pico Green Assay. Data analysis carried out using RM two-way anova with the Geisser-Greenhouse correction and with Turkey's multiple comparison test. For those that are significantly different (*) = $p < 0.05$.

6.3.2 C2C12 Response to Protein Adsorption

C2C12 Viability on Proteins

C2C12s were seeded on to a smaller range of substrate types to investigate the combined effects of the proteins and oriented CNWs on the cell response. Figure 6-8 shows bright field microscope images of the C2C12s 24 h after seeding. Cells are already showing alignment to the oriented topography apart from the C2C12s on laminin.

The initial cell response to the protein treated substrates was examined using bright field light microscope images (Figure 6-8) and metabolic activity (Figure 6-9). The metabolic activity shows an increase between Day 1 and 4 for all the substrates which has been seen before in Section 5.2.1. Some significant differences were found on all the substrate types and all on Day 4. There was a significant difference between the protein treated and non-treated on Glass and between laminin and non-treated on 6CNW. On the ChitCNW and 12CNW substrates, there were significant differences between all of the conditions on Day 4. Notably the metabolic activity was lower on the untreated substrates compared to the protein treated substrates.

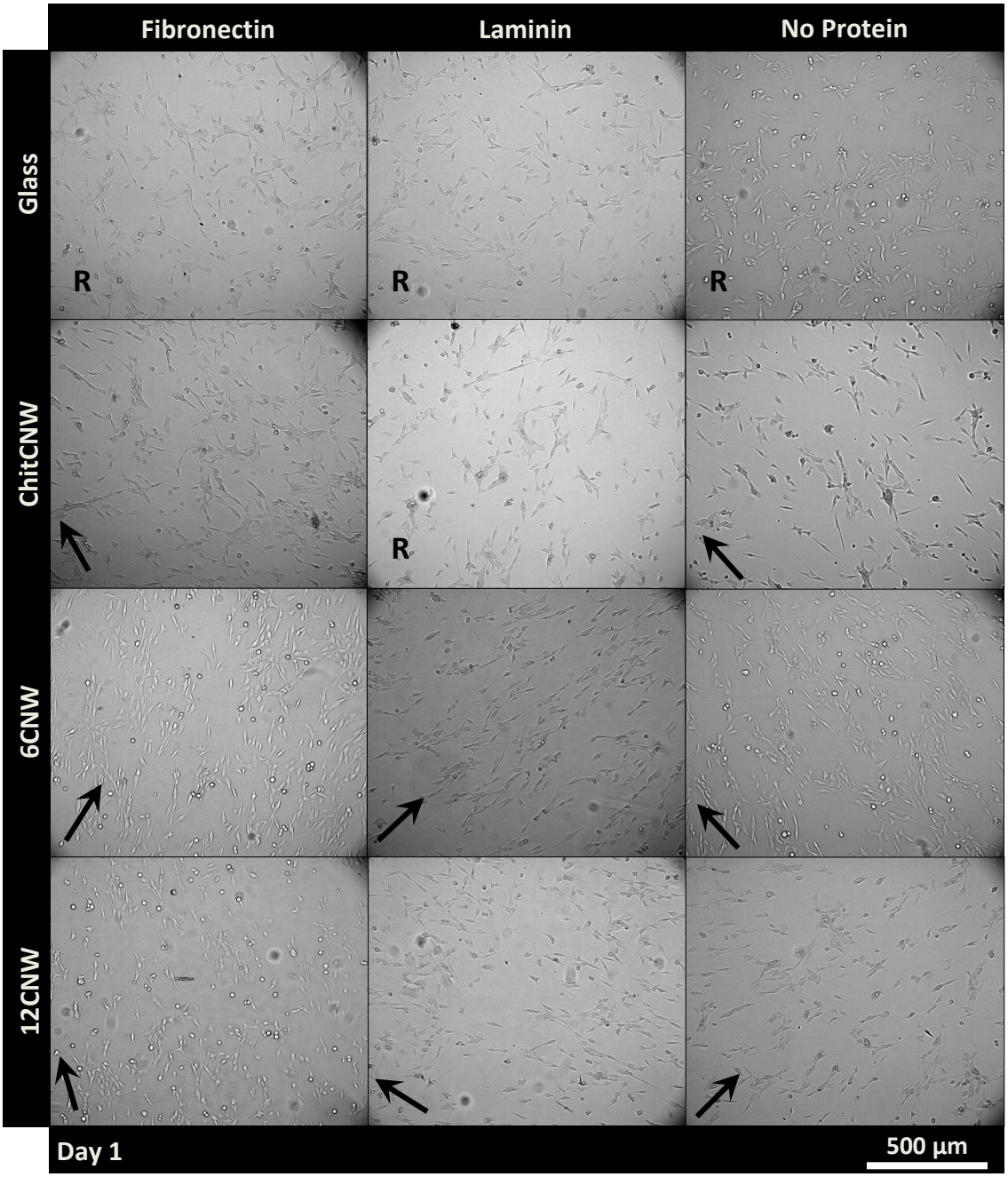

Figure 6-8: Bright field light microscope images taken at 10x mag showing the C2C12s 24 h after seeding. Cell alignment can already be seen on all the oriented substrates apart from the ChitCNW with laminin. The arrows indicate the general direction of the cell alignment and the R denotes where the cells are randomly oriented. Substrates named with CNW have the oriented topography.

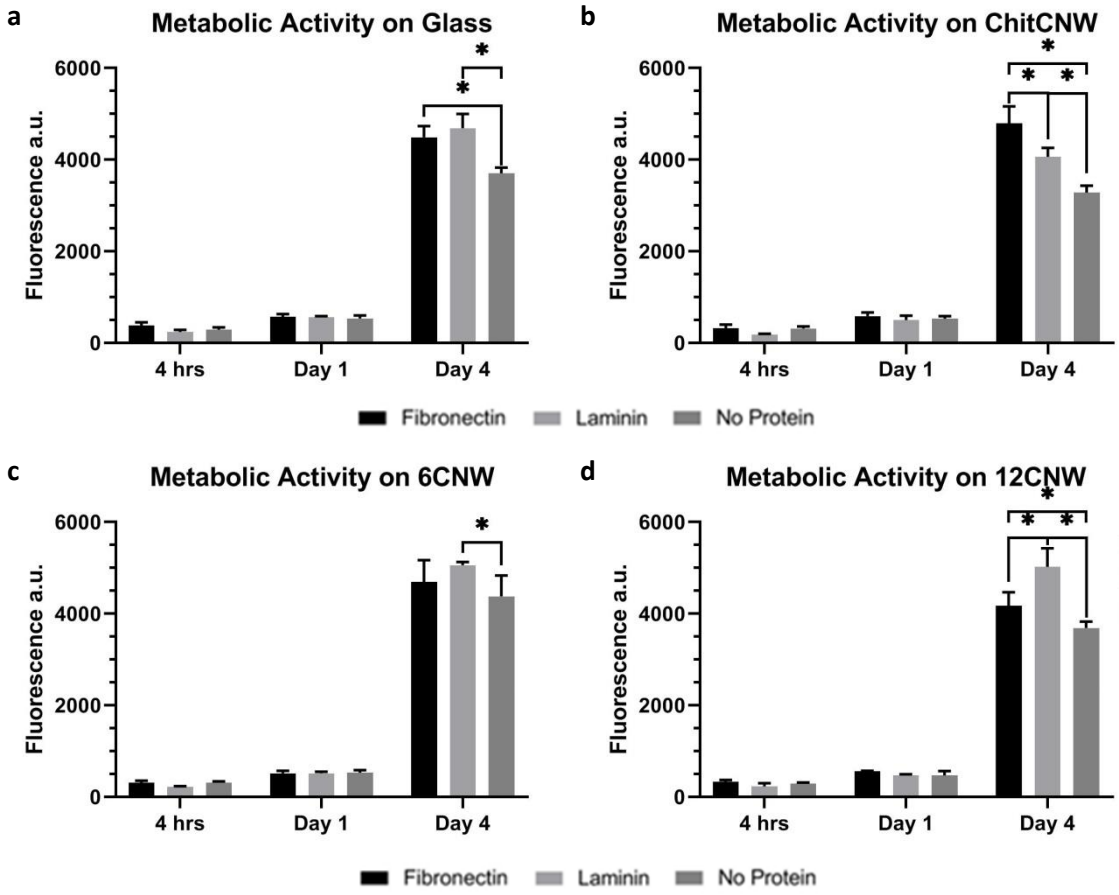

Figure 6-9: Metabolic activity of C2C12s on the (a) Glass, (b) ChitCNW, (c) 6CNW and (d) 12CNW substrates at 4 h, 1 d and 4 d after seeding using the Alamar Blue Assay. Data analysis carried out using RM two-way anova with the Geisser-Greenhouse correction and with Turkey's multiple comparison test. For those that are significantly different (*) = $p < 0.05$.

Cell number was measure using the PicoGreen assay (Figure 6-11) and surface coverage was observed using bright field images (Figure 6-10). Significant differences were found on all of the time points for all the substrate types between the protein treated samples and the non-treated substrates. It is clear that the presence of the proteins increased cell number. Alignment and myotube formation can also be seen in the bright field images in Figure 6-10.

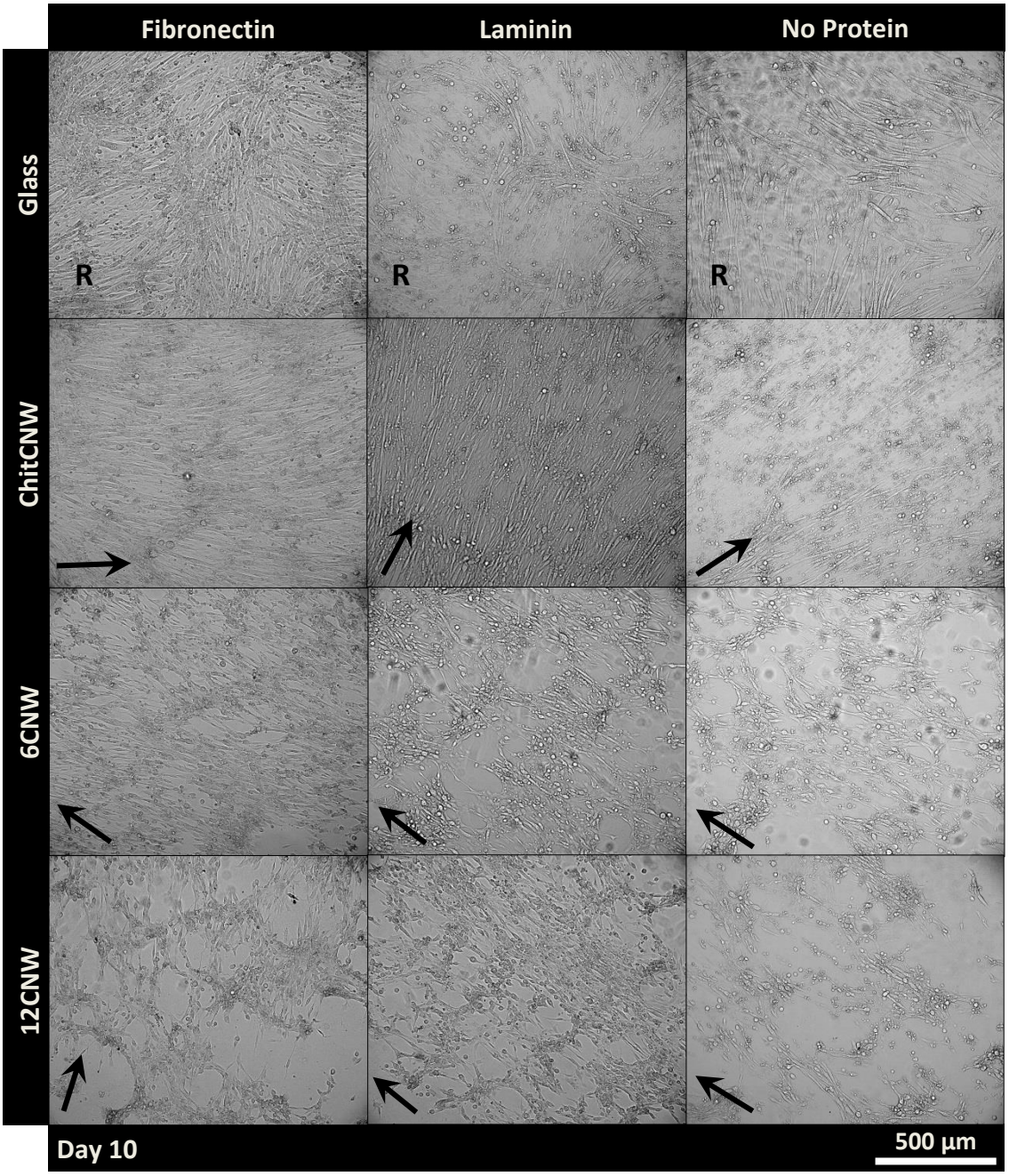

Figure 6-10: Bright field light microscope images taken at 10x mag showing the C2C12s 8 days after seeding. Cell alignment and myotube formation can be seen on all the oriented substrates. The arrows indicate the general direction of the cell alignment and the R denotes where the cells are randomly oriented. Substrates named with CNW have the oriented topography.

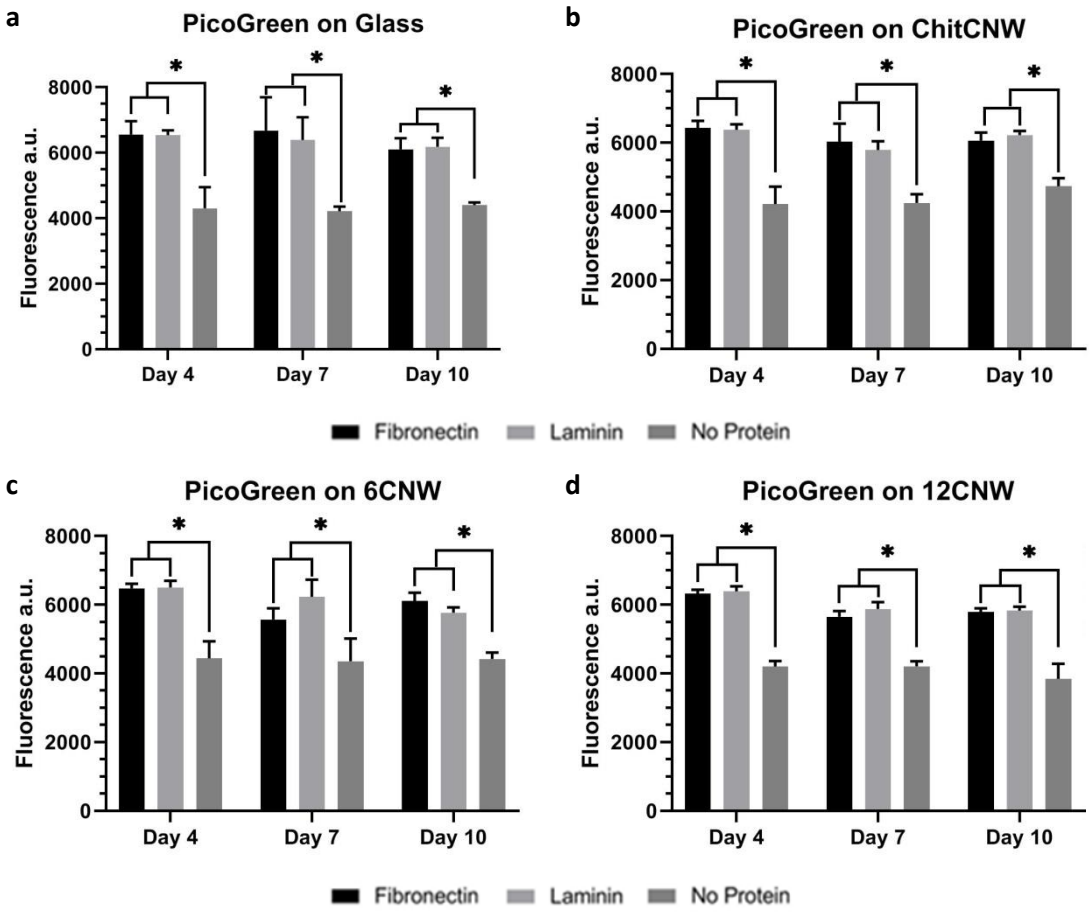

Figure 6-11: Cell number of C2C12s on the (a) Glass, (b) ChitCNW, (c) 6CNW and (d) 12CNW substrates at 4 days, 7 days and 10 days after seeding using the Pico Green Assay. Data analysis carried out using RM two-way anova with the Geisser-Greenhouse correction and with Turkey's multiple comparison test. For those that are significantly different (*) = $p < 0.05$.

Using confocal fluorescence micrographs (examples are shown in Figure 6-13), the number of nuclei per area (μm^2) on Day 7 was measured and shown in Figure 6-12. Within fibronectin samples, Glass and ChitCNW were found to be significantly different to the 12CNW multilayer and this was the same for the untreated substrates. Within the laminin samples, Glass and 6CNW were found to be significantly different to the 12CNW multilayer. Within substrate types, the fibronectin and untreated samples were shown to be significantly different to the laminin. Overall it appears the number of nuclei per area decreases as the number of layers in the substrate increases, however, of further interest is the decrease in nuclei per area between the protein treated and non-treated substrates although not significant.

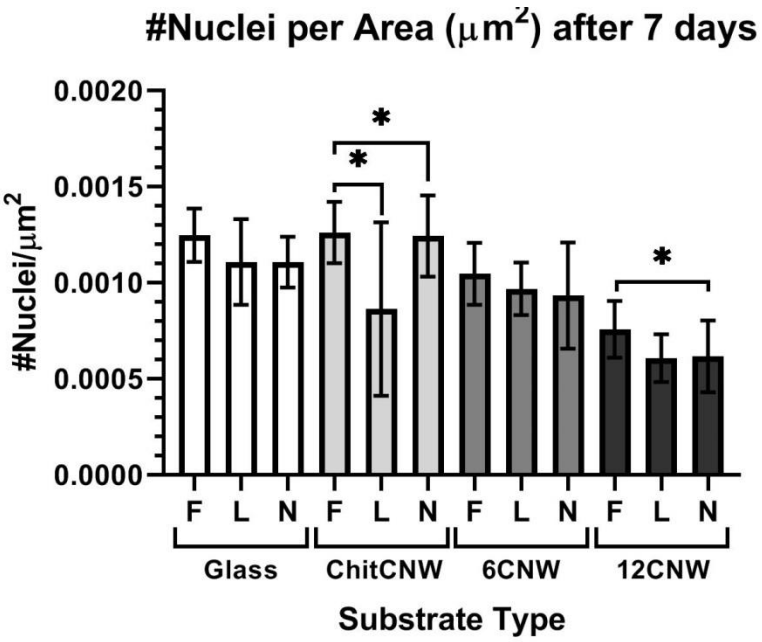

Figure 6-12: The number of nuclei per area (μm^2) was calculated from confocal fluorescence micrographs on Day 7. Data analysis carried out using ordinary one-way anova with Turkey's multiple comparison tests with a single pooled variance. For those that are significantly different (*) = $p < 0.05$. The letters represent the different treatments, F = fibronectin, L = laminin and N = no treatment.

C2C12 Differentiation on Proteins

Differentiation of the C2C12s and myotube formation was observed on all of the substrates regardless of the presence of proteins. Broad alignment can be seen on the oriented substrates in Figure 6-13 and it was also noted that the aggregation of myoblasts and myotubes seen in Section 5.1.2 is also present on the 12CNW multilayer and to some degree the 6CNW. The lengths of the myotubes formed were measured and shown in Figures 6-14 and 6-15. Again, due to the measuring technique and the distribution of data, the lengths >100µm were extracted to better see the spread of longer lengths. The percentages of specific lengths were calculated to show the distribution of the longer myotubes and shown in Table 6-1. Highlighted in bold, the ChitCNW and 6CNW of the fibronectin treated substrates showed the highest number of myotubes over 50 µm, 100 µm and 200 µm on the oriented samples although similar to the value for Glass.

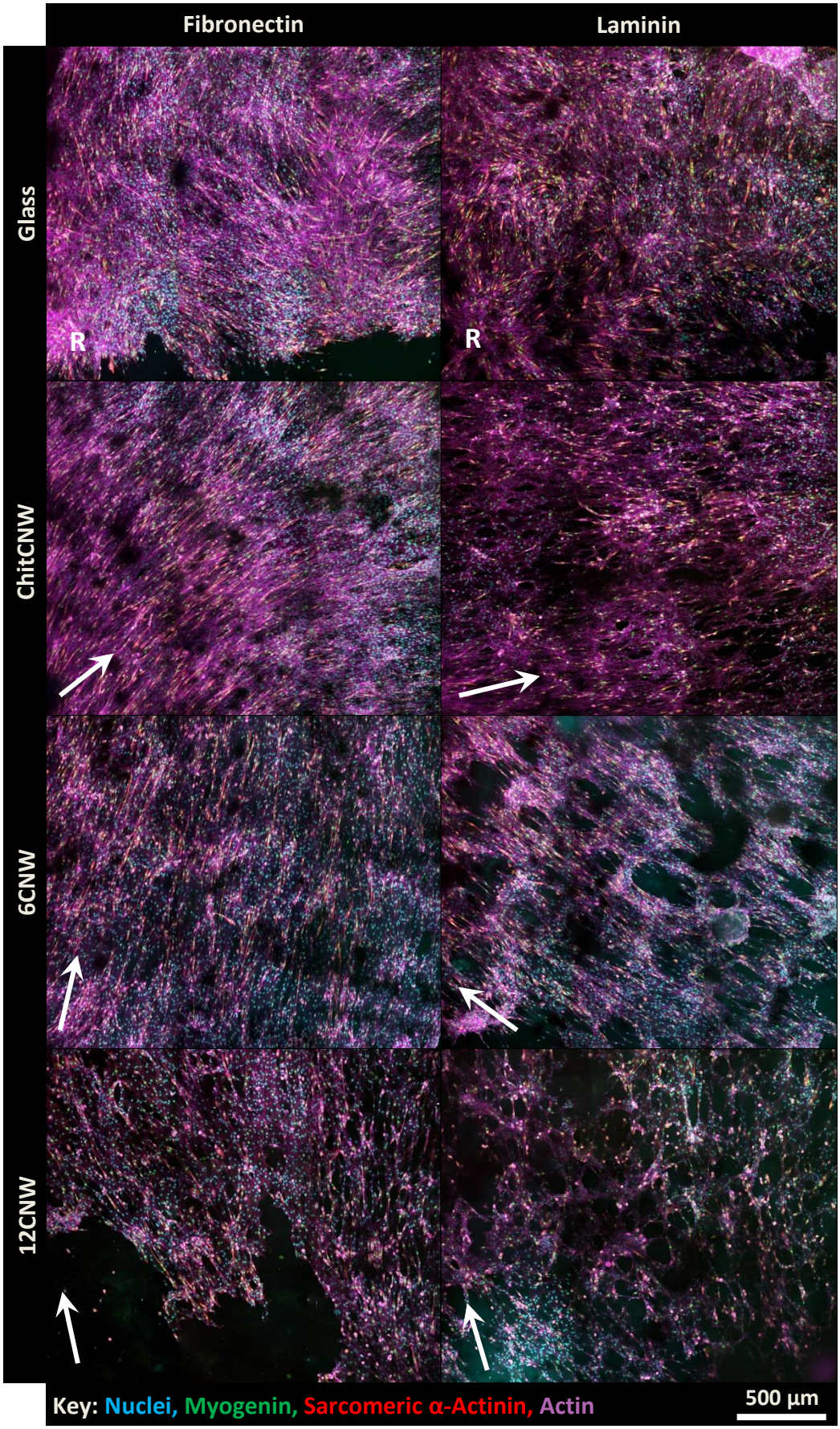

Figure 6-13: Confocal fluorescence micrographs of C2C12s on the fibronectin and laminin treated substrates 7 days after seeding, taken at 20x mag and stitched together in maps of 3x3. The arrows indicate the general direction of the cell alignment and the R denotes where the cells are randomly oriented. Substrates named with CNW have the oriented topography.

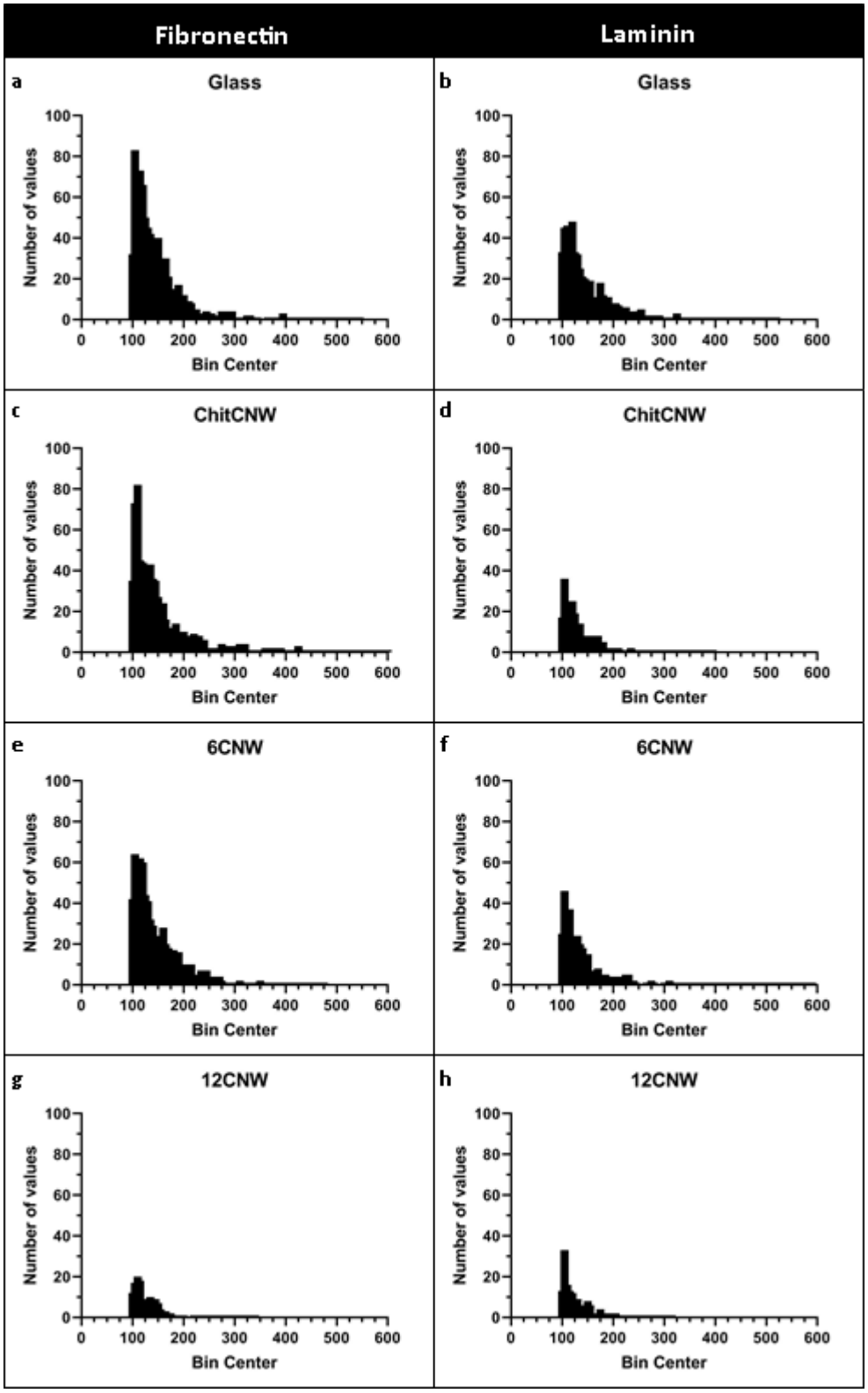

Figure 6-14: The average myotube length was measured for fibronectin and laminin treated substrates. Measurements of myotubes >100 µm were extracted for each protein, fibronectin (a), (c), (e) and (g) and laminin (b), (d), (f) and (h). Full histograms can be found in Appendix H.

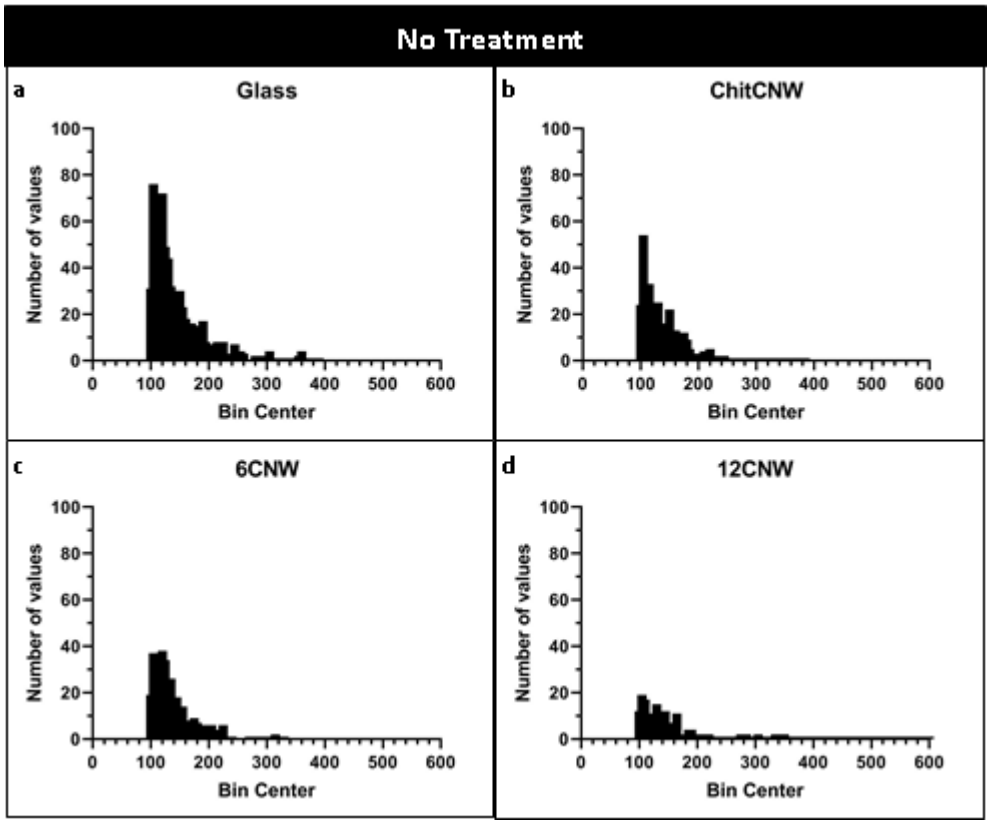

Figure 6-15: The average myotube length was measured for the non- treated substrates. Measurements of myotubes >100 µm were extracted for each substrate type (a) Glass, (b) ChitCNW, (c) 6CNW and (d) 12CNW. Full histograms can be found in Appendix I.

Substrate		Total Count	>50µm (%)	>100µm (%)	>200µm (%)
Fibronectin	Glass	6618	41.83	12.84	1.48
	ChitCNW	**6589**	**39.38**	**11.15**	**1.68**
	6CNW	**7697**	**34.55**	**9.56**	**1.20**
	12CNW	3953	22.36	3.42	0.15
Laminin	Glass	5284	37.13	10.33	1.40
	ChitCNW	4169	29.46	5.73	0.17
	6CNW	5892	28.51	6.25	0.81
	12CNW	4471	22.39	3.47	0.18
No Treatment	Glass	5677	39.18	12.75	1.57
	ChitCNW	5457	31.32	6.93	0.55
	6CNW	6107	27.30	6.57	0.54
	12CNW	3180	23.62	6.01	0.94

Table 6-1: The percentage of myotubes above specific lengths show the distribution of the myotube lengths over 25 µm.

The alignment of the myotubes were quantified and shown in Figure 6-16. Fibronectin treated substrates showed similar alignment to the non-treated substrates however the laminin treated substrates showed less alignment. However, the alignments of the myotubes on the oriented CNWs of the laminin substrates are still a little more aligned than the Glass.

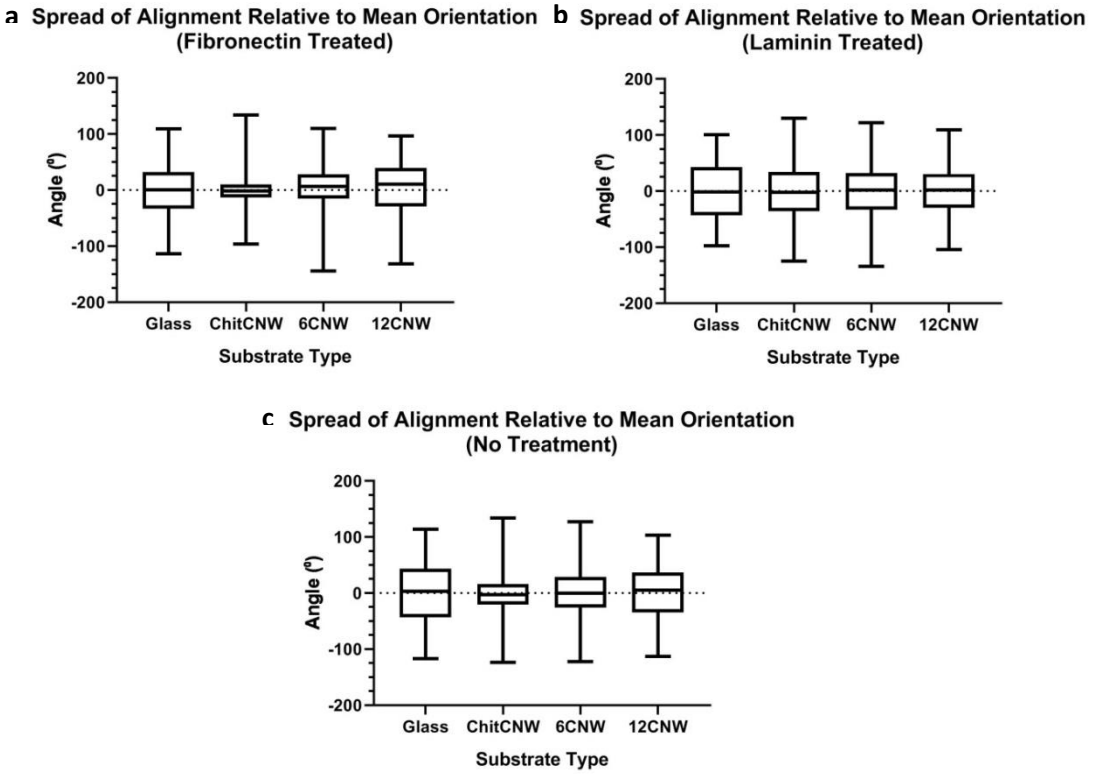

Figure 6-16: Alignment of the myotubes was measured on each substrate type. The distribution of the angles from 0^{o} is shown by the box whisker graph for each treatment and substrate type, (a) fibronectin, (b) laminin and (c) no treatment. A smaller box shows that most of the data (angles) is in a narrower range and therefore the cells are more aligned. A larger box shows that most of the data (angles) is in a wider range and therefore the cells are not as aligned.

Figure 6-17 shows clearly the differentiation of myoblasts and forming of myotubes on the protein treated substrates. Multinucleated tubes can be seen forming where there is sarcomeric alpha actinin (red) and myogenin positive nuclei (green). To investigate the C2C12 differentiation quantitatively, the percentage of nuclei expressing myogenin and the percentage area coverage of sarcomeric alpha actinin (Figure 6-18 (a) and (b)) were measured. For the percentage of nuclei expressing myogenin, significant differences were found within the fibronectin treated samples between the Glass, 6CNW and ChitCNW substrates and within the non-treated samples between the Glass, 6CNW and the ChitCNW, 12CNW substrates. The ChitCNW of the laminin was significantly different to the non-treated ChitCNW and the 12CNW laminin to the 12CNW multilayer of the fibronectin and non-treated. For the percentage area coverage of sarcomeric alpha actinin, significant differences were found between the fibronectin Glass, ChitCNW and 12CNW multilayer, laminin Glass, 6CNW and ChitCNW and non-treated ChitCNW, 12CNW and Glass. The ChitCNW of the fibronectin was significantly different to the non-treated 12CNW and the ChitCNW fibronectin to the ChitCNW multilayer of the laminin and non-treated. Overall, in line with the myotube length data, there is decreasing presence of sarcomeric alpha actinin as the number of layers increase in the substrate, however, this is not shown in the expression of myogenin in the nuclei. No trend was seen per substrate type between the different protein treatments.

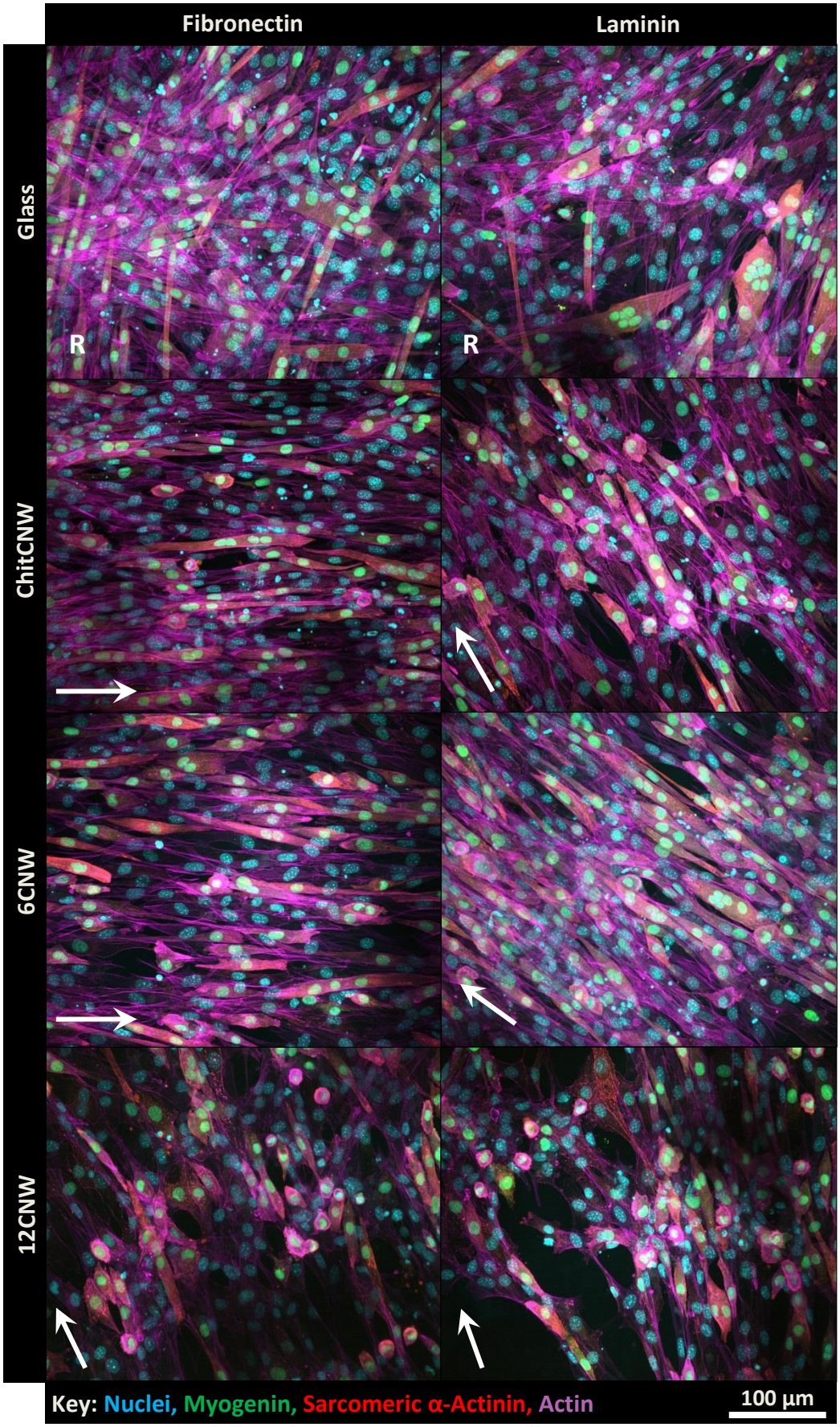

Figure 6-17: Confocal fluorescence micrographs of C2C12s on the fibronectin and laminin treated substrates 7 days after seeding, taken at 40x mag. The arrows indicate the general direction of the cell alignment and the R denotes where the cells are randomly oriented. Substrates named with CNW have the oriented topography.

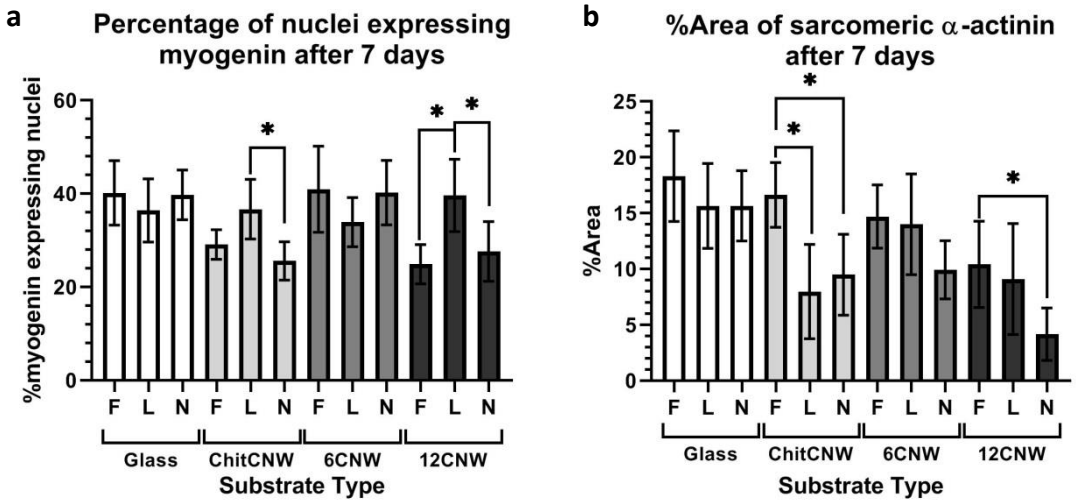

Figure 6-18: Differentiation of the C2C12s was measured on day 7 by (a) the percentage of nuclei expressing myogenin and (b) the percentage area coverage of sarcomeric alpha actinin. Data analysis carried out using ordinary one-way anova with Turkey's multiple comparison tests with a single pooled variance. For those that are significantly different (*) = $p < 0.05$. The letters represent the different treatments, F = fibronectin, L = laminin and N = no treatment.

6.3.3 BM-MSC Response to Protein Adsorption

BM-MSCs from Donor 2 which initially showed a poor response to the CNW multilayers were seeded on to fibronectin and laminin treated substrates. A significant improvement in cell adhesion and spreading was observed of the same BM-MSCs on the fibronectin and laminin treated substrates. Figure 6-19 shows the broad alignment of the BM-MSCs over large areas with arrows indicating the general direction. Figure 6-20 shows the alignment and elongation of the cells in more detail. Actin can be seen stretching unidirectionally.

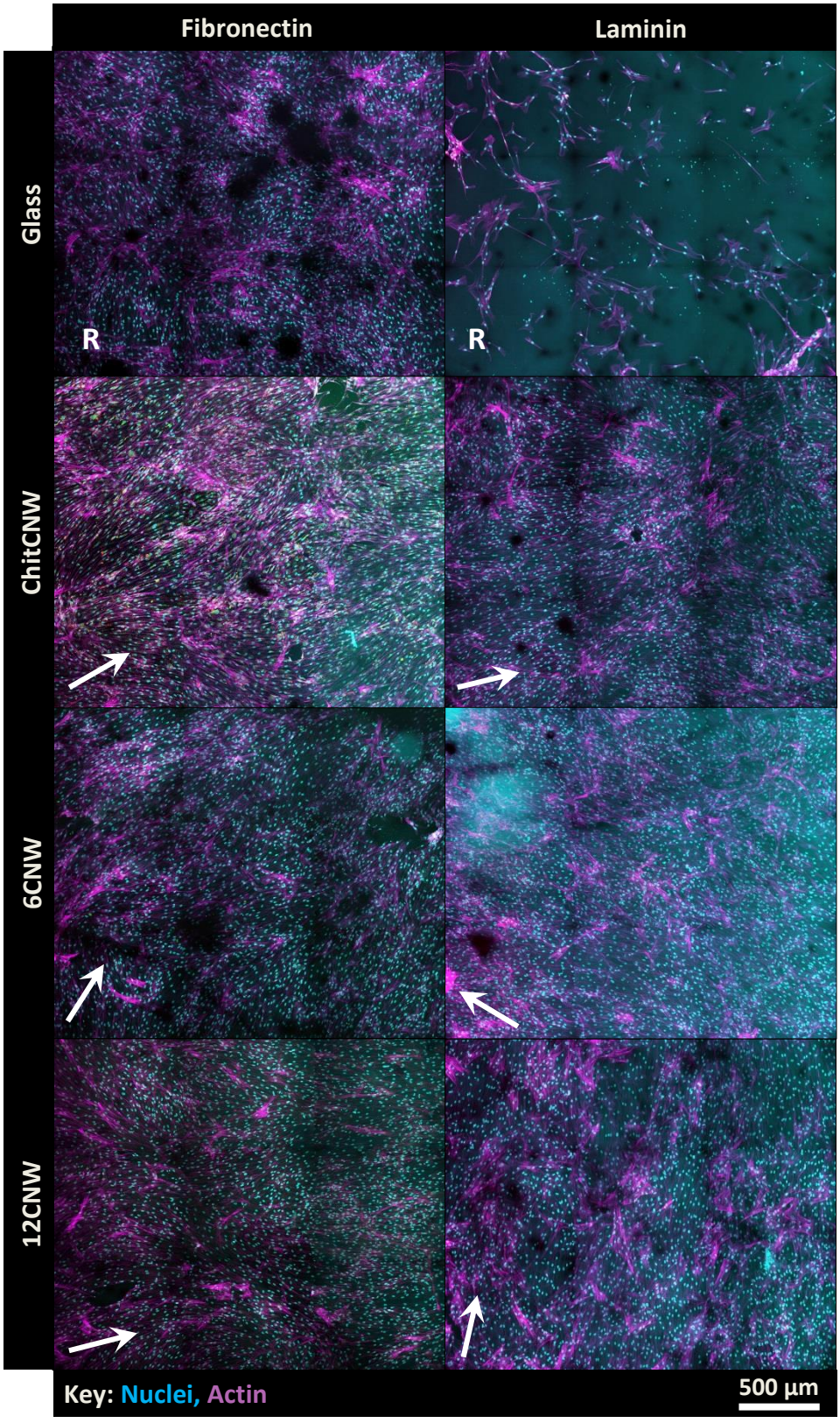

Figure 6-19: Confocal fluorescence micrographs of BM-MSCs on the fibronectin and laminin treated substrates 7 days after seeding, taken at 20x mag and stitched together in maps of 3x3. The arrows indicate the general direction of the cell alignment and the R denotes where the cells are randomly oriented. Substrates named with CNW have the oriented topography.

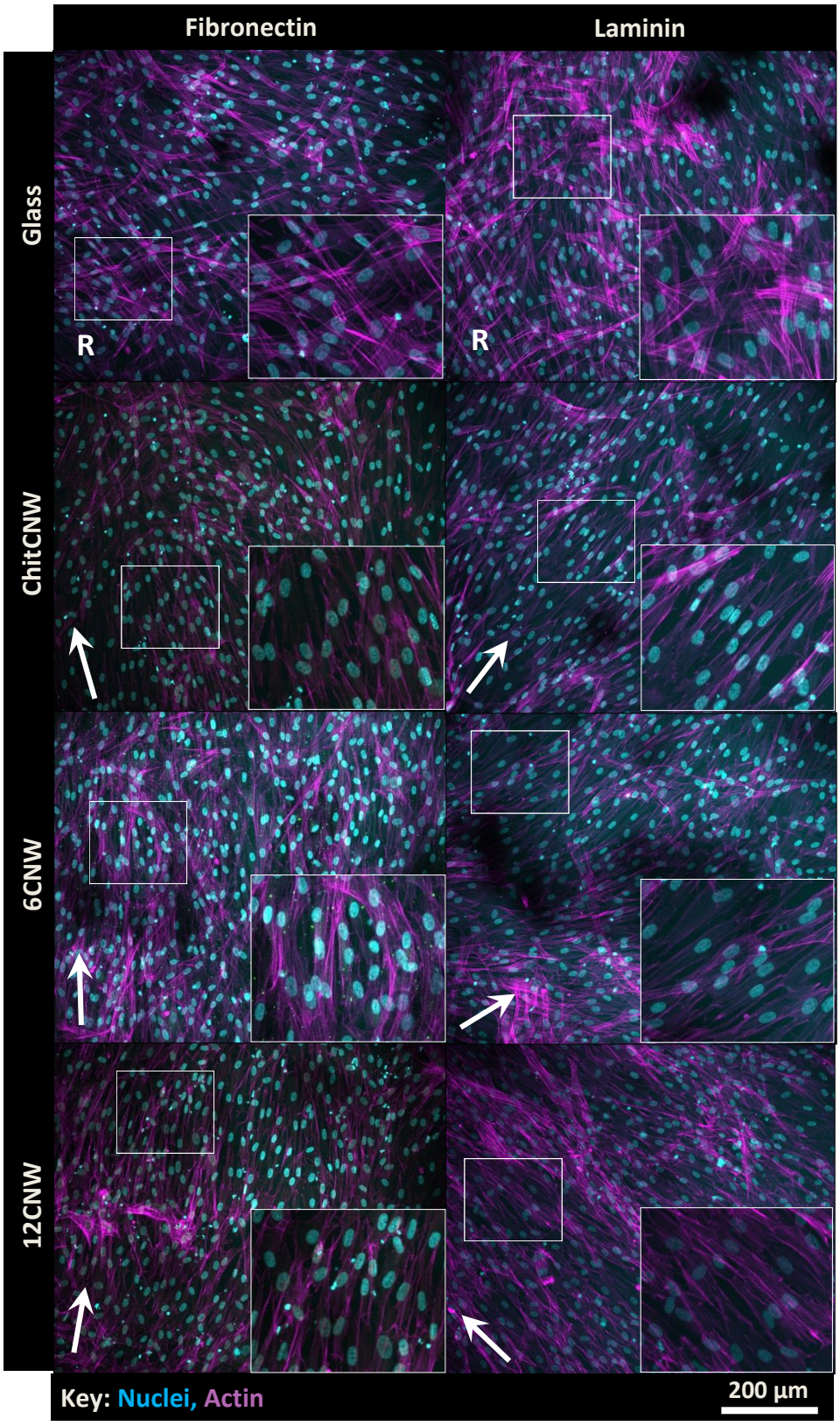

Figure 6-20: Confocal fluorescence micrographs of BM-MSCs on the fibronectin and laminin treated substrates 7 days after seeding, taken at 20x mag and stitched together in maps of 3x3. The arrows indicate the general direction of the cell alignment and the R denotes where the cells are randomly oriented. Substrates named with CNW have the oriented topography.

6.4 Discussion of the Effect of Protein Adsorption

6.4.1 Characterisation of CNW Substrates with Proteins

The substrates were pre-treated with proteins before cell seeding to investigate if there was an improvement in cell response and myotube formation. Fibronectin and laminin were chosen due to their presence in skeletal muscle ECM. Protein adsorption was confirmed using the NanoOrange assay (Section 4.2.4) and further confirmation was shown with immunofluorescence staining (Figure 6-1). Only fibronectin or laminin was adsorbed to each protein, however, all the samples were stained for both antibodies. Negatives showed that only one protein was present on each substrate (Figure 6-2), however, background staining was evident by the cloudy features.

The roughness and wettability of the substrates was re-examined after protein adsorption (Figure 6-3 and 6-4). No difference was observed between the protein treated substrates and the non-treated substrates (shown in Section 4.2.2). For both the fibronectin and laminin samples, the multilayers showed the greatest roughness compared to the thinner substrates. As discussed before, the addition of proteins to a surface can often 'smooth' out the roughness of the topographies and obscure the features (Lampin *et al.*, 1997), however, this has not been seen here. As the magnitude of the roughness values of these substrates are small and in the nanoscale, the protein may have little effect. The addition of proteins did have an effect on the wettability of some of the substrates. The most notable change was the contact angle of the Glass substrate which increased from $10.49^{o} \pm 5.90^{o}$ to $64.05^{o} \pm 14.25^{o}$ on fibronectin and $65.64^{o} \pm 8.86^{o}$ on laminin. These increases show support for the presence of proteins as the surface is now less hydrophilic. Overall the range of contact angle on the fibronectin and laminin samples was approximately between 60-70^{o} which is considered the preferable wettability for cell adhesion (Bačáková *et al.*, 2004; Arima and Iwata, 2007). The results of the NanoOrange assay, immunofluorescence staining and change in wettability strongly suggest that the substrates have adsorbed the proteins; this is further suggested through the difference in cell response discussed further in this section.

6.4.2 Cell Response to the Adsorbed Proteins

The importance of pre-conditioning the multilayers before seeding was investigated. In all of the cell work carried out in Section 5, the substrates were pre-conditioned with media containing serum, i.e. left in growth medium overnight before cell seeding. In order to test the cell response to the addition of proteins, this step needed to be removed to ensure any changes in cell response was due to the addition of the adsorbed proteins. Therefore, C2C12s were seeded on to a range of substrates that had been pre-conditioned in different ways. The conditions were growth media with and without serum, PBS and UltraPure^{TM} dH_2O. UltraPure^{TM} dH_2O was used as this is what the proteins were added to the substrate in. Bright field images, Alamar blue and Pico Green were used to investigate if there was a notable difference in cell response. The cells were cultured on the substrates for 8 days in growth media.

Metabolic activity from the Alamar Blue assay was used to show the initial cell response (Figure 6-5). Although some significant differences were found, the overall metabolic activity was similar across all the pre-conditions. Little difference was seen in the bright field images. Cell spreading and alignment was observed on the oriented substrates regardless of the pre-conditioning (Figure 6-6). The cell number increased on all substrates, however pre-conditioned, over the 8 days as seen in the PicoGreen data (Figure 6-7). This is also clear from the bright field images which show the cells increasing to a high density. There is little difference in cell number across the pre-conditioned substrates and by Day 8 the UltraPure^{TM} dH_2O treated substrates have similar or better cell numbers than the growth media with serum treated substrates. Overall, it was decided there was no negative effect on the cells to remove the pre-conditioning step.

To investigate if fibronectin or laminin made a difference to the cell response, C2C12s were seeded on Glass and the oriented substrates for 10 days. Differentiation media was added through partial media changes every day after 24 h. The initial response was observed through bright field images and Alamar Blue (Figure 6-8 and 6-9). Initially little difference can be seen between the protein treated and non-treated substrates. Alignment can also be seen on the oriented substrates after 24 h. The Alamar Blue assay showed an increase in metabolic activity between Day 1 and 4, similar to the C2C12 response discussed earlier. Overall, the protein treated substrates have a higher

metabolic activity at Day 4 on all the substrates which could be linked to a higher cell number.

The cell number on days 4, 7 and 10 were measured using the PicoGreen assay (Figure 6-11). Cell number remained level during this time. This is due to the reduced myoblast proliferation once myotubes start forming. Noticeably, the cell populations on the protein treated substrates were higher than those on the non-treated substrates. This was significant in all cases. The lower cell number on the non-treated substrates can be seen in the bright field images of Day 10 (Figure 6-10) and also the cells appear denser on the protein treated substrates. Myotube alignment and formation can be seen on all of the oriented CNW surfaces. The cell aggregation on the 12CNW multilayer noted earlier can also be seen. The number of nuclei per area on Day 7 (Figure 6-12) decreases across all protein treated conditions all the number of layers in the substrate increase. Therefore, this is likely the response to the substrate and not the proteins. From this data, there is no clear difference between the cell response of C2C12s on fibronectin or laminin. However, the protein treated substrates appear to enhancing the cells compared to the non-treated substrates. Cronin et al also reported an increase in cell number of C2C12s in response to the adsorption of fibronectin and laminin on to PLLA scaffolds as did Riboldi et al (Cronin *et al.*, 2004; Riboldi *et al.*, 2005).

Broad alignment and myogenic differentiation was observed on all of the oriented substrates (Figure 6-13) although ChitCNW and 6CNW treated with fibronectin had the highest number of myotubes (Figure 6-14, 6-15 and Table 6-1). Multinucleated myotubes were seen forming (Figure 6-17) however the percentage of nuclei expressing myogenin showed no obvious trend (Figure 6-18 (a)). Fibronectin treated substrates produced the most sarcomeric alpha actinin and it was noticeable that the percentage decreased as the number of layers increased (Figure 6-18 (b)).

The principle of using ECMs to coat biomaterials is derived from the knowledge that cell adhesion is mediated by the presence of specific ligand domains found on the proteins that form the native ECM of a tissue. Both fibronectin and laminin have these binding sites or integrins and facilitate the proliferation and differentiation of cells, specifically myoblasts in this case (Riboldi *et al.*, 2005). Fibronectin is known to

mediate cell adhesion and proliferation due to the presence of the RGD (Arg-Gly-Asp) motif which interacts with cells through integrins (Sottile and Hocking, 2002) however has only shown a trivial effect of the differentiation of cells (Kühl *et al.*, 1986). Laminin on the other hand, has been shown to play a crucial role in myogenic differentiation (Bajanca *et al.*, 2006) and its absence can lead to muscle dystrophy (Xu *et al.*, 1994). Lee et al found that fibronectin had a positive influence on the cell spreading and proliferation of C2C12s, however, it was laminin that had a significant effect on the myogenic differentiation (Lee *et al.*, 2015). This model could support the results shown in this work. The fibronectin treated substrates showed consistent cell spreading and proliferation compared to the laminin and non-treated substrates. Although the difference was not large, it could have been enough to result in increased myotube formation. As stated before, it is preferential for the myoblasts to be seeded at a high density (Cronin *et al.*, 2004; Mudera *et al.*, 2010; Wragg *et al.*, 2019) therefore the increased proliferation contributed to improved differentiation. Although laminin has a central role in myogenic differentiation, it may be that the cells had not reach an optimum spreading/proliferation stage for the protein to have a positive effect. Lee et al went on to combine both proteins on the polyurethane acrylate substrate which resulted in thicker and a higher number of myotubes (Lee *et al.*, 2015).

The spread of alignment for the fibronectin treated and non-treated substrates followed the same trend; increased alignment as the number of layers in the substrate decreased. This is likely due to the cells aggregating on the thicker substrates where the myotubes appear aligned but cannot be quantified. The myotube formation on the laminin treated oriented substrates appears aggregated on all of them and therefore quantitatively do not look aligned. Lee et al also combined topography with proteins where C2C12s on 300 nm lines showed higher differentiation than on 5 µm lines irrelevant of protein content. Therefore, they concluded that topography is the heavier influencer for myotube formation although the presence of ECM proteins is beneficial (Lee *et al.*, 2015). Further work is required to see if this point is supported by this work.

BM-MSCs were cultured on the protein treated substrates to explore possible improvements in cell response. This was seen as BM-MSCs of Donor 2, which had a very poor response to the substrates (see Section 6.3), were seeded on both the fibronectin and the laminin treated oriented CNWs and improved cell spreading was

observed. Broad alignment can be seen on all the oriented CNW substrates (Figure 6-19) with high cell densities. The formation of unidirectional actin suggests the cells are influenced by the nanotopography (Figure 6-20) and alignment of the nuclei can also be observed.

It is probable that the influence of the fibronectin and laminin is the positive effect on the BM-MSCs as cell spreading and attachment appears higher than on the untreated substrates. Battista et al (2005) found that the composition of the ECM had more of an effect on cells than the structure or mechanical properties of the scaffold. Significantly different differentiation was observed in cells responding to networks composed of collagen, fibronectin or laminin and concluded that it is the cell adhesion motifs of the ECM proteins that the most influence (Battista *et al.*, 2005). This does not agree with what was discussed earlier where it was suggested that it is the topography that is the heavier influencer. Different cell types express selective integrin and transmemebrane receptors that bind to specific domains on the ECM proteins therefore it could be suggested that there is a higher influence of ECM proteins on BM-MSCs compared to C2C12s. Whereas, the C2C12s are more likely to be influenced by topography than the ECM proteins.

Overall, both cell types showed improvement on the protein treated substrates. Fibronectin was shown to have more of an effect on the C2C12s though the increase in cell adhesion and spreading. On the other hand, C2C12s were shown to form aggregates on the laminin treated substrates. BM-MSCs had a positive effect in response to both ECM proteins. Development of the oriented CNWs with proteins could increase myogenic differentiation in C2C12s and possible direct BM-MSCs towards a myogenic lineage.

Chapter 7: Conclusions and Future Work

7.1 Summary and Overview

As stated in the Project Aims (Section 1), this thesis hypothesises that multilayer substrates of alternating chitosan and CNW layers with an oriented CNW top layer, can be used in the application of skeletal muscle tissue engineering through the alignment of differentiated myoblasts and influence of key ECM proteins. Oriented CNWs on similarly composed substrates have already shown promise in the formation of aligned myotubes, however in the preliminary work a level of toxicity resulted from the choice of material. This thesis seeks to improve both the biocompatibility and functionality of the multilayer substrates, through the addition of fibronectin and laminin, whilst also investigating the cell response of primary cells such as hSkMCs and BM-MSCs. There were three principle aims to achieve this work.

1. *"To create multilayer substrates with an oriented CNW top layer, and to characterise the cell response (guided orientation)."* The desired properties of the substrates were demonstrated by:
    a. High aspect ratio CNWs were produced through the partial acid hydrolysis of cellulose with a mean height of 5.097 nm ± 0.486 nm and lengths ranging from 10's of nanometres to over 2 micrometres (mean = 0.505 µm ± 0.667 µm). These were successfully spin coated to produce a layer of oriented CNWs with 3 times as many whiskers falling within a ±10^{o} range of 0^{o} compared to non-spin coated CNWs.
    b. The presence of sulphate groups was shown on substrates containing CNWs confirming the slight negative charge of the solution required for layer by layer (LbL) assembly. The multilayer substrates had a significantly higher roughness compared to the thinner substrates (Glass, Chitosan, ChitCNW) due to the undulating surface of the layers and not just the CNW topography. Multilayer substrates of alternating polyelectrolyte layers of CNW and chitosan were prepared for cell seeding.
    c. The C2C12s reacted favourably to the multilayer substrates with greater cell spreading observed on the 6CNW and 12CNW multilayers after 24 h.

d. Broad alignment of fused and differentiated C2C12s was seen on the ChitCNW and 6CNW substrates with greater differentiation shown by a higher number of myotubes and presence of sarcomeric alpha actinin. Myotube length was also higher on the ChitCNW and 6CNW substrates with some formed of more than 10 myoblasts.
e. Overall, the ChitCNW and 6CNW substrates showed the highest capacity for increased myotube formation and broad alignment.

2. *"Application and response of primary cells, such as hSkMCs and BM-MSCs, on the oriented multilayer substrates."* The response of the primary cells looked promising:
    a. Unidirectional spreading of hSkMCs after 24 h was observed on the ChitCNW and 6CNW substrates however lower cell numbers were seen on the 12CNW multilayers.
    b. Elongation and broad alignment of hSkMCs on Day 8 was seen all the oriented CNW topographies with the possible presence of myogenin indicating the cells could be in the early stages of myogenic differentiation. However, no sarcomeric alpha actinin was observed.
    c. Similar to the hSkMCs, BM-MSCs were observed spreading and aligning to the ChitCNW and 6CNW substrates after 24 h, however lower cell numbers were seen on the 12CNW multilayer.
    d. Although low initially, the BM-MSCs showed good cell coverage and broad alignment on the 6CNW and 12CNW multilayers after 7 days in differentiation media. However, no myogenic components were observed.

3. *"Investigate the effect on cell response of adsorbed ECM proteins on the oriented CNW topography."* The combination of fibronectin and laminin with the CNWs showed potential:
    a. The NanoOrange assay showed that >64% of both the proteins were adsorbed on to the substrates this was further confirmed by

immunofluorescence staining and the change in wettability of the substrates.

b. The C2C12s showed a positive response to the adsorption of fibronectin and laminin with a higher cell number on the protein treated substrates compared to the control. Cell spreading and alignment was also observed on the protein treated substrates after 24 h.
c. C2C12s on the fibronectin showed greater differentiation after 7 days with the most and longest myotubes, some reaching 400 µm, compared to the myotube formation on the laminin. The cells on the laminin substrates appeared to aggregate, whereas broad alignment could be seen on the fibronectin substrates. C2C12 spreading and differentiation was lower for both proteins on the 12CNW multilayer.
d. The adsorption of the proteins had a positive effect on the BM-MSCs which showed increased cell density and alignment on all the oriented substrate types when compared with the untreated substrate.

The application of oriented CNWs to direct myotube alignment was first explored by Dugan et al (2011) who showed the high aspect ratio of the nanotopography could have potential in guiding cells of highly structured tissues. The concept of LbL assemblies was briefly touched by Dugan, however it was Nikoi (2016) who implemented the techniques of dip coating, with the spin coating, to form polyelectrolyte multilayers of CNW, chitosan and PSS. Nikoi's work considered the cell's response to the material under the oriented CNWs with the idea that myotube formation would be affected by the mechanical properties of the underlying surface. Potential increased myotube formation was observed on the 12 multilayer films of CNW, chitosan and PSS, however the increased number of PSS layers was found to have a cytotoxic effect on the cells. Building on the work carried out by Dugan and Nikoi, this thesis focuses on the further development of polyelectrolyte multilayers with a top layer of oriented CNWs for the engineering of skeletal muscle tissue (Dugan, Gough and Eichhorn, 2013; Nikoi, 2016).

Due to their cytotoxic effect the PSS layers were removed from the multilayers assembled in this work, and other multilayers of different numbers were explored. The multilayer substrates produced in this work are composed of CNWs and chitosan, with a bottom PEI layer on the multilayer layers used for stability. The increasing number of layers of the substrates, ranging from the bilayer ChitCNW to 6CNW and ending with 12CNW were used to explore any trends in cell response to increase in layer number. The response of C2C12 cells to the oriented substrates showed greater differentiation and broad myotube alignment when compared to the non-oriented substrates, Chitosan and 12Chit. Broad alignment is important due to the structural quality of skeletal muscle, and this was observed in large areas on the ChitCNW and 6CNW substrates. These two substrates were found to form the most, and longest, myotubes, with some reaching over 400 μm in length and containing 10+ nuclei per myotube. Glass showed high differentiation and long myotube formation, however the alignment was only local. No cytotoxic effects on cells were found with these CNW and Chitosan substrates, therefore other cells related to skeletal muscle became of interest. The key feature of these substrates is the nanotopography of the CNWs, which could be some of the smallest topographical features to influence the direction of cells.

C2C12s as a murine immortalised cell line are suitable model for exploring the potential of substrates to engineer skeletal muscle, and can spontaneously differentiate at low concentrations of serum (S. Burattini, P. Ferri, M. Battistelli, R. Curci, F. Luchetti, 2004). There has been significantly less research into hSkMCs when compared to the use of C2C12s or satellite cells; however it is of interest if these primary hSkMCs respond to the oriented CNW topography as well as C2C12s. The first observation of the hSkMCs is that their initial response to the multilayer substrates was poor when compared to the C2C12s. However, the cells did broadly align and elongate, which are positive features for myogenic differentiation. No cell fusion was seen although the presence of myogenin around the nuclei indicating potential for myoblast fusion. The lack of differentiation of hSkMCs is likely due to the low cell density and not enough time in culture, observations matched in literature as well (Cronin *et al.*, 2004; Mudera *et al.*, 2010). BM-MSCs are one of the most popular stem cell types, due to the significant body of research already present in literature, and

their potential to differentiate in to wide range of cell types. Two donor lines of BM-MSCs were used in this work, and their response to the multilayer substrates was not consistent. Unlike C2C12s and hSkMCs, there is significantly more variability between donors and this was seen from the initial BM-MSC response. Donor 2 had a poor initial response to the substrates and by day 7 could not be found on the substrates, likely having died or detached due to poor attachment. On the other hand, Donor 1 had a positive response to the substrates and showed alignment and high cell density. No differentiation was observed towards a myogenic lineage therefore it is fair to conclude that topography alone is unlikely to promote myogenic differentiation in BM-MSCs. Overall, both hSkMCs and BM-MSCs require further work to induce differentiation. The hSkMCs could thrive at a higher density with more time given to differentiate, whereas the BM-MSCs may need other stimuli in combination with an aligned topography to reach myogenic differentiation. Generally, the ChitCNW and 6CNW substrates worked the best for the C2C12s and hSkMCs, however it was the 12CNW multilayer and 6CNW substrates which showed the most potential for BM-MSCs.

The incorporation of ECM proteins with both substrates and scaffolds, for the application of tissue engineering, is an approach often used to improve a surface's affinity for cell adhesion, or to promote differentiation of the cells (Bačáková *et al.*, 2004; Lee *et al.*, 2015). Fibronectin and laminin are key ECM proteins in the native structure of skeletal muscle tissue. Their adsorption on to the surface of the oriented CNWs was predicted to increase cell adhesion, proliferation and possibly increase myotube length. There was an initial positive response from C2C12s to the protein treated substrates, with increased cell numbers compared to the untreated substrates. The fibronectin treated substrates had the best overall response from the C2C12s, with formation of the longest and highest number of myotubes when compared to the laminin and untreated substrates. Laminin treated substrates showed a poor response, and broad alignment of myotubes was not observed to the same extent as on the fibronectin treated substrates. Fibronectin is a key protein in cell adhesion and migration, whereas laminin plays a more vital role in myogenic differentiation (Sottile and Hocking, 2002; Bajanca *et al.*, 2006). It could be that the positive initial response of the C2C12s on the fibronectin treated substrates was crucial to support greater

differentiation and formation of myotubes. The untreated substrate showed a decrease in myotube length, and did not as positively respond to the substrates as seen in the first set of studies (Section 6.1). It's suggested that the pre-conditioning step with the media with serum, could have provided the same beneficial effect as the fibronectin, however this step was removed to isolate the effect of the adsorbed fibronectin and laminin. The laminin substrates did not appear to have a significant positive effect on the formation of broadly aligned myotubes; this is potentially a result of the low initial cell response which did not provide the support needed for development to continue. There was, however, some level of aggregation of myotubes on the laminin substrates. These aggregates, although appeared aligned were not quantifiable on the software used as there was some overlap of the cells. This aggregation was only observed on the untreated thicker substrates, and as such suggests that, with optimisation, laminin could be used to improve differentiation. BM-MSCs of Donor 2 used earlier in this work were seeded on to the protein treated substrates and showed a positive initial response. In earlier work, these cells from Donor 2 had a poor response to the multilayer substrates; however the addition of fibronectin and laminin showed an increase in cell adhesion and spreading. Overall, the adsorptions of fibronectin and laminin have shown the potential to improve myogenic differentiation of C2C12s. Both proteins also promote increased cell spreading of BM-MSCs on these substrates. Possible further work could investigate the effect of combining both proteins simultaneously with the oriented CNWs.

The conclusion drawn from this work is that the 6CNW substrate showed the most potential for the alignment and differentiation of multinucleated myotube formation. There was a clear positive response in initial cell proliferation and orientation to the 6CNW substrate from all three cell lines explored in this work. The C2C12s and hSkMCs showed preference for the thinner substrates (ChitCNW and 6CNW), whereas, the BM-MSCs seemed to prefer the multi-layered substrates (6CNW and 12CNW). More work is required to understand the thickness and stiffness of these substrates and how they compare to the ideal stiffness range of skeletal muscle. Skeletal muscle is a 3D tissue and 2D work experimental work only goes so far.

Although the cells showed broad alignment and high proliferation, it was disappointing that it was not further explored if and when the hSkMCs would have differentiated in

to myotubes. In hindsight it was possibly the time in culture and experimental work that could have been a contributing factor. There were also limitations from the sourcing of the BM-MSCs as the cells were not extracted and maintained personally, it is hard to know how much previous treatment of the cells could have influenced the results shown.

The benefits of using ECM proteins with biomaterials are well documented and the conclusions drawn agree with literature. The relationship between the topography and the proteins needs to be further defined to understand how the fibronectin and laminin adsorbed to the CNWs and whether the influence of the protein was purely biochemical or also physical. Fibronectin had the more positive response over laminin although this was likely due to the role fibronectin plays in initial cell response compared to laminin, which become much more vital during differentiation. Again, C2C12s showed a more positive response to the ChitCNW and 6CNW substrates in combinations with the ECM proteins. The improvement in the BM-MSCs proves the importance of ECM proteins and links back to the concept that multiple factors are required to promote and direct MSCs towards specific cell lineages.

This investigation in to the application of CNWs to align and direct the formation of myotubes is a small step in fully exploring the potential of CNWs as a biomaterial.

In summary, the novelty of this work lies in the composition of the multilayer substrates, the application of primary cells and the adsorption of key ECM proteins and the resulting cell response. Polyelectrolyte multilayers composed of CNWs and chitosan with an oriented CNW top layer were shown to promote broad alignment of myotubes from differentiated C2C12s. Primary hSkMCs showed alignment and elongation in response to the oriented topography as did BM-MSCs. The adsorption of fibronectin and laminin to the multilayer substrates showed a positive initial cell response from both C2C12s and BM-MSCs. Broad alignment and greater differentiation was shown by the C2C12s on the fibronectin treated substrates suggesting a positive response to the combination of key ECM proteins and an oriented nanotopography.

7.2 Future Work

The obvious next step for this material would be to explore the possibility of 3D scaffolds. The literature reports that the rate of myogenic differentiation is faster on 3D scaffolds compared to on 2D of the same material (Mudera *et al.*, 2010; Chiron *et al.*, 2012). Due to the nanoscale size of the CNWs, incorporation of the nanowhiskers with other materials that have more structural support is more feasible than using the CNWs alone. He et al (2014) combined electrospun cellulose and cellulose nanocrystals to produce a unidirectional fibre based scaffold that showed potential for skeletal muscle tissue engineering (He *et al.*, 2014). Another possible route is the concept of cell sheet rolling, where initial cell alignment could be guided by the CNWs on a polymer film that could then be rolled in to a 3D scaffold. The incorporation of CNWs in hydrogels has shown promise (Liu *et al.*, 2016; De France *et al.*, 2017), however to take advantage of the high aspect ratio, other methods of CNW orientation would need to be investigated. The CNWs in produced in this group have not been used *in vivo* as of yet. A possible route for this material is to explore its potential inside the body as part of a scaffold which would also help understand the materials full biocompatibility.

Further work on the 2D nanotopography could explore the combined effect of fibronectin and laminin and possibly other ECM proteins, such as collagen which is a major structural protein in the skeletal muscle ECM. The combination of the nano-topography with growth factors could also be considered, especially when exploring the differentiation of MSCs towards a myogenic phenotype. This work briefly touched on the use of satellite cells, however further use of them, such as in co-culture with other relevant cells, could show promise. The application of BM-MSCs with the oriented CNWs could be expanded upon to investigate the use of other stimuli to compliment the nanotopography in promoting myogenic differentiation. For example, media conditioned from injured skeletal muscle cells has been shown to further stimulate myogenic differentiation of BM-MSCs (Santa Maria, Rojas and Minguell, 2004) as have exosomes released from human skeletal muscle cells undergoing differentiation (Choi *et al.*, 2016).

The CNWs could also be used a vehicle to help further understand the mechanics behind cell-material interaction and protein adsorption to nano-scale features.

Although this work focuses on the application of the CNWs to direct skeletal muscle cells, further work could look in to the use of this oriented topography to align other structural tissues, such as tendons.

In conclusion, CNWs are a promising biomaterial and could be used for a wide range of applications. CNWs have been shown successful as a nanotopographical guide for myotube alignment and their use with other cell types for other structural tissues could also be similarly effective.

References

Abujarour, R. *et al.* (2014) 'Myogenic differentiation of muscular dystrophy-specific induced pluripotent stem cells for use in drug discovery.', *Stem cells translational medicine*, 3(2), pp. 149–60. doi: 10.5966/sctm.2013-0095.

Aggarwal, N. *et al.* (2013) 'Effect of molecular composition of heparin and cellulose sulfate on multilayer formation and cell response', *Langmuir*, 29(45), pp. 13853–13864. doi: 10.1021/la4028157.

Anglès, M. N. and Dufresne, A. (2000) 'Plasticized Starch/Tunicin Whiskers Nanocomposites. 1. Structural Analysis', *Macromolecules*, 33(22), pp. 8344–8353. doi: 10.1021/ma0008701.

Anselme, K. and Bigerelle, M. (2011) 'Role of materials surface topography on mammalian cell response', *International Materials Reviews*, 56(4), pp. 243–266. doi: 10.1179/1743280411Y.0000000001.

Arima, Y. and Iwata, H. (2007) 'Effect of wettability and surface functional groups on protein adsorption and cell adhesion using well-defined mixed self-assembled monolayers', *Biomaterials*, 28(20), pp. 3074–3082. doi: 10.1016/j.biomaterials.2007.03.013.

Arjmandi, R. *et al.* (2016) 'Effect of hydrolysed cellulose nanowhiskers on properties of montmorillonite/polylactic acid nanocomposites', *International Journal of Biological Macromolecules*. Elsevier B.V., 82, pp. 998–1010. doi: 10.1016/j.ijbiomac.2015.11.028.

Aviss, K. J., Gough, J. E. and Downes, S. (2010) 'Aligned electrospun polymer fibres for skeletal muscle regeneration', *European Cells and Materials*, 19, pp. 193–204. doi: vol019a19 [pii].

Bacakova, L. *et al.* (2011) 'Modulation of cell adhesion, proliferation and differentiation on materials designed for body implants', *Biotechnology Advances*. Elsevier Inc., 29(6), pp. 739–767. doi: 10.1016/j.biotechadv.2011.06.004.

Bačáková, L. *et al.* (2004) 'Cell Adhesion on Artificial Materials for Tissue Engineering', *Physiological Research*, 53(SUPPL. 1).

Backdahl, H. *et al.* (2006) 'Mechanical properties of bacterial cellulose and interactions with smooth muscle cells', *Biomaterials*, 27(9), pp. 2141–2149. doi: 10.1016/j.biomaterials.2005.10.026.

Bajanca, F. *et al.* (2006) 'Integrin α6β1-laminin interactions regulate early myotome formation in the mouse embryo', *Development*, 133(9), pp. 1635–1644. doi: 10.1242/dev.02336.

Barua, S. *et al.* (2015) 'Sustainable resource based hyperbranched epoxy nanocomposite as an infection resistant, biodegradable, implantable muscle scaffold', *ACS Sustainable Chemistry and Engineering*, 3(6), pp. 1136–1144. doi: 10.1021/acssuschemeng.5b00069.

Battista, O. a. (1950) 'Hydrolysis and Crystallization of Cellulose', *Industrial & Engineering Chemistry*, 42(3), pp. 502–507. doi: 10.1021/ie50483a029.

Battista, S. *et al.* (2005) 'The effect of matrix composition of 3D constructs on embryonic stem cell differentiation', *Biomaterials*, 26(31), pp. 6194–6207. doi: 10.1016/j.biomaterials.2005.04.003.

Beck-Candanedo, S., Roman, M. and Gray, D. (2005) 'Effect of conditions on the properties behavior of wood cellulose nanocrystals suspensions', *Biomacromolecules*, 6, pp. 1048–1054.

Beggs, A. H. *et al.* (1992) 'Cloning and characterization of two human skeletal muscle ?-actinin genes located on chromosomes 1 and 11', *Journal of Biological Chemistry*, 267(13), pp. 9281–9288.

Belton, P. S. *et al.* (1989) 'High-Resolution Solid-State 13 C Nuclear Magnetic Resonance Spectroscopy of Tunicin, an Animal Cellulose', *Macromolecules*, 22(4), pp. 1615–1617. doi: 10.1021/ma00194a019.

Benton, M. (2004) *No TitleVertebrate Palaeontology, 3rd Edition*. Blackwell Publishing Ltd.

Bian, W. and Bursac, N. (2009) 'Engineered skeletal muscle tissue networks with controllable architecture', *Biomaterials*. Elsevier Ltd, 30(7), pp. 1401–1412. doi: 10.1016/j.biomaterials.2008.11.015.

Biela, S. A. *et al.* (2009) 'Different sensitivity of human endothelial cells, smooth muscle cells and fibroblasts to topography in the nano-micro range', *Acta Biomaterialia*. Acta Materialia Inc., 5(7), pp. 2460–2466. doi: 10.1016/j.actbio.2009.04.003.

Biggs, M. J. P., Richards, R. G. and Dalby, M. J. (2010) 'Nanotopographical modification: A regulator of cellular function through focal adhesions', *Nanomedicine: Nanotechnology, Biology, and Medicine*. Elsevier Inc., 6(5), pp. 619–633. doi: 10.1016/j.nano.2010.01.009.

Blais, A. *et al.* (2005) 'An initial blueprint for myogenic differentiation', *Genes and Development*, 19(5), pp. 553–569. doi: 10.1101/gad.1281105.

den Braber, E. T. *et al.* (1998) 'Orientation of ECM protein deposition, fibroblast cytoskeleton, and attachment complex components on silicone microgrooved surfaces.', *Journal of biomedical materials research*, 40(2), pp. 291–300. doi: 10.1002/(SICI)1097-4636(199805)40:2<291::AID-JBM14>3.0.CO;2-P.

Brandan, E. and Inestrosa, N. C. (1987) 'Isolation of the heparan sulfate proteoglycans from the extracellular matrix of rat skeletal muscle', *Journal of Neurobiology*, 18(3), pp. 271–282. doi: 10.1002/neu.480180303.

Buckingham, M. and Montarras, D. (2008) 'Chapter 2 the Origin and Genetic Regulation of Myogenic Cells : From the Embryo To the Adult', *Most*, pp. 19–44.

Bumgardner, J. D. *et al.* (2012) 'Contact angle, protein adsorption and osteoblast precursor cell attachment to chitosan coatings bonded to titanium', *Journal of Biomaterials Science, Polymer Edition*, 14(12), pp. 1401–1409. doi: 10.1163/156856203322599734.

Caplan, A. (1991) 'Mesenchymal stem cells.', *Journal of orthopaedic research : official publication of the Orthopaedic Research Society*, 9(5), pp. 641–50. doi: 10.1002/jor.1100090504.

Caplan, A. I. and Bruder, S. P. (2001) 'Mesenchymal stem cells: Building blocks for molecular medicine in the 21st century', *Trends in Molecular Medicine*, 7(6), pp. 259–264. doi: 10.1016/S1471-4914(01)02016-0.

Chae, S. J., Lee, J. U. and Kim, G. H. (2019) 'Skeletal myotube formation enhanced through fibrillated collagen nanofibers coated on a 3D-printed polycaprolactone surface', *Colloids and Surfaces B: Biointerfaces*. Elsevier, 181(January), pp. 408–415. doi: 10.1016/j.colsurfb.2019.05.043.

Charest, J. L., Garcia, A. J. and King, W. P. (2007) 'Myoblast alignment and differentiation on cell culture substrates with microscale topography and model chemistries', *Biomaterials*, 28(13), pp. 2202–2210. doi: 10.1016/j.biomaterials.2007.01.020.

Chargé, S. B. P. and Rudnicki, M. (2004) 'Cellular and molecular regulation of muscle regeneration.', *Physiological reviews*, 84(1), pp. 209–238. doi: 10.1152/physrev.00019.2003.

Chiron, S. *et al.* (2012) 'Complex interactions between human myoblasts and the surrounding 3D fibrin-based matrix', *PLoS ONE*, 7(4). doi: 10.1371/journal.pone.0036173.

Chiu, C. *et al.* (2010) 'Mutations in Alpha-Actinin-2 Cause Hypertrophic Cardiomyopathy. A Genome-Wide Analysis', *Journal of the American College of Cardiology*. Elsevier Inc., 55(11), pp. 1127–1135. doi: 10.1016/j.jacc.2009.11.016.

Choi, J. S. *et al.* (2008) 'The influence of electrospun aligned poly(e-caprolactone)/collagen nanofiber meshes on the formation of self-aligned skeletal muscle myotubes', *Biomaterials*, 29(19), pp. 2899–2906. doi: 10.1016/j.biomaterials.2008.03.031.

Choi, J. S. *et al.* (2016) 'Exosomes from differentiating human skeletal muscle cells trigger myogenesis of stem cells and provide biochemical cues for skeletal muscle regeneration', *Journal of Controlled Release*. Elsevier B.V., 222, pp. 107–115. doi: 10.1016/j.jconrel.2015.12.018.

Christ, G. J. *et al.* (2015) *Skeletal Muscle Tissue Engineering*, *Stem Cell Biology and Tissue Engineering in Dental Sciences*. Elsevier Inc. doi: 10.1016/B978-0-12-397157-9.00047-3.

Clark, P. *et al.* (1991) 'Cell guidance by ultrafine topography in vitro.', *Journal of cell science*, 99 (Pt 1), pp. 73–77.

Clem, W. C. *et al.* (2008) 'Mesenchymal stem cell interaction with ultra-smooth nanostructured diamond for wear-resistant orthopaedic implants', *Biomaterials*, 29(24–25), pp. 3461–3468. doi: 10.1016/j.biomaterials.2008.04.045.

Clift, M. J. D. *et al.* (2011) 'Investigating the interaction of cellulose nanofibers derived from cotton with a sophisticated 3D human lung cell coculture', *Biomacromolecules*, 12(10), pp. 3666–3673. doi: 10.1021/bm200865j.

Constantinides, P., Jones, P. and Gevers, W. (1977) 'Functional striated muscle cells from non-myoblast precursors following 5-azacytidine treatment', *Nature Publishing Group*, 267, pp. 364–366. doi: 10.1038/267364a0.

Cossu, G. *et al.* (2000) 'Determination, diversification and multipotency of mammalian myogenic cells', *International Journal of Developmental Biology*, 44(6), pp. 699–706.

Cranston, E. D. and Gray, D. G. (2006) 'Morphological and optical characterization of polyelectrolyte multilayers incorporating nanocrystalline cellulose', *Biomacromolecules*, 7(9), pp. 2522–2530. doi: 10.1021/bm0602886.

Cranston, E. D. and Gray, D. G. (2008) 'Birefringence in spin-coated films containing cellulose nanocrystals', *Colloids and Surfaces A: Physicochemical and Engineering Aspects*, 325(1–2), pp. 44–51. doi: 10.1016/j.colsurfa.2008.04.042.

Cronin, E. M. *et al.* (2004) 'Protein-coated poly(L-lactic acid) fibers provide a substrate for differentiation of human skeletal muscle cells', *Journal of Biomedical Materials Research - Part A*, 69(3), pp. 373–381. doi: 10.1002/jbm.a.30009.

Crouch, A. S. *et al.* (2009) 'Correlation of anisotropic cell behaviors with topographic aspect ratio', *Biomaterials*. Elsevier Ltd, 30(8), pp. 1560–1567. doi: 10.1016/j.biomaterials.2008.11.041.

Curtis, A. and Wilkinson, C. (1997) 'Topographical control of cells', *Biomaterials*, 18(24), pp.

1573–1583. doi: 10.1016/S0142-9612(97)00144-0.

Dang, J. M. and Leong, K. W. (2007) 'Myogenic induction of aligned mesenchymal stem cell sheets by culture on thermally responsive electrospun nanofibers', *Advanced Materials*, 19(19), pp. 2775–2779. doi: 10.1002/adma.200602159.

Decher, G., Hong, J. D. and Schmitt, J. (1992) 'Buildup of ultrathin multilayer films by a self-assembly process: III. Consecutively alternating adsorption of anionic and cationic polyelectrolytes on charged surfaces', *Thin Solid Films*, 210–211(PART 2), pp. 831–835. doi: 10.1016/0040-6090(92)90417-A.

Domingues, R. M. A., Gomes, M. E. and Reis, R. L. (2014) 'The potential of cellulose nanocrystals in tissue engineering strategies', *Biomacromolecules*, 15(7), pp. 2327–2346. doi: 10.1021/bm500524s.

Dong, X. (1998) 'Effect of microcrystallite preparation conditions on the formation of colloid crystals of cellulose', *Cellulose*, 5, pp. 19–32. doi: 10.1023/A:1009260511939.

Dugan, J. (2011) 'Cellulose Nanowhiskers for Tissue Engineering Skeletal Muscle A thesis submitted to the University of Manchester for the degree of Doctor of Philosophy in the Faculty of Engineering and Physical Sciences 2011'.

Dugan, J. M. *et al.* (2013) 'Oriented surfaces of adsorbed cellulose nanowhiskers promote skeletal muscle myogenesis.', *Acta biomaterialia*. Acta Materialia Inc., 9(1), pp. 4707–15. doi: 10.1016/j.actbio.2012.08.050.

Dugan, J. M., Gough, J. E. and Eichhorn, S. J. (2010) 'Directing the morphology and differentiation of skeletal muscle cells using oriented cellulose nanowhiskers', *Biomacromolecules*, 11(9), pp. 2498–2504. doi: 10.1021/bm100684k.

Dugan, J. M., Gough, J. E. and Eichhorn, S. J. (2013) 'Bacterial cellulose scaffolds and cellulose nanowhiskers for tissue engineering.', *Nanomedicine (London, England)*, 8(2), pp. 287–98. doi: 10.2217/nnm.12.211.

Ebrahimi, M. *et al.* (2018) 'Enhanced skeletal muscle formation on microfluidic spun gelatin methacryloyl (GelMA) fibres using surface patterning and agrin treatment', *Journal of Tissue Engineering and Regenerative Medicine*, 12(11), pp. 2151–2163. doi: 10.1002/term.2738.

Eichhorn, S. J. (2011) 'Cellulose nanowhiskers: Promising materials for advanced applications', *Soft Matter*, 7(2), pp. 303–315. doi: 10.1039/c0sm00142b.

Elazzouzi-Hafraoui, S. *et al.* (2008) 'The shape and size distribution of crystalline nanoparticles prepared by acid hydrolysis of native cellulose', *Biomacromolecules*, 9(1), pp. 57–65. doi: 10.1021/bm700769p.

Engler, A. J. *et al.* (2006) 'Matrix Elasticity Directs Stem Cell Lineage Specification', *Cell*, 126(4), pp. 677–689. doi: 10.1016/j.cell.2006.06.044.

Entcheva, E. *et al.* (2004) 'Functional cardiac cell constructs on cellulose-based scaffolding', *Biomaterials*, 25(26), pp. 5753–5762. doi: 10.1016/j.biomaterials.2004.01.024.

Favier, V., Chanzy, H. and Cavaillé, J. Y. (1995) 'Polymer Nanocomposites Reinforced by Cellulose Whiskers', *Macromolecules*, 28(18), pp. 6365–6367. doi: 10.1021/ma00122a053.

Ferri, P. *et al.* (2009) 'Expression and subcellular localization of myogenic regulatory factors during the differentiation of skeletal muscle C2C12 myoblasts', *Journal of Cellular Biochemistry*, 108(6), pp. 1302–1317. doi: 10.1002/jcb.22360.

De France, K. J. *et al.* (2017) 'Injectable Anisotropic Nanocomposite Hydrogels Direct in Situ Growth and Alignment of Myotubes', *Nano Letters*, 17(10), pp. 6487–6495. doi: 10.1021/acs.nanolett.7b03600.

Gang, E. J. *et al.* (2004) 'Skeletal myogenic differentiation of mesenchymal stem cells isolated from human umbilical cord blood.', *Stem cells (Dayton, Ohio)*, 22(4), pp. 617–24. doi: 10.1634/stemcells.22-4-617.

Gang, E. J. *et al.* (2008) 'Pax3 activation promotes the differentiation of mesenchymal stem cells toward the myogenic lineage', *Experimental Cell Research*, 314(8), pp. 1721–1733. doi: 10.1016/j.yexcr.2008.02.016.

Gentile, A. *et al.* (2011) 'Human epicardium-derived cells fuse with high efficiency with skeletal myotubes and differentiate toward the skeletal muscle phenotype: a comparison study with stromal and endothelial cells.', *Molecular biology of the cell*, 22(5), pp. 581–92. doi: 10.1091/mbc.E10-06-0537.

George, J. and Sabapathi, S. (2015) 'Cellulose nanocrystals: synthesis, functional properties, and applications', *Nanotechnology, Science and Applications*, Volume 8, p. 45. doi: 10.2147/NSA.S64386.

Gillies, A. R., Lieber, B. . and Lieber, R. L. (2012) 'Structure and Function of the Skeletal Muscle Extracellular Matrix', *Muscle Nerve*, 44(3), pp. 318–331. doi: 10.1002/mus.22094.Structure.

Gingras, J. *et al.* (2009) 'Controlling the orientation and synaptic differentiation of myotubes with micropatterned substrates', *Biophysical Journal*. Biophysical Society, 97(10), pp. 2771–2779. doi: 10.1016/j.bpj.2009.08.038.

Guilak, F. *et al.* (2009) 'Control of Stem Cell Fate by Physical Interactions with the Extracellular Matrix', *Cell Stem Cell*. Elsevier Inc., 5(1), pp. 17–26. doi: 10.1016/j.stem.2009.06.016.

Guo, Y. *et al.* (2019) 'Modified cell-electrospinning for 3D myogenesis of C2C12s in aligned fibrin microfiber bundles', *Biochemical and Biophysical Research Communications*, 516(2), pp. 558–564. doi: 10.1016/j.bbrc.2019.06.082.

Habibi, Y., Lucia, L. A. and Rojas, O. J. (2010) 'Cellulose nanocrystals: Chemistry, self-assembly, and applications', *Chemical Reviews*, 110(6), pp. 3479–3500. doi: 10.1021/cr900339w.

Hart, J. *et al.* (2002) 'The role of oxidised regenerated cellulose/collagen in wound repair: Effects in vitro on fibroblast biology and in vivo in a model of compromised healing', *International Journal of Biochemistry and Cell Biology*, 34(12), pp. 1557–1570. doi: 10.1016/S1357-2725(02)00062-6.

He, X. *et al.* (2014) 'Uniaxially aligned electrospun all-cellulose nanocomposite nanofibers reinforced with cellulose nanocrystals: Scaffold for tissue engineering', *Biomacromolecules*, 15(2), pp. 618–627. doi: 10.1021/bm401656a.

Hernández-Hernández, J. M. *et al.* (2017) 'The myogenic regulatory factors, determinants of muscle development, cell identity and regeneration', *Seminars in Cell and Developmental Biology*. Elsevier Ltd, 72, pp. 10–18. doi: 10.1016/j.semcdb.2017.11.010.

Hornyak, G. L. (2008) *Fundamentals of Nanotechnology*. CRC Press. doi: 10.1201/9781315222561.

Hu, Y. and Catchmark, J. M. (2011) 'In vitro biodegradability and mechanical properties of bioabsorbable bacterial cellulose incorporating cellulases', *Acta Biomaterialia*. Acta Materialia Inc., 7(7), pp. 2835–2845. doi: 10.1016/j.actbio.2011.03.028.

Huang, N. F. *et al.* (2006) 'Myotube assembly on nanofibrous and micropatterned polymers', *Nano Letters*, 6(3), pp. 537–542. doi: 10.1021/nl060060o.

Hynes, R. O. (2009) 'The extracellular matrix: Not just pretty fibrils', *Science*, 326(5957), pp. 1216–1219. doi: 10.1126/science.1176009.

Jangid, N. K., Hada, D. and Rathore, K. (2019) 'Chitosan as an emerging object for biological and biomedical applications', *Journal of Polymer Engineering*, 39(8), pp. 689–703. doi: 10.1515/polyeng-2019-0041.

Jarvinen, T. A., Jarvinen, M. and Kalimo, H. (2013) 'Regeneration of injured skeletal muscle after the injury.', *Muscles, ligaments and tendons journal*, 3(4), pp. 337–45. doi: 10.11138/mltj/2013.3.4.337.

Jenkins, A. D. *et al.* (1996) 'Glossary of basic terms in polymer science (IUPAC Recommendations 1996)', *Pure and Applied Chemistry*, 68(12), pp. 2287–2311. doi: 10.1351/pac199668122287.

Jia, B. *et al.* (2013) 'Effect of microcrystal cellulose and cellulose whisker on biocompatibility of cellulose-based electrospun scaffolds', *Cellulose*, 20(4), pp. 1911–1923. doi: 10.1007/s10570-013-9952-0.

Jones, J. M. *et al.* (2018) 'An assessment of myotube morphology, matrix deformation, and myogenic mRNA expression in custom-built and commercially available engineered muscle chamber configurations', *Frontiers in Physiology*, 9(MAY), pp. 1–9. doi: 10.3389/fphys.2018.00483.

Juhas, M., Ye, J. and Bursac, N. (2015) 'Design, Evaluation, and Application of Engineered Skeletal Muscle.', *Methods (San Diego, Calif.)*. Elsevier Inc., 99, pp. 81–90. doi: 10.1016/j.ymeth.2015.10.002.

Jun, I. *et al.* (2016) 'Creating Hierarchical Topographies on Fibrous Platforms Using Femtosecond Laser Ablation for Directing Myoblasts Behavior', *ACS Applied Materials & Interfaces*, p. acsami.5b11418. doi: 10.1021/acsami.5b11418.

Kimura, S. and Itoh, T. (2007) 'Biogenesis and function of cellulose in the tunicates', *Cellulose: molecular and structural biology*, pp. 217–236. doi: 10.1007/978-1-4020-5380-1_13.

Klemm, D. *et al.* (2005) 'Cellulose: Fascinating biopolymer and sustainable raw material', *Angewandte Chemie - International Edition*, 44(22), pp. 3358–3393. doi: 10.1002/anie.200460587.

Kontturi, E. *et al.* (2007) 'Cellulose nanocrystal submonolayers by spin coating', *Langmuir*, 23(19), pp. 9674–9680. doi: 10.1021/la701262x.

Kopecek, M. *et al.* (2008) 'Improved adhesion, growth and maturation of human bone-derived cells on nanocrystalline diamond films', *Physica Status Solidi (A) Applications and Materials Science*, 205(9), pp. 2146–2153. doi: 10.1002/pssa.200879729.

Kühl, U. *et al.* (1986) 'Role of laminin and fibronectin in selecting myogenic versus fibrogenic cells from skeletal muscle cells in vitro', *Developmental Biology*, 117(2), pp. 628–635. doi: 10.1016/0012-1606(86)90331-3.

Lam, M. T. *et al.* (2006) 'The effect of continuous wavy micropatterns on silicone substrates on the alignment of skeletal muscle myoblasts and myotubes', *Biomaterials*, 27(24), pp. 4340–4347. doi: 10.1016/j.biomaterials.2006.04.012.

Lampin, M. *et al.* (1997) 'Correlation between substratum roughness and wettability, cell adhesion, and cell migration', *Journal of Biomedical Materials Research*, 36(1), pp. 99–108. doi: 10.1002/(SICI)1097-4636(199707)36:1<99::AID-JBM12>3.0.CO;2-E.

Langer, R. and Vacanti, J. P. (1993) 'Tissue Engineering', *Science*, 260(May), pp. 920–926. doi: 10.1126/science.8493529.

Laurie, G. W. *et al.* (1986) 'Localization of binding sites for laminin, heparan sulfate proteoglycan and fibronectin on basement membrane (type IV) collagen', *Journal of Molecular Biology*, 189(1), pp. 205–216. doi: 10.1016/0022-2836(86)90391-8.

Lee, E. A. *et al.* (2015) 'Extracellular matrix-immobilized nanotopographical substrates for enhanced myogenic differentiation', *Journal of Biomedical Materials Research - Part B Applied Biomaterials*, 103(6), pp. 1258–1266. doi: 10.1002/jbm.b.33308.

Li, H. *et al.* (2012) 'Direct laser machining-induced topographic pattern promotes up-regulation of myogenic markers in human mesenchymal stem cells', *Acta Biomaterialia*. Acta Materialia Inc., 8(2), pp. 531–539. doi: 10.1016/j.actbio.2011.09.029.

Lieber, R. L. and Fridén, J. (2000) 'Functional and Clinical Significance', *Muscle Nerve*, 23(November), pp. 1647–1666. doi: 10.1002/1097-4598(200011)23:11<1647::AID-MUS1>3.0.CO;2-M [pii].

Lim, J. Y. *et al.* (2007) 'The regulation of integrin-mediated osteoblast focal adhesion and focal adhesion kinase expression by nanoscale topography', *Biomaterials*, 28(10), pp. 1787–1797. doi: 10.1016/j.biomaterials.2006.12.020.

Liu, L. *et al.* (2016) 'Mechanically strong and thermosensitive hydrogels reinforced with cellulose nanofibrils', *Polymer Chemistry*. Royal Society of Chemistry, 7(46), pp. 7142–7151. doi: 10.1039/c6py01652a.

Loesberg, W. A. *et al.* (2007) 'The threshold at which substrate nanogroove dimensions may influence fibroblast alignment and adhesion', *Biomaterials*, 28(27), pp. 3944–3951. doi: 10.1016/j.biomaterials.2007.05.030.

Luo, H. *et al.* (2019) 'Advances in tissue engineering of nanocellulose-based scaffolds: A review', *Carbohydrate Polymers*. Elsevier, 224(May), p. 115144. doi: 10.1016/j.carbpol.2019.115144.

Madden, L. *et al.* (2015) 'Bioengineered human myobundles mimic clinical responses of skeletal muscle to drugs', *eLife*, 2015(4), pp. 1–14. doi: 10.7554/eLife.04885.

Mahmoud, K. A. *et al.* (2010) 'Effect of surface charge on the cellular uptake and cytotoxicity of fluorescent labeled cellulose nanocrystals', *ACS Applied Materials and Interfaces*, 2(10), pp. 2924–2932. doi: 10.1021/am1006222.

Marieb, E. N. and Hoehn, K. N. (2014) *Human Anatomy & Physiology*. Pearson Education Limited.

Michell, A. J. (1993) 'Second-derivative FTIR spectra of native celluloses from Valonia and tunicin', *Carbohydrate Research*, 241(C), pp. 47–54. doi: 10.1016/0008-6215(93)80093-T.

Mills, M. (2001) 'Differential expression of the actin-binding proteins, alpha-actinin-2 and -3, in different species: implications for the evolution of functional redundancy', *Human Molecular Genetics*, 10(13), pp. 1335–1346. doi: 10.1093/hmg/10.13.1335.

Miyamoto, T. *et al.* (1989) 'Tissue biocompatibility of cellulose and its derivatives.', *Journal of*

biomedical materials research, 23(1), pp. 125–133. doi: 10.1002/jbm.820230110.

Mudera, V. *et al.* (2010) 'The effect of cell density on the maturation and contractile ability of muscle derived cells in a 3D tissue-engineered skeletal muscle model and determination of the cellular and mechanical stimuli required for the synthesis of a postural phenotype', *Journal of Cellular Physiology*, 225(3), pp. 646–653. doi: 10.1002/jcp.22271.

Murphy, W. L., McDevitt, T. C. and Engler, A. J. (2014) 'Materials as stem cell regulators', *Nature Materials*, 13(6), pp. 547–557. doi: 10.1038/nmat3937.

NHS (2018) *Overview: Muscular dystrophy*. Available at: https://www.nhs.uk/conditions/muscular-dystrophy/.

Nickerson, R. F. and Habrle, J. A. (1947) 'Cellulose Intercrystalline Structure', *Industrial & Engineering Chemistry*, 39(11), pp. 1507–1512. doi: 10.1021/ie50455a024.

Nikoi, N.-D. (2016) *Cellulose Nanowhiskers for Skeletal Muscle Engineering*, *PhD Thesis*. University of Manchester, Manchester, UK.

Nishiyama, Y. *et al.* (2003) 'Crystal structure and hydrogen bonding system in cellulose I(alpha) from synchrotron X-ray and neutron fiber diffraction.', *Journal of the American Chemical Society*, 125(47), pp. 14300–14306. doi: 10.1021/ja037055w.

North, K. N. and Beggs, A. H. (1996) 'Deficiency of a skeletal muscle isoform of α-actinin (α-actinin-3) in merosin-positive congenital muscular dystrophy', *Neuromuscular Disorders*. Elsevier Science B.V. All rights reserved, 6(4), pp. 229–235. doi: 10.1016/0960-8966(96)00361-6.

Nunes, V. a *et al.* (2007) 'Stem cells from umbilical cord blood differentiate into myotubes and express dystrophin in vitro only after exposure to in vivo muscle environment.', *Biology of the cell / under the auspices of the European Cell Biology Organization*, 99(4), pp. 185–96. doi: 10.1042/BC20060075.

Ohara, P. T. and Buck, R. C. (1979) 'Contact guidance in vitro. A light, transmission, and scanning electron microscopic study', *Experimental Cell Research*, 121(2), pp. 235–249. doi: 10.1016/0014-4827(79)90002-8.

Penton, C. M. *et al.* (2016) 'Laminin 521 maintains differentiation potential of mouse and human satellite cell-derived myoblasts during long-term culture expansion', *Skeletal Muscle*. Skeletal Muscle, 6(1), p. 44. doi: 10.1186/s13395-016-0116-4.

Pooyan, P., Tannenbaum, R. and Garmestani, H. (2012) 'Mechanical behavior of a cellulose-reinforced scaffold in vascular tissue engineering', *Journal of the Mechanical Behavior of Biomedical Materials*. Elsevier Ltd, 7, pp. 50–59. doi: 10.1016/j.jmbbm.2011.09.009.

Porter, J. D. *et al.* (2001) 'Extraocular muscle is defined by a fundamentally distinct gene expression profile', *Proceedings of the National Academy of Sciences of the United States of America*, 98(21), pp. 12062–12067. doi: 10.1073/pnas.211257298.

Powell, C. A. *et al.* (2002) 'Mechanical stimulation improves tissue-engineered human skeletal muscle', *American Journal of Physiology - Cell Physiology*, 283(5 52-5), pp. 1557–1565.

Pownall, M. E., Gustafsson, M. K. and Emerson, C. P. (2002) 'Myogenic Regulatory Factors and the Specification of Muscle Progenitors in Vertebrate Embryos', *Annual Review of Cell and Developmental Biology*, 18(1), pp. 747–783. doi: 10.1146/annurev.cellbio.18.012502.105758.

Price, R. L. *et al.* (2004) 'Nanometer surface roughness increases select osteoblast adhesion on

carbon nanofiber compacts', *Journal of Biomedical Materials Research - Part A*, 70(1), pp. 129–138. doi: 10.1002/jbm.a.30073.

Qian, Q. *et al.* (2012) '5-Azacytidine Induces Cardiac Differentiation of Human Umbilical Cord-Derived Mesenchymal Stem Cells by Activating Extracellular Regulated Kinase', *Stem Cells and Development*, 21(1), pp. 67–75. doi: 10.1089/scd.2010.0519.

Ranby, B. G. (1949) 'Aqueous colloidal solutions of cellulose micelles', *Acta Chem. Scand.,* pp. 649–650. doi: 10.3891/acta.chem.scand.03-0649.

Revol, J. F. *et al.* (1992) 'Helicoidal self-ordering of cellulose microfibrils in aqueous suspension', *International Journal of Biological Macromolecules*, 14(3), pp. 170–172. doi: 10.1016/S0141-8130(05)80008-X.

Ribeiro, S. *et al.* (2018) 'Electroactive biomaterial surface engineering effects on muscle cells differentiation', *Materials Science and Engineering C*, 92(November 2017), pp. 868–874. doi: 10.1016/j.msec.2018.07.044.

Riboldi, S. A. *et al.* (2005) 'Electrospun degradable polyesterurethane membranes: Potential scaffolds for skeletal muscle tissue engineering', *Biomaterials*, 26(22), pp. 4606–4615. doi: 10.1016/j.biomaterials.2004.11.035.

Riboldi, S. A. *et al.* (2008) 'Skeletal myogenesis on highly orientated microfibrous polyesterurethane scaffolds', *Journal of Biomedical Materials Research - Part A*, 84(4), pp. 1094–1101. doi: 10.1002/jbm.a.31534.

Ricotti, L. *et al.* (2010) 'Adhesion and proliferation of skeletal muscle cells on single layer poly(lactic acid) ultra-thin films', *Biomedical Microdevices*, 12(5), pp. 809–819. doi: 10.1007/s10544-010-9435-0.

S. Burattini, P. Ferri, M. Battistelli, R. Curci, F. Luchetti, E. F. (2004) 'C 2 C 12 murine myoblasts as a model of skeletal muscle development: morpho-functional characterization', pp. 223–233. Available at: http://www.ejh.it/index.php/ejh/article/viewFile/891/1003.

Santa Maria, L., Rojas, C. V. and Minguell, J. J. (2004) 'Signals from damaged but not undamaged skeletal muscle induce myogenic differentiation of rat bone-marrow-derived mesenchymal stem cells', *Experimental Cell Research*, 300(2), pp. 418–426. doi: 10.1016/j.yexcr.2004.07.017.

Saxena, I. M. and Brown, R. M. (2005) 'Cellulose biosynthesis: Current views and evolving concepts', *Annals of Botany*, 96(1), pp. 9–21. doi: 10.1093/aob/mci155.

Sengupta, D. *et al.* (2012) 'Protein-Engineered Biomaterials to Generate Human Skeletal Muscle Mimics', *Advanced Healthcare Materials*, 1(6), pp. 785–789. doi: 10.1002/adhm.201200195.

Shi, D. *et al.* (2004) 'Myogenic fusion of human bone marrow stromal cells , but not hematopoietic cells', *Bone*, 104(1), pp. 290–294. doi: 10.1182/blood-2003-03-0688.Supported.

Shimizu, K., Fujita, H. and Nagamori, E. (2009) 'Alignment of skeletal muscle myoblasts and myotubes using linear micropatterned surfaces ground with abrasives', *Biotechnology and Bioengineering*, 103(3), pp. 631–638. doi: 10.1002/bit.22268.

Soleimani-Gorgani, A. (2016) 'Inkjet Printing', in *Printing on Polymers*. Elsevier, pp. 231–246. doi: 10.1016/B978-0-323-37468-2.00014-2.

Sottile, J. and Hocking, D. C. (2002) 'Fibronectin Polymerization Regulates the Composition and

Stability of Extracellular Matrix Fibrils and Cell-Matrix Adhesions', *Molecular Biology of the Cell*, 14(December), pp. 3546–3559. doi: 10.1091/mbc.E02.

Svensson, A. *et al.* (2005) 'Bacterial cellulose as a potential scaffold for tissue engineering of cartilage', *Biomaterials*, 26(4), pp. 419–431. doi: 10.1016/j.biomaterials.2004.02.049.

Tapscott, S. J. (2005) 'The circuitry of a master switch: Myod and the regulation of skeletal muscle gene transcription.', *Development (Cambridge, England)*, 132(12), pp. 2685–95. doi: 10.1242/dev.01874.

Thayer, M. J. *et al.* (1989) 'Positive autoregulation of the myogenic determination gene MyoD1', *Cell*, 58(2), pp. 241–248. doi: 10.1016/0092-8674(89)90838-6.

Trappmann, B. *et al.* (2012) 'Extracellular-matrix tethering regulates stem-cell fate', *Nature Materials*. Nature Publishing Group, 11(7), pp. 642–649. doi: 10.1038/nmat3339.

Ul-Islam, M. *et al.* (2015) 'Bacterial cellulose composites: Synthetic strategies and multiple applications in bio-medical and electro-conductive fields', *Biotechnology Journal*, 10(12), pp. 1847–1861. doi: 10.1002/biot.201500106.

Wada, M., Heux, L. and Sugiyama, J. (2004) 'Polymorphism of cellulose I family: Reinvestigation of cellulose IVl', *Biomacromolecules*, 5(4), pp. 1385–1391. doi: 10.1021/bm0345357.

Wakitani, S., Saito, T. and Caplan, A. (1995) 'Myogenic cells derived from rat bone marrow mesenchymal stem cells exposed to 5-azacytidine', *Muscle & nerve*, 18(December), pp. 1417–1426. Available at: http://onlinelibrary.wiley.com/doi/10.1002/mus.880181212/abstract.

Wang, P. Y., Yu, H. Te and Tsai, W. B. (2010) 'Modulation of alignment and differentiation of skeletal myoblasts by submicron ridges/grooves surface structure', *Biotechnology and Bioengineering*, 106(2), pp. 285–294. doi: 10.1002/bit.22697.

Webster, T. J. *et al.* (2000) 'Specific proteins mediate enhanced osteoblast adhesion on nanophase ceramics', *Journal of Biomedical Materials Research*, 51(3), pp. 475–483. doi: 10.1002/1097-4636(20000905)51:3<475::AID-JBM23>3.0.CO;2-9.

Weiss, P. (1934) 'In vitro experiments on the factors determining the course of the outgrowing nerve fiber', *Journal of Experimental Zoology*, 68(3), pp. 393–448. doi: 10.1002/jez.1400680304.

Wells, R. G. (2008) 'The role of matrix stiffness in regulating cell behavior', *Hepatology*, 47(4), pp. 1394–1400. doi: 10.1002/hep.22193.

Wertz, J.-L. and Bédué O, M. J. (2010) *Cellulose Science and Technology*. EPFL Press, Lausanne, Switzerland.

Winter, H. T. *et al.* (2010) 'Improved colloidal stability of bacterial cellulose nanocrystal suspensions for the elaboration of spin-coated cellulose-based model surfaces', *Biomacromolecules*, 11(11), pp. 3144–3151. doi: 10.1021/bm100953f.

Wippermann, J. *et al.* (2009) 'Preliminary Results of Small Arterial Substitute Performed with a New Cylindrical Biomaterial Composed of Bacterial Cellulose', *European Journal of Vascular and Endovascular Surgery*. Elsevier Ltd, 37(5), pp. 592–596. doi: 10.1016/j.ejvs.2009.01.007.

Wragg, N. M. *et al.* (2019) 'Development of tissue-engineered skeletal muscle manufacturing variables', *Biotechnology and Bioengineering*. John Wiley & Sons, Ltd, 116(9). doi: 10.1002/bit.27074.

Xu, H. *et al.* (1994) 'Murine muscular dystrophy caused by a mutation in the laminin α2 (Lama2) gene', *Nature Genetics*, 8(3), pp. 297–302. doi: 10.1038/ng1194-297.

Yang, C. *et al.* (2011) 'Preparation and characterization of three-dimensional nanostructured macroporous bacterial cellulose/agarose scaffold for tissue engineering', *Journal of Porous Materials*, 18(5), pp. 545–552. doi: 10.1007/s10934-010-9407-z.

Yang, G. H., Lee, J. U. and Kim, G. H. (2019) 'The fabrication of uniaxially aligned micro-textured polycaprolactone struts and application for skeletal muscle tissue regeneration', *Biofabrication*. IOP Publishing, 11(2). doi: 10.1088/1758-5090/ab0098.

Yeo, M. and Kim, G. H. (2019) 'Nano/microscale topographically designed alginate/PCL scaffolds for inducing myoblast alignment and myogenic differentiation', *Carbohydrate Polymers*. Elsevier, 223(July), p. 115041. doi: 10.1016/j.carbpol.2019.115041.

Yeung, T. *et al.* (2005) 'Effects of substrate stiffness on cell morphology, cytoskeletal structure, and adhesion', *Cell Motility and the Cytoskeleton*, 60(1), pp. 24–34. doi: 10.1002/cm.20041.

Yim, E. K. F., Pang, S. W. and Leong, K. W. (2007) 'Synthetic nanostructures inducing differentiation of human mesenchymal stem cells into neuronal lineage', *Experimental Cell Research*, 313(9), pp. 1820–1829. doi: 10.1016/j.yexcr.2007.02.031.

Yokota, S., Kitaoka, T. and Wariishi, H. (2008) 'Biofunctionality of self-assembled nanolayers composed of cellulosic polymers', *Carbohydrate Polymers*, 74(3), pp. 666–672. doi: 10.1016/j.carbpol.2008.04.027.

Zahari, N. K., Idrus, R. B. H. and Chowdhury, S. R. (2017) 'Laminin-coated poly(Methyl methacrylate) (PMMA) nanofiber scaffold facilitates the enrichment of skeletal muscle myoblast population', *International Journal of Molecular Sciences*, 18(11). doi: 10.3390/ijms18112242.

Zammit, P. S. (2008) 'Chapter 3 the Muscle Satellite Cell : the Story of a Cell on the Edge !', *Cell*, pp. 45–64.

Zhang, Q., Lin, D. and Yao, S. (2015) 'Review on biomedical and bioengineering applications of cellulose sulfate', *Carbohydrate Polymers*. Elsevier Ltd., 132, pp. 311–322. doi: 10.1016/j.carbpol.2015.06.041.

Zhang, W., Behringer, R. R. and Olson, E. N. (1995) 'Inactivation of the myogenic bHLH gene MRF4 results in up-regulation of myogenin and rib anomalies', *Genes and Development*, 9(11), pp. 1388–1399. doi: 10.1101/gad.9.11.1388.

Zuk, P. a *et al.* (2001) 'Multilineage cells from human adipose tissue: implications for cell-based therapies.', *Tissue engineering*, 7(2), pp. 211–228. doi: 10.1089/107632701300062859.

Appendix

Appendix A: Repeats of Alamar Blue assays for C2C12s Section 6.1.1

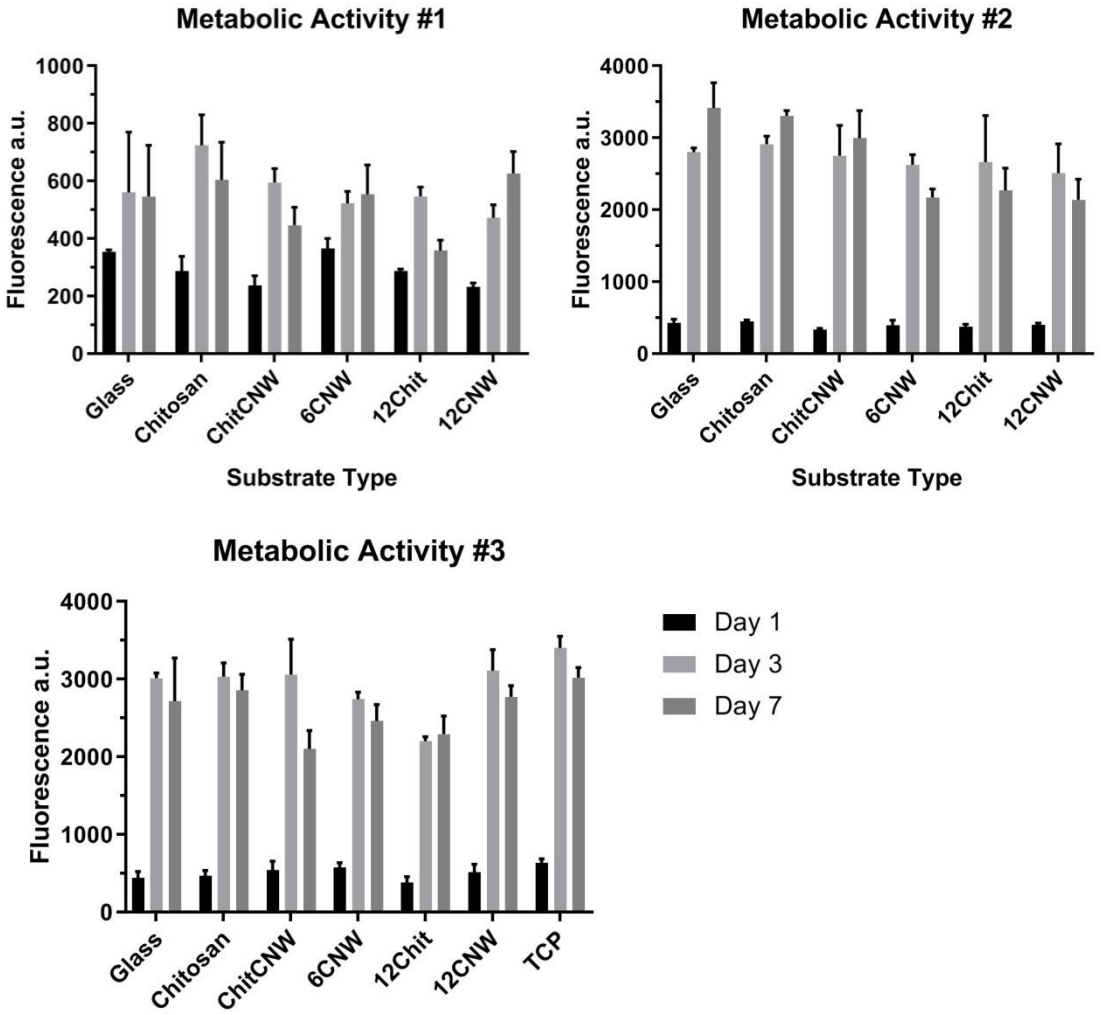

Appendix B: Repeats of PicoGreen assays for C2C12s Section 6.1.1

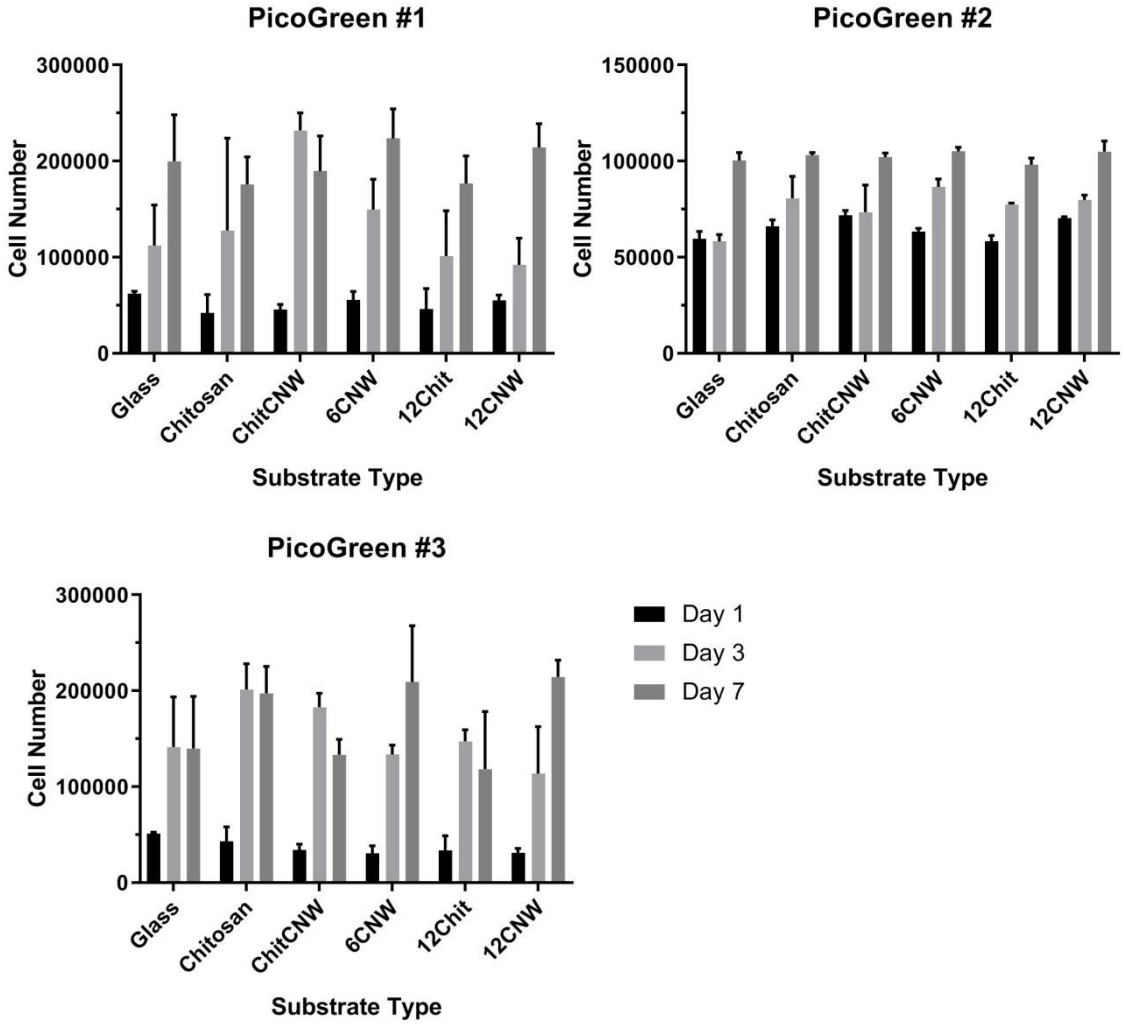

Appendix C: Full histograms of myotube length for C2C12s Section 6.1.2

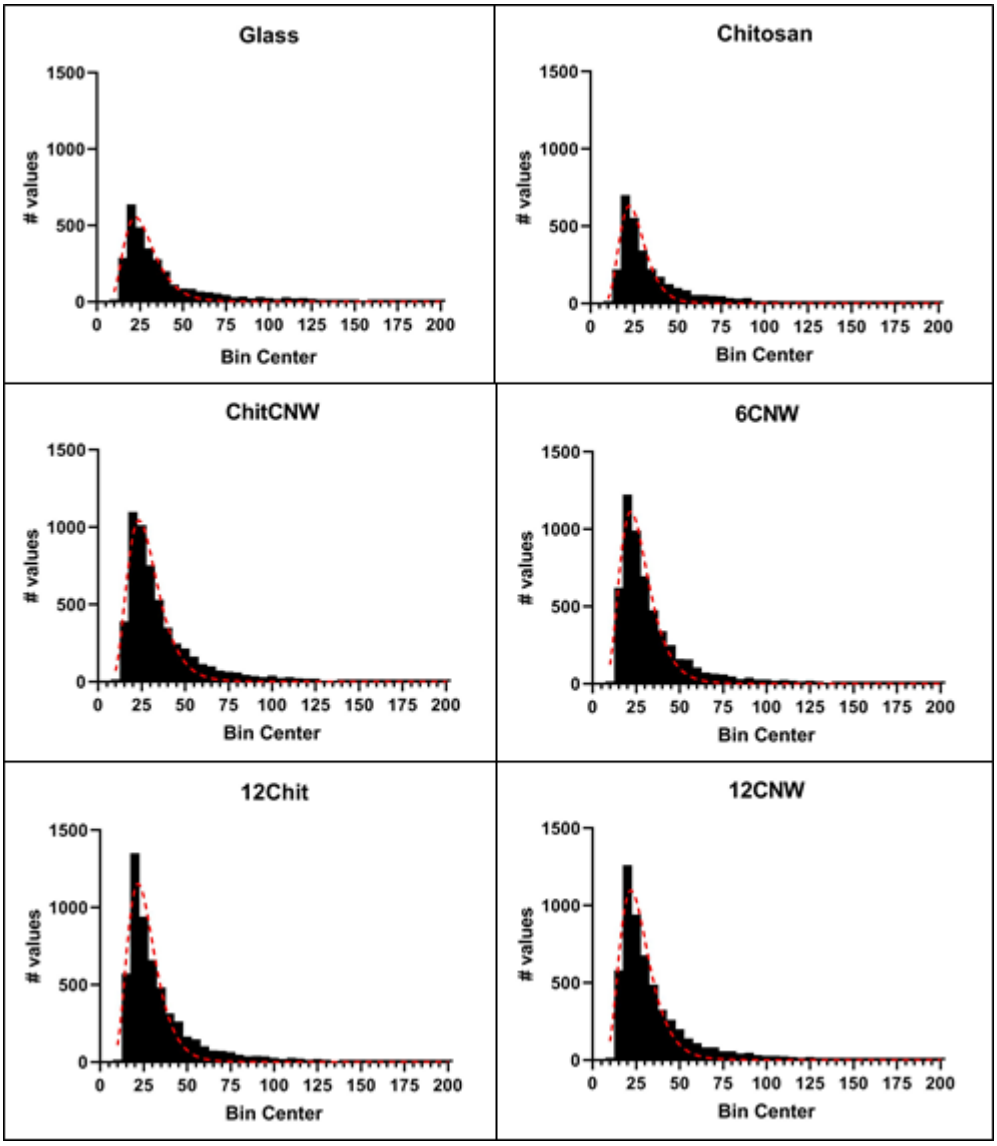

Appendix D: Repeats of Alamar Blue assays for hSkMCs Section 6.2.1

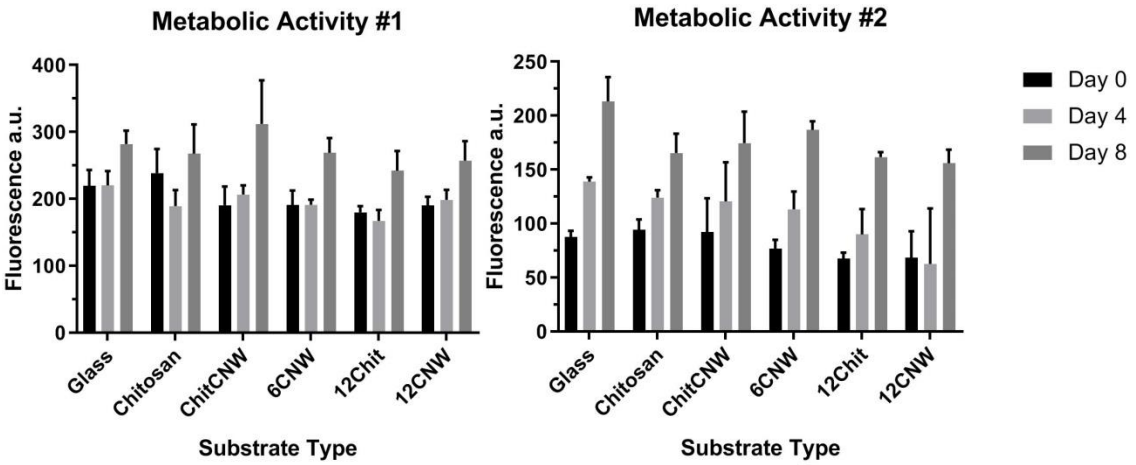

Appendix E: Repeats of PicoGreen assays for hSkMCs Section 6.2.1

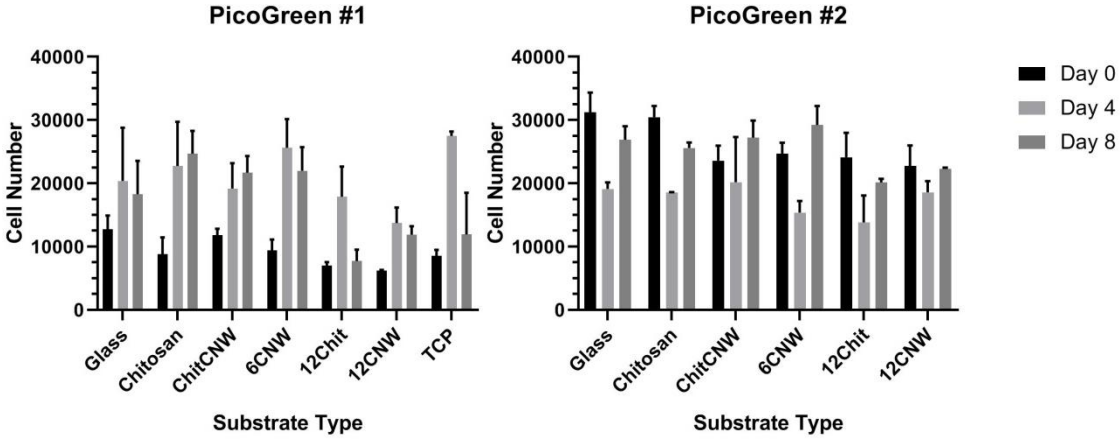

Appendix F: Alamar Blue assays for Glass and 6CNW substrates in response to pre-conditioning, Section 7.2.1

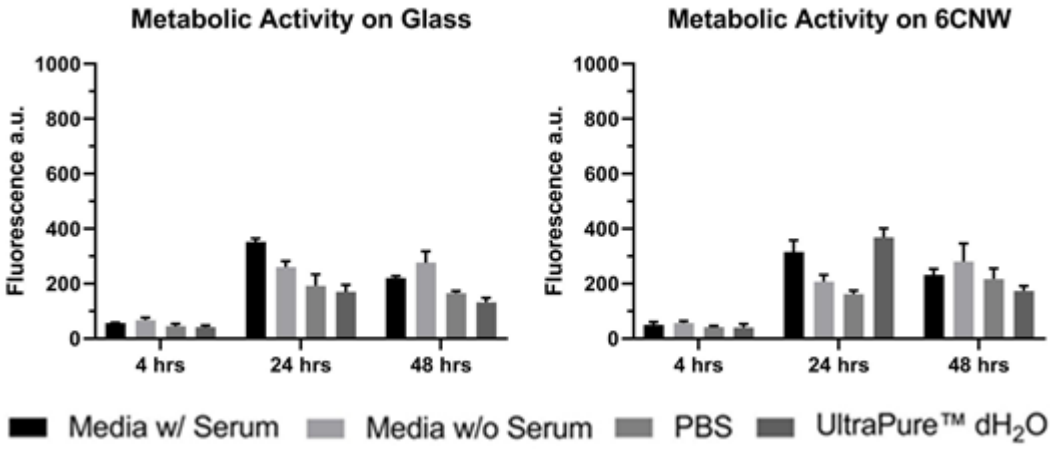

Appendix G: PicoGreen assays for Glass and 6CNW substrates in response to pre-conditioning, Section 7.2.1

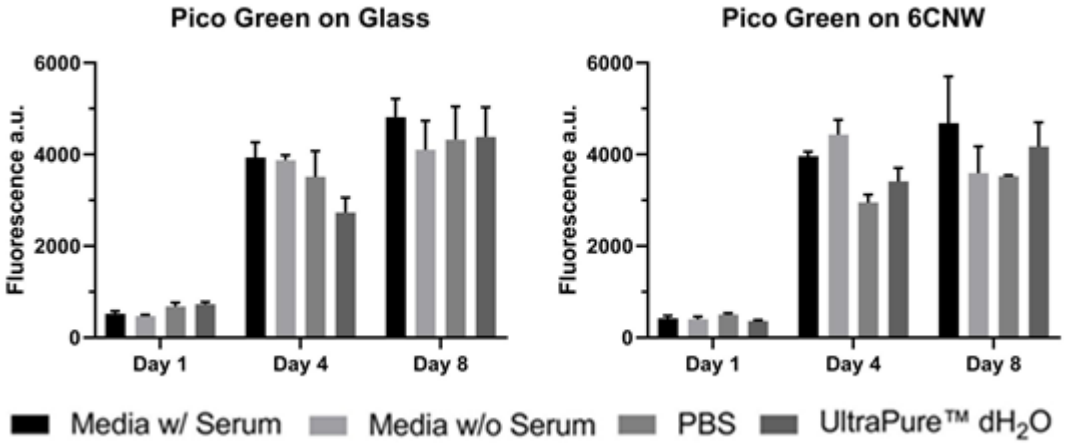

Appendix H: Full histograms of myotube length for C2C12s on fibronectin and laminin treated substrates, Section 7.2.2

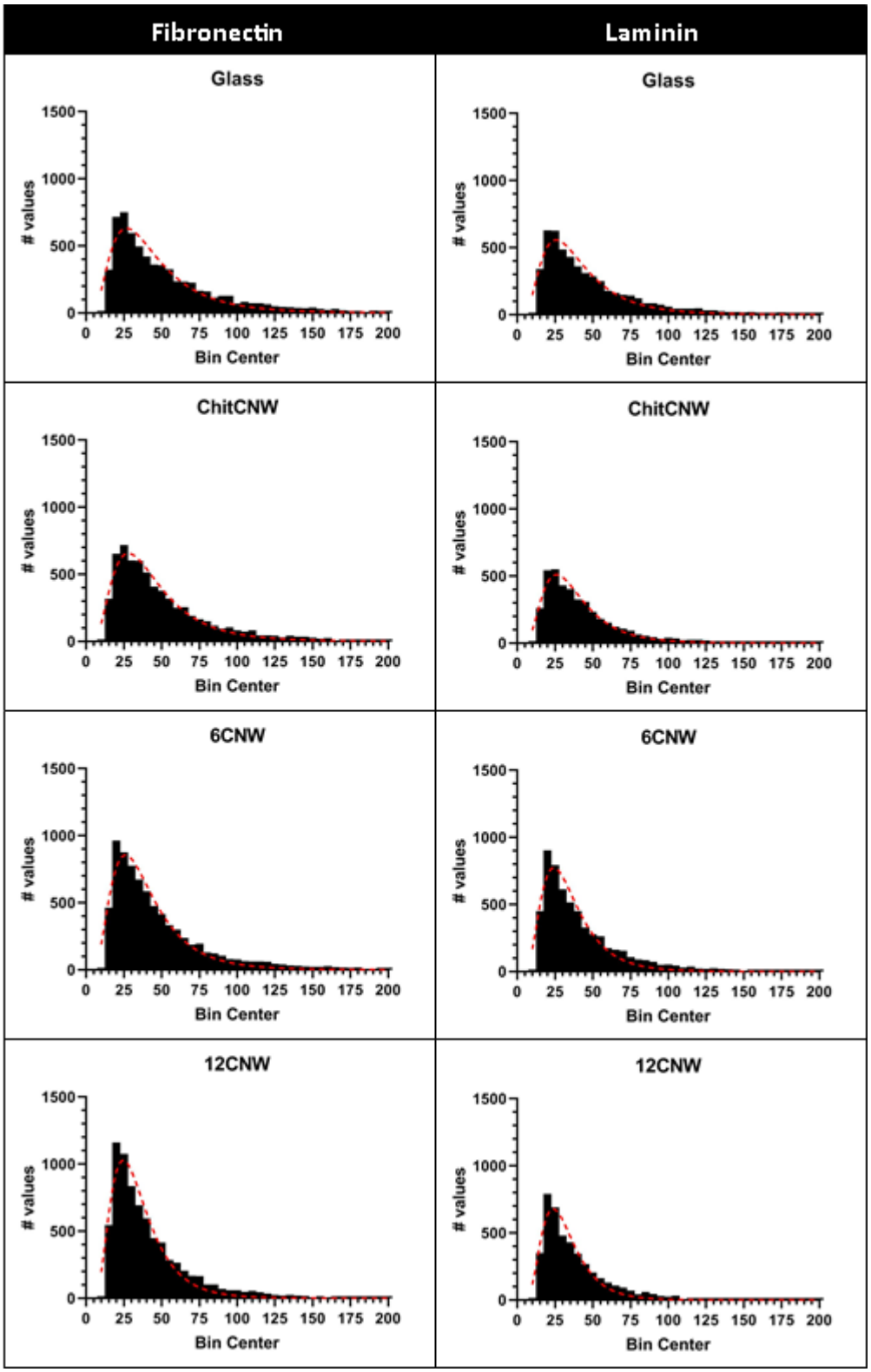

Appendix I: Full histograms of myotube length for C2C12s untreated substrates, Section 7.2.2